Université Ferhat ABBAS Sétif 1

UNIVERSITE FERHAT ABBAS SETIF 1

FACULTE DE TECHNOLOGIE

THESE

Présentée au Département de Génie des Procédés

Pour l'obtention du diplôme de

DOCTORAT
Domaine : Sciences et Technologie

Filière: Génie des procédés   **Option : Génie des procédés pharmaceutiques**

Par

SID Dounia

THEME

Conception et évaluation *in vitro*/*in vivo* de nouvelles formulations pharmaceutiques microparticulaires à base de complexes d'inclusion

Soutenue le 14/05/2022 devant le Jury :

OUARI Kamel	Professeur	Univ. Ferhat Abbas Sétif 1	Président
BAITICHE Milad	Professeur	Univ. Ferhat Abbas Sétif 1	Directrice de thèse
LE BORGNE Marc	Professeur	Univ. Claude Bernard Lyon 1	Co-Directeur
REZGUI Farouk	Professeur	Univ. Abderrahmane Mira Béjaïa	Examinateur
ZOUAI Foued	M.C.A.	Univ. Ferhat Abbas Sétif 1	Examinateur
Zineb EL BAHRI	Professeur	Univ. Djillali Liabès Sidi Belabès	Invité
BOUTAHALA Mokhtar	Professeur	Univ. Ferhat Abbas Sétif 1	Invité

Acknowledgements

First and foremost, I would like to thank my supervisors, Professor **Milad BAITICHE** and Professor **Marc LE BORGNE**, for their kind support and guidance over the four years which the preparation of this thesis took. With their patience and unrelenting help, I have learned not only scientific knowledge and experience, but also an attitude of doing research which will help me for my professional life.

I thank also members of the jury, Professor **Kamel OUARI**, Professor **Farouk REZGUI** and Doctor **Foued ZOUAI** for accepting to be readers and to judge my thesis work as well as for agreeing to attend the presentation of the thesis defense.

Thank you very much Professor **Zineb EL BAHRI** for having accepted to be present for my thesis presentation. I would like to express my sincere gratitude for your initial guidance and contribution for the thesis project.

I am very grateful to my professor **Mokhtar BOUTAHALA** for his support. His contribution in the implementation of the experimental work which has been of great help. Receive my immense appreciation for all what you did for me.

I would like to deeply express my gratitude to my Professor **Ferhat DJERBOUA**, for the scientific guidance, transmitted knowledge, consideration and availability. His amazing energy and competence absolutely make him an example for me, as a professional and as a person. My eternal gratitude for everything.

I would also like to express my gratitude to Professor **Lekhmici ARRAR** for assisting the in vivo tests. Working in his laboratory was a very enriching scientific opportunity for me.

I would also like to express my gratitude to Doctor **Christelle MARMINON** and Professor **Zouhair BOUAZIZ** for the kind and excellent reception, for their contributions and advice, and for all their availability.

I would also like to express my gratitude to Professor **Laurent DAVID** for the excellent reception in his laboratory, for all contributions and advice, and for his availability.

Dedication

Many people have contributed to this work and made my graduate experience one of the most enriching and interesting steps in my life. First, I have to dedicate this work to my **family**, with special gratitude to my **parents**, who were always behind me. None of this would have been possible without their love and prayers. I have been fortunate to have them in my life; I wish I could thank them.

I want to express my deepest gratitude and appreciation to my dear friends **Manel, Milled, Soumaya, Imane, Ikram, Chahinez** and **Walid** who gave me all their support and love. They were the source of encouragement and confidence during my graduate academic background. I want to express my immense appreciation for all they have done for me.

Dounia

List of abbreviations

°C: Celcius Degree

A: Alunite

Å: Ångström

Abs: Absorbency

APIs: Active Pharmaceutical Ingredients

BCS: Biopharmaceutics Classification System

BSA: Bovine Serum Albumin

CA: Citric Acid

CD: Cyclodextrin

CGTase: Glucosyltransferase

CPCSEA: Committee for the Purpose of Control and Supervision of Experiments on Animal

D: Drug

DDS: Drug Delivery System

DFT: Density Functional Theory

DNA: Deoxyribonucleic Acid

Dp: Pore Diameter

DSC: Differential Scanning Calorimetry

FDA: Food and Drug Administration

FTIR: Fourier-Transform Infrared Spectroscopy

GI: Gastrointestinal

GIT: Gastrointestinal Tract

HAL: Halloysite

HPLC: High Performance Liquid Chromatography

HRBC: Human Red Blood Cell

HSM: Hot Stage Microscopy

IUPAC: International Union of Pure and Applied Chemistry

K_c: Stability/Equilibrium constant

KET: Ketoprofen

KN: Kneading

MA: Mefenamic Acid

MC: Monte-Carlo

MDS: Molecular Dynamic Simulation

MPE: Maximum Possible Effect

NMR: Nuclear Magnetic Resonance

NSAID: Non-Steroidal Anti-Inflammatory Drug

PDB: Protein Data Bank

PY: Practical Yield

Q: Quartz

QM: Quantum Mechanics

SEM: Scanning Electron Microscopy

T: Temperature

TEM: Transmission Electronic Microscopy

TGA: Thermal Gravimetric Analysis

TMS: Tetra Methyl Silane

UV-VIS: Ultra-Violet Visible spectroscopy

Vp: Pore Volume

XP: Extra-Precision

XRF: X-Ray Fluorescence

XRPD: X-Ray Powder Diffraction

ΔG: The binding affinity

ΔG^0: Gibbs free energy

ΔH^0: Standard Enthalpy

ΔS^0: Standard Entropy

List of figures

List of tables

List of contents

Chapter I: Literature Review

Chapter II: Solubility enhancement of active pharmaceutical ingredients

Chapter III: Controlled release of active pharmaceutical ingredients

Summary

Introduction

In the late Middle Age, when Paracelsus (1493-1541), a physician-alchemist, made his famous statement, "All the substances are poisons; there is none that is not a poison, the right dose differentiates a poison from a remedy". So by this, he laid the ground work for the later development of the modern toxicology by promoting the importance of the dose-response relationship [1]. Many of his revolutionary views remain an integral part of toxicology, pharmacology and therapeutics, and his concept is considered as the basis for pharmaceutical therapy. With the advancement of the pharmaceutical sciences, the industry has certainly observed the discovery of several new drug molecules ranging from small drug molecules to macromolecules, but the ultimate goal of achieving disease-free conditions in the patients is often left hanging due to several obstacles related to physicochemical and molecular complexities of the free drugs and the inaccessibility and under-dosing for most of the biological/pathological targets [2].

The acquisition and development of knowledge on how active pharmaceutical ingredients (APIs) exert their pharmacological effect, particular information such as dose-response, onset, duration of action and pharmacodynamic and pharmacokinetic relationships, has required attention and stimulated interest in order to deliver APIs at rates (and to locations) that optimize the therapeutic effects.

Drug delivery systems (DDS) are used to improve pharmacokinetics, biodistribution profiles, efficacy and safety of the drug. Often, APIs considered hopeless have been revived through the design of drug delivery systems [3]. Thus, controlling drug release has evolved as a multidisciplinary science, requiring knowledge in polymer science, engineering technologies, and awareness of the complexities and vagaries of gastrointestinal conditions that affect the transit of dosage forms. In fact, the therapeutic effect of traditional and novel APIs is enhanced via the development of galenic formulation, which ensures targeting of APIs to a particular tissue, cell or intracellular compartment, optimization of physicochemical properties of APIs poorly water-soluble, the control over release kinetics, the protection of the active agent, enhancement of the biological activities of the API, decrease in side effects, improve patient compliance or a combination of all these [4]. Therefore, the development of a galenic formulation is an essential step in the development of medicines and pharmaceutical research is constantly exploring new approaches to improve the efficiency of drug delivery.

In this context, the major purposes of this PhD thesis were:

- To examine the capacity of CDs specifically β-cyclodextrin and hydroxypropyl β-cyclodextrin to encapsulate and improve the water solubility and the biological efficiency of two APIs, namely the non-steroidal anti-inflammatory, mefenamic acid (MA), and a new Ser/Thr kinase CK2 inhibitor named NB4 respectively. It is well established that inclusion complexes are products with a high importance and their optimal therapeutic properties are related to their mode of preparation which is not easy to assess. Therefore, it is essential in our case to study the likely interactions between CDs and APIs for a better understanding of the encapsulation process and tailor make the factors involved in the inclusion process for these systems.

- Contrary to the above study where the host is relatively a small organic molecule with a cavity capable of hosting APIs, another part of the work explore the possible use of a pure tubular mineral namely halloysite which has been modified by citric acid (CA) as a galenic model for the sustained release of a non-steroidal anti-inflammatory drug, ketoprofen (KET).

- The developed formulations were physically and chemically characterized and evaluated *in vitro* and *in vivo* with regard to their release kinetic parameters, safety and efficiency.

This doctoral thesis consists of three main chapters, namely:

- The first chapter is a bibliographical review on the background related to the work undertaken in this thesis, presenting the main microparticulate and nanoparticulate galenic systems widely studied in the experimental part. Actually, most advanced ideas put forward concerning the cyclodextrins as drug carriers highlight their history and contributions of different scientists who have worked with CDs, their physical and chemical properties and pharmaceutical applications with typical examples and especially the advantages of using CDs for molecular encapsulation of APIs. In addition, the preparation and characterization of inclusion complexes in solution, and solid phase are described. Chapter one also gives a clear idea about halloysite, its physical and chemical properties, methods used to prepare pharmaceutical formulations and its applications in the drug delivery field. Moreover, studies conducted to ensure its biocompatibility are mentioned. The last part briefly introduces the possible halloysite

modification techniques for increasing the pore volume, loading efficiency, and extending release time, including functionalization by cyclodextrins.

- The second chapter is composed of three parts: the first one is a brief introduction describing the problem of poor water-solubility drugs, the different approaches to improve drug solubility, and the potential of cyclodextrins as drug solubilizer agents. The second part represents the published research on how to enhance the solubility of mefenamic acid (MA) and the last part corresponds to the research work done on NB4 in order to improve its water solubility by complexation with cyclodextrins.

- The last chapter presents four parts, a brief introduction about the sustained release systems and their advantages. The second and third parts are based on the theoretical and experimental studies of halloysite and citric acid modified halloysite as ketoprofen drug carriers, where two research manuscripts published are described.

References

[1] P. Grandjean, Paracelsus Revisited: The Dose Concept in a Complex World, Basic Clin Pharmacol Toxicol. 119 (2016) 126–132. https://doi.org/10.1111/bcpt.12622.

[2] B.S. Pattni, V.P. Torchilin, Targeted Drug Delivery Systems: Strategies and challenges in Target/Concepts and Design, (ed), Springer, Cham, 2014.

[3] P.M. Glassman, V.R. Muzykantov, Pharmacokinetic and Pharmacodynamic Properties of Drug Delivery Systems, J Pharmacol Exp Ther. 370 (2019) 570–580. https://doi.org/10.1124/jpet.119.257113.

[4] C. Wilson, P. Crowley, Controlled Release in Oral Drug Delivery, (ed), Springer, Science & Business Media, 2011.

Chapter I

Literature Review

I.1 Introduction

Humankind's efforts to fight against diseases date back to the dawn of civilization. Substances extracted from nature have been tested and used to treat physiological processes dysfunctions, pain, and discomfort. With the advancement of science, the active ingredients of these materials, the drugs, were identified, isolated, and in many cases, their mechanism of action elucidated [1]. New drug candidates are tested even today in the quest to add increasingly effective tools against diseases. They may be a top priority with the evolution of diseases (e.g., cancers) and the mutation of viruses (e.g., coronavirus).

Active pharmaceutical ingredients (APIs) properties differ drastically; even those designed to treat the same symptom, chemical structure, size, hydrophilicity, and potency identify the drug molecules whose function may be specific or highly complex. Even additional applicants, such as peptides and nucleic acids, have been introduced because of a growing understanding of cellular biology at the molecular level, as well as the (decoding) of the human genome and technological breakthroughs in the fields of proteomics and DNA micro-arrays [2].

Drug activity results from molecular interaction(s) in specific cells, which is necessary to reach the site of action following administration (oral, intravenous, local, transdermal, etc.) at sufficient concentrations [2]. The field that studies how to deliver the drug at the right place, at the right concentration for a suitable time, is known as drug delivery. However, it is not straightforward to deliver the drug by simply selecting an appropriate administration way; strategies based on the association of the API with a carrier (a drug delivery system – DDS) are an alternative solution. DDS, ranging from implantable electronic devices to single polymer chains, are required to be compatible with processes in the body (biocompatibility) as well as with the drug to be delivered [3].

In general, release dosage forms are thought to deliver an initial burst of API while allowing no control over the release rate. Dosage control is required to achieve and maintain therapeutic plasmatic concentrations (**Fig. I.1**). Indeed, DDSs alter the associated drug biodistribution and pharmacokinetics: the percentages of the delivered dose in the body various organs that change over time. Minimizing the drug fluctuation in plasma level and extending its action duration are ideal drug carriers robust functions. Furthermore, obstacles arising from low drug solubility, degradation (environmental or enzymatic), fast clearance rates, non-specific toxicity, inability to cross biological barriers, may be addressed by DDS. Overall, the

challenge of increasing the therapeutic effect of drugs, with a concurrent minimization of side effects, can be tackled through proper design and engineering of the DDS. Therefore the frequency of dosing of drugs can be reduced, and patient compliance increased [4,5].
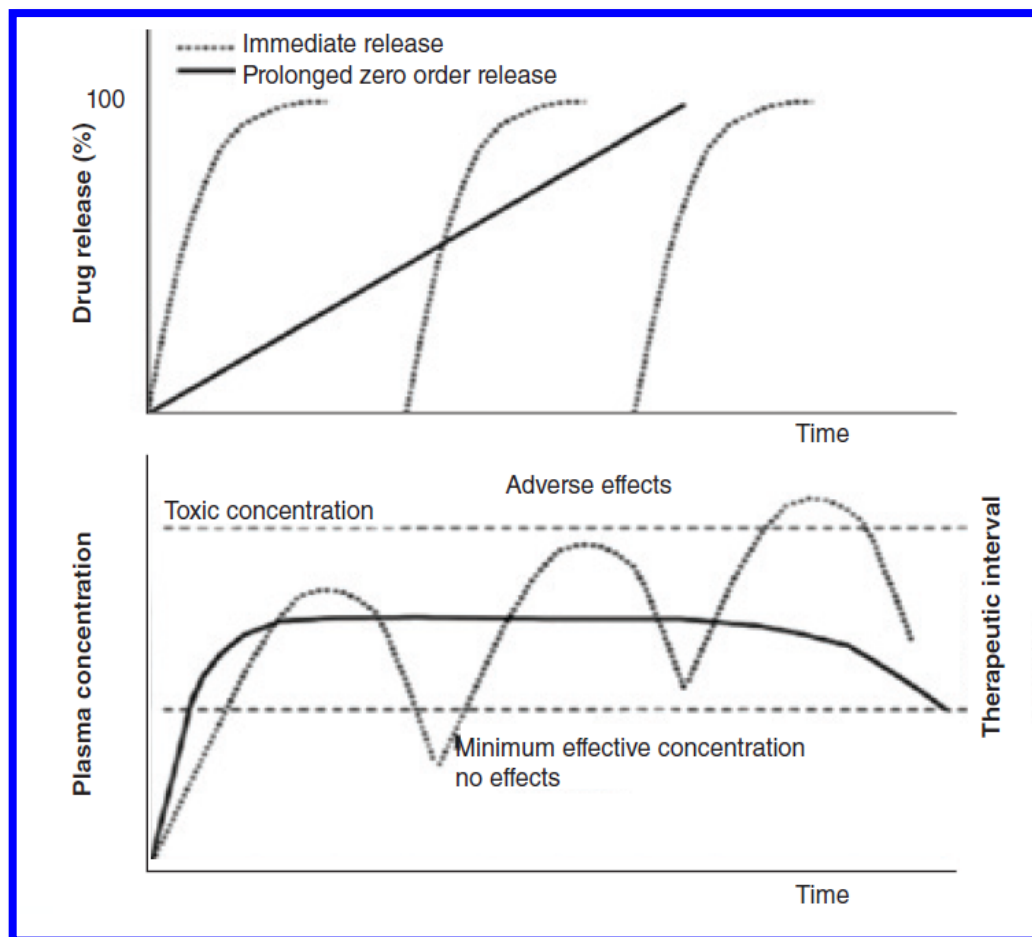
Fig. I.1: Correlation between drug-release profiles and its plasma concentration [4].

This chapter aims to present a state-of-the-art of bioavailable DDSs widely studied in the experimental part of the thesis, with particular attention to studies interested in modifying these DDSs to improve APIs efficiency. More specifically, studies concerning cyclodextrins and halloysite as natural vectors of drugs highlight their properties and the contributions of the various scientists who have worked with these two materials with examples showing the advantages of their use for the administration of APIs.

I.2 Cyclodextrins

I.2.1 Brief history

Although Scientists and regulators consider cyclodextrins (CDs) as new excipients for drug formulations, but the fact that they were reported in literature more than one hundred years ago. CDs materials were first isolated by Antoine Villiers in 1891 as a digest of *Bacillus amylobacter* on potato starch. The main events of their historical development are shown in **Table I.1**. CDs are cyclic carbohydrates formed during the bacterial (*Bacillus macerans*) degradation of starch molecules by CD glucosyltransferase enzyme (CGTase). Cyclodextrins possess interesting structures, they present a hydrophilic outer surface and a hydrophobic central cavity that can trap or encapsulate other molecules (**Fig. I.2**). This aptitude may lead to the formation of complexes of specific properties. So since their discovery, CDs have received a great attention by the scientists and according to Grégorio Crini **[6]**, the CDs history evolution can be divided into five quite distinct periods, namely:

- From 1891 to 1911, the first period covers their discovery by Antoine Villiers and characterization by Franz Schardinger.
- From 1911 to 1935 came a period of doubt and disagreement about the likely structures of CDs, between the laboratories of Hans Pringsheim and Paul Karrer.
- From 1935 to 1950, the third period was marked by the results obtained by Karl Freudenberg and Dexter French on the preparation, separation, and purification of cycloamylose.
- The period of exploration between 1950 and 1970 focused on inclusion complexes, with the work of Friedrich Cramer at the forefront.
- The period of utilization has been in progress since 1970 until now and CDs found numerous industrial applications.

Table I.1: Historical evolution of CDs and achievements **[6,7]**.

Year	Occurrence
1891	Villiers published his discovery of cellulosine (cyclodextrin)
1903	Schardinger isolated and purified α- and β-CDs
1911	Schardinger did lay the foundation of CD chemistry
1924	Methylation of CDs first described
1935	Freudenberg and Jacobi discovered γ-CD

1935-1955	Research on structure and function of CDs complexes by Freudenberg, Cramer, French, Rundle, Saenger, Bender, and Breslow
1953	The first CD patent was issued in Germany to Freudenberg, Cramer and Plieninger
1954	Cramer's book on inclusion complexes was published
1957-1965	French described the existence of large natural CDs with up to 12 glucose units. First fundamental review on CDs containing first misinformation on toxicity of CD was published
1960-1970	First analytical methods of CDs were developed
1965	Higuchi and Connors published their article about phase solubility profiles
1969	Launch DDS Research Institute of ALZA Co. in Kansas University
1975	First publication on CD polymers by M. Furue
1976	Manufacturing of natural CDs using alkaline CGTase in Japan
1976	Approval in Japan of the first pharmaceutical product with PGE_2/β-CD (Prostarmon E^{TM} sublingual tablets)
1978	Approval of natural CDs as food additives in Japan
1981	First International CD Symposium organized in Budapest (Hungary)
1981	First CD book is published
1983-1985	Brauns and Müller (Europe) and Pitha (USA) filed for patents on hydroxypropyl-β-CD
1983	First suggestion of self-association of parent CDs by K. Miyajima
1985	The first patent registering the pharmacological benefits of the complexation of analgesics compounds in CDs
1987	Approval of benexate HCl/β-CD capsules in Japan
1988	Approval of piroxicam/β-CD tablets (Brexin®) in Europe
1990	Stella and Rajewski filed for a patent on sulfobutyl ether-β-CD
1990	Approval of hydroxypropyl-β-CD containing cosmetics in Japan
1994	α-CD and β-CD listed in Japanese Pharmaceutical Excipients
1997	Approval of itraconazole/hydroxypropyl-β-CD oral solution (Sporanox®) in United States
1997	Founding of CD Society in Japan
1997	First monograph on β-CD appeared in the European Pharmacopoeia
2001	Approval of sulfobutyl ether-β-CD containing injections in United States
2005	Publication of "Nanomaterial Cyclodextrin"
2006	First CD Workshop in Japan
2008	Approval of sugammadex (Bridion®) in Europe
2010	Approval of sugammadex (Bridion®) in Japan
2011	Launch DDS Research Institute of Sojo University (Kumamoto)
2015	Approval of sugammadex (Bridion®) in United States
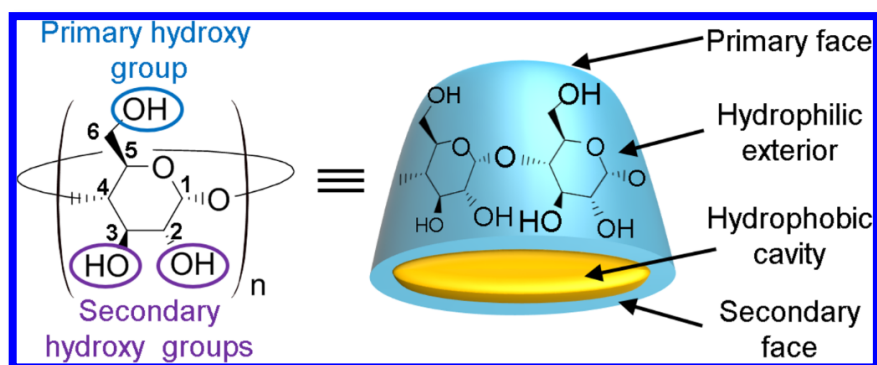
Fig. I.2: Cyclodextrins structural characteristics **[8]**.

I.2.2 Native cyclodextrins

Cyclodextrins are enzymatically modified starches by the action of glucosyltransferase, a unique enzyme able to convert starch or starch derivates into CDs, via the cyclization reaction **[9]**. CDs are cyclic oligosaccharides, containing a minimum of six D-(+) -glucopyranose units attached by α-1,4-linkages and exhibiting no reducing power. This arrangement is the origin of the conical cylinder shape of the CDs. Three native/natural/parent CDs contain 6, 7, and 8 glucose units and are designated alpha-cyclodextrin (α-CD), beta-cyclodextrin (β-CD), and gamma-cyclodextrin (γ-CD), respectively (**Fig. I.3**). These compounds are crystalline, conical, and hygroscopic substances **[10]**.
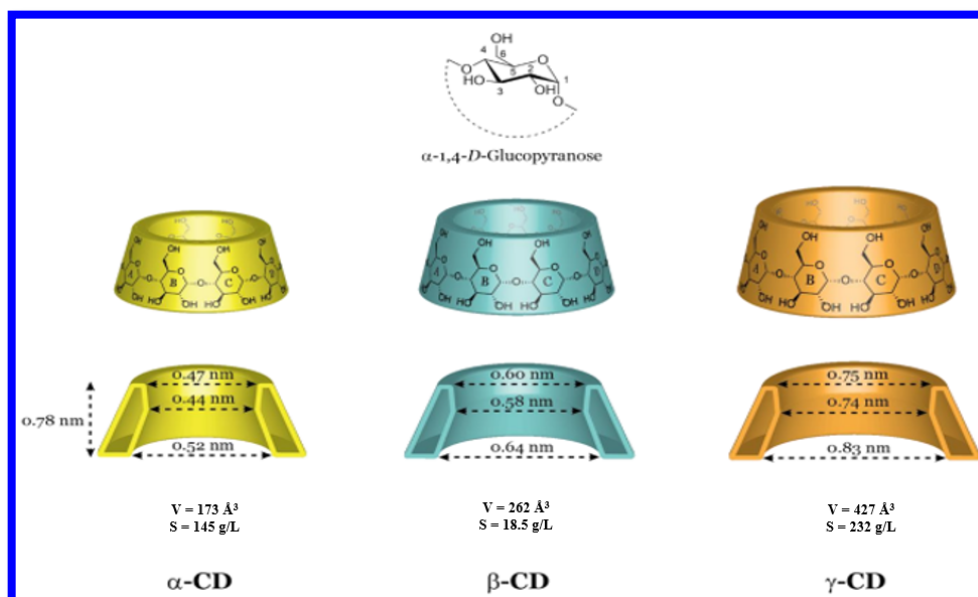
Fig. I.3: Structural characteristics of native cyclodextrins **[7]**.

Cyclodextrins are toroidal compounds with a truncated cone shape possessing secondary hydroxyl groups on the C-2 and C-3 atoms located on wider side of the torus, while

the primary hydroxyl groups on C-6 are situated on the opposite, narrower side of the torus. The CH groups carrying the protons H-1, H-2, and H-4 are located outside the molecule; thus, the outer surface of CDs is hydrophilic. The interior of the torus presents a much lower polarity than water; then, it can be seen as a hydrophobic cavity, which is lined by two rings of CH groups (H-3 and H-5) and by a ring of glucosidic "ether oxygens" (O-4), with H-6 situated near the cavity. This structure and these properties allow several kinds of drugs (guests) to be encased, originating non-covalently bonded inclusion complexes [11,12].

The cavity diameter varies with glucopyranose units' number, while the height is the same for all three CDs. Thus, the external diameter and the volume of the cavity increase from α-CD to γ-CD. The aqueous solubility varies less regularly (**Fig. I.3**), with β-CD having the lowest solubility. This can be explained by the fact that the proximity of the secondary hydroxyls of β-CD promoting the formation of a complete belt of hydrogen bonds which gives it a robust stabilization. However, β-CD is the most interesting from the complexation point of view and represents at least 95% of the production of CDs. According to the dimensions, α-CD complexes are low molecular weight compounds or molecules with aliphatic side chains, β-CD complexes aromatics, heterocycles, and γ-CD can include compounds with high molecular weight like macrocycles and steroids [13].

I.2.3 Cyclodextrins derivatives

In general, natural CDs have been modified with various types of substituents in distinct positions and with several degrees of substitution to improve their physicochemical properties (enhance the solubility of the CD derivative and its complexes) and inclusion ability (stabilization of the guest), decreasing its reactivity and mobility. In fact, the number of potential derivatives is limitless, because CDs exhibit 18, 21, or 24 substitutable hydroxyl groups for α-CD, β-CD and γ-CD, respectively [14].

The hydrophilic or ionizable CDs are mainly used to increase the uptake of drugs, while hydrophobic CDs may act as sustained-release agents of water-soluble drugs, integrating peptides and proteins. Anionic CDs show improved characteristics for drug inclusion compared with natural CDs (**Fig. I.4**), they have more excellent solubility in water and greater cavity. They form stronger inclusion complexes with polar guests or guests bearing a positive charge at a given pH, enabling the release of drugs controlled by pH [15] and they find pharmaceutical applications in different fields.
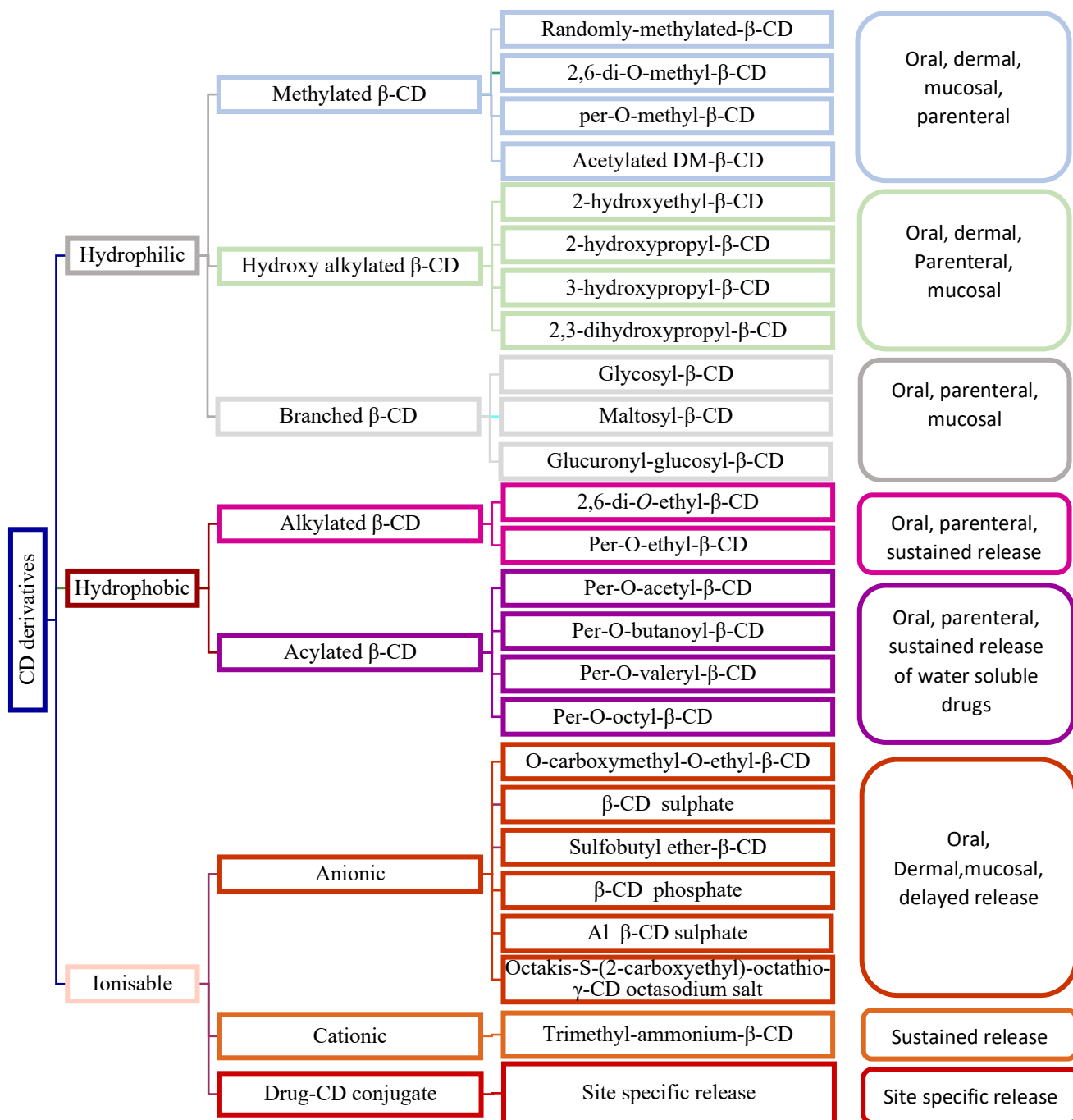
Fig. I.4: Diagram showing derivatives of cyclodextrins and their biomedical applications **[7]**.

I.2.4 Inclusion complex formation

The most notable feature of cyclodextrins is their ability to form inclusion complexes (host–guest complexes) with a very wide range of solid, liquid, and gaseous compounds by a molecular complexation. The formation of an inclusion complex may occur in solution and in the solid state, and after administration, it dissociates, releasing the drug into the organism in a quick and uniform mode. Inclusion constitutes a true molecular encapsulation; a guest molecule is held within the cavity of the cyclodextrin host molecule. Complex formation is a dimensional fit between host cavity and guest molecule. The lipophilic cavity of cyclodextrin molecules provides a microenvironment into which appropriately sized non-polar moieties can enter to form inclusion complexes. No covalent bonds are broken or formed during formation of the inclusion complex. The driving forces that lead to the CD complexation are electrostatic interaction, van der Waals interaction, hydrophobic interaction, hydrogen bonding, and charge-transfer interaction. As far as most inclusion possesses for drugs are carried out in water, overall, there are four energetically favourable factors that help shift the equilibrium to form the inclusion complex, namely [16,17]:

- The displacement of water molecules from the CD cavity
- The increased number of hydrogen bonds formed as the displaced water returns to the larger pool (Inclusion complexation can be accomplished in a co-solvent system)
- A decrease of the repulsive connections between the hydrophobic guest and the aqueous environment
- A rise in the hydrophobic interactions as the guest inserts itself into the non polar CD cavity.

. Inclusion in cyclodextrins exerts a profound effect on the physicochemical properties of guest molecules as they are temporarily locked or caged within the host cavity giving rise to beneficial modifications of guest molecules, which are not achievable otherwise. With pharmaceutical applications, these properties are solubility enhancement of highly insoluble guests (class 2 and 4 drugs of the biopharmaceutics classification system) (**Fig. I.5**) (**Table I.2**), stabilisation of labile guests against the degradative effects of oxidation, visible or UV light and heat effects, control of volatility and sublimation, physical isolation of incompatible compounds, chromatographic separations, taste modification by masking off flavours, unpleasant odours and controlled release of drugs and flavours. Therefore, and in general cyclodextrins based complexes found applications in food, pharmaceuticals, cosmetics, environment protection, bioconversion, packaging and the

textile industry. We should add that the formation of an inclusion complex cyclodextrins guests depends on several factors **[18]**, such as:

- Sizes of the CD and the guest molecule or some major functional groups within the guest moiety
- Thermodynamic connections between the different components of the system (CD, guest, and solvent)
- Structure of added substituent to the CD for (CD derivative)
- Location of substituent within the CD derivative molecule.
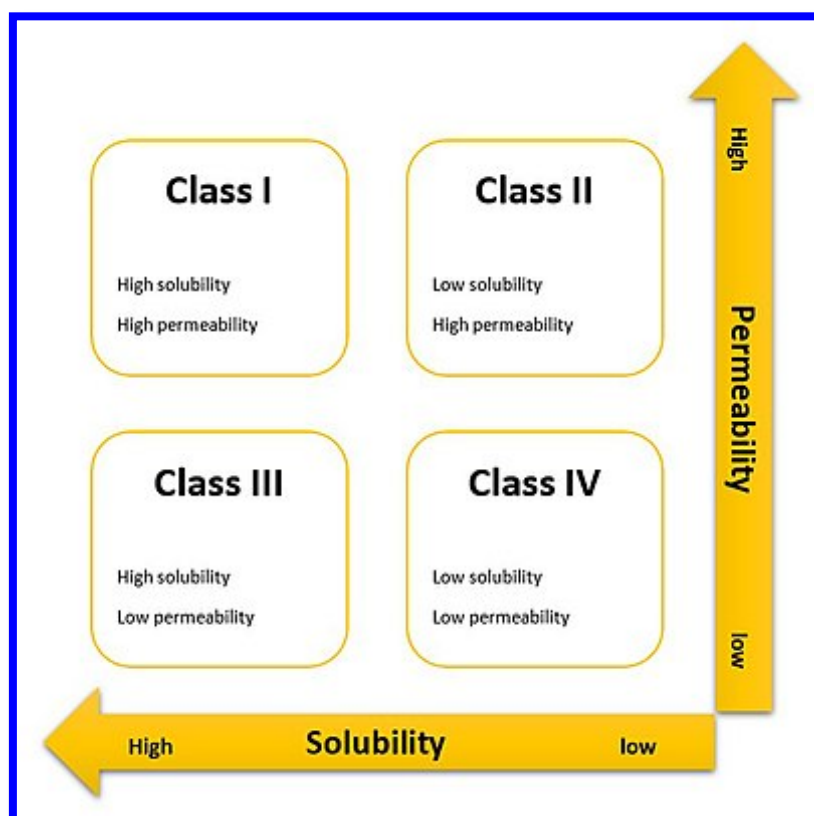
Fig. I.5: Diagram showing the biopharmaceutics classification system of drugs **[19]**.

Table I.2: Water improved drug solubility by complexing with CDs [20].

Drug/compound	Cyclodextrin	Solubility enhancement
Meloxicam	α-CD, β-CD, γ-CD, HP-β-CD	1.2 to 3-fold
Imatinib	β-CD, RM-β-CD	10-fold
Bupivacaine	HP-β-CD	1.5 to 4.5-fold
Omeprazole	β-CD, M-β-CD	1.7 to 3.4-fold
Sidenafil	β-CD, HP-β-CD, γ-CD, α-CD	1.6 to 3.2-fold
Progesterone	HP-β-CD, HPγ-CD, PM-β-CD, SBE-β-CD	4-3600-fold
Ginseng saponin	β-CD, HP-β-CD	40 to 80-fold
Naftifine	α-CD, β-CD, γ-CD, M-β-CD, HP-β-CD	0 to 21-fold
Disoxaril	DM-β-CD	3800-fold
Valsartan	HP-β-CD	18-fold
Gossypol	β-CD	2.5-fold
Celecoxib	α-CD, β-CD, γ-CD, HP-β-CD	2.5 to 20-fold
Valdecoxib	β-CD	3.5-fold
Benzocaine	β-CD	3-fold
Hesperetin	HP-β-CD	10-fold
Flurbiprofen	β-CD, HEβ-CD, M-β-CD	8-160-fold
Quercetin	β-CD, HP-β-CD, SBE-β-CD	21-55-fold
Valdecoxib	β-CD, HP-β-CD, SBE-β-CD	60-250-fold
Risperidone	α-CD, β-CD, γ-CD, HP-β-CD	0 to 70-fold
Celecoxib	β-CD	5-fold
3-Hydroxyflavones	α-CD, β-CD	6-fold
Triamterene	β-CD	3-fold
Camptothecin	HP-β-CD	30 to 50-fold
Furnidine	β-CD	3.4-fold
Celecoxib	β-CD	2.3-fold
Furan derivative G1	β-CD	3.3-fold
Rofecoxib	β-CD, SBE-β-CD	2-fold
Furosemide	HP-β-CD	11-fold
Natamycin	β-CD, γ-CD, HP-β-CD	16 to 152-fold
Bisabolol	β-CD	1.7-fold
Acitretin	HP-β-CD, RM-β-CD	N 1000-fold
Fentanyl	HP-β-CD, SBE-β-CD, G2β-CD	1-10-fold
Rofecoxib	β-CD	3-fold
Artemisinin	HP-β-CD	15-fold

Ketoconazole	HP-β-CD, M-β-CD	320 to 900-fold
Carprofen	HP-β-CD	52-fold
Diclofenac	β-CD	5-fold

In fact, there is not an ideal method for obtaining drug-CD complexes, and the best method, as well the best experimental conditions, must be selected case by case, depending on both the host and guest characteristics and the goal to be achieved by this CD complexation. In general there are an essential physical parameter that can be determined for the inclusion process [20]:

- The complexation strength or stability/equilibrium constant (K_c) shown in **(Fig. I.6),** known as the binding constant as defined in **Eq. I.1**, where [CD] and [D] are the concentrations of free CD and free drug molecule respectively. The constants K_f and K_r are the forward and reverse rate constants, respectively.

$$K_c = \frac{K_f}{K_r} = \frac{[D-CD]}{[D][CD]} \textbf{(Eq. I.1)}$$
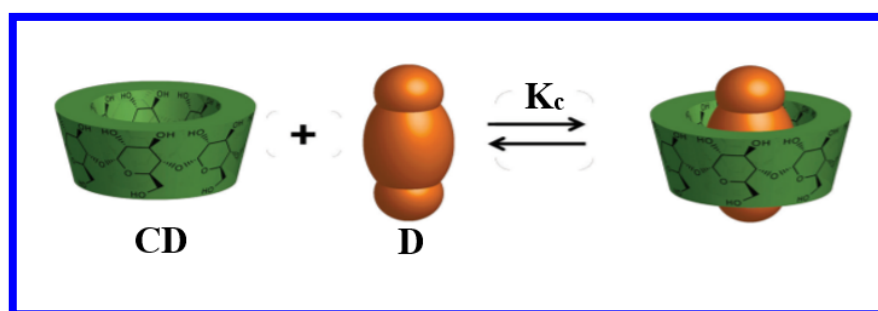
FigI.6: Scheme showing the interaction of guest (drug) (D) with a cyclodextrin (CD) forming an inclusion complex (D-CD) of 1:1 stoichiometry with a binding constant K_c [21].

In general, as it can be seen in **Fig. I.7,** different order complexes can be formed depending on the relative number of cyclodextrin molecules to those of guest ones in the complexation process. The order of the complex can be predicted when considering the thermodynamic of the complex formation. For this, the Gibbs free energy (ΔG^0) of complexation of 1:1 stoichiometry can be calculated from **Eq. I.2**, where R is the gas constant, T is the absolute temperature, ΔH^0 is the standard enthalpy of complexation, $K_{1:1}$ is the equilibrium constant for 1:1 drug: cyclodextrin inclusion complex, and ΔS^0 is the standard entropy of complexation [22,23].

$$\Delta G^0 = -RT \ln K_{1:1} = \Delta H^0 - T\Delta S^0 \quad \textbf{(Eq. I.2)}$$
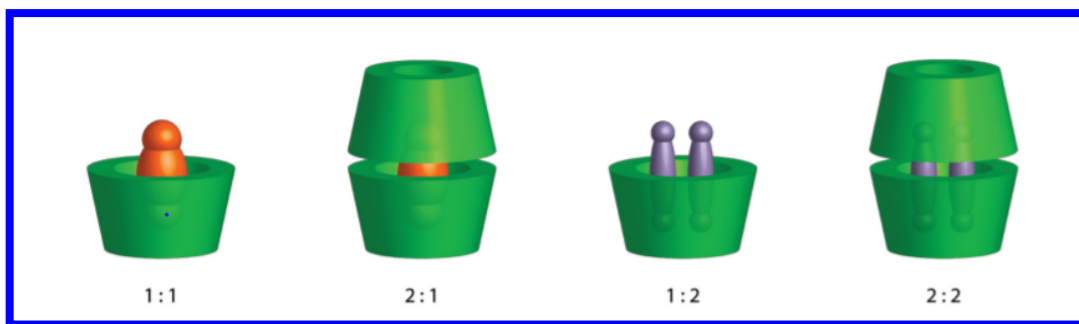
Fig. I.7: Different stoichiometries of inclusion complexes **[21]**.

Various values of K_C of 0 to about 100,000 M^{-1} have been described for CD complexes, with 0 meaning the absence of binding. Very weak binding is characterized by a K_C less than 500 M^{-1}, while weak, moderate, strong, and very strong binding are characterized by K_C in the ranges of 500-1000 M^{-1}, 1000-5000 M^{-1}, 5000-20,000 M^{-1}, and greater than 20,000 M^{-1}, respectively.

I.2.4.1 Inclusion complexes in solution

In aqueous solutions, CDs form inclusion complexes by replacing water molecules located within the relatively hydrophobic central cavity with some lipophilic drug moiety. Drug-CD complexes are continuously forming and dissociating with lifetimes in the range of milliseconds or less. In fact, in aqueous solutions, water molecules occupy the slightly non polar CD cavity via energetically unfavourable polar non-polar interactions and consequently can be promptly substituted by suitable "guest molecules" that show lower polarity than water. The dissolved CD acted as a "host molecule" and the "driving force" of the complex formation was the replacement of the high-enthalpy water molecules by these guests. The most frequently claimed stoichiometric ratio for CD complexes is 1:1. Nevertheless, other ratios are recognised, and the most usual of these possibly is 1:2. The stoichiometry of drug-CD complexes and the values of their K_C are often acquired from phase-solubility profiles (**Fig. I.8**), that is, plots of drug solubility versus CD concentration. The phase-solubility technique was developed by Higuchi and Connors, and it is based on research associated to how complexes of diverse complexing agents influence the drugs aqueous solubility. Phase solubility profiles are classified into A and B types: A type diagrams designate the formation of soluble inclusion complexes while B type indicate the formation of inclusion complexes with poor solubility. The B_S type corresponds to complexes with limited solubility and the BI profile indicates the presence of insoluble complexes. On the other hand, the A-type profile is subdivided into A_L

(linear increase of drug solubility as a function of CD concentration), A_P (positively deviating isotherms), and A_N (negatively deviating isotherms) subtypes [24].
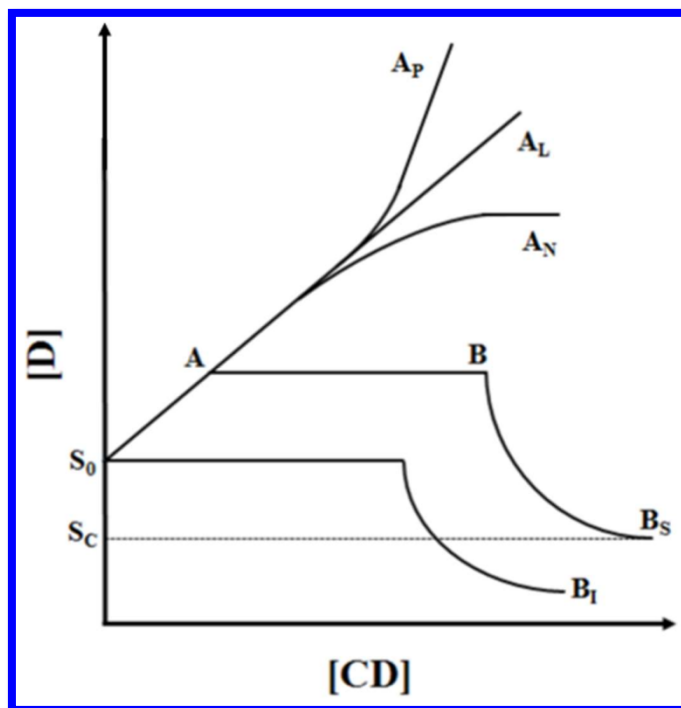
Fig. I.8: Phase-solubility diagram of cyclodextrin in water [21].

The principal analytical methods utilized for the characterization of CD inclusion complexation in solution are as follows:

- spectroscopic methods (ultraviolet-visible, circular dichroism, fluorescence, nuclear magnetic resonance (NMR), and electron spin resonance)
- electroanalytical methods (polarography, voltammetry, potentiometry, and conductimetry)
- separation methods (high performance liquid chromatography (HPLC) and capillary electrophoresis)
- polarimetry
- isothermal titration calorimetry.

Spectroscopic techniques, and especially NMR, have a crucial role in the characterization of inclusion complexes in solution [25].

I.2.4.2 Inclusion complexes in solid state

The technique utilized to prepare inclusion complexes by the solid-state technique can affect then physico-chemical characteristics of the obtained product. Currently, the main methods used to prepare the CD inclusion complexes by this method are as follows:

- methods in the solid state (milling/co-grinding method, supercritical fluid technology or microwave irradiation)
- methods in the semi-solid state (kneading method)
- methods in solution (co-precipitation technique, solvent evaporation method, neutralization precipitation method, lyophilisation /freeze drying method or atomization/spray-drying method)

The importance of water molecules in drug-CD inclusion complex formation in aqueous solutions has been extensively studied; however, in the solid state it has not received enough attention. It should be noted that a full characterization of the formation of a drug-CD inclusion complex in solution does not demonstrate its presence also in the solid state. Furthermore, the techniques that can be applied for preparing solid complexes can influence the final product properties. The principal analytical methods for the characterization of drug-CD solid systems are the following:

- thermal analysis methods (differential scanning calorimetry (DSC), thermal gravimetric analysis (TGA), and hot stage microscopy (HSM))
- X-ray diffraction (single crystal X-ray diffraction and powder X-ray diffraction)
- spectroscopic methods (Fourier-transform infrared (FTIR) spectroscopy, attenuated total reflectance-FTIR spectroscopy, and Raman spectroscopy)
- scanning electron microscopy (SEM).

DSC with X-ray diffraction methods are considered the methods of choice [26].

I.3 Clays and clay minerals

Often the terms clay and clay minerals are used as one and the same, but they are not exactly synonymous. The meaning of "clay" indicates a rock, a sedimentary deposit, and the alteration products of primary silicate minerals. The definition of clay, according to Joint Nomenclature Committees, and Clay Mineral Society is "…a naturally occurring material composed primarily of fine grained minerals, which is generally plastic at the appropriate water contents and will harden when dried or heated". The plasticity, in general, is a property of all materials which can deform irreversibly without breaking. Instead, clay mineral are phyllosilicate minerals and minerals which give plasticity to clay, have the tendency to harden upon drying or heating and can also be defined as the major constituents of clay, being responsible for their primary characteristics [27].

I.3.1 Origin and terminology

The origin of clay materials in nature is due to weathering, hydrothermal and diagenetic actions on sediments. Physical and chemical weathering interaction with the rocks forms silica, alumina and other rocks materials (primary minerals) that can develop in secondary minerals after a recrystallization process [27,28].

For example, the CO_2 gas dissolves easily in water forming carbonic acid, which hydrolyzes in hydrogen and bicarbonate ions making the water slightly acidic. Then the acidic water reacts with the rocks surfaces dissolving the potassium ions and silica to form feldspar, a potassium aluminosilicate. After that, the feldspar is transformed into kaolinite as indicated below [27,28].

$$2KAlSi_3O_8 + 2H^+ + H_2O \rightarrow Al_2Si_3O_5(OH)_4 + 2K^+ + 4SiO_2$$

The assembly of the particles brings the formation of aggregates. Accordingly, we may distinguish between interlayers, interparticles and interoperate cavities. All clays minerals are porous, containing pores of varied size and shapes which will act as sites of the host that can interact with the guest [27,28].

Kaolinite is known with the commonly used name kaolin, which is a corruption of the Chinese Gaoling, meaning "high ridge," the name of a hill near Jingdezhen where the occurrence of the mineral is known as early as the 2nd century B.C.. Montmorillonite and nontronite are named after the localities Montmorillon and Nontron, located in France where these minerals were first discovered. The name of Celadonite is from the French céladon

(meaning greyish yellow green) in allusion to its color. Sepiolite is a light and porous material, and its name is based on the Greek word for cuttlefish, the bone of which is similar in nature. The name saponite comes from the Latin sapon (meaning soap), because of its appearance and cleaning ability. Vermiculite derived from the Latin vermiculari ("to breed worms"), related to the physical characteristic of exfoliation upon heating, which causes the mineral to exhibit a spectacular volume change, from small grains to long wormlike threads. Baileychlore, brindleyite, corrensite, sudoite, and tosudite are instead examples of clay minerals that were named after distinguished clay mineralogists—Sturges W. Bailey, George W. Brindley, Carl W. Correns, and Toshio Sudō, respectively **[28]**.

I.3.2 Classifications of clay minerals

The classification of clay minerals can be made in different ways, mainly based on morphology and chemical structure (**Fig. I.9**). The arrangement of the particles or aggregates leads, as mentioned above, to different morphologies: road-like (palygorskite), fibrous (sepiolite), tubular (Hal), lamellar (MTM), layer-pillared (Hydrotalcite). Some clay minerals may be expressed using a general chemical formula as the following: $2SiO_2Al_2O_32H_2O$ (kaolinite), $4SiO_2Al_2O_3H_2O$ (pyrophyllite), $4SiO_23MgOH_2O$ (talc), and $3SiO_2Al_2O_35FeO4H_2O$ (chamosite) **[28]**.

The term phyllosilicate originates from the greek, "phyllon", meaning leaf. The phyllosilicates are constituted of alumina and silica sheets combined to form layers that may condense in either 1:1 or 2:1 proportion. The 1:1 group is constituted by the kaolin in which the most abundant minerals are the kaolinite, and halloysite, with an interlayer space of about 7 Å **[28]**.
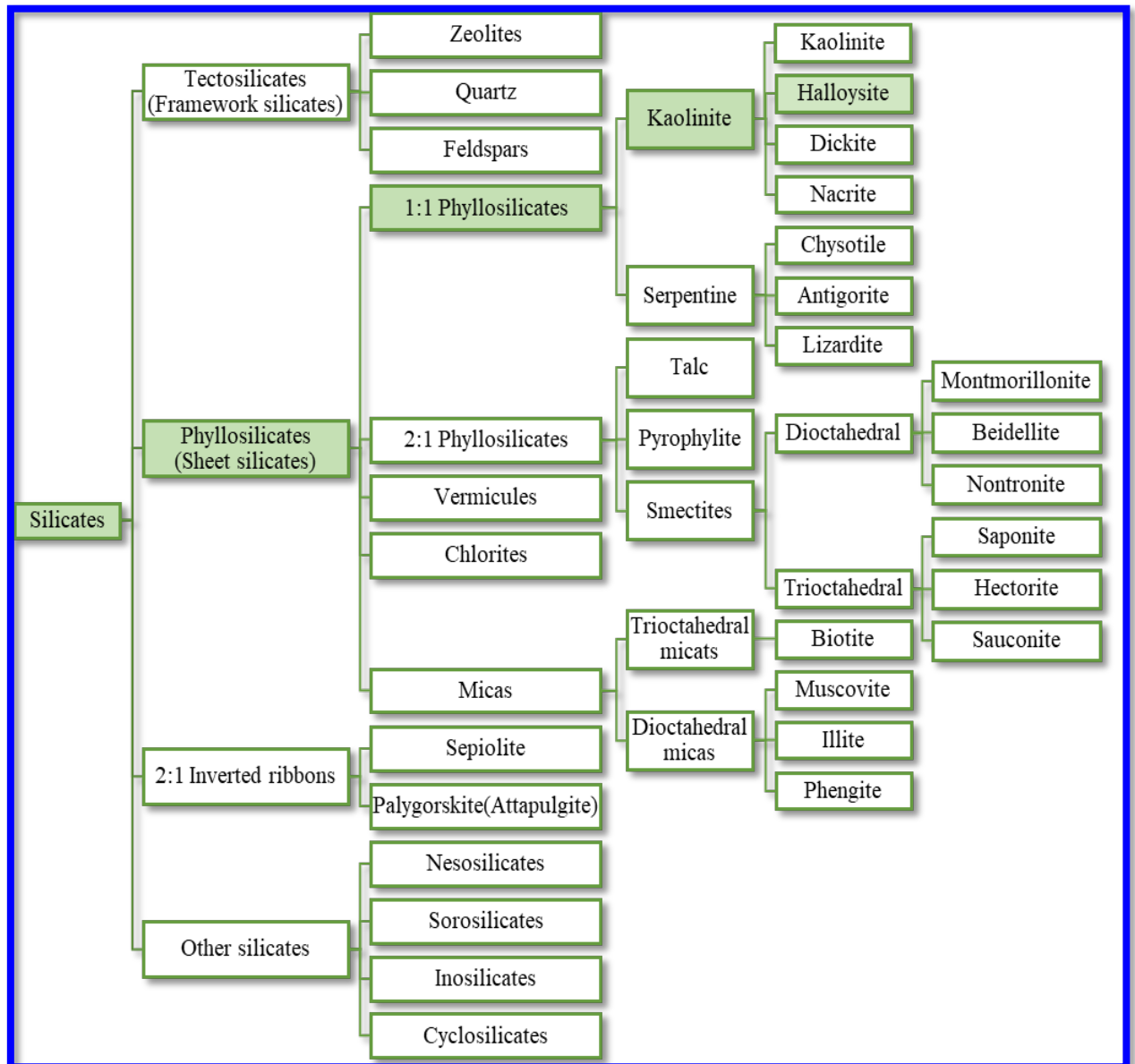
Fig. I.9: Clay minerals classification **[28]**.

In detail, the structure of clay materials consists of two basic units: an octahedral and a tetrahedral sheet. The octahedral sheet includes a closely packed oxygen and a hydroxyl group in which aluminum or magnesium atom are arranged in octahedral coordination (**Fig. I.10 a**). When aluminum is present in the sheets, only two out of three octahedral sites are occupied by the trivalent ions, to balance the total charge (this type of minerals is named "dioctahedral"). Instead, when magnesium is present, all three positions are filled to balance the structure and this type of mineral is named trioctahedral. The second structural unit is the silica tetrahedral layer, in which the silicon atoms, in the center of a tetrahedral, are equidistant from four oxygen

atoms (**Fig. I.10 b**). The tetrahedrons are arranged to form a hexagonal network repeated infinitely into two horizontal directions to form what is called the "silica tetrahedral sheet". The silica tetrahedral sheet and the octahedral sheet are joined by sharing the apical oxygen or hydroxyl to form what is named the 1:1 clay materials layer or the 2:1 clay material layer (**Fig. I.10 c-d**). According to this disposition, several types of surfaces are present, like the external, internal and edge surfaces **[27]**.
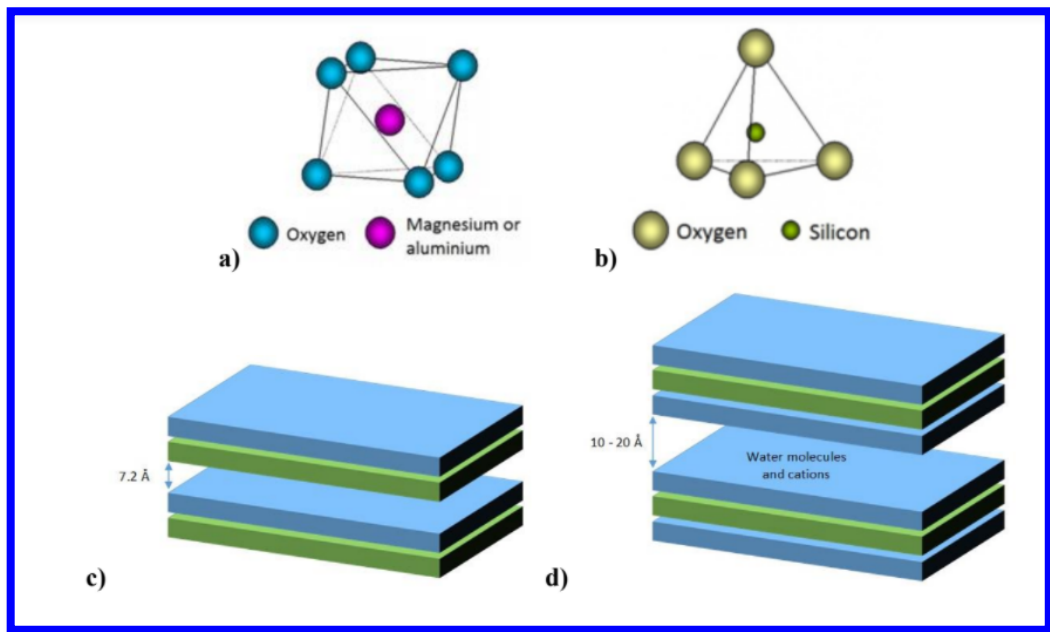
Fig. I.10: Representation of a) octahedral coordination; b) tetrahedral coordination c-d) building blocks of clays **[29]**.

I.3.3 Halloysite nanotubes

Halloysite (Hal) is a clay mineral of the kaolin group, with a dioctahedral 1:1 structure. In terms of chemistry, Hal composition is the same as kaolinite with water present between Hal monolayers. Thus, it is known as the hydrated kaolinite phase. Hal particles can adopt different morphologies such as tubes, fibers, spheres, plates, laths, etc. The tubular morphology of Hal is the most common one. They consist of predominately hollow cylinders (Hal nanotubes). These are made of multiple rolled layers composed of a sheet of corner-sharing SiO_4 tetrahedral bonded to a sheet of edge-sharing AlO_6 octahedral, creating in this way a 1:1 layer silicate. There are crystallographic water molecules and kaolinite OH groups in the gaps between the aluminosilicate layers of the structures (**Fig. I.11**). Layered Hal occurs mainly in two different polymorphs, the hydrated form with the formula $AlSi_2O_5(OH)_4\ 2H_2O$ and the anhydrous form

with the formula $Al_2Si_2O_5(OH)_4$, with an interlayer spacing of 10 Å and 7 Å, respectively (**Fig. I.12**). Typically, 10–15 aluminum-silicate bilayers roll into the cylinder giving an external surface composed of siloxane (Si-O-Si) groups, an internal surface that consists of gibbsite - like array of aluminol (Al-OH) groups, and Al-OH and Si-OH groups at the edges of the material. Due to this characteristic structure, Hal has negative charges on its external surface, positive on the inner lumen surface, and negative/positive charges at its edges at pH values ranging from 3 to 10. Generally, Hal nanotubes have an external diameter of 40-70 nm, an internal diameter of 10-40 nm, length of 0.2µm-1m. These characteristics depend on many factors, such as the extraction site and purification procedures. For example, in some deposits, were observed Hal tubes with lengths up to 3-5 µm, but in the size distribution curve, they have a minor fraction. The smaller clay nanotubes are most interesting for composites with sustained drug delivery formulations. The commercially available Hal tubes are the shorter ones (0.4-0.5 µm length) because of harsh milling during industrial processing **[30]**.
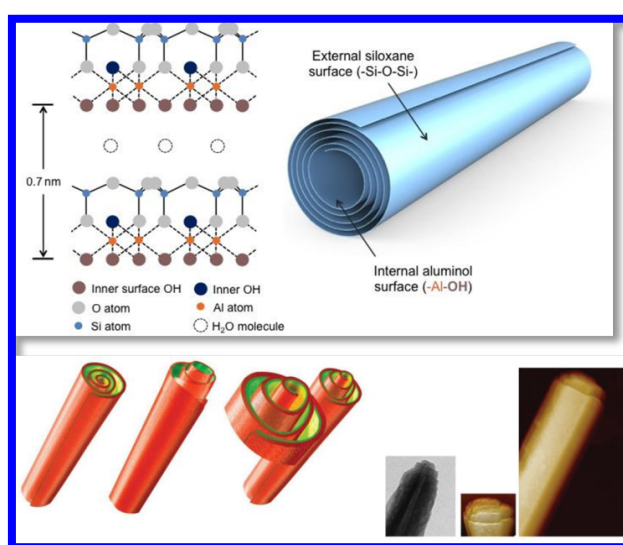
Fig. I.11: Schematic illustration of the crystalline structure and rolling of Hal nanotubes **[31]**.

Hal nanotubes shape and properties make them very versatile in terms of drug-carrying and drug release applications, including proteins as active substances. These substances can also be loaded into the lumen of Hal under vacuum or using immersion techniques. Research activities in this area have gained significant attention in recent years due to the obvious benefits of Hal, such as elongated shape, empty lumen, and ease of mixing with a broad range of polymers, biocompatibility, and availability. In addition, Hal has an easily modifiable surface

chemistry that differs at the external surface and inner pores (exterior silica, interior aluminum oxide), allowing for the selective modification of each of them. The peculiarity to have different charges between the inner and outer side of the Hal nanotubes, among other things, allows for the selective loading of negatively charged molecules into their lumen [28,31].
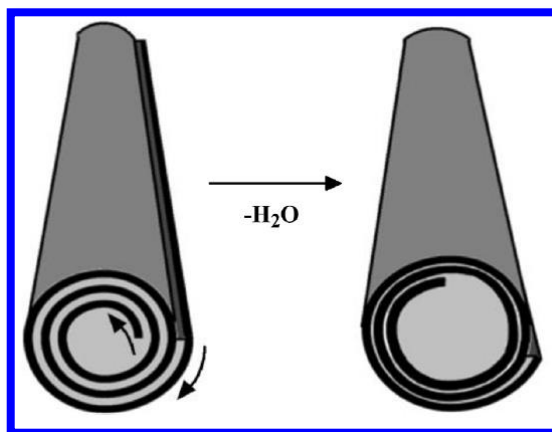
Fig. I.12: Scheme of the Hal dehydration ($10 \rightarrow 7$ Å) [31].

The hydrated Hal presents a water layer between two adjacent sheets of about 12% mass that evaporates under heating, giving a compression of the layers and a smaller packing spacing. The interlayer water molecules can be classified into two types: The first type is that the whole water molecules are embedded into the ditrigonal cavities in the basal oxygen site with two different main orientations and forming hydrogen bonds with the basal oxygen. Instead, in the second one, the associated molecules are located at different levels in the interlayer space with an ice-like configuration, forming a network of hydrogen bonds with each other and/or with inner surface hydroxyls with a high degree of mobility. Because of the different stability, the whole water is lost more slowly than the associated one. The dehydration process gives an intermediate state between a fully hydrated and fully dehydrated form with two intermediate states of Hal nanotubes (8.6 Å) and Hal nanotubes (7.9 Å). The dehydration process is irreversible and can have different effects on Hal nanotubes, such as reducing particle size, unfolding, or changes in diameter [32].

I.3.4 Halloysite biocompatibility and toxicity

Cytocompatibility is the prerequisite for the Hal usage in drug release applications. A large amount of work has been done in this area, showing the biocompatible nature of Hal. In *vitro* cell toxicity tests on breast cancer and human dermal fibroblast cells showed that raw Hal is 50 times less toxic than sodium chloride. Penetration and accumulation of Hal within MCF-

7 and HeLa cell membranes did not prevent their proliferation, as evidenced by confocal microscopy research. Hal nanotubes were found safe for a soil nematode model type (*Caenorhabditis elegans*) at concentrations below 1 mg/mL **[33]**.

Figure I.13 summarizes the toxicity threshold values reported for various Hal nanotubes administration routes in murine models. Oral administration of a high dosage of Hal nanotubes (50 mg per kg body weight daily for 30 days) was found to be toxic and the mice suffered from pulmonary fibrosis, possibly caused by the accumulation of aluminum in their lungs. Yet, no adverse effects were observed at a lower dosage of 5 mg/kg body weight. These results are further confirmed in a recent study of the same group, showing normal mice weight gain at a lower oral dose of 5 mg /kg body for 30 days, whereas, a higher dose (50 mg/kg) incited a reversible inflammation of the small intestine. Although the intravenous administration of non-biodegradable substances is usually ruled out, Wu et al. reported that the tail intravenous injection of short Hal nanotubes (<200 nm) to mice (5 mg/kg body weight twice a week for 3 weeks) had no significant effect on the mice body weight after 21 days **[33]**.
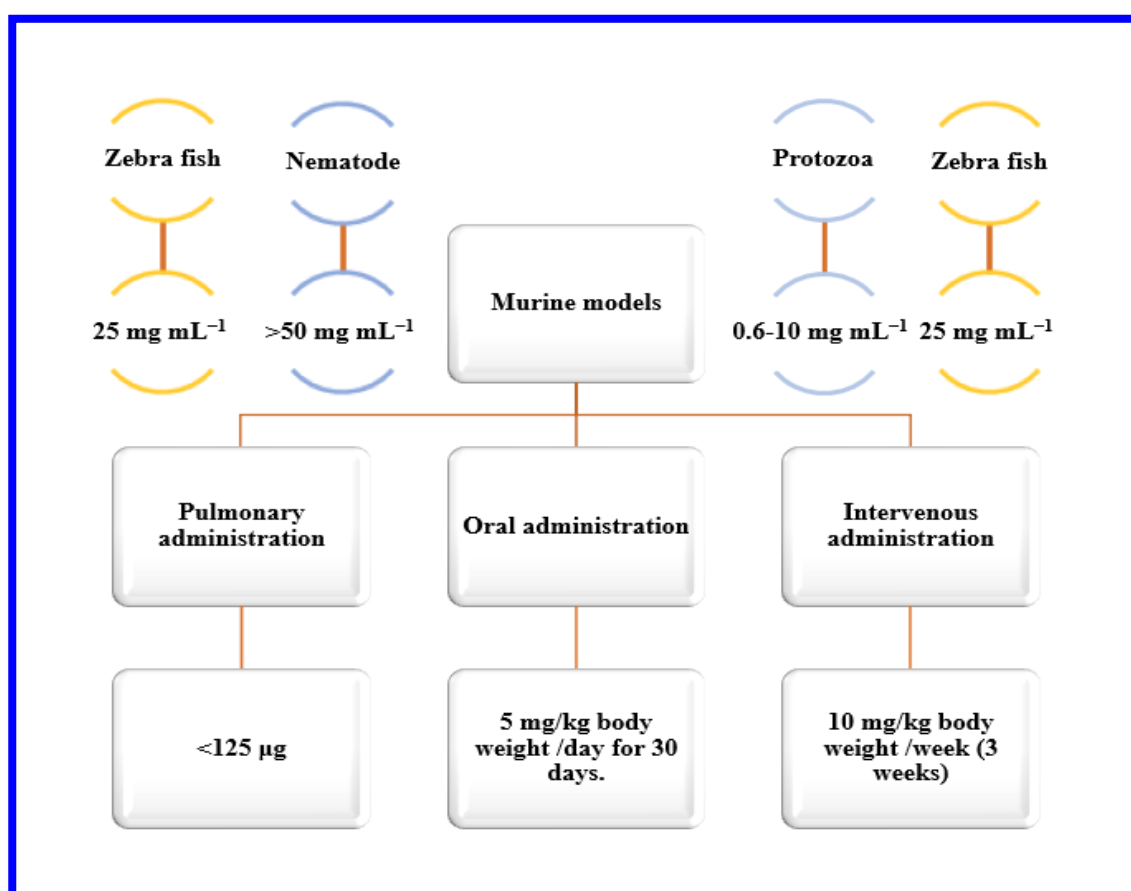
Fig. I.13: Toxicity threshold values of Hal nanotubes **[33]**.

The cytotoxicity of Hal nanotubes towards cancer and human cells was thoroughly studied; (**Table I.3**), revealing intracellular accumulation of Hal and a concentration dependent effect. Yet, Hal nanotubes concentration in these studies was limited to less than<1000 µg mL^{-1}, and at 1000 µg mL^{-1} a clear cytotoxic effect was observed. Moreover, we should highlight that as Hal nanotubes are of a natural resource, their characteristics (namely, dimensions and impurities) are highly origin-dependent and thus, any toxicity study should be coupled with a thorough physiochemical characterization **[33]**.

Hal nanotubes toxicity was also studied in few non-mammalian animal models, including *Caenorhabditis elegans* (C. elegans), *Paramecium caudatum* and (*Danio Rerio* (zebrafish). For the latter, high concentrations (25 mg mL^{-1}) were not found to exert adverse effects on embryos and even promoted their hatchability **[33]**.

To summarize, the origin of Hal nanotubes toxicity stems from the combination of their nanoscale diameter, high aspect ratio, and chemical composition. Yet, the role of each of these properties is contextual and depends on the target organism, tissue and cell type. In addition, from a regulatory point of view, although kaolin clay minerals are affirmed as generally recognized as safe (GRAS) for indirect food contact by the United States Food and Drug Administration (FDA), Hal as a nanomaterial is not yet approved for any sort of intake. Indeed, work is underway to regularize Hal nanotubes for future applications **[33]**.

Table I.3: Cytotoxicity of Hal nanotubes towards cancer and human cells **[33]**.

Cell type	Time frame	Toxicity threshold
A549 (human lung epithelial cancer cell line)	24 h	No toxic effect up to 100 µg mL^{-1}
HUVECs (umbilical vein endothelial cells) MCF-7 (human breast adenocarcinoma)	72 h	No significant apoptosis up to 200 µg mL^{-1}
HeLa (human cervical carcinoma) MCF-7 cell line	24–72 h	No toxic effect up to 75 µg mL^{-1}
Caco-2/HT29-MTX (intestinal cell co-culture cells)	6 h	No cytotoxic effect up to 100 µg mL^{-1}
		Proteomics suggests processes of cell growth and cell injury
HepG2 (hepatocellular carcinoma) HCT116 (colorectal carcinoma cells)	24–72 h	Cytostatic at 500 µg mL^{-1}
		Cytotoxic at 1000 µg mL^{-1}
Human peripheral blood lymphocytes	24–72 h	Cytogenetic toxicity at only 1000 µg mL^{-1} by blocking the passage of cel

I.3.5 Halloysite for drug loading

Hal nanotubes were successfully loaded with diverse types of active agents, including pharmaceutical agents. Hal entraps molecules in three different ways:

- Adsorption to the external and internal walls of the tubes,
- Loading into lumen,
- Intercalation of substance between layers.

The most important of these three ways is the lumen loading, as this provides the highest loading capability. Most likely, the real distribution of the drug molecules occurs both in the inner lumen along with the outer surfaces, but drug bound to the outer surface may be easily washed out. In addition, the wall interlayer spaces can also be filled with the small drug molecules. These approaches may be combined providing initial drug burst release from the outer surface of the tubes followed by slower leakage of the drug from tubes interior lumens [34,35].

Lumens of the Hal nanotubes correspond to about 20% of the total volume, which makes them suitable for loading with about 10–15% of the active agents within internal lumens. There are some studies claiming even higher loading efficiency, which could be associated with the external adsorption of active agents along with the lumen loading. A general procedure for the Hal lumen loading, shown in **Fig. I.14**, is as follows. Hal is mixed as a dry powder with a saturated (highly concentrated) solution of the active agent. Solvents are generally chosen among liquids of low viscosity that dissolve active agents and wet Hal walls. Water, acetone and ethanol are among the most commonly used solvents. The dispersion of Hal is stirred and transferred to a jar for evacuation with a vacuum pump, which then should be kept in à vacuum for 10–30 min, allowing air bubbles to be removed from Hal pores, which is generally indicated by a slight fizzing of the solution. Once the vacuum is broken, the solution enters the lumen. This is generally repeated three to four times to increase the loading efficiency. After loading, the Hal nanotubes are washed to remove unloaded substance and dried [34,35].
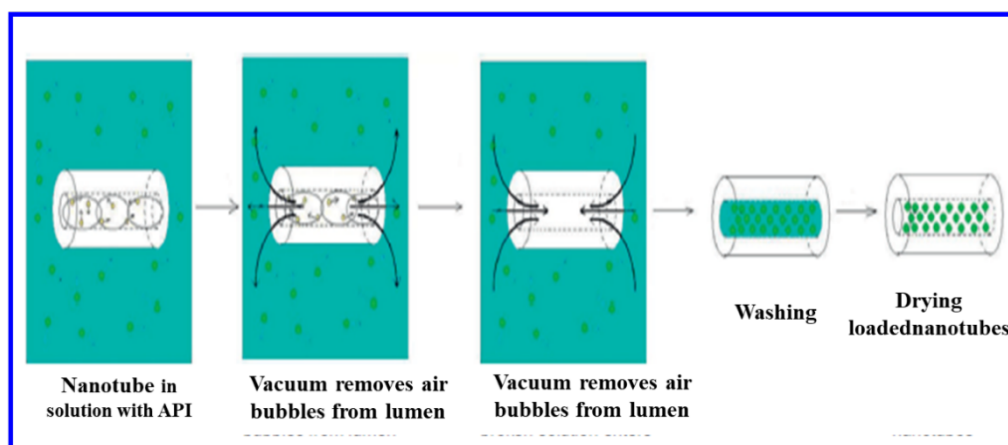
Fig. I.14: Scheme showing steps in Hal nanotubes drug loading with API **[31]**.

The concentration gradient of the active agent between Hal pores and external solution is important for reaching maximum loading efficiency. This is usually maintained by drying of the solution while loading (generally in a moderate vacuum). On the other hand, drying speed has to be relevant to the diffusion rate of the active agents. Therefore, volatile and low-viscosity solvents like acetone or ethanol are preferable in order to increase the process speed. Water is generally used for medicines, enzymes and proteins when the stability of the active agent in the above mentioned solvents is questionable, or in cases when solubility is not sufficiently high. Some of the active agents successfully encapsulated by Hal nanotubes are presented in **Table I.4**. The loading efficiency of the unmodified Hal nanotubes lies in the range of 5–13% for low-molecular-mass substances and about 1–2% for enzymes **[34,35]**.

Table I.4: Drug encapsulated and released by halloysite nanotubes **[31]**.

API	Loading effeciency	Drug release
Verapamil HCl	9.32%	99% (pH 1.2) 12 h
		77% (pH 4.5) 12h
		100% (pH 6.8) 8h
Flurbiprofen	8.741%	11% (pH 1.2) 12 h
		35% (pH 4.5) 12h
		100% (pH 6.8) 12h
Atenolol	8.59%	76% (pH 1.2) 12 h
		99% (pH 4.5) 12h
		67% (pH 6.8) 12h
Furosemide	8%	35% (pH 1.2) 12 h

		34% (pH 4.5) 12h
		32% (pH 6.8) 12h
Dexamethasone	5%	80% (pH 7.4) 5h
Ibuprofen	12%	92% (pH 7.4) 25h
Salicylic acid	3.5%	99% (pH 7.4) 25h
Diclofenac	3.5%	99% (pH 7.4) 10h
5-flurouracil	40%	98% (pH 7.4) 6h
Paclitaxel	7%	100% (pH 7.4) 24h
Nifedipine	5	30.4% (pH 7.4) 5h

Loading of the API into Hal nanotubes is determined by Si–OH and Al–OH functional groups existing on their external and internal surfaces, respectively. Deprotonation of silanol groups is responsible for the negative net charge of Hal nanotubes at pH above 3. Consequently, the anionic nature of the external Hal nanotubes surface enables it to interact with cationic compounds, while aluminol groups located on the internal lumen surface carry positive charge and support the loading of anionic molecules. In addition to electrostatics, interaction of molecules and their assemblies with Hal nanotubes might involve hydrogen binding, van der Waals and other specific interactions. However, Hal provides complete isolation of the loaded active agent from surrounding media, which is critical for both sustained and controlled release [33].

I.3.6 Halloysite for drug release

Hal nanotubes can show several advantages in drug delivery applications due to its submicron size and 10 nm pores that are suitably fitted for loading medicines with a broad molecular range. The lumen loading provides controlled release. Release from Hal lumen typically lasts from several hours to days, depending on molecular mass, structure, and solubility of the active agent in the release medium. Several drugs have been effectively encapsulated within Hal lumens. These show that release kinetics takes place in two stages: namely, fast desorption of externally adsorbed molecules and slow drug release from nanotubes lumen. Desorption rate increased in acidic and buffer solutions as compared to purified water, which was ascribed to the increased ionic strength of the release medium. Encapsulation in Hal reduced drug-release time by more than 20 times [31].

I.3.7 Halloysite nanotubes modifications

Enhanced loading efficiency and extended-release rates are possible through the chemical modification and surface functionalization of Hal nanotubes. These methods not only help in improving loading and release behaviour, but also allow for rendering nanotubes lumen suitable for each specific target active agent to obtain maximum chemical stability, such as favourable pH within nanotubes lumen for acid or base-sensitive actives. Reactive aluminol groups within Hal lumen and nanotube edges, as well as OH groups at nanotube defects, are useful for surface functionalization, while negative surface charge allows for building polyelectrolyte shells. Selective etching aluminum of oxide from Hal lumens allowed for increasing the pore volume and loading efficiency **[36]**.

I.3.7.1 Selective lumen etching Halloysite nanotubes

Selective etching of aluminum oxide from Hal lumens is one of the most effective ways to improve loading efficiency. Aluminum oxide from Hal lumen can be leached with strong acids like sulphuric and hydrochloric acids. External silicone dioxide sheets remain intact with acid treatment due to the high acid stability of SiO_2. However, care must be taken not to collapse the tubular structure by over etching the aluminum oxide. Typically, up to 40% removal of aluminum oxide is possible without degrading the tubular structure **[37]**.

Such treatment allowed for increasing the lumen diameter from the original 15 nm up to 25 nm, resulting in 30–40% loading efficiency. This is higher than most of the siliceous templates, and comparable with polymeric capsules. Al–OH sheet removal from the nanotubes takes place in three steps:

- Diffusion of hydrogen ions of the acid into the inner lumen,
- Chemical reaction with an octahedral (Al–OH) sheet on the tube inner wall,
- Transport of the reaction products out of the lumen.

In the Al-OH sheet removal process, significant changes in Hal morphology was observed, holes in the Hal walls, free silica nanoparticles were formed, and finally, the tubular Hal transformed into porous silica nanorods **[37]**.

I.3.7.2 Formation of halloysite nanotubes release stoppers

Hal nanotubes allow synthesising release stoppers to control the release rate of the loaded active agents. Caps were formed on Hal tube endings by melting and crystallisation of
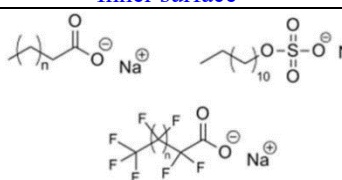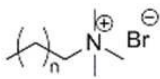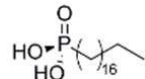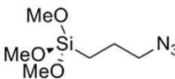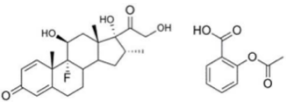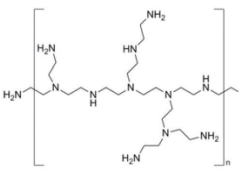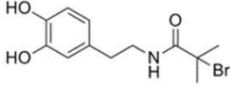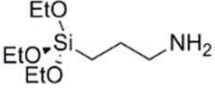
starch at the Hal tube ends at 200°C. This method was not very practical due to the requirement of such a high temperature. Other methods include formation of thin films, precipitate, or both at the tube endings by the interaction of triazole and imidazole derivatives with transition metal salts and polyelectrolyte complexation through layer-by-layer nano-assembly [31].
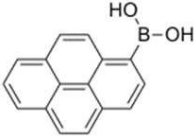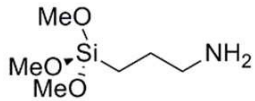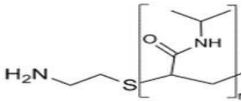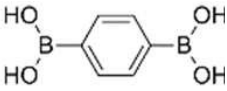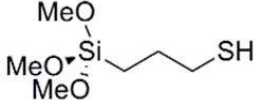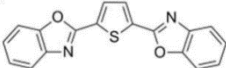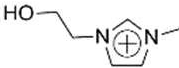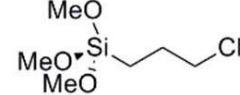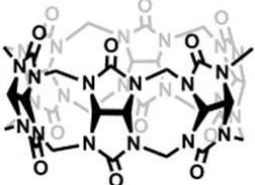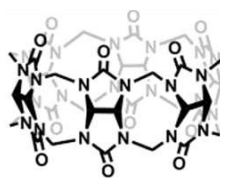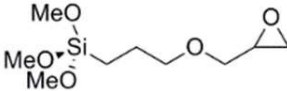
I.3.7.3 Surface functionalisation of halloysite nanotubes for controlled release

Hal nanotubes external surfaces and inner lumen walls have been modified with a variety of surface-modifying agents through interaction with reactive aluminol and silanol groups (at surface defects) and ionic and hydrogen bonding. These surface modifiers include silane-coupling agents, alkyl phosphonic acid derivatives, quaternary ammonium salts, fatty acid salts, polymers, ionic liquids and various metal and metal oxide nanoparticles [31].

The most common purpose of Hal surface modification involves its compatibilization with polymer matrices to obtain enhanced dispersion. However, surface modification was also shown to increase the loading and release properties of active agents. **Table I.5** summarizes the different methods adopted for the Hal surfaces functionalization.

Table I.5: Overview of the different Hal functionalization methods [38].

Supramolecular Functionalization		Covalent Modification	
Inner surface	Outer surface	Inner surface	Outer surface
Anionic surfactants	Alkyltrimethyl ammonium bromide (Cationic surfactants)	Octadecyl posphonic acid	3-azidopropyltrimethoxysilane
Dexamethasone,Aspirin (Drugs)	Poly(ethyleneimine)	2-bromo-N- [2-(3,4-dihydroxyphenyl) ethyl]-isobutyryl amide31	3-aminopropyltriethoxysilane

Lipase, Glucose, oxidase, Albumin Laccase and Pepsin (ph<pI), Binase	Lipase, Glucose oxidase, Albumin Laccase and Pepsin (ph>pI)	HO–B–OH (structure)	MeO Si propyl-NH₂ (structure)
Co-enzymes or enzymes	Enzymes	1-pyrenyl boronic acid	3- aminomethyltrimethoxy-silane
Pectin, Alginate	(PNIPAAM structure)	(1,4-phenylenebisdiboronic acid structure)	(mercaptopropyl silane structure)
Anionic polymers	Amine terminated PNIPAAM (cationic polymers)	1,4-phenylenebisdiboronic acid	3- Mercaptopropyl-trimethoxysilane
(Carbon dots image)	(benzoxazolyl thiophene structure)	(imidazolium structure)	(chloropropyl silane structure)
Carbon dots	2,5-bis(2-benzoxazolyl) thiophene	3-(2-hydroxyethyl)-1-methylimidazolium	3-chloropropyl-trimethoxysilane
(Cucurbituril structure)	(Cucurbituril structure)		(glicidoxypropyl silane structure)
Cucurbituril	Cucurbituril		γ−glicidoxypropyltrimethoxysilane

I.4 Multicavity halloysite–amphiphilic cyclodextrin hybrids

The novel hybrid based on Hal nanotubes covalently linked to amphiphilic-cyclodextrin units results are promising as a carrier for biologically active molecules, since it possesses two cavities (Fig. I.15), the Hal lumen and the hydrophobic cyclodextrin cavity. The advantages of multifunctional nanocarriers with the presence of two cavities, indeed, offers the remarkable possibility for a simultaneous encapsulation of one or more drug molecules with different physicochemical properties, followed by a different path release in agreement with the cavity that interacts with drugs. Therefore, the introduction of cyclodextrin moieties was crucial to obtain a high drug load and a sustained release within time [39].
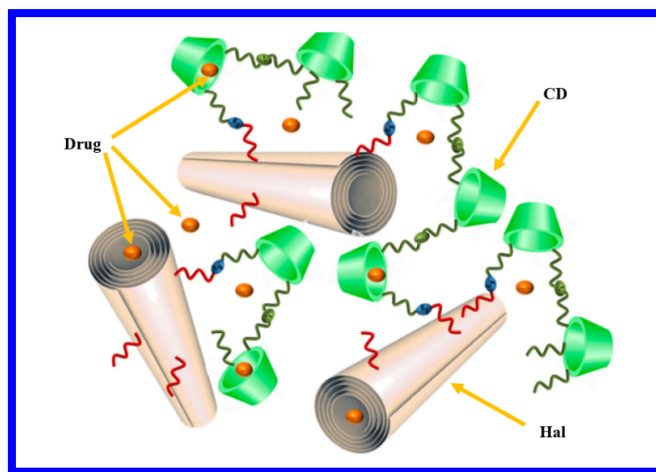
Fig. I.15: Scheme showing Halloysite nanotubes -amphiphilic cyclodextrin drug carrier **[39].**

I.5. References

[1] N.S. Dey, S. Majumdar, M.E.B. Rao, Multiparticulate Drug Delivery Systems for Controlled Release, Tropical Journal of Pharmaceutical Research. 7 (2008) 1067–1075. https://doi.org/10.4314/tjpr.v7i3.14692.

[2] B.G. Katzung, S.B. Masters, A.J. Trevor, Basic & clinical pharmacology, McGraw-Hill Medical ; McGraw-Hill [distributor, New York; London, 2012. http://accessmedicine.mhmedical.com/book.aspx?bookid=388 (accessed November 13, 2021).

[3] G. Tiwari, R. Tiwari, B. Sriwastawa, L. Bhati, S. Pandey, P. Pandey, S.K. Bannerjee, Drug delivery systems: An updated review, Int J Pharm Investig. 2 (2012) 2–11. https://doi.org/10.4103/2230-973X.96920.

[4] Giuseppe Lazzara, S. Riela, R.F. Fakhrullin, Clay-based drug-delivery systems: what does the future hold?, Therapeutic Delivery. 8 (2017) 633–646. https://doi.org/10.4155/tde-2017-0041.

[5] S. Wang, R. Liu, Y. Fu, W.J. Kao, Release mechanisms and applications of drug delivery systems for extended-release, Expert Opinion on Drug Delivery. 17 (2020) 1289–1304. https://doi.org/10.1080/17425247.2020.1788541.

[6] G. Crini, Review: A History of Cyclodextrins, Chem. Rev. 114 (2014) 10940–10975. https://doi.org/10.1021/cr500081p.

[7] J. Conceicao, O. Adeoye, H.M. Cabral-Marques, J.M.S. Lobo, Cyclodextrins as Drug Carriers in Pharmaceutical Technology: The State of the Art, Current Pharmaceutical Design. 24 (2018) 1405–1433. https://doi.org/10.2174/1381612824666171218125431.

[8] L. Leclercq, Interactions between cyclodextrins and cellular components: Towards greener medical applications?, Beilstein J. Org. Chem. 12 (2016) 2644–2662. https://doi.org/10.3762/bjoc.12.261.

[9] A. Biwer, G. Antranikian, E. Heinzle, Enzymatic production of cyclodextrins, Appl Microbiol Biotechnol. 59 (2002) 609–617. https://doi.org/10.1007/s00253-002-1057-x.

[10] D. Duchěne, D. Wouessidjewe, Pharmaceutical Uses of Cyclodextrins and Derivatives, Drug Development and Industrial Pharmacy. 16 (1990) 2487–2499. https://doi.org/10.3109/03639049009058543.

[11] S.P. Jones, D.J.W. Grant, J. Hadgraft, G.D. Parr, Cyclodextrins in the pharmaceutical sciences. I: Preparation, structure and properties of cyclodextrins and cyclodextrin inclusion compounds, Acta Pharm. Technol. 30 (1984) 213–223.

[12] W. Saenger, Cyclodextrin Inclusion Compounds in Research and Industry, Angewandte Chemie International Edition in English. 19 (1980) 344–362. https://doi.org/10.1002/anie.198003441.

[13] B. Kost, M. Brzeziński, M. Socka, M. Baśko, T. Biela, Biocompatible Polymers Combined with Cyclodextrins: Fascinating Materials for Drug Delivery Applications, Molecules. 25 (2020) 3404. https://doi.org/10.3390/molecules25153404.

[14] J. Szejtli, Past, present and futute of cyclodextrin research, Pure and Applied Chemistry. 76 (2004) 1825–1845. https://doi.org/10.1351/pac200476101825.

[15] I.M. Mavridis, K. Yannakopoulou, Anionic cyclodextrins as versatile hosts for pharmaceutical nanotechnology: Synthesis, drug delivery, enantioselectivity, contrast agents for MRI, International Journal of Pharmaceutics. 492 (2015) 275–290. https://doi.org/10.1016/j.ijpharm.2015.06.004.

[16] E.M.M. Del Valle, Cyclodextrins and their uses: a review, Process Biochemistry. 39 (2004) 1033–1046. https://doi.org/10.1016/S0032-9592(03)00258-9.

[17] L. Liu, Q.-X. Guo, The Driving Forces in the Inclusion Complexation of Cyclodextrins, Journal of Inclusion Phenomena. 42 (2002) 1–14. https://doi.org/10.1023/A:1014520830813.

[18] N. Sharma, A. Baldi, Exploring versatile applications of cyclodextrins: an overview, Drug Delivery. 23 (2016) 729–747. https://doi.org/10.3109/10717544.2014.938839.

[19] T. Loftsson, Cyclodextrins and the Biopharmaceutics Classification System of Drugs, Journal of Inclusion Phenomena. 44 (2002) 63–67. https://doi.org/10.1023/A:1023088423667.

[20] M.E. Brewster, T. Loftsson, Cyclodextrins as pharmaceutical solubilizers, Advanced Drug Delivery Reviews. 59 (2007) 645–666. https://doi.org/10.1016/j.addr.2007.05.012.

[21] M. Kfoury, D. Landy, S. Fourmentin, Characterization of Cyclodextrin/Volatile Inclusion Complexes: A Review, Molecules. 23 (2018) E1204. https://doi.org/10.3390/molecules23051204.

[22] V.J. Stella, V.M. Rao, E.A. Zannou, V. Zia, Mechanisms of drug release from cyclodextrin complexes, Advanced Drug Delivery Reviews. 36 (1999) 3–16. https://doi.org/10.1016/S0169-409X(98)00052-0.

[23] D. Cagno, M. Pio, The Potential of Cyclodextrins as Novel Active Pharmaceutical Ingredients: A Short Overview, Molecules. 22 (2017) 1. https://doi.org/10.3390/molecules22010001.

[24] S.S. Jambhekar, P. Breen, Cyclodextrins in pharmaceutical formulations I: structure and physicochemical properties, formation of complexes, and types of complex, Drug Discov Today. 21 (2016) 356–362. https://doi.org/10.1016/j.drudis.2015.11.017.

[25] P. Mura, Analytical techniques for characterization of cyclodextrin complexes in aqueous solution: A review, Journal of Pharmaceutical and Biomedical Analysis. 101 (2014) 238–250. https://doi.org/10.1016/j.jpba.2014.02.022.

[26] P. Mura, Analytical techniques for characterization of cyclodextrin complexes in the solid state: A review, Journal of Pharmaceutical and Biomedical Analysis. 113 (2015) 226–238. https://doi.org/10.1016/j.jpba.2015.01.058.

[27] F. Bergaya, G. Lagaly, Chapter 1 General Introduction: Clays, Clay Minerals, and Clay Science, in: F. Bergaya, B.K.G. Theng, G. Lagaly (Eds.), Developments in Clay Science, Elsevier, 2006: pp. 1–18. https://doi.org/10.1016/S1572-4352(05)01001-9.

[28] M. Khalid, R. Walvekar, M.R. Ketabchi, H. Siddiqui, M.E. Hoque, Rubber/Nanoclay Composites: Towards Advanced Functional Materials, in: M. Jawaid, A. el K. Qaiss, R. Bouhfid (Eds.), Nanoclay Reinforced Polymer Composites: Nanocomposites and Bionanocomposites, Springer, Singapore, 2016: pp. 209–224. https://doi.org/10.1007/978-981-10-1953-1_9.

[29] Synthesis, Characterization, and Study, of New Nanostructured Materials, (n.d.). https://iris.unipa.it/handle/10447/264743#.YZDrP2DMI2w (accessed November 14, 2021).

[30] G.J. Churchman, R.M. Carr, The Definition and Nomenclature of Halloysites, Clays Clay Miner. 23 (1975) 382–388. https://doi.org/10.1346/CCMN.1975.0230510.

[31] E. Abdullayev, Y. Lvov, Chapter 22 - Halloysite for Controllable Loading and Release, in: P. Yuan, A. Thill, F. Bergaya (Eds.), Developments in Clay Science, Elsevier, 2016: pp. 554–605. https://doi.org/10.1016/B978-0-08-100293-3.00022-4.

[32] H. Yang, Y. Zhang, J. Ouyang, Chapter 4 - Physicochemical Properties of Halloysite, in: P. Yuan, A. Thill, F. Bergaya (Eds.), Developments in Clay Science, Elsevier, 2016: pp. 67–91. https://doi.org/10.1016/B978-0-08-100293-3.00004-2.

[33] O.P. Setter, E. Segal, Halloysite nanotubes – the nano-bio interface, Nanoscale. 12 (2020) 23444–23460. https://doi.org/10.1039/D0NR06820A.

[34] Y. Lvov, E. Abdullayev, Functional polymer–clay nanotube composites with sustained release of chemical agents, Progress in Polymer Science. 38 (2013) 1690–1719. https://doi.org/10.1016/j.progpolymsci.2013.05.009.

[35] L. Lisuzzo, G. Cavallaro, P. Pasbakhsh, S. Milioto, G. Lazzara, Why does vacuum drive to the loading of halloysite nanotubes? The key role of water confinement, Journal of Colloid and Interface Science. 547 (2019) 361–369. https://doi.org/10.1016/j.jcis.2019.04.012.

[36] E. Abdullayev, A. Joshi, W. Wei, Y. Zhao, Y. Lvov, Enlargement of Halloysite Clay Nanotube Lumen by Selective Etching of Aluminum Oxide, ACS Nano. 6 (2012) 7216–7226. https://doi.org/10.1021/nn302328x.

[37] Y. Lvov, W. Wang, L. Zhang, R. Fakhrullin, Halloysite Clay Nanotubes for Loading and Sustained Release of Functional Compounds, Advanced Materials. 28 (2016) 1227–1250. https://doi.org/10.1002/adma.201502341.

[38] M. Massaro, G. Cavallaro, C.G. Colletti, G. Lazzara, S. Milioto, R. Noto, S. Riela, Chemical modification of halloysite nanotubes for controlled loading and release, J. Mater. Chem. B. 6 (2018) 3415–3433. https://doi.org/10.1039/C8TB00543E.

[39] M. Massaro, S. Riela, Organo-Clay Nanomaterials Based on Halloysite and Cyclodextrin as Carriers for Polyphenolic Compounds, Journal of Functional Biomaterials. 9 (2018) 61. https://doi.org/10.3390/jfb9040061.

Chapter II
Solubility enhancement of active pharmaceutical ingredients

II.1 Introduction

Solubility and dissolution are the core concepts of any physical and chemical research including that related to the biopharmaceutical and pharmacokinetic considerations in the treatment with any medicines. As a result, recently more than 40% of new chemical compounds developed for the purpose to be used in the treatment of specific diseases fail before entering into the drug developmental process because of their non-optimal biopharmaceutical properties especially their poor solubility in biological media that is necessary for good bioavailability **[1]**.

In general, solubility is the property of a solid, liquid or gaseous chemical substance called solute to dissolve in a solid, liquid, or gaseous solvent to form a homogeneous solution. The solubility of a substance fundamentally depends on the solvent used, the physical form of solute as well as on the temperature and the pressure. The extent of solubility of a substance in a specific solvent is measured as the saturation concentration where adding more solute does not increase its concentration in the solution **[2]**.

The Solubility occurs under dynamic equilibrium, which means that solubility results from the simultaneous and opposing processes of dissolution and phase joining (e.g., precipitation of solids). Solubility equilibrium occurs when the two processes proceed at equal rates. Solubilization may be defined as the preparation of a thermodynamically stable solution of a substance that is normally insoluble or very slightly soluble in a solvent, by the introduction of one or more amphiphilic components. The approximate solubilities of Pharmacopoeial and National Formulary substances are indicated by the descriptive terms in the **table II.1 [3]**.

Table II.1: Terms of solubility.

Descriptive term	Parts of solvent required for 1 part of solute
Very soluble	Less than 1
Freely soluble	From 1 to 10
Soluble	From 10 to 30
Sparingly soluble	From 30 to 100
Slightly soluble	From 100 to 1000
Very slightly soluble	From 1000 to 10000
Practically insoluble, or insoluble	10000 and over

The bioavailability of a drug is mainly dependent on its solubility in the gastrointestinal tract and its permeability through the intestinal wall. Therefore, a drug with poor aqueous

solubility will typically exhibit a low dissolution rate and consequently limited absorption. And to overcome this problem there are several methodologies that can be engaged to improve its bioavailability as well as its therapeutic efficacy.

II.2. Solubilization Techniques to Improve Bioavailability

The three major approaches in overcoming the bioavailability problem are:

✓ The Pharmaceutical approach, which involves modification of formulation, manufacturing process or the physicochemical properties of the drug without changing the chemical structure.

✓ The chemical approach in which the pharmacokinetics of the drug is altered by modifying its chemical structure. This approach includes salt formation or incorporating polar or ionizable groups in the main drug structure resulting in the formation of prodrug.

✓ The biologic approach where by the route of drug administration may be changed such as changing from oral to parenteral route.

The attempts, whether optimizing the formulation, manufacturing process or physicochemical properties of the drug, are mainly aimed to enhance dissolution rate, as it is the major rate-limiting step in the absorption of most drugs. Increasing the effective surface of the drugs will be discussed briefly as it follows: **[2]**.

✓ **Solid dispersions**

Chiou and Riegelman defined the term solid dispersion as "a dispersion of one or more active ingredients in an inert carrier or matrix in solid state, prepared by the melting (fusion), solvent, or melting-solvent method". Dispersions obtained through the fusion process are often called melts, and those obtained by the solvent method are frequently referred to as co-precipitates or co-evaporates. The matrix can be either crystalline or amorphous. The drug can be dispersed molecularly, as an amorphous particle (clusters) or as crystalline particles.

When dissolving the solid dispersions, it is believed that the drug substance is released as small discrete units owing to a fast dissolution of the easily soluble carrier. If the drug solubility in the carrier is high enough, a so-called solid solution can be obtained. Sekiguchi and Obi first introduced the concept of using solid dispersions to improve bioavailability of poorly water-soluble drugs in 1961. They demonstrated that the eutectic of sulfathiazole and the physiologically inert water-soluble carrier urea exhibited higher absorption and excretion after oral administration than sulfathiazole alone **[4]**.

✓ **Particles size reduction**

Micronization occurs as an increase of surface area which enhances the dissolution rate and bioavailability of drug. The particle size after micronization is 1-10 microns. This method involves spray drying and attrition methods. For many new chemical entities with very low solubility, oral bioavailability enhancement by micronization is not sufficient because micronized product has the tendency to agglomerate, which leads to decrease effective surface area for dissolution. Recently research is focusing on the use of particles of nanoscale. Various nanonization strategies have emerged to increase the dissolution rates and bioavailability of numerous drugs that are poorly soluble in water. Nanonization broadly refers to the study and use of materials and structures at the nanoscale level of approximately 100 nm or less. Nanonization can result in improved drug solubility and pharmacokinetics, and it might also decrease systemic side-effects. There are different techniques used for nanonization of drug including Wet milling, Homogenization, Emulsification-solvent evaporation technique, Pear milling, Spray drying etc… **[5]**.

✓ **Use of Surfactants**

A conventional approach to solubilise a poorly soluble substance is to reduce the interfacial tension between the surface of solute and solvent for better wetting solvation interaction. A wide variety of surfactants like tweens, spans, polyoxyethylene glycerides, polyoxyethylene stearates and synthetic block copolymers etc…, are very successful as excipients and carriers for dissolution enhancement **[6]**.

✓ **pH Adjustment**:

Adjustment of micro-environmental pH to modify the ionization behavior is the simplest and most commonly used method to increase the water solubility behavior. Therefore, in accordance with the pH partition hypothesis and Handerson- Hesselbatch equation, ionization of a compound is dependent on the pH of media and pKa of drug. Also the change in the ionic compound can result to in–situ salt formation. Therefore, this salt formation is infeasible for unionized compounds. The formed salts may also converse to respective acid or base forms in gastrointestinal tract(GIT) **[2]**.

✓ **Manipulation of solid state**

From the stability and bioavailability aspects, the crystalline form of a drug is of pharmaceutical importance. Polymorphism (existence of a drug substance in multiple

crystalline forms) can cause variations in melting point, density, stability and drug solubility as these properties depend on the escaping tendency of the molecules from a particular crystalline structure. As a rule, for a drug that has the highest order of crystallinity is the most stable form, exists in multiple polymorphic forms, i.e. with the least amount of free energy, and, consequently, possesses the highest melting point and the least solubility. By controlling the crystallization process, amorphous or meta stable forms of drugs possessing high free energy can be forcibly created. They offer the advantage of higher solubility but suffer from stability issues unless intense stabilizers to inhibit crystal growth are incorporated in the formulation [7].

A typical example for this is a high-profile case involving polymorphism was withdrawal of ritonavir (Norvir®) capsules from the market in 1998 because a less soluble (and consequently less bioavailable) polymorph was identified two years after the product was approved and marketed, causing a decrease in bioavailability of the drug. This incident sensitized the pharmaceutical industry to the critical importance of polymorphism and encouraged the inclusion of polymorph screening as a routine component of preformulation studies [8].

✓ **Self- emulsifying drug delivery system**

A self-emulsifying or self-micro emulsifying system is the concept of in-situ formation of emulsion in the gastrointestinal tract. It is defined as the mixture of oil, surfactant, co-surfactant, one or more hydrophilic solvents and drug which forms a transparent isotropic solution in the absence of external phase (water) and forms fine oil/water emulsions or micro-emulsions spontaneously upon dilution by the aqueous phase in the GIT and is used for improving lipophillic drug dissolution and absorption. So the ease of emulsification could be associated with the ease of water penetrating into the various liquids crystalline or gel phases formed on the surface of the droplet. The large quantity of surfactant in self-emulsifying formulations (30- 60%) irritates GIT. Most self emulsifying systems are limited to administration in lipid filled soft or hard-shelled gelatin capsules due to the liquid nature of the product. Interaction between the capsule shell and the emulsion should be considered so as to prevent the hygroscopic contents from dehydrating or migrating into the capsule shell.

✓ **Complexation**

This is the most widely method to enhance the water solubility and increase the stability of hydrophobic drugs. Cyclodextrins (CDs) interact with poorly-water soluble compounds to

increase their apparent solubility. The most prominent mechanism by which this solubilization occurs is inclusion complex formation in which the guest and host molecules are in dynamic equilibrium with the complex. There are certain forces which play an important role for the complexation and which are attributed to:

- The exclusion of high energy water from the cavity,
- The release of ring strain particularly in the case of CD,
- Hydrogen and hydrophobic bindings,
- Van der Waals interactions.

In fact, no covalent bonds are formed or ruptured during the drug/CD complex formation and in aqueous solutions, the complexes are readily dissociated.

The world's first CD-containing pharmaceutical product, prostaglandin E2/β-CD (sublingual tablets), was marketed in Japan in 1976. Twelve years later, the first European CD-based pharmaceutical product, piroxicam/β-CD (Brexin® tablets), was marketed and in 1997, the first US-approved product, itraconazole/2-hydroxypropyl-β-CD oral solution (Sporanox®) was introduced. Worldwide, 35 different drugs are currently marketed as solid or solution-based CD complex formulations (**Table II.2**). In these pharmaceutical products, CDs are mainly used as complexing agents to increase the aqueous solubility of poorly water-soluble drugs, to increase their bioavailability and stability **[9]**.

Table II.2: Some marketed pharmaceutical products containing cyclodextrins **[9]**

Drug/cyclodextrin	Trade name	Formulation	Company (country)
α-Cyclodextrin			
Alprostadil	Caverject Dual	i.v. solution	Pfizer (Europe)
Cefotiam-hexetilHCl	Pansporin T	Tablet	Takeda (Japan)
OP-1206	Opalmon	Tablet	Ono (Japan)
PGE1	Prostavastin	Parenteral solutions	Ono (Japan); Schwarz (Europe)
β-Cyclodextrin (βCD)			
BenexateHCl	Ulgut, Lonmiel	Capsule	Teikoku (Japan); Shionogi (Japan)
Cephalosporin	Meiact	Tablet	Meiji Seika (Japan)
Cetirzine	Cetrizin	Chewing	Losan Pharma

		Tablet	(Germany)
Chlordiazepoxide	Transillium	Tablet	Gador (Argentina)
Dexamethasone	Glymesason	Ointment, tablet	Fujinaga (Japan)
Dextromethorphan	Rynathisol		Synthelabo (Europe)
Diphenhydramin and chlortheophyllin	Stada- Travel	Chewing tablet	Stada (Europe)
Iodine	Mena-Gargle	Solution	Kyushin (Japan)
Meloxicam	Mobitil	Tablet and suppository	Medical Union Pharmaceuticals (Egypt)
Nicotine	Nicorette	Sublingual tablets	Pfizer (Europe)
Nimesulide	Nimedex	Tablets	Novartis (Europe)
Nitroglycerin	Nitropen	Sublingual tablet	Nihon Kayaku (Japan)
Omeprazole	Ombeta	tablet	Betafarm (Europe)
PGE2	Prostarmon E	Sublingual tablet	Ono (Japan)
Piroxicam	Brexin, Flogene, Cicladon	Tablet, suppository	Chiesi (Europe);Aché (Brazil) Aché (Brazil)
Tiaprofenicacid	Surgamyl	Tablet	Roussel-Maestrelli (Europe)
2-Hydroxypropyl-β-cyclodextrin			
Cisapride	Propulsid	Suppository	Janssen (Europe)
Hydrocortisone	Dexocort	Solution	Actavis (Europe)
Indomethacin	Indocid	Eye drop solution	Chauvin (Europe)
Itraconazole	Sporanox	Oral and i.v. olutions	Janssen (Europe, USA)
Mitomycin	MitoExtra, Mitozytrex	i.v. infusion	Novartis (Europe)

Sulfobutylether β-cyclodextrin sodium salt (SBEβCD)			
Aripiprazole	Abilify	im solution	Bristol-Myers Squibb (USA); Otsuka Pharm. (USA)
Maropitant	Cerenia	Parenteral Solution	Pfizer Animal Health (USA)
Voriconazole	Vfend	i.v. solution	Pfizer (USA, Europe, Japan)
Ziprasidone mesylate	Geodon, Zeldox	im solution	Pfizer (USA, Europe)
Randomly methylated β-cyclodextrin			
17β-Estradiol	Aerodiol	Nasal Spray	Servier (Europe)
Cloramphenicol	Clorocil	Eye drop Solution	Oftalder (Europe)
Insulin		Nasal spray	Spain
2-Hydroxypropyl-γ-cyclodextrin			
Diclofenac sodium salt	Voltaren	Eye drop Solution	Novartis (Europe)
Tc-99 Teoboroxime	CardioTec	i.v. solution	Bracco (USA)

II.3. References

[1] S. Stegemann, F. Leveiller, D. Franchi, H. de Jong, H. Lindén, When poor solubility becomes an issue: From early stage to proof of concept, European Journal of Pharmaceutical Sciences. 31 (2007) 249–261. https://doi.org/10.1016/j.ejps.2007.05.110.

[2] A. Mahapatra, V. Patil, R. Patil, Solubility Enhancement of Poorly soluble Drugs by using Novel Techniques : A Comprehensive Review, International Journal of PharmTech Research. 13 (2020) 80–93. https://doi.org/10.20902/IJPTR.2019.130211.

[3] K.T. Savjani, A.K. Gajjar, J.K. Savjani, Drug Solubility: Importance and Enhancement Techniques, ISRN Pharmaceutics. 2012 (2012) 1–10. https://doi.org/10.5402/2012/195727.

[4] T. Vasconcelos, B. Sarmento, P. Costa, Solid dispersions as strategy to improve oral bioavailability of poor water soluble drugs, Drug Discovery Today. 12 (2007) 1068–1075. https://doi.org/10.1016/j.drudis.2007.09.005.

[5] J. Leleux, R.O. Williams, Recent advancements in mechanical reduction methods: particulate systems, Drug Development and Industrial Pharmacy. 40 (2014) 289–300. https://doi.org/10.3109/03639045.2013.828217.

[6] K. Kawakami, N. Oda, K. Miyoshi, T. Funaki, Y. Ida, Solubilization behavior of a poorly soluble drug under combined use of surfactants and cosolvents, European Journal of Pharmaceutical Sciences. 28 (2006) 7–14. https://doi.org/10.1016/j.ejps.2005.11.012.

[7] R. Censi, P. Di Martino, Polymorph Impact on the Bioavailability and Stability of Poorly Soluble Drugs, Molecules. 20 (2015) 18759–18776. https://doi.org/10.3390/molecules201018759.

[8] A. Chaudhary, U. Nagaich, N. Gulati, V.K. Sharma, R.L. Khosa, Enhancement of solubilization and bioavailability of poorly soluble drugs by physical and chemical modifications: A recent review, (2012) 32–67.

[9] M.E. Brewster, T. Loftsson, Cyclodextrins as pharmaceutical solubilizers, Advanced Drug Delivery Reviews. 59 (2007) 645–666. https://doi.org/10.1016/j.addr.2007.05.012.

II.3. Publication: Solubility Enhancement of Mefenamic Acid by Inclusion Complex with β-Cyclodextrin: In Silico Modelling, Formulation, Characterization and In *Vitro* Studies

ABSTRACT

The aim of the present study was to prepare and characterize inclusion complexes of a low water-soluble drug, mefenamic acid (MA), with -cyclodextrin (β-CD). Firstly, the phase solubility diagram of MA in β-CD was drawn from 0 to 21 x10^{-3} M of β-CD concentration. A job's plot experiment was used to determine the stoichiometry of the MA:β-CD complex (2:1). The stability of this complex was confirmed by molecular modeling simulation. Three methods, namely solvent co-evaporation (CE), kneading (KN) and physical mixture (PM), were used to prepare the (2:1) MA:β-CD complexes. All complexes were fully characterized. The drug dissolution tests were established in simulated liquid gastric and the MA water solubility at pH 1.2 from complexes was significantly improved. The mechanism of MA released from the β-CD complexes was illustrated through a mathematical treatment. Finally, two *in vitro* experiments confirmed the interest to use a (2:1) MA:β-CD complex.

Keywords: mefenamic acid; β-cyclodextrin inclusion complexes; solubility; characterization; *in vitro* studies.

Introduction

The access of drugs to biological targets is essential for producing biological effect(s) in living organisms. Globally physicochemical properties and ADME (Absorption, Distribution, Metabolism, Elimination) parameters of a drug substance are essential to ensure the accessibility to target(s)[1]. Moreover, only the free part of the drug substance diffuses in tissues from the blood and then can access to the active binding site of the desired target. Among all parameters to control for a successful treatment, an acceptable level of drug substance solubility is required. In the case of low solubility drug substances, inclusion complexes can be an interesting alternative to facilitate drug administration. Additionally, *in silico* methods were also developed to optimize this approach and then improve the use of low solubility drug substances[2].

Actually, many efficiency issues caused by low solubility drugs are highlighted in recent works, for instance, according to Kalepu *et al.*[3], more than 80% of drugs are sold as tablets, in which 40% have low water solubility. The same study illustrates more serious situation concerning R&D drug candidates, in which 90% could fail due to low solubility problems.

However, to improve the dissolution profile of poorly soluble drugs, various approaches are proposed such as particle size reduction[4], drug dispersion in carrier[5], modification of crystal habit[6], use of surfactant[7], self-emulsifying formulations[8] and complexation with cyclodextrins (CDs)[9]. This later is one of the frontier techniques that are employed in almost 56 pharmaceutical products [10], where these oligomers obtained from enzymatic degradation of starch are exploited. These cycloamyloses are composed of D-glucopyranoside units linked by α(1→4)-glycosidic bonds. Typical native CDs involve six, seven or eight glucose units, denoted α-, β- and γ-CDs, respectively. CDs belong to cage molecules family due to their hydrophobic cavity structure, and hydrophilic outer surface. Indeed, the most significant characteristic of CDs is their ability to form inclusion complexes with various molecules through host-guest interactions[11,12]. These inclusion complexes have been revealed to improve the apparent stability, solubility, dissolution rate, and bioavailability of the guest bioactive molecules[13-16]. Among various cyclodextrins, β-CD is the most frequently used in pharmaceutical excipient due to its wide availability, low cost, excellent biocompatibility, preferred cavity dimension and wide regulatory acceptance[17]. We note that two other naturally occurring cyclodextrins (α- and γ-CDs) are more cost effective compared to β-CD. Moreover, a recent report provided that a β-CD derivative known as the hydroxypropyl-β-CD, even though it has a better solubility than β-CD, is undesirable due to its toxicity[18].

Mefenamic acid (MA), 2-[(2,3-dimethylphenyl)amino]benzoic acid, was selected as a drug model for our study. It is a potent non-steroidal anti-inflammatory drug (NSAID) of the anthranilic acid class. Moreover, it shows preferential inhibition of cyclo-oxygenase-2 (COX-2), inhibiting the action of prostaglandin synthetase[19-21]. Furthermore, MA is approved by the food and drug administration (FDA) in 1965[22]. Due to its low solubility in water and high permeability in the gastrointestinal (GI) tract, MA is classified in the biopharmaceutics classification system (BCS) as class II drug[23,24]. It is widely indicated for inflammatory diseases and also as an analgesic for the treatment of musculoskeletal, osteoarthritis, rheumatoid arthritis, menstrual symptoms and headach[19,25-27]. Furthermore, MA has been shown to have therapeutic effects in neurodegenerative disease (e.g. Alzheimer disease)[28]. In addition, MA, like other anti-inflammatory drugs, is emerging as new chemopreventive agents against cancer[29]. However, due to its low water solubility, high doses (250 mg or 500 mg twice a day administration) and side effects, mainly related to gastrointestinal adverse consequences, including bleeding, ulceration or colitis lesions and steatorrhea, which can be sometimes fatal, made the use of MA limited[19,30-32].

On the other hand, the study of the formation and the stability of guest-host complexes can be assisted by molecular modeling methods, like docking and quantum mechanics (QM), which may mimic the behavior of inclusion systems at the atomistic level[33]. These modeling methods have been playing an important role in providing 3D simulation structures in order to understand the mechanism of CDs inclusion formation systems, assist the formulation design and simplify the formulation screening procedures followed by the delivery studies[34,35].

In the present study, we investigated the complexation of MA with β–CD for improving both solubility and dissolution rate. We were motivated by the fact that β-CD complexation enhanced the solubility of other acidic NSAIDs, including tolfenamic acid[36], niflumic acid[37], indomethacin[38] and ketoprofen[39]. Some (1:1) complexes' types of MA:β-CD have been previously developed by authors using precipitation[40,41].or kneading[42] methods In these studies, the molar concentration of β-CD did not exceed 10 mM, the solubility phase diagram was A_L type and so the proposed MA:β-CD complex ratio was 1 to 1 of MA and β-CD. In these previous works[40-42], the Job's plot method was not also investigated. In this work, phase solubility diagram of MA using increasingly high β-CD concentrations (from 0 to 21 x10^{-3} M), job's plot and molecular modeling simulation were associated to study MA:β-CD inclusion complexes. Three methods were carried out using solvent co-evaporation (CE), kneading (KN) and physical mixture (PM) for the preparation of these complexes. Then selective physicochemical determinations based on Fourier-transform infrared spectroscopy (FTIR), differential scanning calorimetry (DSC), X-ray powder diffraction (XRPD) and scanning electron microscopy (SEM) were performed to characterize all complexes. *In vitro* aqueous solubility and dissolution rate profiles of the complexes were also performed. Finally, the resulting inclusion complexes were evaluated *in vitro* using protein denaturation and membrane stabilization methods.

Materials and methods

Chemicals

Mefenamic acid (MA), $C_{15}H_{15}NO_2$, molecular weight: 241.29 g/mol was a gift from SALEM Laboratories El-Eulma, Algeria. β-Cyclodextrin (β-CD) [$C_{42}H_{70}O_{35}$, molecular weight: 1134.00 g/mol] was purchased from Sigma–Aldrich, USA. All other chemicals used were of analytical grades. All reagents were used as received.

Phase solubility studies

The phase solubility investigation was performed in order to find out the apparent stability constant (K) that represents the affinity of MA to the β-CD in water. For this, studies were carried out in triplicate following the Higuchi and Connors method[43]. Samples were prepared by mixing in sealed 50 mL Erlenmeyer flasks excess of MA (4.11×10^{-3} g) with 30 mL of aqueous solutions containing successively increasing concentrations (0, 3, 6, 9, 12, 15, 18 and 21) $\times 10^{-3}$ M of β-CD. Then, the solutions were kept under agitation for 5 days at 25 °C. The solutions were then filtered through 0.45 μm filter pore size and the filtrate was assayed for drug concentration by ultra-violet spectroscopy (SHIMADZU UV-1800) at 282 nm where no absorbance due to the β-CD was observed.

Determination of complex stoichiometry

The continuous variation method otherwise known as Job's plot was used to ascertain the stoichiometry for MA:β-CD complexation[16]. The experiments were carried out in duplicate by mixing two equimolar solutions (10^{-3} M) of β-CD (in water) and MA (in ethanol) in different molar ratio from 0-1 without variation of the final volume. After seven days of stirring at 25 °C, solutions were analyzed by ultra-violet spectroscopy at 282 nm. The absorbency changes ($\Delta Abs = Abs-Abs_0$) of MA in the presence (Abs) and absence (Abs_0) of β-CD were plotted versus R, where $R = [MA]/([MA]+[\beta\text{-CD}])$. The Job's plot showed a maximum at a specific molar ratio indicating the stoichiometry of the complexes.

In silico molecular modeling studies

The molecular docking simulations were carried out in the Glide (grid-based ligand docking) application implemented in the Maestro 9.3 software (Schrodinger, LLC, New York, 2012)[44,45]. The crystal structure of β-CD was obtained from the Protein Data Bank PDB (ID: 1BFN). For adding the missing hydrogen, we used the Protein Preparation Wizard. Then, β-CD crystal structure was separated from α-amylase, followed by energy minimization at RMSD convergence (0.30 Å with OPLS_2005 as a force field). In order to obtain possible MA conformers, the MA structure was designed using the Maestro structure builder and optimized with LigPrep tool. To get the appropriate ionization state, LigPrep was run with the Epik option set (version 3.7, Schrödinger) to generate a possible state at pH 7.4. Finally, the geometrical optimization was performed using the OPLS-2005 force field. The "Generate Grid" sub-application of the Glide tool allowed the generation of the grid by selecting the entire β-CD structure as the receiving site to locate the coordinates of the center of the targeted receptor

cavity. Then, the generated grid was configured as the MA docking receiver using the "extra-precision" (XP) flexible docking method, from the Glide tool. The binding affinity "ΔG" was calculated using the Prime MM-GBSA module (version 4.5, Schrödinger). The same work was done for the 2:1 MA:β-CD inclusion complex.

On the other hand, in order to study the MA:β-CD interaction in the 1:2 complex, the β-CD structure was extracted from the crystallographic parameters. This last was provided by the structural database system of the Cambridge Crystallographic Data Center and optimized by minimizing energy to get the most stable state. These results were obtained using the Materials Studio 6.0 software[44]. Then, the resulting structure was simulated in the Maestro 9.3 software[45]. We followed the same steps for the first two conjugates.

Once the docking search was completed, the conformations were applied with the best binding energy. The complex inclusion structures resulted from the docking calculations were computed with Materials Studio using the Dmol3 method with the database (B3LYP / 6-31g (d, p))[46,47]. This last allowed the computation of the descriptor dielectric energy (solvation). We noted that this last provided more information on the solubility of inclusion complexes between MA with β-CD.

Preparation of solid complexes

Solvent co-evaporation method

MA (0.723 g, 0.003 mol) and β-CD (1.700 g, 0.0015 mol) were dissolved in ethanol (100 mL) and distilled water (100 mL), respectively. Then, these solutions were mixed in a flask and stirred at 600 rpm for 2 h at 50 °C. The obtained clear solution was evaporated at 45 °C using a rotary evaporator (BÜCHI, rotavapor R-215) rolling at 100 rpm. The solid residue was further dried at 50 °C for 24 h and stored in bottles and kept in the refrigerator.

Kneading method

The calculated and exactly weighed amounts of β-CD (1.700 g) were wetted with a minimum water volume (1 mL) and mixed in a ceramic mortar to get a homogeneous paste. Then, MA (0.723 g) was progressively introduced; while kneading, a small quantity of ammonium hydroxide (0.5 mL of 35% solution), was added to assist the dissolution of MA. The mixture was then blended for 1 h. During this process, a small quantity (1.5 mL) of water was added to the mixture in order to keep an appropriate consistency. The paste was dried in an oven at 50 °C for 24 h then grinded into a fine powder and stored in bottles and kept in the refrigerator.

Physical mixture

The physical mixture was prepared by simple blending for 30 min in a ceramic mortar pulverized powders (0.723 g of MA and 1.700 g of β-CD). The resulting material was sieved and stored in bottles and kept in the refrigerator.

Percentage practical yield

The percentage practical yield helps in selecting the appropriate method of preparation and it gives efficiency of any method. So, these were determined to know about percent practical yield (PY) from the following equation[10]:

$$\text{PY (\%)} = \frac{\text{Practical Mass (Inclusion complex)}}{\text{Theoretical Mass (Drug + Carrier)}} *100 \qquad (1)$$

Percentage drug extract

The percentage drug extract was determined by extraction of the MA from the complexes and its amount measured using a SHIMADZU-1800 UV-visible spectrophotometer. Therefore, a known amount of each complex (25 mg) was placed in a 25 mL volumetric flask, and ethanol was then added. The mixture was shaken for 5 h. Hence, the MA extractable amount was obtained through its UV photometric analysis (λ_{max}=282 nm) using the standard curve of a bunch of known MA concentrations. The extractions were carried out in triplicate and the drug content in the complex was obtained using the following equation:

$$\text{MA content in complex (\%)} = \left[\frac{\text{mass of MA extracted}}{\text{mass of complex}}\right] *100 \qquad (2)$$

Characterization of the ingredients and their complexes

Fourier transform infrared spectroscopy

The infrared spectra of MA, β-CD and their complexes were recorded with an IRAffinity-1S SHIMADZU spectrometer using the potassium bromide (KBr) disk technique (1% w/w of the samples in KBr). The scanning range was 4500-500 cm^{-1}.

Differential scanning calorimetry

DSC analysis for MA, β-CD and their inclusion complexes were carried out using a DSC SETARAM instrument. The samples (10-15 mg) were placed in sealed aluminum pans under nitrogen flow (20 mL/min) at a scanning rate of 10 °C/min, over the temperature range of 25 to 340 °C.

X-Ray powder diffraction

X-ray powder diffractograms of individual components and those of complex systems were obtained on a PAN analytical kind X' PERTPRO diffractometer. The radiation used was generated by a copper filter, wavelength 1.54 Å at 40 kV and 30 mA. Glass slide was covered with the sample to be analyzed and scanned over a 2θ range from 10 to 40 degrees, using a scan rate of 1 degree per min and a step scan of 0.02 degree.

Nuclear magnetic resonance (NMR)

The ^{1}H and ^{13}C NMR spectra were recorded at 100 MHz and 400 MHz, respectively, on a Brücker DRX 400 spectrometer in DMSO-d_6. Chemical shifts are expressed in ppm (δ) downfield from internal tetramethylsilane (TMS). The NMR spectra were processed and analyzed by MestReNova software 11.02.18153.

Scanning electron microscopy

The surface morphology of MA, β-CD and binary complexes were captured by a scanning electron microscope (JSM 6360A, JOEL) equipped with secondary electron detector. The samples were examined at an accelerating voltage of 10 kV.

In vitro drug release test

The *in vitro* release test of pure MA and its complexes was performed using the United States Pharmacopeia Paddle Method (Apparatus II) on Heidolph RZR 2041. Samples equivalent to 50 mg of MA were placed into a hard gelatin capsule, and then soaked into 900 mL of the simulated gastric medium (0.1 M HCl, pH 1.2) for 2 h. The dissolution media was maintained at 37 ± 0.5 °C and stirred at 100 rpm. At suitable time intervals, 3 mL of the dissolution medium was withdrawn, using a syringe, and filtered through 0.45 μm nylon disc filter. Then, an equivalent volume offresh medium was added in order to maintain sinking conditions. The MA content was determined at 282 nm using an UV-VIS spectrophotometer. We noted that each dissolution test was carried out in duplicate. The kinetics of the MA released from inclusion complexes

were determined by fitting the release profiles to the first order (3), Korsmeyer–Peppas (4) and Higuchi (5) theoretical models:

$$F_t = 1 - \exp(-K_1 \cdot t) \tag{3}$$

where F_t is the fraction of drug dissolved in time t and K_1 is the first order release constant.

$$\frac{M_t}{M_i} = K_{KP} t^n \tag{4}$$

where M_t/M_i is the fractional release of drug into the dissolution media, Mt is the release accumulation and M_i is the initial drug amount. K_{KP} is the Korsmeyer–Peppas constant, and n is the release exponent indicative of the drug release mechanism.

$$F_t = K_H t^{0.5} + a \tag{5}$$

where K_H is the Higuchi release constant and a is a constant characterizing the initial drug release.

Then, the selection of the best fit model is based on the regression coefficient value R^2 which should be close to one[48].

In Vitro anti-inflammatory activities

Protein denaturation method

The binary inclusion complexes were evaluated by using inhibition of bovine serum albumin (BSA) denaturation technique. This assay was done according to Muzushima and Kobayashi[49] with minor modification. The MA drug and tested complexes (1 mL) containing 100 µg/mL of drug were mixed with 1 mL of 1% w/v BSA in phosphate buffer (pH 6.4) and incubated at 27 ± 1 °C for 15 min. The denaturation was induced by maintaining the reaction mixture at 75 ± 1 °C in a water bath for 10 min. Then, after cooling, the turbidity was measured at 660 nm (λ_{max} bovine serum albumin). The percentage inhibition of denaturation can be calculated from reference where no drug was added. We noted that each experiment was done in triplicate and an average value was taken.

Membrane stabilization method

The binary inclusion complexes were assayed by using human red blood cell (HRBC) membrane stabilization method[50]. For this, fresh whole human blood (10 mL) was collected and transferred to heparinized centrifuge tubes. The tubes were centrifuged for 5 min at 3000

rpm, and washed three times with an equal volume of normal saline. The volume of the blood was measured and reconstituted as a 40% v/v suspension with isotonic buffer solution (10 mM sodium phosphate buffer pH 7.4). The activity of MA from all drug-carrier systems was analyzed at the concentration of 100 µg/mL with the same dose of standard drug of pure MA.

Results and discussion

Phase solubility studies

The phase solubility diagram of MA with various concentrations of β-CD in water is illustrated in Figure 1. β-CD formed A_N-subtype complexes with MA. We note that the MA solubility increases with the β-CD concentration. However, a negative curvature occurs at higher cyclodextrin concentrations (15-21 mM). This fact implies that β-CD is proportionally less effective at higher concentrations. This may occur as a result of the change of physical properties of the solution at higher β-CD concentration and the self-association of free β-CD molecules, thereby reducing the available concentration of free β-CD[15]. It should be noted that other researchers[40,42] revealed A_L type phase solubility of MA:β-CD where the used β-CD concentration was lower than 10^{-2} M.

Equation	y = a + b*x
Intercept	7.97851E-5 ± 3.64631E-6
Slope	0.01813 ± 4.962E-4
Adj. R-Square	0.99701
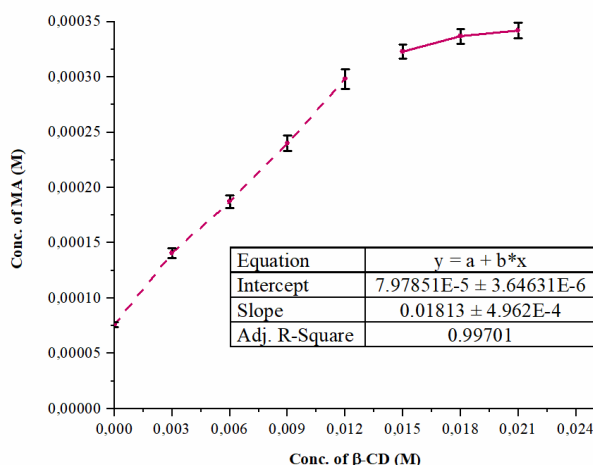
Figure 1. Phase solubility diagram of MA with β-CD in aqueous solution at 25 °C.

Similar phase solubility profiles (curvature shapes) have been found by Pradines*et al.*[51], for an antiparasitic drug complexed with a methyl-β-CD in water. Buchanan *et al.*[52] also reported other similar profiles for some antifungal drugs and hydroxybutenyl-β-CD in some buffer. Equivalently, Rudrangi *et al.*[53] presented similar profile for indomethacin and methyl-β-CD in phosphate buffer (pH 7.4) solution.

Determination of complex stoichiometry

Job's continuous variation technique is applied to determine the stoichiometry by utilizing the absorption spectral data. As seen in Figure 2, the maximum ΔAbs variation was observed at mole fraction value of 0.67. This suggests a 2:1 stochiometric ratio of MA:β-CD.
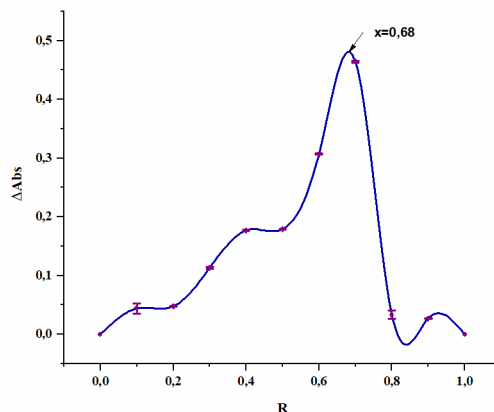
Figure 2. Continuous variation plot (Job's plot) for the complexation of MA/β-CD (25 °C).

In silico molecular modeling studies

The molecular docking was used to explore the interaction of β-CD with MA in the inclusion complexes with different stoichiometry. The best pose of MA in inclusion complexes is illustrated in Figure 3.

The binding affinity expressed in the form of Glide docking score for the MA with β-CD is given by -7.890 kcal.mol^{-1} for IC1. Actually, this value is comparable to that of the IC3 (-7.375 kcal.mol^{-1}), where the IC2 presents the lowest docking score. However, for complex stabilization, contribution (from Van der Waals interaction) it takes higher value compared to lipophilic and hydrogen bonding interactions for all binary complexes (Table 1).

On the other hand, Prime MM-GBSA module (version 4.5, Schrödinger) is used to obtain the binding affinity (ΔG) that represents the free energy change upon formation of the complex, in comparison to total individual energy based on change in the solvent accessible surface area. It allows the stability determination of binary inclusion complexes[54]. In fact, the ΔG binding energy exhibits a similar behavior as that of docking score calculations. The IC1 is the most stable complex (-37.698 kcal.mol^{-1}) followed by IC3 (-35.995 kcal.mol^{-1}) and IC2 (-21.468 kcal.mol^{-1}) (Table 1). The introduction of a second MA molecule in the primary complex will enhance the stability (Figure 3). This is a consequence of further hydrogen electrostatic

interaction and improved filling of the β-CD cavity. Figure 4 provides more details about the hydrophobic and hydrophilic surface areas of MA, β-CD and the binary complexes. From Figure 4, the hydrophilic area increases upon formation of IC1. In fact, higher polar surface area of the supramolecular inclusion complex improved the MA solubility.

Table 1. Prime MM-GBSA calculations.

ΔG values in Kcal.mol⁻¹						
Ratio (MA:β-CD)	Bind[a]	Docking score	Glide Lipo[b]	Glide vdw[c]	Glide Hbond[d]	Glide Emodel
1:1 (IC2)	-21.468	-4.575	-2.179	-21.123	-0.042	-26.612
2:1 (IC1)	-37.698	-7.890	-3.454	-37.387	-0.202	-46.262
1:2 (IC3)	-35.995	-7.375	-3.139	-28.990	-0.160	-50.976

[a] free energy of binding (Glide energy); [b] free energy of binding from lipophilic binding; [c] free energy of binding from van der Waals energy; [d] free energy of binding from hydrogen bonding.
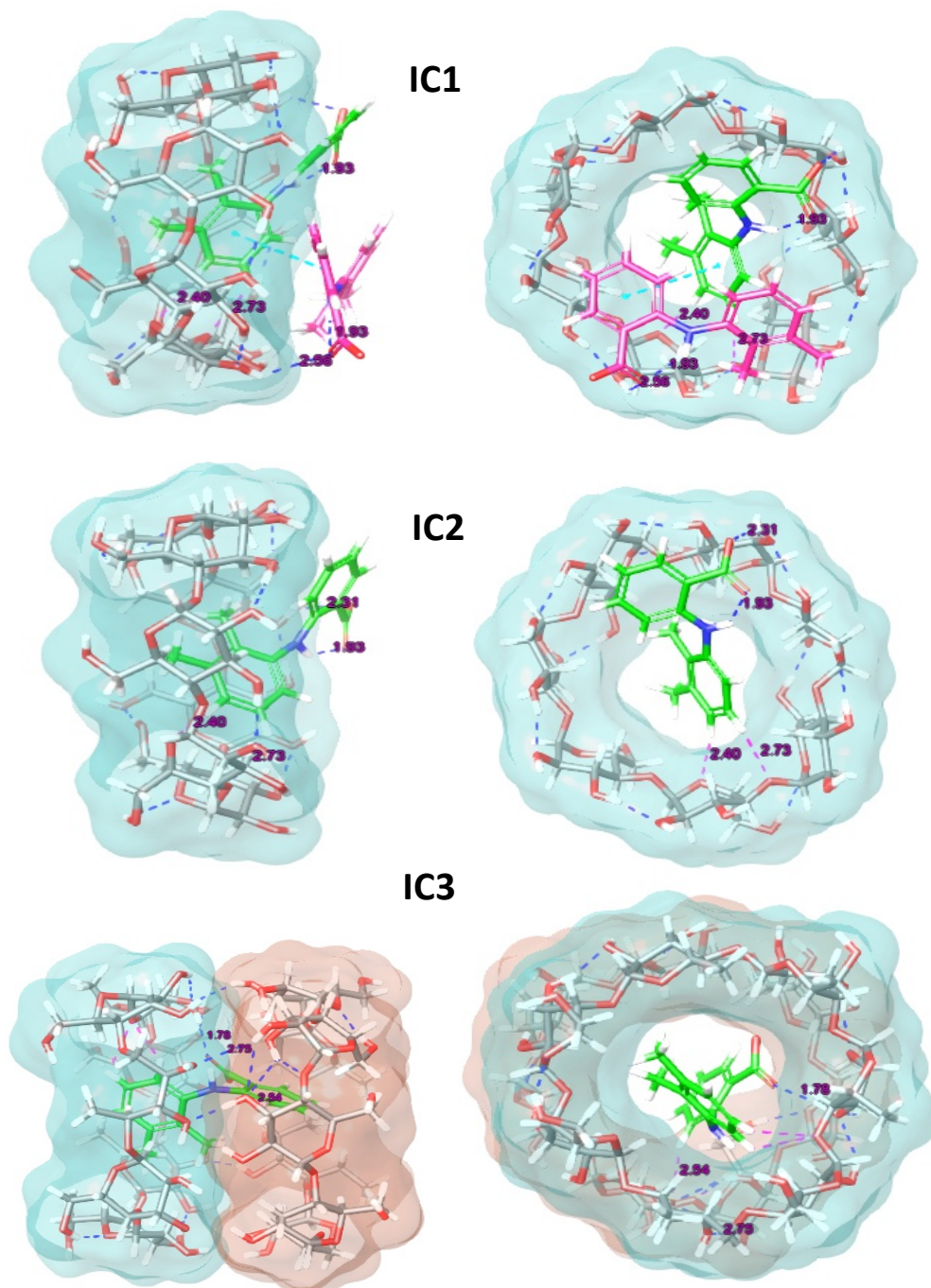
Figure 3. Docking binding poses of the inclusion complexes.
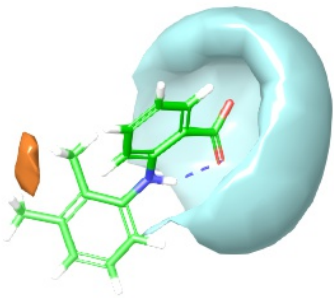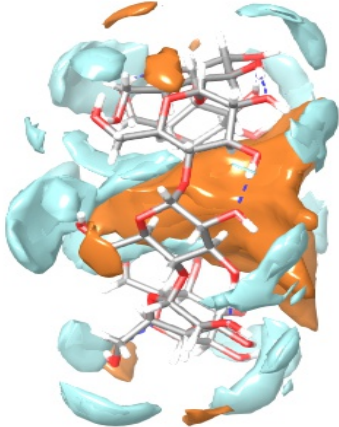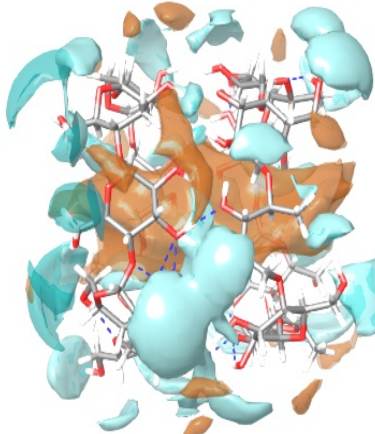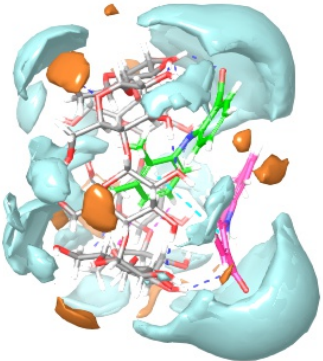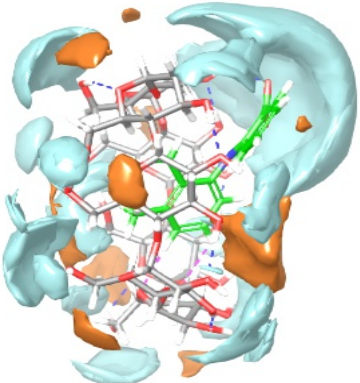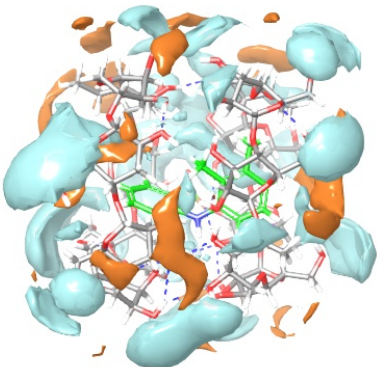
MA	β-CD	2 β-CD
Phobic: 5.28 CÅ	Phobic: 264.75 CÅ	Phobic: 371.46 CÅ
Phillic: 234.95 CÅ	Phillic: 348.44 CÅ	Phillic: 610.83 CÅ

IC1	IC2	IC3
Phobic: 89.80 CÅ	Phobic: 137.09 CÅ	Phobic: 552.53 CÅ
Phillic: 692.85 CÅ	Phillic: 525.07 CÅ	Phillic: 727.03 CÅ
Dielectric (solvation) energy:	Dielectric (solvation) energy:	Dielectric (solvation) energy:
-118.67 Kcal.mol^{-1}	-115.89 Kcal.mol^{-1}	-162.72 Kcal.mol^{-1}

Figure 4. Hydrophobic (brown) and hydrophilic (blue) surface area of MA, β-CD and MA:β-CD binary inclusion complexes (CÅ, cubic Angströms).

Preparation of solid complexes and loading

According to job's plot results and the molecular docking observations, (2:1) MA:β-CD complexes were prepared by PM, KN and CE methods. In all inclusion methods, loss of complexes' mass was observed. In CE method, large volumes of organic solvent and longer

process causes more important loss of mass. So an experimental yield was calculated (Table 2) for CE. With an experimental loading value of 28.96%, the ratio of (2:1) MA:β-CD complex was also confirmed.

Table 2. Experimental yield and drug extraction from CE binary inclusion complex.

Complex	CE
Experimental yield (%)	90.1
Drug content (%)	28.96 ± 0.39
Experimental molar ratio MA:β-CD	1.9:1

Characterization of the ingredients and their complexes

Fourier-transform infrared spectroscopy

In order to examine the plausible interactions between MA and β-CD in the solid state, the IR spectra of binary complexes are compared to those of the physical mixture and the pure drug (Figure 5). The spectrum of the pure drug shows many intense and sharp absorption bands. Actually, this fact is due to the different functional groups existing in MA, for instance: the aromatic ring, the carboxylic group, the amine group and the methyl group. In fact, the band recorded in the high wave numbers' region can be used to distinguish the polymorph forms of MA. This very weak band at 3310 cm^{-1} is assigned to N−H stretching modes of the most stable polymorphism form I of MA[55]. The band at 2915 cm^{-1} is attributed to the ν(O−H) out-of-phase mode. Very intense and sharp band (recorded at 1649 cm^{-1}) is due to stretching mode ν(C=O) of the carboxylic group. The bands due to the ν(C–C) stretching modes of the aromatic rings are recorded between 1500 and 1450 cm^{-1}, where the band due to the deformation mode δ(N–H) of the amine group is recorded at 1574 cm^{-1}. The bands for the methyl group δ(CH$_3$) are recorded between 1470–1430 cm^{-1} and the band originated from the ν(C–N) stretching mode is recorded between 1160–1250 cm^{-1}. Bands due to out-of-plane deformations, δ(N–H) and δ(C–H), are recorded below 1000 cm^{-1}[55].

FTIR spectrum of β-CD (Figure 5) shows that prominent absorption band at 3393 cm^{-1} is due to the O-H stretching vibration. A further peak appearing in the region of 2800-3000 cm^{-1} represents the stretching vibrations of CH and CH$_2$ groups. The peaks appearing at 1022 cm^{-1} and 1162 cm^{-1} can be assigned to the stretching vibrations of C-OH and C-O-C groups of β-

CD. The peak at 750 cm^{-1} also represents the pyranose ring vibration[56]. Finally, the peak at 650 cm^{-1} is due to the presence of water in β-CD cavity.
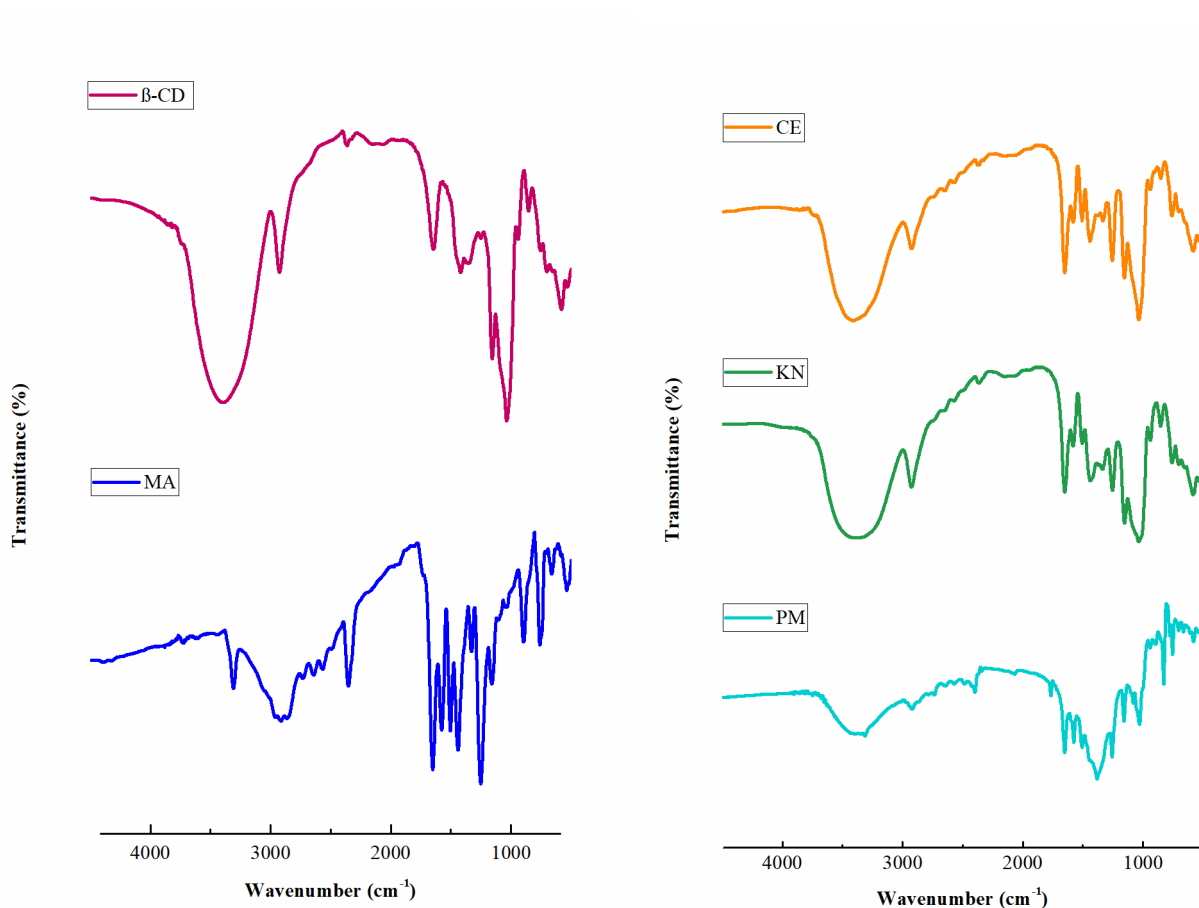
Figure 5. FT-IR spectra of MA, β-CD and MA:β-CD binary inclusion complexes.

The FTIR spectrum of the PM imitates both peaks of MA and β-CD, which could be considered as simple superimposition of MA and β-CD spectra. Therefore, the presence of chemical incompatibility among pure MA and β-CD is ruled out.

However, in the FTIR spectra of complexes prepared by CE andKN, MA bands are almost masked by the very intense and broad β-CD bands. The results indicate interactions of MA into the β-CD cavity. We notice that the CO band of MA at 1649 cm^{-1} is shifted to 1656 cm^{-1} in CE spectrum and to 1647 cm^{-1} in KN spectrum. Also, the N-H band at 1574 cm^{-1} is 1586 cm^{-1} in CE spectrum and 1577cm^{-1} in KN spectrum. This is a usual phenomenon observed by researchers in synthesizing the inclusion complexes between β-CD and a guest molecule[38,57,58].

We can add that the inclusion of the MA molecule with its aromatic rings into the electron rich cavity of the β-CD may amplify the density of the electron cloud. This last can lead to an increase in energy and consequently higher IR frequency absorption. The hydrogen bonding contacts and Van der Waals forces in complexes could also alter the microenvironment and eventually could decline the frequency between the inclusion complex and its constituent molecules[57].

The broad hydroxyl band of pure β-CD at 3393 cm^{-1} is shifted to higher frequency region in the FTIR spectra for the KN and CE complexes. This last can be considered as a good indication of the inclusion complex formation. Additionally, the aromatic C-H and N-H deformation bands for binary complexes strongly drifted towards lower wave number. Overall, the binary inclusion complexes did not display any new IR peaks signifying that no chemical bonds are formed with the obtained complexes.

Differential scanning calorimetric analysis

The DSC technique is significantly important to understand the compatibility between the drug and CD in its complexes. When guest molecules are included in CD cavities, their melting, boiling, and sublimation points can shift to different temperatures or disappear[18]. The DSC thermograms for MA, β-CD and binary systems are depicted in Figure 6.

The DSC thermogram of MA shows two endodermic peaks at 174 °C and 232 °C which correspond to the transition from form I to form II and to the fusion of form II, respectively. MA decomposes after fusion and completely decarboxylates at 300 °C[59]. The thermal curve of β-CD shows a loss of physical water starting from 50 °C with a strong endotherm at 130 °C, which is caused by the liberation of crystal water molecules from the cavity. However, the peak corresponding to the decomposition process of β-CD is observed around 310 °C[60]. The thermal curves of the complexes show the endothermic peaks of the two individual components at their corresponding temperatures. This fact indicates the absence of chemical interaction between them. The thermogram of binary inclusion complexes illustrates the characteristic endothermic peak of the drug with reduced sharpness and intensity as compared to the pure drug, indicating an incomplete inclusion of the drug in the β-CD cavity. Hirlekar et al.[61] described that similar phenomenon previously. Furthermore, in the DSC curves of the inclusion complexes, a small decrease of the endothermic peaks corresponding to β-CD dehydration indicates that the water molecules are present in a low quantity in the internal cavity of β-CD. This may be caused by

the replacement of water molecules in the cavity by MA molecules occupying the same space. This in turn referred to the formation of inclusion complexes[18].
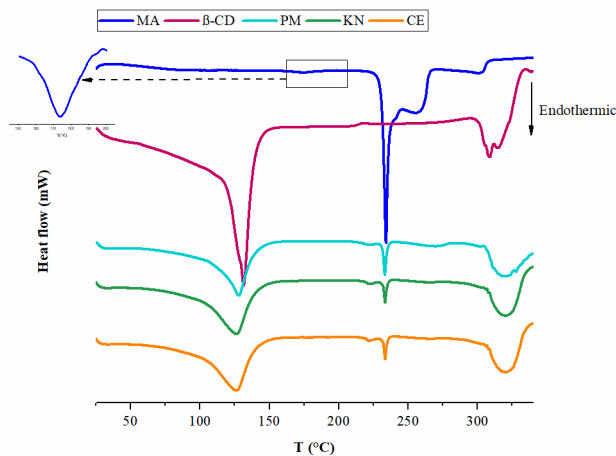
Figure 6. DSC thermograms of MA, β-CD and MA:β-CD binary inclusion complexes

X-Ray powder diffraction

XRPD is a useful tool for the detection of β-CD complexation in powder state. XRD studies could be employed to detect any change of crystallinity of a compound upon host–guest interactions [29]. The X-ray diffraction patterns of MA, β-CD and binary systems are presented in Figure 7.

MA showed characteristic peaks at 2Ө equal to 13.8, 14.28, 15.8, 20.1, 21.4, 26.3, 27.7 and 32.8°. This corresponds to the I polymorph crystalline form of MA[55]. In addition, the diffractogram of β-CD displayed several sharp and intense diffraction peaks between 5° and 40° (2Ө), which are indicative of its crystalline structure[18], which corresponds to the well-known cage packing. The same diffraction peaks of MA and β-CD clearly appear in the physical mixture, which indicates the absence of interaction between them. The binary physical mixture shows also relatively less intense peaks of MA, but the crystallinity is evident. On the other hand, diffraction pattern of KN and CE complexes seems to be more diffused and the intensities of the characteristic peaks of MA are further reduced but still present. This suggests incomplete complexation between MA and β-CD leading to partial loss of the crystalline nature of MA. This observation is in accordance with the obtained results in the molecular modeling studies. Fernandes et al.[62], while working with nicardipine-CD complexes, obtained similar results.
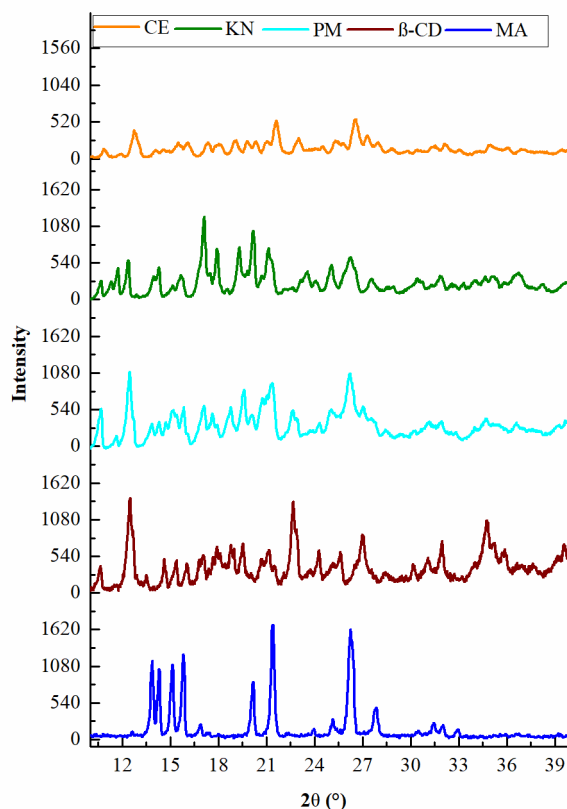
Figure 7. XRPD patterns of MA, β-CD and MA:β-CD binary inclusion complexes.

Nuclear magnetic resonance

The inclusion of a guest molecule in a host molecule is mainly based on intermolecular interactions (e.g. H bonds, van der Waals). NMR is a method of choice for studying such systems and the chemical shift analysis indicate intermolecular interactions between MA and β-CD. ^{1}H NMR spectrum of MA displays OH proton signal at 12.98 ppm (H-1) (Figure. S1). The signal at 9.45 ppm is attributed to NH (H-2). The characteristic aromatic signatures are captured in the region 7.89–6.68 ppm (H-3-H-9). Sharp singlets corresponding to methyl protons (H-10 and H-11) are detected at 2.29 and 2.10 ppm, respectively. β-CD NMR spectrum shows signals at the δ value of 4.89 (H-1), 3.37 (H-2), 3.7 (H-3), 3.42 (H-4), 3.64 (H-5) and 3.76 ppm (H-6) (Figure S2). However, in order to confirm the inclusion of MA into β-CD, a comparison of the ^{1}H NMR spectra of β-CD in the presence or absence of MA (Figures S3-S5) is necessary. Then chemical inclusion shifts (CIS) were calculated and listed in Table 3 (CIS with δ_{guest}) and Table S1 (CIS with δ_{host}). For complexes prepared by CE and KN methods, MA

protons showed [1]H-chemical shifts upon interaction with β-CD (Table 3). For example, all aromatic protons of MA (H-4, H-5, H-6 and H-7, H-8, H-9) are shifted, except for H-3. In addition, the NH function of MA also participates in the formation of the inclusion complex with a significant variation in CIS values (1.30 ppm for CE, 0.72 ppm for KN). Moreover, the chemical shift of ^{1}H from COOH group in CE complex (CIS = -2.23 ppm) is the CIS value that has changed the most. All these variations clearly indicate that the guest-host interaction results in chemical shift changes. On the other hand, no shift was observed on all protons of MA when the PM method is used to get the corresponding inclusion complex. This last can be considered as a simple superimposition of MA and β-CD spectra. The overall analysis of CIS values for CH protons of β-CD also shows variations, both for the 6 protons of the 3 complexes (Table S1). By comparing the ^{13}C NMR signals of the CE and KN complexes with MA alone (Figures S6-S10), large shifts of all carbon atoms of MA were observed (Table 4). As seen with ^{1}H NMR spectra, the greatest changes are observed for the CE and KN complexes. The amplitude of the chemical shifts can reach values greater than 2, as for C-5 carbon (-2.76 ppm for CE, 2.22 ppm for KN).

In conclusion, the presence of H-bond interactions should lead to more stable complexes, specially here for CE and KN complexes and then should increase the solubility of MA.Among the three methods investigated, the CE complex is the most stable complex prepared, with highest CIS values.

Table 3. ^{1}H NMR Chemical shifts (δ, ppm) for protons of MA alone (δ$_{guest}$) and their complexation induced shifts (CIS = δ$_{complex}$ − δ$_{guest}$) in DMSO-d_6 at 25 °C.

MA Protons	δ$_{guest}$	CIS (CE)	CIS (KN)	CIS (PM)
H-1	12.98	-2.23	-	0
H-2	9.45	1.30	0.72	0
H-3	7.89	0	0	0
H-4	7.03	-0.21	0.05	0
H-5	7.12	-0.10	0.01	0
H-6	7.31	-0.18	-0.09	0
H-7	6.68	-0.08	-0.05	0
H-8	6.70	-0.09	-0.05	0
H-9	6.72	-0.09	-0.05	0

H-10	2.29	-0.03	-0.01	0
H-11	2.10	0.01	0.01	0

Table 4.^{13}C NMR Chemical shifts (δ, ppm) for carbons of MA alone (δ_{guest}) and their complexation induced shifts (CIS = $\delta_{complex} - \delta_{guest}$) in DMSO-$d_6$ at 25 °C.

MA Carbons	δ_{guest}	CIS (CE)	CIS (KN)	CIS (PM)
C-1	170.66	-	0.34	0
C-2	149.22	-2.2	-1.43	-0.02
C-3	138.81	1.4	0.57	0
C-4	138.35	-0.93	-0.72	0
C-5	134.66	-2.76	-2.22	0
C-6	132.17	-1.16	-0.35	0
C-7	131.71	-2.64	-1.68	-0.02
C-8	129.89	-1.26	-1.08	-0.01
C-9	126.49	-2.22	-1.28	0.01
C-10	122.66	-	-2.31	-0.02
C-11	116.71	2.16	-0.60	0.01
C-12	113.55	2.43	-0.62	-0.01
C-13	111.69	1.11	-	0.03
C-14	20.69	-0.31	-0.38	0.01
C-15	14.14	-0.45	-0.45	0

Scanning electron microscopy

Figure 8 presents the micrographs of MA, β-CD and MA:β-CD binary systems prepared by various processing methods. The morphological changes may be used as an evidence for the interactions between molecules. β-CD (Figure 8a) exists as broken bricks, distributed in parallelogram, which are well separated from each other[63]. MA takes the form of flake crystalline particles (Figure 8b), irregularly sized with a tendency to self-agglomerate[64]. The PM method respects the original morphology of each component, the MA crystals are adhered to smooth surface of β-CD (Figure 8c). It is possible to distinguish a reduction in the agglomerated drug on the surface of β-CD in the case of KN product (Figure 8d) when

compared with the PM complex. A significant change in the morphology of the inclusion complex was observed using CE method (Figure 8e). In fact, it is found that the crystal nature of MA disappeared. Micrographs show small, more agglomerated, and amorphous smooth structures, which suggest that MA molecules are well dispersed in the β-CD cavities. These results are consistent with the data obtained with the DSC and XRPD studies

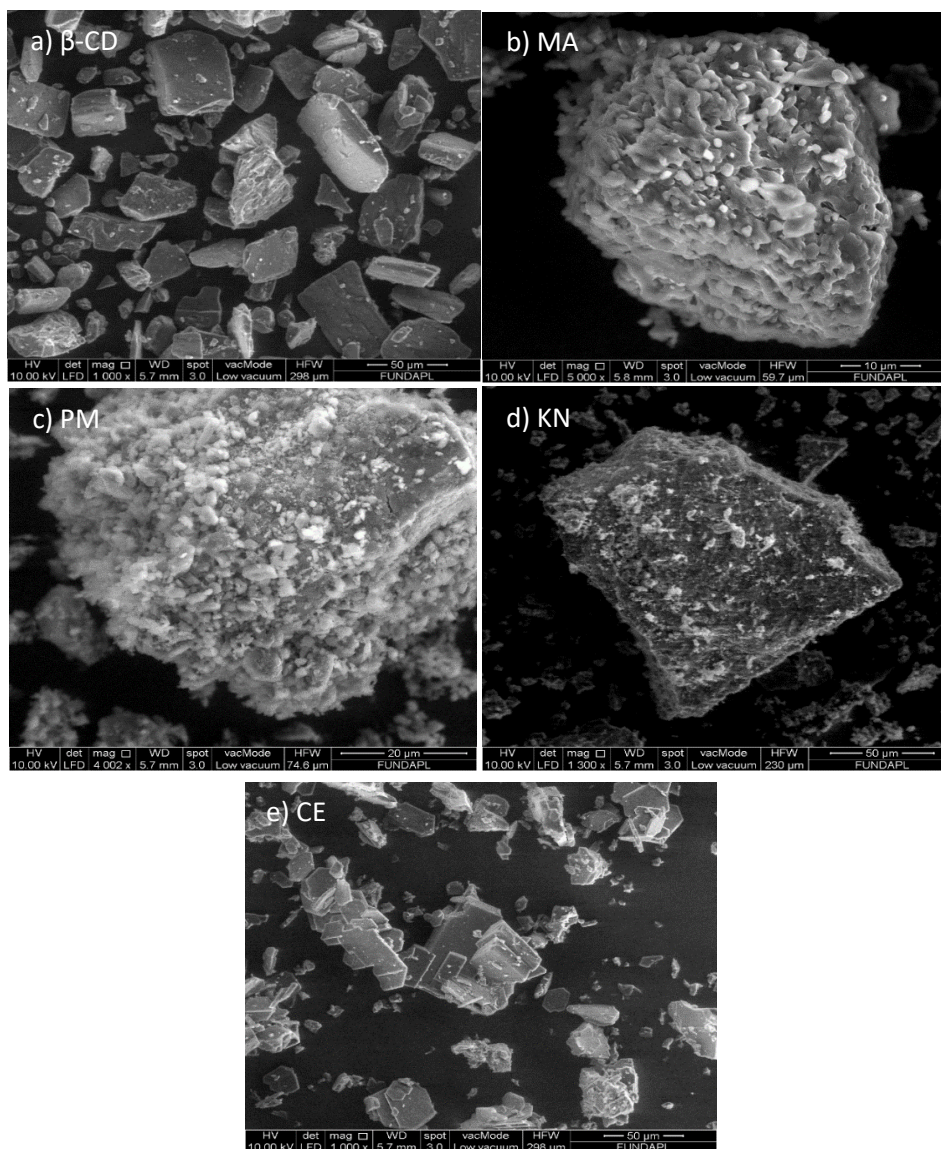**Figure 8.** SEM micrographs of β-CD (a), MA (b) and MA:β-CD binary inclusion complexes (c-e).

In vitro drug release test

Figure 9 illustrates the dissolution profiles of MA from various (2:1) binary systems in 0.1 M HCl (pH 1.2). In fact, all the binary systems exhibit a more rapid release and a greater extent of dissolution compared to the drug alone. The most important enhancement of the drug

dissolution properties is observed with the binary mixture prepared by CE, followed by KN and PM.

The improved MA dissolution characteristics of the PM binary system may be explained by the drug wettability enhancement at the early stages of dissolution process, due to the coexistence of drug and β-CD in the dissolution medium and/or the existence of interaction(s) between external β-CD cavity and MA. Indeed, because of the hydrophilicity of its outer surface, β-CD acts as a surfactant. Thus, it reduces the interfacial tension between the poorly soluble drug and the dissolution medium, resulting in a higher dissolution rate of the drug as proposed by Hriday et al.[18]. Moreover, KN and CE binary systems showed a greater extent of dissolution than those of the pure drug and the PM. This enhancement may be due to partial trapping of the drug in β-CD verified by molecular modeling, FTIR, DSC, XRPD and SEM experiments. It may confer a certain hydrophilicity and then may increase the solubility and wettability of MA. Furthermore, the reduced crystallinity of MA in the KN and CE binary mixtures is considered as an important point in the improvement of its dissolution. This could be related to the higher Gibbs free energy[65] of the amorphous form.
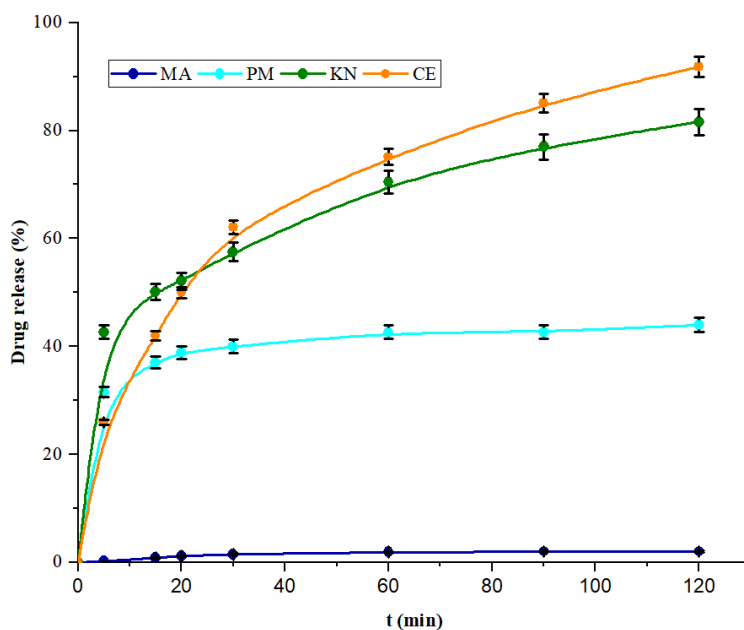
Figure 9. Dissolution profiles of MA and MA:β-CD binary inclusion complexes.

In order to study the mechanism of release of MA from the different complexes, three kinetic models were used. The fitting results are summarized in Table 5. On the basis of the R^2 values, the Higuchi model is the most appropriate model for the KN and signified that the mechanism of MA release from β-CD is governed by diffusion. The K_H release constant of the PM is the lowest (0.012 min$^{-1/2}$), that confirmed no appreciable interaction between MA and β-

CD. However, CE formulation presented a higher value of K_H release constant (0.074 min$^{-1/2}$) which indicated the complex formation and the enhancement of drug dissolution compared to all formulations. In addition, the exponent (n) of the Korsmeyer–Peppas model indicated that the drug release is related to a quasi- Fickian diffusion since the values of n are lower than 0.5.

Table 5. Mathematical models of drug release kinetics: application to MA:β-CD binary inclusion complexes.

MA:β-CD	First order		Higuchi			Kosmeyer-Peppas			% Drug release after 120 min
	R^2	K_1 (min^{-1})	R^2	K_H x100 (min$^{-1/2}$)	a	R^2	K_{KP}	n	
PM	0.6553	0.0022	0.8363	1.2367	31.7150	0.9424	3.5851	0.0997	44.00
KN	0.9113	0.0054	0.9934	4.6504	32.2330	0.9784	3.4922	0.2154	81.60
CE	0.7551	0.0090	0.9688	7.4297	14.7730	0.9832	6.8865	0.3980	91.80

In vitro anti-inflammatory activities

The last stage of our study was to evaluate the real potency of (2:1) MA:β-CD binary inclusion complexes in vitro. Since MA has marked anti-inflammatory activity, two assays were used, namely BSA denaturation and HRBC membrane stabilization, to investigate the anti-inflammatory activity of studied complexes[48,49]. In certain inflammatory and arthritic diseases, protein denaturation leads to the production of autoantigen. In addition, neutrophils appear to be activated inappropriately and then release lysosomal enzymes that further promote inflammation like chemo-attractants (eicosanoids and chemokines) or cytokines. Additionally, due to the close similarity of the erythrocyte and lysosome membranes, stabilization of erythrocyte membrane is considered as a preventive measure for the treatment of inflammation disorders. Then the prevention of hypotonicity induced HRBC membrane lysis is a good marker for estimating the anti-inflammatory property of products[66].

The obtained results are shown in Figure 10. Inclusion complexes have considerably protected the BSA from denaturation (inhibition > 69%). With the CE complex, the percentage rises up to 88%. This observation is well correlated to the rate of MA release (CE > KN > PM, see Figure 9). Additionally, the inclusion complexes are able to protect the membrane of erythrocyte from lysis induced by heat and hypotonicity. We also observed the best result with CE complex, the inhibition of heat-induced hemolysis and hypotonic-induced hemolysis are equal to 37 and 52%, respectively.
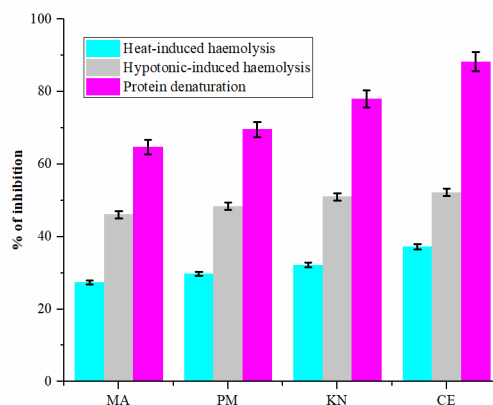
Figure 10. Comparison of the activity of MA and MA:β-CD binary inclusion complexes on BSA denaturation and HRBC membrane stabilization.

Conclusions

In this work, the phase solubility diagram and job's plot experiment were used to determine the stoichiometry of the MA:β-CD complex. Then molecular modeling approach helped (i) to select the most stable inclusion complex (2:1), (ii) to determine intermolecular energy contributions, and (iii) to predict hydrophilic surfaces and drug solubility (e.g. solvation energy). Inclusion complexes of MA:β-CD in the 2:1 molar ratio were prepared using three methods, namely PM, KN and CE. FTIR and NMR studies showed no evidence of chemical reactions between the drug and β-CD. DSC, XRPD and SEM experiments confirmed partial amorphism of the MA after inclusion complexation indicating that MA was well dispersed in the β-CD cavities. These results suggest an enhanced dissolution profile compared to the crystalline form. All three formulations showed a significant improvement of the MA dissolution; however, the CE complex exhibited the highest K_H value. The CE method is thus the most appropriate method to get improved MA dissolution properties. Actually, the (2:1) MA:β-CD binary complex obtained by CE method constitutes an interesting alternative to formulate MA. Protein denaturation and membrane stabilization assays also confirmed the therapeutic benefits of MA when used as (2:1) MA:β-CD complex. Finally, this approach of preparing inclusion complexes in an optimized ratio could allow other poor-water soluble NSAIDs to be studied again.

References

1. Benet LZ, Kroetz D, Sheiner L, et al. Pharmacokinetics: the dynamics of drug absorption, distribution, metabolism, and elimination. In: *Hardman JG, Limbert LE, Molinoff PB, Ruddon RW, Gilman AG, editors.*Goodman and Gilman's the Pharmacological Basis of Therapeutics. 9th ed. New York (USA): *McGraw-Hill Inc.;* 1996. p. 3–27.

2. Wei M, Yang X, Watson P, et al. Development of QSAR model for predicting the inclusion constants of organic chemicals with α-cyclodextrin. Environ Sci Pollut Res 2018;25:17565–74.

3. Kalepu S, Nekkanti V. Insoluble drug delivery strategies: review of recent advances and business prospects. Acta Pharm Sin B 2015;5:442–53.

4. Dizaj SM, Vazifehasl Z, Salatin S, et al. Nanosizing of drugs: effect on dissolution rate. Res Pharm Sci 2015;10:95–108.

5. Ren F, Jing Q, Tang Y, et al. Characteristics of bicalutamide solid dispersions and improvement of the dissolution. Drug Dev Ind Pharm 2006;32:967–72.

6. Wang N, Xie C, Lu H, et al. Cocrystal and its application in the field of active pharmaceutical ingredients and food ingredients. Curr Pharm Des 2018;24:2339–48.

7. Chaudhari SP, Dugar RP. Application of surfactants in solid dispersion technology for improving solubility of poorly water soluble drugs. J Drug Deliv Sci Technol 2017;41:68–77.

8. Gursoy RN, Benita S. Self-emulsifying drug delivery systems (SEDDS) for improved oral delivery of lipophilic drugs. Biomed Pharmacother 2004;58:173–82.

9. Priya AS, Sivakamavalli J, Vaseeharan B, Stalin T. Improvement on dissolution rate of inclusion complex of rifabutin drug with β-cyclodextrin. Int J Biol Macromol 2013;62:472–80.

10. Crini G, Fourmentin S, Fenyvesi É, et al. Fundamentals and applications of cyclodextrins. In Fourmentin S, Crini G, Lichtfouse E, editors. Cyclodextrin fundamentals, reactivity and analysis. 1st ed. Cham (Switzerland): Springer International Publishing; 2018. p. 1–55.

11. Conceição J, Adeoye O, Cabral-Marques HM, Lobo JMS. Cyclodextrins as excipients in tablet formulations. Drug Discov Today 2018;23:1274–84.

12. Jambhekar SS, Breen P. Cyclodextrins in pharmaceutical formulations I: structure and physicochemical properties, formation of complexes, and types of complex. Drug Discov Today 2016;21:356–62.

13. Kontogiannidou E, Ferrari M, Deligianni AD, et al. In vitro and ex vivo evaluation of tablets containing piroxicam-cyclodextrin complexes for buccal delivery. Pharmaceutics 2019;11:398.

14. Prandina A, Herfindal L, Radix S, et al. Enhancement of iodinin solubility by encapsulation into cyclodextrin nanoparticles. J Enzyme Inhib Med Chem 2018;33:370–75.

15. Perret F, Marminon C, Zeinyeh W, et al. Preparation and characterization of CK2 inhibitor-loaded cyclodextrin nanoparticles for drug delivery. Int J Pharm 2013;441:491–8.

16. Nacereddine A, Bollacke A, Róka E, et al. Self-assembled supramolecular nanoparticles improve the cytotoxic efficacy of CK2 inhibitor THN7. Pharmaceuticals 2018;11:E10.

17. Kurkov SV, Loftsson T. Cyclodextrins. Int J Pharm 2013;453:167–80.

18. Bera H, Chekuri S, Sarkar S, et al. Novel pimozide-β-cyclodextrin-polyvinylpyrrolidone inclusion complexes for tourette syndrome treatment. J Mol Liq 2016;215:135–43.

19. Cimolai N. The potential and promise of mefenamic acid. Expert Rev Clin Pharmacol 2013;6:289–305.

20. Cryer B, Feldman M. Cyclooxygenase-1 and cyclooxygenase-2 selectivity of widely used nonsteroidal anti-inflammatory drugs. Am J Med Sci 1998;104:413–21.

21. Winder CV, Kaump DH, Glazko AJ, Holmes EL. Experimental observations on flufenamic, mefenamic, and meclofenamic acids. I. Pharmacology. Ann Phys Rehabil Med 1966;8(Supl.1):7–49.

22. Baum C, Kennedy DL, Forbes MB. Utilization of nonsteroidal anti-inflammatory drugs. Arthritis Rheum 1985;28:686–92.

23. Abdul Mudalip S.K, Abu Bakar MR, Jamal P, Adam F. Solubility and dissolution thermodynamic data of mefenamic acid crystals in different classes of organic solvents. J Chem Eng Data 2013;58:3447–52.

24. Kafarska K, Gacki M, Wolf WM. Synthesis, spectroscopic, and thermal investigations of metal complexes with mefenamic acid. J Chem 2017;2017, 6172626.

25. Stephens WH, El-Ghobarey AF, Macleod MM, Watson Buchanan WA. double-blind, crossover trial of mefenamic acid, sulindac and flurbiprofen in rheumatoid arthritis.Curr Med Res Opin 1979;5:754–8.

26. Ozgoli G, Goli M, Moattar F. Comparison of effects of ginger, mefenamic acid, and ibuprofen on pain in women with primary dysmenorrhea. J Altern Complement Med 2009;15:129–32.

27. Mavrikakis ME, Madkour MM, Buchanan WW. The place of mefenamic acid in the treatment of rheumatoid arthritis. Scott Med J 1978;23:189–90.

28. Joo Y, Kim HS, Woo RS, et al. Mefenamic acid shows neuroprotective effects and improves cognitive impairment in in vitro and in vivo alzheimer's disease models. Mol Pharmacol 2006;69:76–84.

29. Ghanghas P, Jain S, Rana C, Sanyal SN. Chemopreventive action of non-steroidal anti-inflammatory drugs on the inflammatory pathways in colon cancer. Biomed Pharmacother 2016;78:239–47.

30. Lee FD. Drug-related pathological lesions of the intestinal tract. Histopathology 1994;25:303–8.

31. Zentler-Munro PL, Northfield TC. Drug-induced gastrointestinal disease. Br Med J 1979;1:1263–5.

32. Gibson GR, Whitacre EB, Ricotti CA. Colitis induced by nonsteroidal anti-inflammatory drugs: report of four cases and review of the literature. J Gen Intern Med 1992;152:625–32.

33. Zhao Q, Miriyala N, Su Y, et al. Computer-aided formulation design for a highly soluble lutein–cyclodextrin multiple-component delivery system. Mol Pharm 2018:15:1664–73.

34. Quevedo MA, Zoppi A. Current trends in molecular modeling methods applied to the study of cyclodextrin complexes. J Incl Phenom Macro 2018;90:1–14.

35. Mazzaferro S, Bouchemal K, Gallard JF, et al. Bivalent sequential binding of docetaxel to methyl-β-cyclodextrin. Int J Pham 2011;416:171–80.

36. Vavia PR, Adhage NA. Freeze-dried inclusion complexes of tolfenamic acid with β-cyclodextrins. Pharm Dev Technol 2000;5:571–4.

37. Terekhova IV, Volkova TV, Perlovich GL. Experimental analysis of complex formation of niflumic acid with β-Cyclodextrins. J Incl Phenom Macro 2006;55:335–40.

38. Jambhekar S, Casella R, Maher T. The physicochemical characteristics and bioavailability of indomethacin from β-cyclodextrin, hydroxyethyl-β-cyclodextrin, and hydroxypropyl-β-cyclodextrin complexes. Int J Pharm 2004;270:149–66.

39. Tayade PT, Vavia PR. Inclusion complexes of ketoprofen with beta-cyclodextrins: Oral pharmacokinetics of ketoprofen in human. Indian J Pharm Sci 2006;68:164–70.

40. Siva S, Kothai Nayaki S, Rajendiran N. Spectral and molecular modeling investigations of supramolecular complexes of mefenamic acid and aceclofenac with α- and β-cyclodextrin. Spectroc Acta A 2017;174:349–62.

41. Hładoń T, Pawlaczyk J, Szafran B. Stability of mefenamic acid in the Inclusion complex with β-cyclodextrin in the solid phase. J Incl Phenom 1999;35:497–506.

42. Derle DV, Bele M, Kasliwal N. In vitro and in vivo evaluation of mefenamic acid and its complexes with β-cyclodextrin and HP-β-cyclodextrin. Asian J Pharm 2014;2:30–4.

43. Higuchi T. A phase solubility technique. Adv Anal Chem Instrum 1965;4:117–211.

44. Accelrys Materials Studio, versions v 5.5.0.0 (2010) and v 6.0.0.0. (2012), Accelrys Inc, San Diego, CA, USA.

45. Maestro*, version 9.3, Schrödinger, LLC, New York, NY, USA, 2012.*

46. Delley B. An all-electron numerical method for solving the local density functional for polyatomic molecules. J Chem Phys1990;92:508–17.

47. Zhao Y, Truhlar DG. Density functionals with broad applicability in chemistry. Acc Chem Res 2008;41:157–67.

48. Assas N, Elbahri Z, Baitiche M, Djerboua F. Effects of some process parameters on the niflumic acid controlled release polymeric microspheres: Optimization using designs of experiments. Asia-Pac J Chem Eng 2019;14:e2283.

49. Mizushima Y, Kobayashi M. Interaction of anti-inflammatory drugs with serum proteins, especially with some biologically active proteins. J Pharm Pharmacol 1968;20:169–73.

50. Bulani VD, Kothavade PS, Kundaikar HS, et al. Inclusion complex of ellagic acid with β-cyclodextrin: characterization and in vitro anti-inflammatory evaluation. J Mol Struct 2016;1105:308–15.

51. Pradines B, Gallard JF, Iorga BI, et al. Investigation of the complexation of albendazole with cyclodextrins for the design of new antiparasitic formulations. Carbohydr Res 2014;398:50–5.

52. Buchanan CM, Buchanan NL, Edgar KJ, et al. Building new drug delivery systems: In vitro and in vivo studies of drug-hydroxybutenyl cyclodextrin complexes. In Edgar KJ, Heinze T, Buchanan CM, editors. Polysaccharide materials: Performance by design. Washington, DC (USA): American Chemical Society Books; 2009. p. 31–64.

53. Rudrangi SRS, Bhomia R, Trivedi V, et al. Influence of the preparation method on the physicochemical properties of indomethacin and methyl-β-cyclodextrin complexes. Int J Pharm 2015;479:381–90.

54. Sherje AP, Kulkarni V, Murahari M, et al. Inclusion complexation of etodolac with hydroxypropyl-beta-cyclodextrin and auxiliary agents: formulation characterization and molecular modeling studies. Mol Pharm 2017;14:1231–42.

55. Cunha VR, Izumi CM, Petersen PA, et al. Mefenamic acid anti-inflammatory drug: probing its polymorphs by vibrational (IR and Raman) and solid-state NMR spectroscopies. J Phys Chem B 2014;118:4333–44.

56. Fateminasab F, Bordbar AK, Shityakov S, Gholami S. Diadzein complexation with unmodified cyclodextrins: A detailed experimental and theoretical study. J Mol Liq 2018;271:80–95.

57. Sambasevam K, Mohamad S, Sarih N, Ismail N. Synthesis and characterization of the inclusion complex of β-cyclodextrin and azomethine. Int J Mol Sci 2013;14:3671–82.

58. Khoukhi OE, Elbahri Z, Diaf K, Baitiche M. Piroxicam/β-cyclodextrin complex included in cellulose derivatives-based matrix microspheres as new solid dispersion-controlled release formulations. Chem Pap 2016;70:828–39.

59. Romero S, Escalera B, Bustamante P. Solubility behavior of polymorphs I and II of mefenamic acid in solvent mixtures. Int J Pharm 1999;178:193–202.

60. Giordano F, Novak C, Moyano JR. Thermal analysis of cyclodextrins and their inclusion compounds. Thermochim Acta 2001;380:123–51.

61. Hirlekar RS, Sonawane SN, Kadam VJ. Studies on the effect of water-soluble polymers on drug–cyclodextrin complex solubility. AAPS Pharm Sci Tech 2009;10:858.

62. Fernandes CM, Vieira MT, Veiga FJB. Physicochemical characterization and in vitro dissolution behavior of nicardipine–cyclodextrins inclusion compounds. Eur J Pharm Sci 2002;15:79–88.

63. Shanmuga PA, Balakrishnan BS, Veerakanellore GB, Stalin T. In-vitro dissolution rate and molecular docking studies of cabergoline drug with β-cyclodextrin. J Mol Struct 2018;1160:1–8.

64. Panchagnula R, Sundaramurthy P, Pillai O, et al. Solid-state characterization of mefenamic acid. J Pharm Sci 2004;93:1019–29.

65. Khadka P, Ro J, Kim H, et al. Pharmaceutical particle technologies: an approach to improve drug solubility, dissolution and bioavailability. Asian J Pharm Sci 2014;9:304–16.

66. Chippada SC, Volluri SS, Bammidi SR, Vangalapati M. In vitro anti-inflammatory activity of methanolic extract of *Centella asiatica* by HRBC membrane stabilization. Rasayan J Chem 2011;4:457–60.

Supplementary information for the publication: Solubility Enhancement of Mefenamic Acid by Inclusion Complex with β-Cyclodextrin: In Silico Modelling, Formulation, Characterization and *In Vitro* Studies

Figure S1. ^{1}H NMR Spectrum of MA.

CMDS6.100.fid — no_title — 1H_8 DMSO /opt/topspin ea4446 :
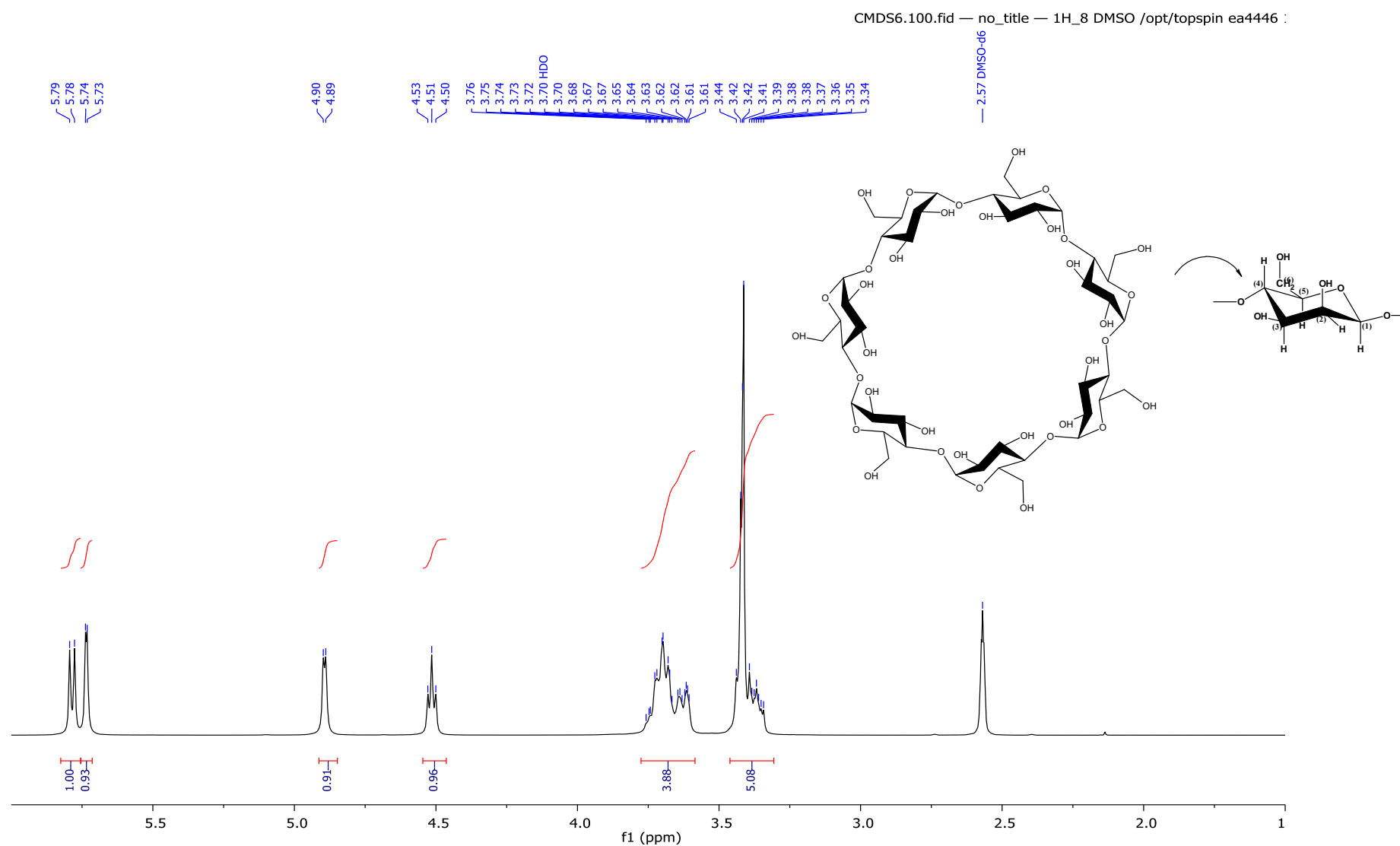
Figure S2. ^{1}H NMR Spectrum of β-CD.

Figure S3. ^{1}H NMR Spectrum of CE inclusion complex.

Figure S4. ^{1}H NMR Spectrum of KN inclusion complex.
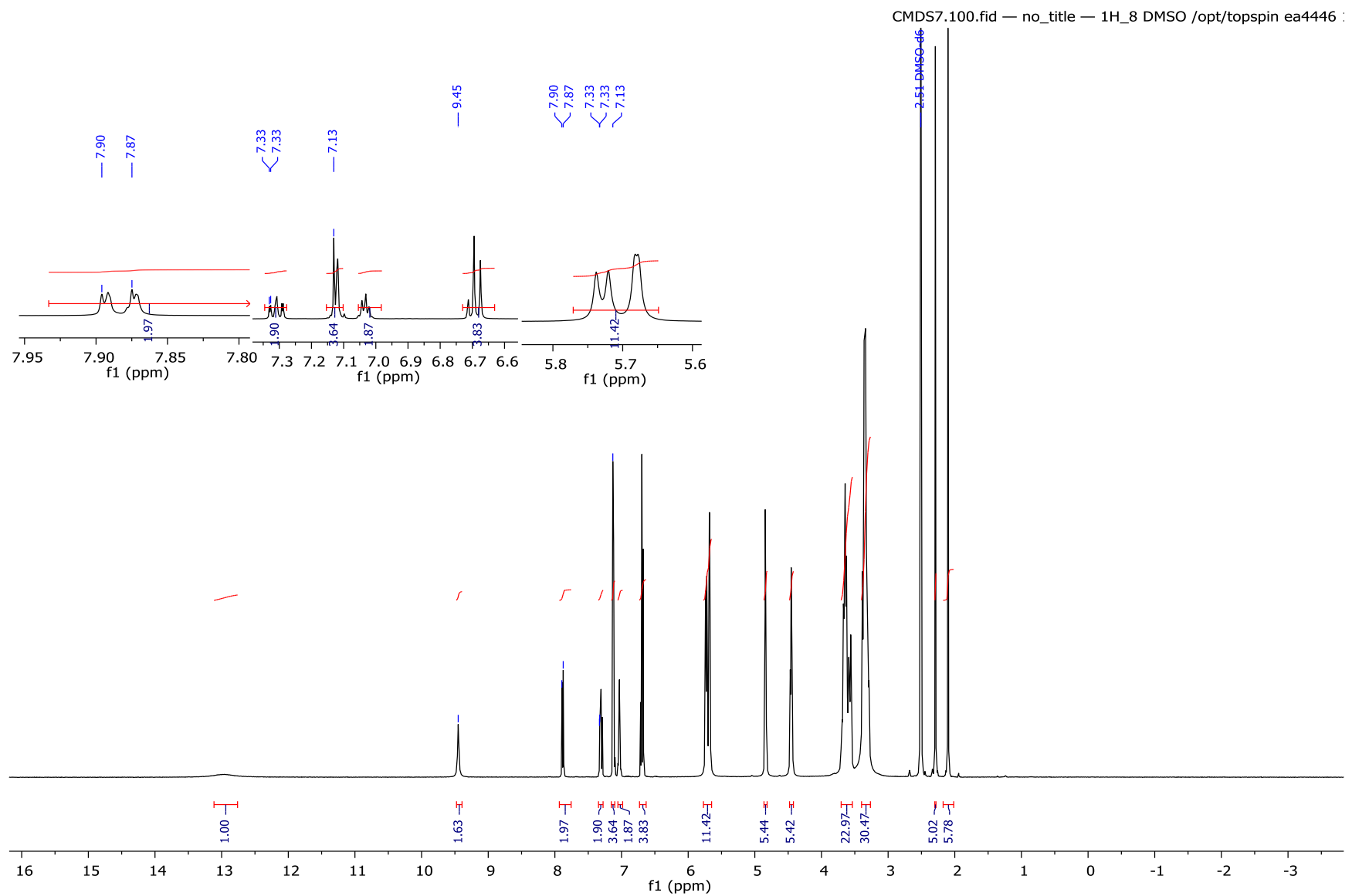
Figure S5.^{1}H NMR Spectrum of PM inclusion complex.

CMDS5.101.fid — no_title — 13C_CPD_1k DMSO /opt/topspin ea4446
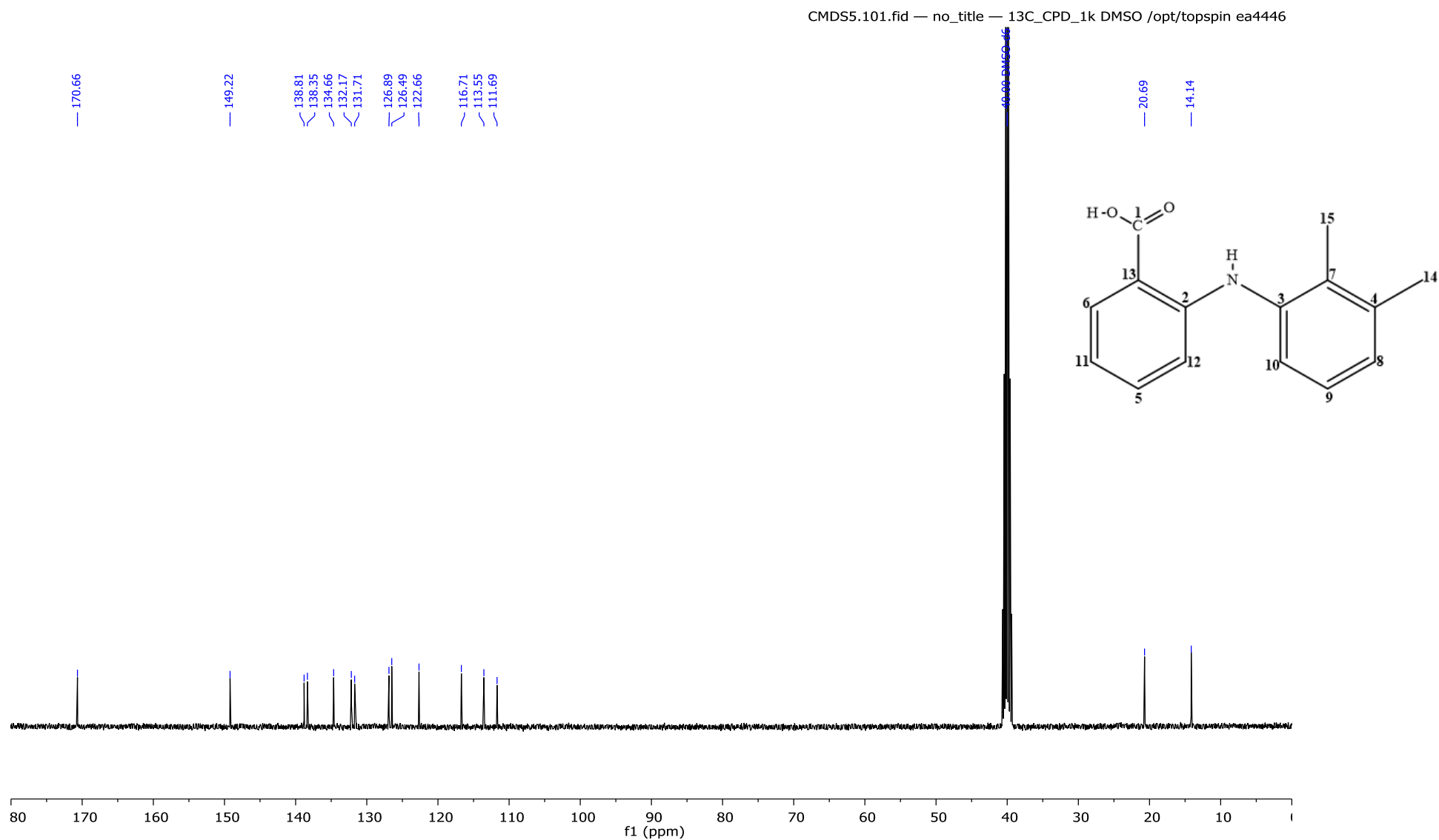
Figure S6. ^{13}C NMR Spectrum of MA.
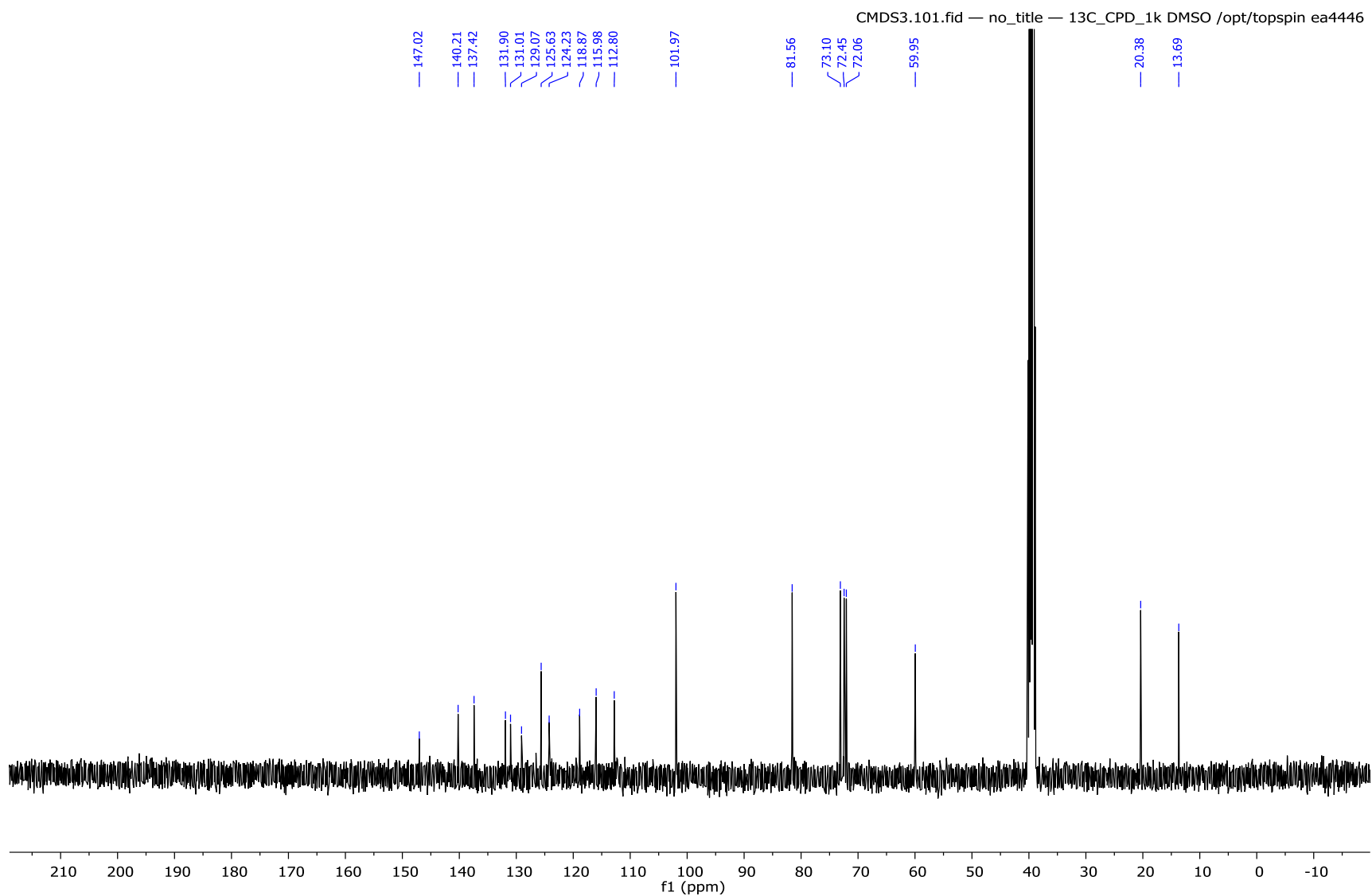
Figure S7. ^{13}C NMR Spectrum of CE inclusion complex.
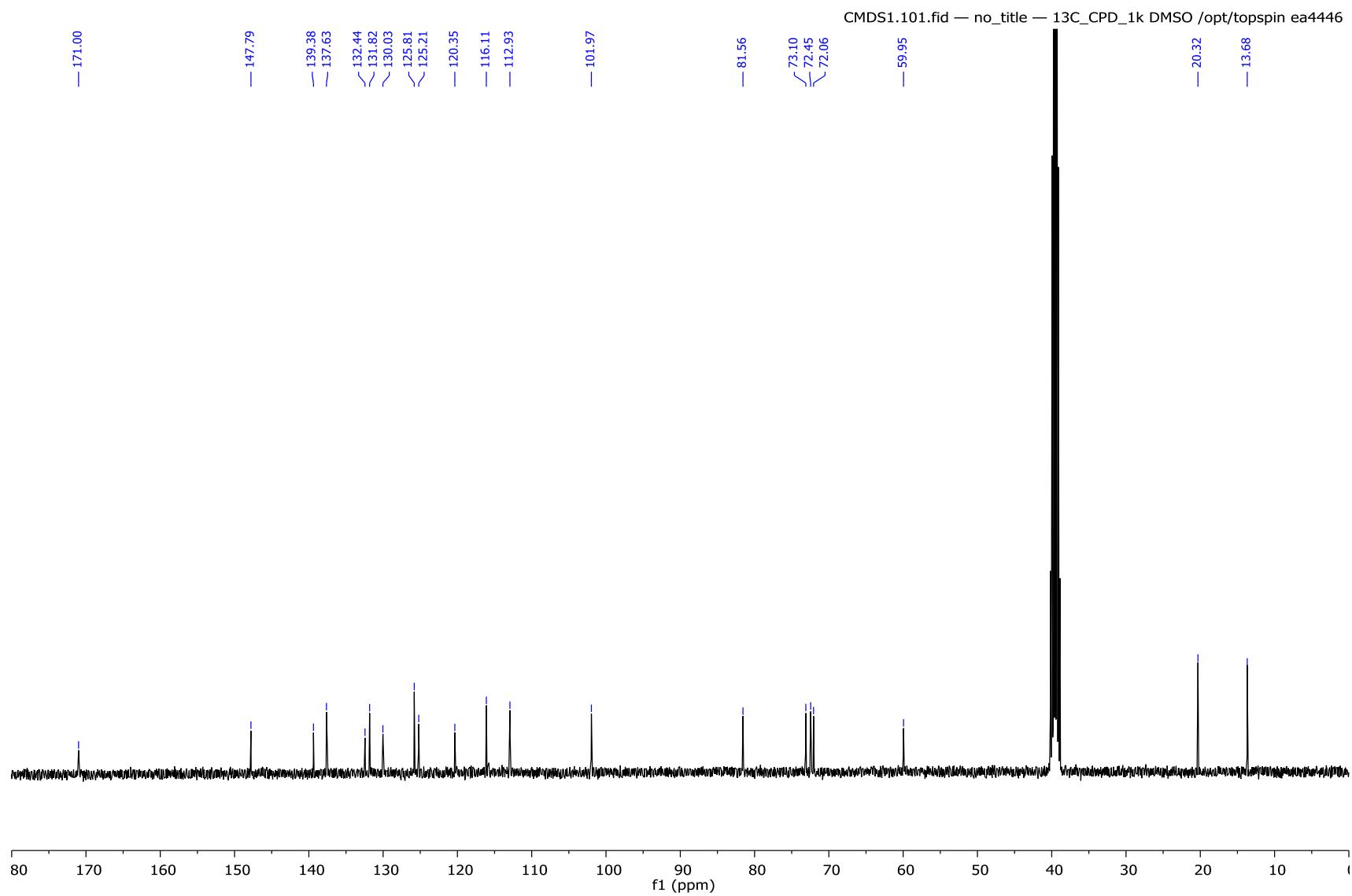
Figure S8. ^{13}C NMR Spectrum of KN inclusion complex.

CMDS7.101.fid — no_title — 13C_CPD_1k DMSO /opt/topspin ea4446
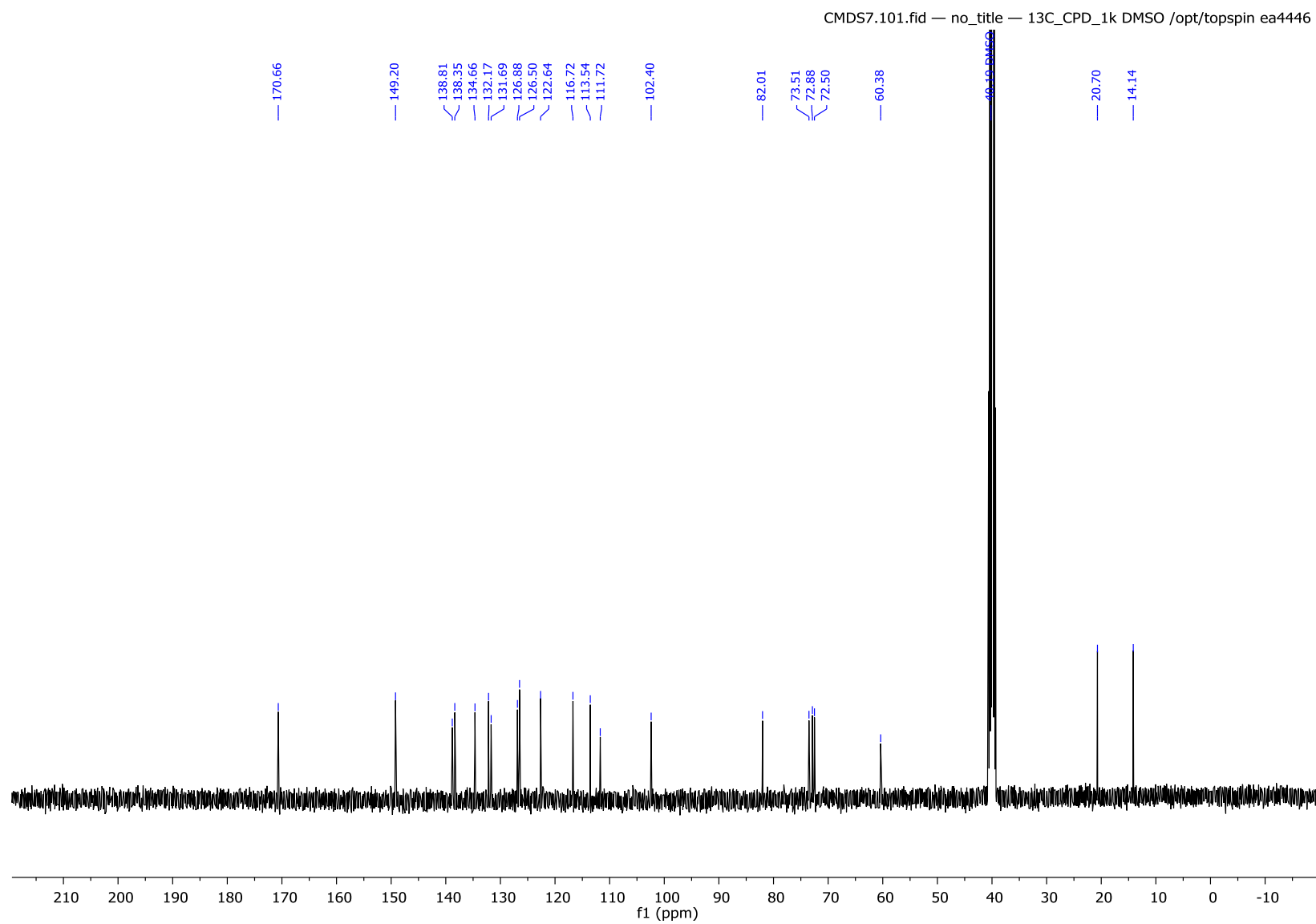
Figure S9.^{13}C NMR Spectrum of PM inclusion complex.

Table S1. ^{1}H NMR Chemical shifts (δ, ppm) for CH protons of β-CD alone (δ_{host}) and their complexation induced shifts (CIS = $\delta_{complex} - \delta_{host}$) in DMSO-$d_6$ at 25 °C.

CH Protons of β-CD	δ_{host}	CIS (CE)	CIS (KN)	CIS (PM)
H-1	4.89	-0.05	-0.05	-0.06
H-6	3.76	-0.05	-0.06	-0.06
H-3	3.70	-0.05	-0.04	-0.05
H-5	3.64	-0.05	-0.04	-0.05
H-4	3.42	-0.06	-0.06	-0.06
H-2	3.37	-0.04	-0.04	-0.04

II.4. Future Publication: Solubility Enhancement of a New Inhibitor of the Ser/Thr Kinase CK2 by Inclusion Complexation with Hydroxypropyl-β-Cyclodextrin: A Joint Experimental and Theoretical Investigation

ABSTRACT

The present investigation was aimed to optimize the hydrosolubility of a new small-molecule called NB4 (1,2,3,4-tetrabromo-5-isopropyl-7,8-dihydroindeno[1,2-b] indole-9,10(5H,6H) -dione) having a marked inhibitory activity on the Ser/Thr kinase CK2 (IC_{50} = 16 nM). NB4 also demonstrated an anti-leukemic activity on multidrug-resistant lines (IPC, Bcl-2) using hydroxypropyl-β-CD (HP-β-CD) as a pharmaceutical carrier. A job's plot experiment was used to determine the stoichiometry of the NB4:HP-β-CD complex (1:1). The freeze dried (FD) and physical mixture (PM) were used to prepare complexes. The interaction between the NB4 molecules and HAL has been investigated experimentally by FTIR spectroscopy, DSC and ^{1}H NMR. In addition, this interaction was studied theoretically by using molecular docking. Finally, the solubility of NB4 was measured in water.

Keywords: Hydrosolubility; NB4; Hydroxypropyl-β-CD; Freeze drying; Molecular docking.

Introduction

CK2 is a constitutively active acidophilic Ser/Thr protein kinase. It is expressed in all tissues of all eukaryotic organisms, and is essential for normal embryo development[1], usually present in a tetrameric form composed of (i) catalytic CK2α subunit and its isoforms CK2α' and CK2α", (ii) regulatory CK2β subunit, and (iii) heterotetramer. CK2 phosphorylates hundreds of substrates, involved in practically all cellular processes, but its main functions are related to cell growth, proliferation, and survival.

A high activity of this protein has been reported in many human diseases[2] such as inflammatory processes, neurodegenerative disorders, viral infections, cardiovascular diseases. Moreover, protein kinase CK2 activity is associated with the proliferative status of several tumor cells such as glioblastoma[3], breast carcinoma[4], prostate carcinoma[5], pancreatic cancer[6], leukemia[7] and hepatocellular carcinoma[8]. In most cases a remarkable hyperactivity of CK2 has been observed. It seems to be linked to an overexpression of the kinase considering that no protein mutations have been found until now. Initial studies of down-regulation of CK2 expression in cells or cell treatment with CK2 inhibitors allowed to postulate the anti-apoptotic role of this kinase. Later, it was clear that the prevention of caspase action, but also the

potentiation of different survival signaling and a multitude of other mechanisms, contribute to mediate a global anti-apoptotic function of CK2[9].

On the other hand, ABCG2 is overexpressed in many types of tumors, and is recognized to play a role in their multidrug resistance by catalyzing the efflux of anticancer drugs[10]. A number of tyrosine kinase inhibitors were found to strongly inhibit the cancer resistance protein ABCG2: canertinib (CI1033), imatinib, gefitinib, nilotinib and dasatinib, vandetinib, pelitinib and neratinib, erlotinib, sorafenib, sunitinib and linsitinib which inhibit various serine/threonine kinases, were also found to inhibit ABCG2[11]. Potent, selective and nontoxic inhibitors might constitute a good therapeutic strategy to improve anticancer drugs efficiency by increasing their bioavailability, and then sensitize tumor growth to their cytotoxicity. New inhibitors should therefore be investigated[12].

Recently, the series of indeno[1,2-b] indoles has revealed great interest as potent and selective CK2ATP-competitive inhibitors. Among them, a new small-molecule called NB4 (1,2,3,4-tetrabromo-5-isopropyl-7,8-dihydroindeno[1,2-b] indole-9,10(5H,6H) -dione) having a marked inhibitory activity on the Ser/Thr kinase CK2 (IC50 = 16 nM). NB4 also demonstrated an anti-leukemic activity on multidrug-resistant lines (IPC, Bcl-2). However, the water solubility of NB4 is almost nil (<< 0.002 mg/mL), there is a need to increase its hydrosolubility using a pharmaceutical carrier like cyclodextrins (hydroxypropyl-β-CD)[13].

Cyclodextrins, a family of cyclic amylose-derived oligomers with a hydrophilic outer surface and a lipophilic central cavity, are well known for its abilities to form inclusion complex with various guest molecules[14]. Druing the past decades, cyclodextrins has been successfully used as comlexing agents to enhance the solubility, stability and bioavailabilty of drug molecules[15]. The α-, β-, and γ-cyclodextrin are the most common cyclodextrins used as formulation vehicles consisting of six, seven, and eight D-(+)-glucopyranose units attached by α-1,4 linkage[16]. β-cyclodextrin is the most useful and the lowest price, however, its solubility in water is relatively low (approximately 2% w/v) wich limit its further application in pharmaceutical formulations[14]. 2-hydroxylpropyl-β-cyclodextrin (HP-β-CD) is an alternative to β-cyclodextrin having a higher aqueous solubility (above 60% w/v). Recently, HP-β-CD has been widely used to improve the solubility of poorly water-soluble drugs[17].

In the present study, with the aim to increase the aqueous solubility of NB4. The stoichiometry of the complex was obtained using the continuous variation method of Job. he complexes of NB4 with HP-β-CD in 1:1 stoichiometry was prepared by a simple physical

mixing (PM) and freeze dried method (FD). Then selective physicochemical determinations based on Fourier-transform infrared spectroscopy (FTIR) and differential scanning calorimetry (DSC) were performed to characterize complexes. The mechanism of inclusion interaction of guest and host was established through ^{1}H NMR, molecular docking, and molecular dynamics studies. Finally, aqueous solubility of the complexes was also estimated.

Materials and methods

Materials

All chemicals and phosphate buffer solution were purchased from Acros Organics or Sigma Aldrich and used without further purification. Other solvents were of chemical grade and were used as received. The (1,2,3,4-tetrabromo-5-isopropyl-7,8-dihydroindeno[1,2-b] indole-9,10(5H,6H) -dione) NB4 (Molecular weight=594.92 g/mol) was synthetized by the EA 4446 B2MC team. The HP-β-CD (Molecular weight= 1135 g/mol) was purchased from Roquette Frères (Lestrem, France).

The physical chemical properties of NB4 can be summarised as follows: it is a dark orange solid. NB4's solubility in different solvent can be summarised in the following table:

Table 1. Solubilty of NB4 in different solvent.

Solvent	Solubility (mg/ml)
Chloroform	9.09
Dichloromethane	2.5
N,N dimethylformamide	2.32
Methanol	1.5
Ethanol	1.17
75% Tetrahydrofuran 25% Acetone	0.5
Tetrahydrofuran	0.24
Acetone	0.20
Acetonitrile	0.11
Dioxane	0.093
Prpan-2-ol	<< 0.08
Water	<< 0.002

It thus appears that NB4 is a bioactive molecule, which is difficult to manage in most biological investigations. To overcome this issue, we envisaged to complex NB4 with Hydroxypropyl cyclodextrin to increase aqueous solubility.

Determination of complex stoichiometry

The continuous variation method otherwise known as Job's plot was used to ascertain the stoichiometry for NB4: HP-β-CD complexation[1] The experiments were carried out in triplicate by mixing two equimolar solutions (8.41×10^{-4}) of HP-β-CD in water and NB4 in ethanol in different molar ratio from 0-1 without variation of the final volume and stirred during 5 days, solutions were analyzed by ultra-violet spectroscopy at 283 nm. The absorbency changes ($\Delta Abs = Abs-Abs_0$) of NB4 in the presence (Abs) and absence (Abs_0) of HP-β-CD were plotted versus R, where R = [NB4]/([NB4] +[HP-β-CD]). The Job's plot showed a maximum or a minimum at a specific molar ratio indicating the stoichiometry of the complexes. For the determination of the equilibrium constant ($K_{1:1}$), the double-reciprocal (Benesi/Hildebrand) plot was used:

$$\frac{l}{\Delta A} = \frac{1}{\Delta \varepsilon 1:1 \, K1:1[\mathrm{HP}-\beta-\mathrm{CD}][\mathrm{NB4}]} + \frac{1}{\Delta \varepsilon 1:1 \, [\mathrm{NB4}]} \qquad (\mathbf{1})$$

where *l* is the path length, ΔA the absorbance change, [NB4] theorical NB4 concentration, K1:1 the stability constant, $\Delta \varepsilon 1:1$ the molar absorptivity change and HP-β-CD the total cyclodextrin concentration. Absorption intensity of NB4 at constant concentration was measured at room temperature at 283 nm as function of added HP-β-CD.

Preparation of solid complexes

The inclusion complex of NB4:HP-β-CD was prepared freeze-drying method. Equimolar quantities of NB4 (0.125 g) and HP-β-CD (0.323 g) were solubilized in ethanol (150mL) and distilled water (1mL), respectively, these solutions were mixed in a flask and stirred at 600 rpm for 2 h at 50 °C. Then, the solvent removed under vacuum at 30 °C. In the next step, 50 mL of water was added to the powder formed, the orange filtrate obtained by centrifugation (4000 rpm for 10 min) was then frozen at −40 °C and freeze-dried for 72 h. The resulting material stored in bottles and kept in the refrigerator.

The physical mixture was prepared by simple blending for 30 min in a ceramic mortar pulverized powders (0.125 g of NB4 and 0.323 g of HP-β-CD). The resulting material was sieved and stored in bottles and kept in the refrigerator.

Percentage drug extract

For measuring the loading efficiency, a known amount of the freeze-dried complex (5 mg) was placed in a 25 mL volumetric flask, and methanol was then added. The mixture was shaken for 24 h. Hence, the NB4 extractable amount was obtained through its UV photometric analysis (λmax=283 nm) using the standard curve of a bunch of known NB4 concentrations. The extractions were carried out in triplicate and the drug content in the complex was obtained using the following equation:

$$\text{NB4 content in complex (\%)} = \frac{\text{masse of NB4 extracted}}{\text{mass of complex}} * 100 \qquad (2)$$

Characterization of inclusion complex

Fourier transform infrared (FTIR) spectroscopy

Formation of the inclusion complex was verified by infrared spectroscopy (FTIR, Perkin Elmer, USA) in the frequency range between 4000 and 400 cm^{-1}. The infrared spectra of NB4:HP-β-CD inclusion complexes at 1:1 loading mole ratio were recorded and analyzed in comparison with those of NB4 and HP-β-CD.

Differential scanning calorimetry (DSC)

DSC analysis for NB4, HP-β-CD and the inclusion complexes were carried out using a DSC SETARAM instrument. The samples (about 4 mg) were placed in sealed aluminum pans under nitrogen flow (20 mL/min) at a scanning rate of 10 °C/min, over the temperature range of 25 to 340 °C.

Nuclear magnetic resonance (NMR)

The ^{1}H NMR spectra were recorded at 400 MHz on a Brücker DRX 400 spectrometer in DMSO-d_6. Chemical shifts are expressed in ppm (δ) downfield from internal tetramethylsilane (TMS). The NMR spectra were processed and analyzed by MestReNova software 11.02.18153.

In silico molecular modelling studies

The molecular modeling studies of NB4 with HP-β-CD was carried out using the Schrödinger software (Schrödinger, LLC, New York) in the Maetsro module (version 9.3). Using Chem 3D Ultra, the initial geometry of HP-β-CD was constructed from the crystallographic parameters of β-CD taken from the Cambridge Structural Database (CSD). The H-atoms in the 2-OH of each glucose unit for *β*-CD were replaced with 2-hydroxypropyl groups [18].

Using the Maestro structure builder, the structure of NB4 was drawn, and the obtained structure were optimized using the LigPrep (version 3.9, Schrödinger) module. To generate the proper ionization state, LigPrep was run with the Epik (version 3.7, Schrödinger) option set to generate a possible state at target pH 7.4. Finally, the geometry optimization was carried out using the OPLS2005 force field [19]. The *"Generate Grid"* sub-application of the Glide tool allowed the generation of the grid by selecting the entire HP-β-CD structure as the receiving site to locate the coordinates of the centre of the targeted receptor cavity [20]. Then, the generated grid was configured as the NB4 docking receiver using the *"extra-precision"* (XP) flexible docking method, from the Glide tool. The binding affinity *"ΔG"* was calculated using the Prime MM-GBSA [21] module version 4.5 (Schrodinger). The properties including H-bond energy, van der Waals energy, lipophilic energy, and generalized borne electrostatic solvation energy were calculated for complexes, ligand, and receptor.

Solubility test

Solubility test was performed to determine the solubility enhancement of NB4 by the inclusion into cyclodextrin. For this purpose, samples (PM or FD) equivalent to 5 mg of NB4 soaked into 20 mL of distilled water for 5 h and stirred using magnetic stirrer at 100 rpm at room temperature. After this, solutions were filtered through 0.45 μm nylon disc filter. The obtained solution was dried under vacuum at 30 °C. In the next step, 1 mL of chloroform was added to the powder formed, and analyzed at 283 nm using UV-spectrophotometer. We noted that each experiment was done in triplicate and an average value was taken.

Results and discussion

Determination of complex stoichiometry

UV/vis spectroscopy has first been chosen for the characterization of the inclusion complex between -hydroxy propyl beta cyclodextrin and NB4. This technique allowed the determination of the stoichiometry, the stability constant(K11). The Job plots, shows a maximum at a molar ratio of 0.5 indicating a 1:1 stoichiometry of the complex (Figure 1.).
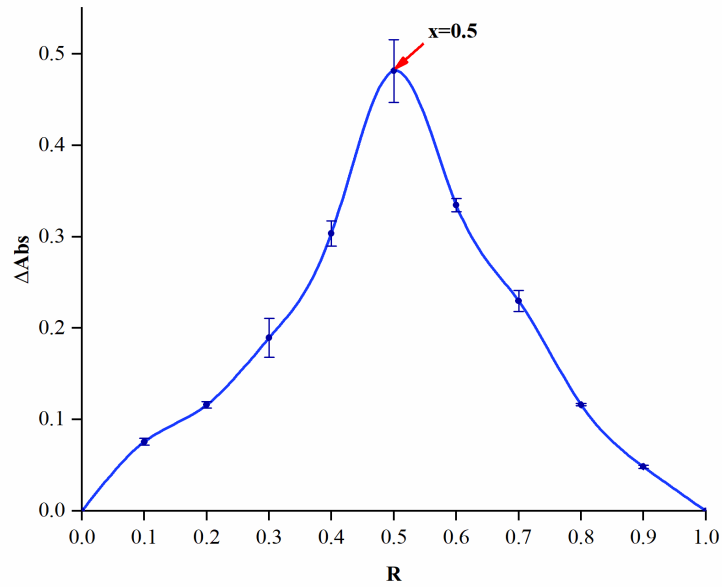
Figure 1. Continuous variation plot (Job's plot) for the complexation of NB4:HP-β-CD (25 °C).

The Benesi–Hildebrand plot was used to calculate the stability constants (Figure 2). The plot shows a good linearity (correlation coefficient from 0.996) which confirms the formation of 1:1 inclusion complex between NB4 and HP-β-CD. From the slope of the straight line, binding constant calculated as 2366 M^{-1}.
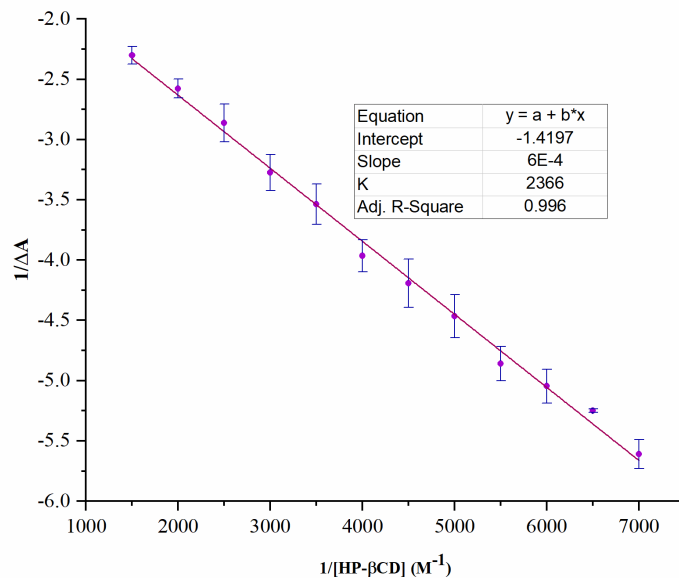
Figure 2. The Benesi–Hildebrand plot for the complexation of NB4:HP-β-CD (25 °C).

Preparation of solid complexes and loading

According to job's plot results, (1:1) NB4:HP-β-CD complexes were prepared by PM and FD methods. In all inclusion methods, loss of complexes' mass was observed. In FD method, large volumes of organic solvent and longer process causes more important loss of mass. So an experimental yield was calculated (Table 2) for FD. With an experimental loading value of 28.96%, the ratio of (1:1) NB4:HP-β-CD complex was also confirmed.

Table 2. Experimental yield and NB4 extraction from FD binary inclusion complex.

Complex	FD
Experimental yield (%)	70
Drug content (%)	34 ± 0.92
Experimental molar ratio NB4:HP-β-CD	1:1.02

Characterization of the ingredients and their complexes

Fourier transform infrared (FTIR) spectroscopy

FT-IR technique is a valuable analytical tool to analyze the possible interaction of drug with cyclodextrin molecules in the solid state. The infrared spectra of NB4:HP-β-CD inclusion complexes at 1:1 loading mole ratio were recorded and analyzed in comparison with those of NB4 and HP-β-CD (Figure 3). The FT-IR spectrum of pure NB4 showed C−H stretch, C=O stretch (cyclopentene), C=O (cyclohexene), stretch and C−Br stretch at 2934, 1712, 1658, and 650 cm^{-1}, respectively. The FT-IR spectrum of HP-β-CD showed absorption bands at 3346 cm^{-1} (O−H, stretch), 2921 cm^{-1} (C−H, stretch), and 1024 cm^{-1} (C−O−C stretch)[22].

The FTIR spectrum of the PM imitates both peaks of NB4 and HP-β-CD, which could be considered as simple superimposition of NB4 and HP-β-CD spectra. Therefore, the presence of chemical incompatibility among pure NB4 and HP-β-CD is ruled out. However, in the FTIR spectra of complexes prepared by FD, NB4 bands are almost masked by the very intense and broad HP-β-CD bands. The results indicate interactions of NB4 into the HP-β-CD cavity. The broad hydroxyl band of pure HP-β-CD at 3346 cm^{-1} is shifted to higher frequency region in the FTIR spectra for the FD complex. This last can be considered as a good indication of the inclusion complex formation. Additionally, we notice that the C=O band of NB4 at 1712 cm^{-1} is shifted to 1727 cm^{-1} in FD spectrum. In addition, a disappearance of intense bands at 1658 cm^{-1} were observed in FD complex, which corresponds to C=O stretching frequency of

cyclohexene. Overall, the binary inclusion complexes did not display any new IR peaks signifying that no chemical bonds are formed with the obtained complexes.
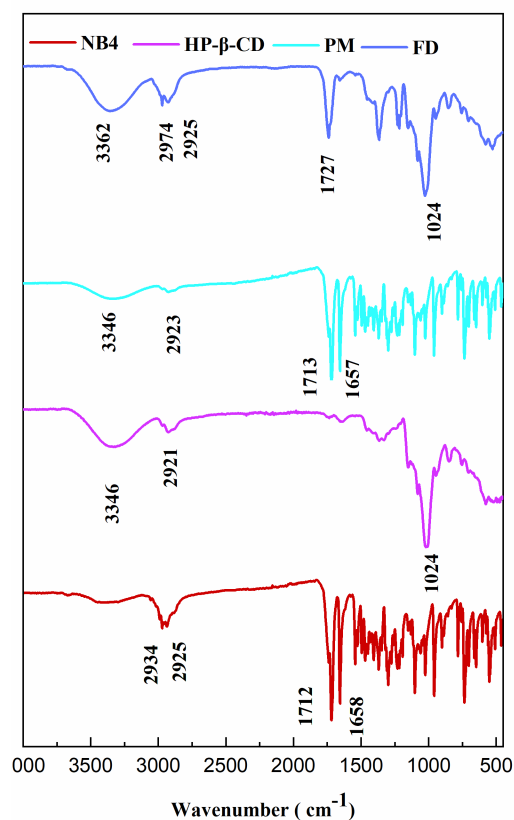
Figure 3. FT-IR spectra of NB4, HP-β-CD and NB4:HP-β-CD binary inclusion complexes.

Differential scanning calorimetric analysis

DSC curves of the pure materials, PM, and FD inclusion complex are displayed in Figure 4. NB4 showed a principal sharp endothermic peak at 305 °C corresponding to its melting point. In addition, HP-β-CD presented a large endothermic band ranging between 45-135 °C due to the loss of adsorbed water molecules and an endothermic band at 352 °C corresponding to its decomposition temperature[23]. On the other hand, the thermogram of PM and FD binary inclusion complexes illustrate the characteristic endothermic peak of the NB4 with reduced sharpness and intensity as compared to the pure drug, indicating an incomplete inclusion of the drug in the HP-β-CD cavity. Furthermore, it should be noted that the degradation temperature of both NB4 and HP-β-CD in the PM and FD inclusion complexes determined by DSC is different than that of pure materials. This in turn referred to the formation of inclusion complexes.
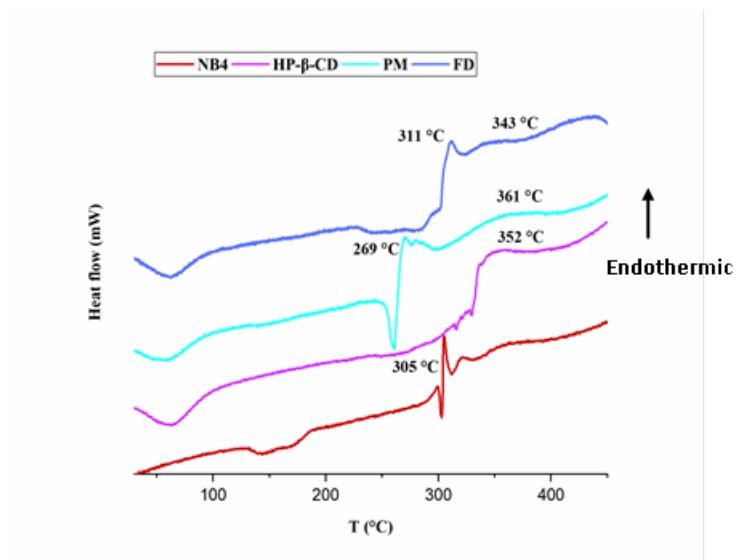
Figure 4. DSC thermograms of NB4, HP-β-CD and NB4:HP-β-CD binary inclusion complexes.

Nuclear magnetic resonance (NMR)

Inclusion of a guest molecule into the hydrophobic cavity of a cyclodextrin molecule generally modifies the environment of the protons of the guest moiety which is included and of the host cavity. Therefore, ^{1}H NMR can provide direct information on the complex structure from the comparison of the proton chemical shifts observed for the guest/host mixture with those found for the individual species. ^{1}H NMR spectrum of HP-β-CD shows signals at the δ value of 0.86 (H-1), 3.46 (H-2), 3.76 (H-3), 3.31 (H-4), 3.58 (H-5), 3.56 (H-6), 3.23 (H-7), 3.61 (H-8) and 1.03 ppm (H-9) (Figure S1)[24]. ^{1}H NMR spectrum of NB4 displays signals at 0.86, 3.05, 2.09, 2.40 and 1.58 ppm attributed to H-1, H-2, H-3, H-4 and H-5, respectively (Figure. S2). However, in order to confirm the inclusion of NB4 into HP-β-CD, a comparison of the ^{1}H NMR spectra of HP-β-CD in the presence or absence of NB4 (Figures S3-S4) is necessary. Then chemical inclusion shifts (CIS) were calculated and listed in Table 3. (CIS with δ_{host}).

In FD inclusion complex (Table 3) we could see the signals disappearance of H-1, H-6 and H-7. In addition, the H-4 and H-5 shift in the outer surface changed by approximately −0.05 and 0.02 ppm, respectively. While significant chemical shift changes were exhibited by H-3

proton in the inner surface of HP-β-CD with a field shift of -0.13 ppm. All these variations clearly indicate that the guest-host interaction results in chemical shift changes. It is noteworthy that the chemical shift variation for H-5 (0.01) was smaller than H-3 after resulting FD inclusion complex. Since both H-3 and H-5 protons from each sugar unit are located in the internal cavity of HP-β-CD, and H-3 protons are near the wide side of the cavity while H-5 protons near the narrow side (Bernini, 2004), we can propose from the ^{1}H NMR data that NB4 was interacted in the HP-β-CD outer surface of the wide side and with Hydroxypropyl moiety.

On the other hand, a smal shift observed on the H2, H4 and H6 protons of HP-β-CD when the PM method is used to get the corresponding inclusion complex. This last can be considered as a simple interaction of NB4 and HP-β-CD.

Table 3.^{1}H NMR Chemical shifts (δ, ppm) for protons of HP-β-CD alone (δ_{host}) and their complexation induced shifts (CIS = $\delta_{complex} - \delta_{host}$) in DMSO-$d_6$ at 25 °C.

HP- β-CD Protons	δhost	CIS (FD)	CIS (PM)
H-1	5.03	-	0
H-2	3.46	-0.05	0.01
H-3	3.76	-0.13	0
H-4	3.31	0.02	0.05
H-5	3.58	0.01	0
H-6	3.56	-	0.06
H-7	3.23	-	0
H-8	3.61	0	0
H-9	1.03	0.01	0

In silico molecular modelling studies

The molecular docking was used to explore the interaction of HP-β-CD with NB4 in the inclusion complex. The best pose of NB4 in inclusion complexes is illustrated in Figure 5.
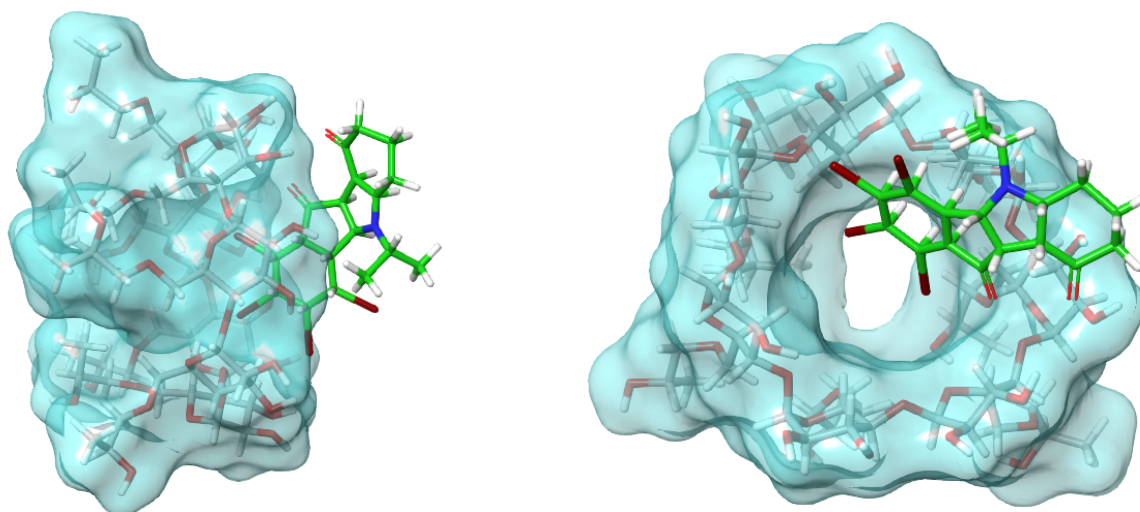
Figure 5. Docking binding poses of the inclusion complexes.

The Prime MM-GBSA method estimates the energy based on the difference in solvent accessible surface area. The "ΔG Bind" is a measure of binding affinity, calculated considering strain energy terms of the ligand and the host. The binding affinity (GLIDE emodel), van der Waals energy and docking score for the inclusion of NB4 in HP-β-CD are -28.363 kcal mol^{-1}, -23.155 kcal mol^{-1} and -5.234 kcal mol^{-1}, respectively (Table 4). Furthermore, the molecular docking showed low hydrogen bond, probably because most of the forces involved in its complexation are Van der Walls interactions.

Table 4. Prime MM-GBSA Calculations

Molar ratio	ΔG values in Kcal/mol				
	Glide emodel	ΔG bind docking score	ΔG bind Lipo	ΔG bind vdw	ΔG bind Hbond
1:1	-28.363	-5.234	-2.456	-23.155	-0.038

ΔG bind, free energy of binding; ΔG bind Hbond, free energy of binding from hydrogen bonding; ΔG bind Lipo, free energy of binding from lipophilic binding; ΔG bind vdW, free energy of binding from van der Waals energy.

However, for complex stabilisation, contribution (from Van der Waals interaction) it takes higher value compared to lipophilic and hydrogen bonding interactions for all binary complexes Table 5.

Table 5. Electrostatic, binding, Kinetic and Dielectric (solvation) energy of NB4:HP-β-CD inclusion complex in vacuum condition.

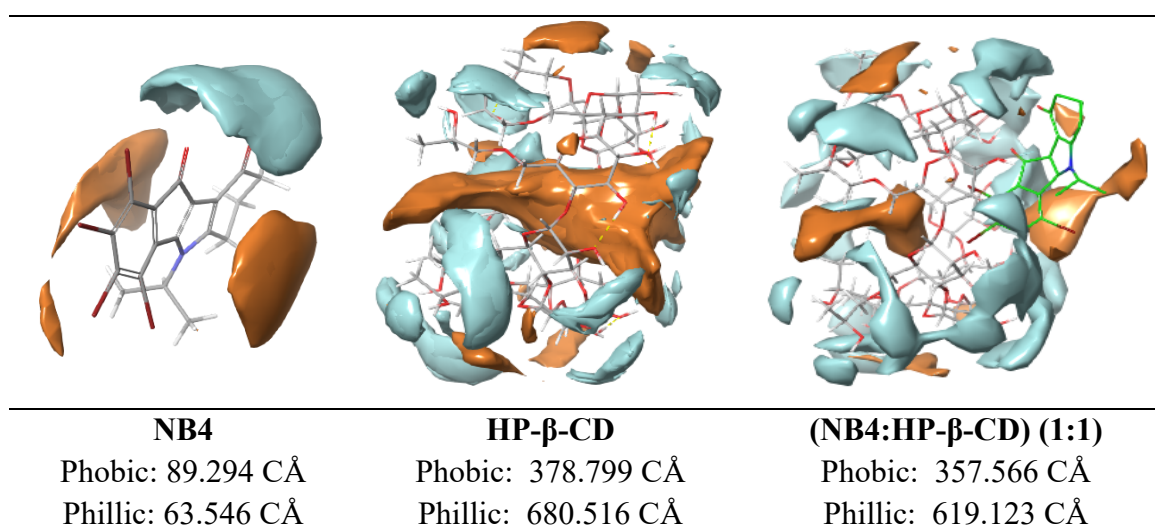| Molar ratio atio	E (Kcal/mol)			
	Electrostatic	Binding energy	Kinetic	Dielectric (solvation) energy
1:1	13.019	-28695.326	-82.325	-116.325

Figure 6. shows details of the hydrophobic and hydrophilic surface areas of NB4, the HP-β-CD, and the complexes. It is evident from Figure 6. that the hydrophilic area increased upon formation of the complex, and it further improved upon addition of NB4 which could be the reason for the observed better complexation efficiency (CE).

NB4	HP-β-CD	(NB4:HP-β-CD) (1:1)
Phobic: 89.294 CÅ	Phobic: 378.799 CÅ	Phobic: 357.566 CÅ
Phillic: 63.546 CÅ	Phillic: 680.516 CÅ	Phillic: 619.123 CÅ

Figure 6. Hydrophobic (brown) and hydrophilic (blue) surface area of NB4, HP-β-CD and HP-β-CD: NB4 binary inclusion complexes (CÅ, cubic Angstroms).

Solubility test

The solubility test of binary complexes exhibit a enhancement in NB4 dissolution properties. FD complex dissolved in water very well, indicating that the complex was water soluble at this concentration.PM did not dissolve in water, and an orange solid residue was observed at the bottom of the vial. After analysis with UV the quantity of NB4 is 4,8 and 0.01mg for FD and PM, respectively. These results suggest that the solubility of NB4 was improved by complexation with HP-β-CD especially with FD method. This enhancement may be due to

partial trapping of the NB4 in HP-β-CD verified by molecular modeling, FTIR, DSC and 1H NMR experiments.

Conclusion

In this work, the job's plot experiment were used to determine the stoichiometry of the NB4:HP-β-CD complex. Inclusion complexes of NB4:HP-β-CD in the 1:1 molar ratio were prepared using PM and FD methods. FTIR and NMR studies showed no evidence of chemical reactions between the NB4 and HP-β-CD. DSC experiment and molecular modeling approach confirmed partial inclusion of NB4 into HP-β-CD. These results suggest an enhanced dissolution profile compared to the pure NB4. FD showed a significant improvement of the NB4 dissolution.

References

1. Pinna, L. A. Protein kinase CK2: a challenge to canons. *J Cell Sci* **115**, 3873–3878 (2002).
2. Guerra, B. & Issinger, O.-G. Protein kinase CK2 in human diseases. *Curr Med Chem* **15**, 1870–1886 (2008).
3. Kaminska, B. *et al.* Efficacy and mechanism of anti-tumor action of new potential CK2 inhibitors toward glioblastoma cells. *International Journal of Oncology* **35**, 1091–1100 (2009).
4. Rabjerg, M. *et al.* Nuclear localization of the CK2α-subunit correlates with poor prognosis in clear cell renal cell carcinoma. *Oncotarget* **8**, 1613–1627 (2016).
5. Götz, C., Gratz, A., Kucklaender, U. & Jose, J. TF--a novel cell-permeable and selective inhibitor of human protein kinase CK2 induces apoptosis in the prostate cancer cell line LNCaP. *Biochim Biophys Acta* **1820**, 970–977 (2012).
6. Hamacher, R. *et al.* Casein kinase II inhibition induces apoptosis in pancreatic cancer cells. *Oncol Rep* **18**, 695–701 (2007).
7. Piazza, F. *et al.* Protein kinase CK2 in hematologic malignancies: reliance on a pivotal cell survival regulator by oncogenic signaling pathways. *Leukemia* **26**, 1174–1179 (2012).
8. Yu, W. *et al.* The phosphorylation of SEPT2 on Ser218 by casein kinase 2 is important to hepatoma carcinoma cell proliferation. *Mol Cell Biochem* **325**, 61–67 (2009).
9. Borgo, C., D'Amore, C., Sarno, S., Salvi, M. & Ruzzene, M. Protein kinase CK2: a potential therapeutic target for diverse human diseases. *Signal Transduct Target Ther* **6**, 183 (2021).
10. Choi, Y. H. & Yu, A.-M. ABC Transporters in Multidrug Resistance and Pharmacokinetics, and Strategies for Drug Development. *Curr Pharm Des* **20**, 793–807 (2014).
11. Baker, S. J. & Reddy, E. P. TARGETED INHIBITION OF KINASES IN CANCER THERAPY. *Mt Sinai J Med* **77**, 573–586 (2010).
12. Senapati, S., Mahanta, A. K., Kumar, S. & Maiti, P. Controlled drug delivery vehicles for cancer treatment and their performance. *Signal Transduct Target Ther* **3**, 7 (2018).
13. Hundsdörfer, C. *et al.* Indeno[1,2-b]indole derivatives as a novel class of potent human protein kinase CK2 inhibitors. *Bioorg Med Chem* **20**, 2282–2289 (2012).
14. Davis, M. E. & Brewster, M. E. Cyclodextrin-based pharmaceutics: past, present and future. *Nat Rev Drug Discov* **3**, 1023–1035 (2004).
15. Kim, D.-H., Lee, S.-E., Pyo, Y.-C., Tran, P. & Park, J.-S. Solubility enhancement and application of cyclodextrins in local drug delivery. *J. Pharm. Investig.* **50**, 17–27 (2020).
16. Qiu, N. *et al.* Inclusion complex of barbigerone with hydroxypropyl-β-cyclodextrin: Preparation and in vitro evaluation. *Carbohydrate Polymers* **101**, 623–630 (2014).
17. Taupitz, T., Dressman, J. B., Buchanan, C. M. & Klein, S. Cyclodextrin-water soluble polymer ternary complexes enhance the solubility and dissolution behaviour of poorly soluble drugs. Case example: Itraconazole. *European Journal of Pharmaceutics and Biopharmaceutics* **83**, 378–387 (2013).
18. Shi, J., Su, Y. & Jiang, W. Enantioseparation and chiral recognition of α-cyclohexylmandelic acid and methyl α-cyclohexylmandelate on hydroxypropyl-β-cyclodextrin as chiral selector: HPLC and molecular modeling. *J Chromatogr Sci* **51**, 8–16 (2013).
19. Jorgensen, W. L. & Tirado-Rives, J. The OPLS [optimized potentials for liquid simulations] potential functions for proteins, energy minimizations for crystals of cyclic peptides and crambin. *J. Am. Chem. Soc.* **110**, 1657–1666 (1988).

20. Friesner, R. A. *et al.* Glide: A New Approach for Rapid, Accurate Docking and Scoring. 1. Method and Assessment of Docking Accuracy. *J. Med. Chem.* **47**, 1739–1749 (2004).

21. Mulakala, C. & Viswanadhan, V. N. Could MM-GBSA be accurate enough for calculation of absolute protein/ligand binding free energies? *J Mol Graph Model* **46**, 41–51 (2013).

22. Lin, S.-Y., Hsu, C.-H. & Sheu, M.-T. Curve-fitting FTIR studies of loratadine/hydroxypropyl-β-cyclodextrin inclusion complex induced by co-grinding process. *Journal of Pharmaceutical and Biomedical Analysis* **53**, 799–803 (2010).

23. Yang, B., Lin, J., Chen, Y. & Liu, Y. Artemether/hydroxypropyl-β-cyclodextrin host–guest system: Characterization, phase-solubility and inclusion mode. *Bioorganic & Medicinal Chemistry* **17**, 6311–6317 (2009).

24. Chen, T. C., Yu, S.-C., Hsu, C.-M., Tsai, F.-J. & Tsai, Y. Minoxidil–2-hydroxypropyl-β-cyclodextrin inclusion complexes: characterization and in vivo evaluation of an aqueous solution for hair growth in rats. *J Incl Phenom Macrocycl Chem* **88**, 27–34 (2017).

Supplementary information for the publication: Solubility Enhancement of a New Inhibitor of the Ser/Thr Kinase CK2 by Inclusion Complexation with Hydroxypropyl-β-Cyclodextrin: A Joint Experimental and Theoretical Investigation
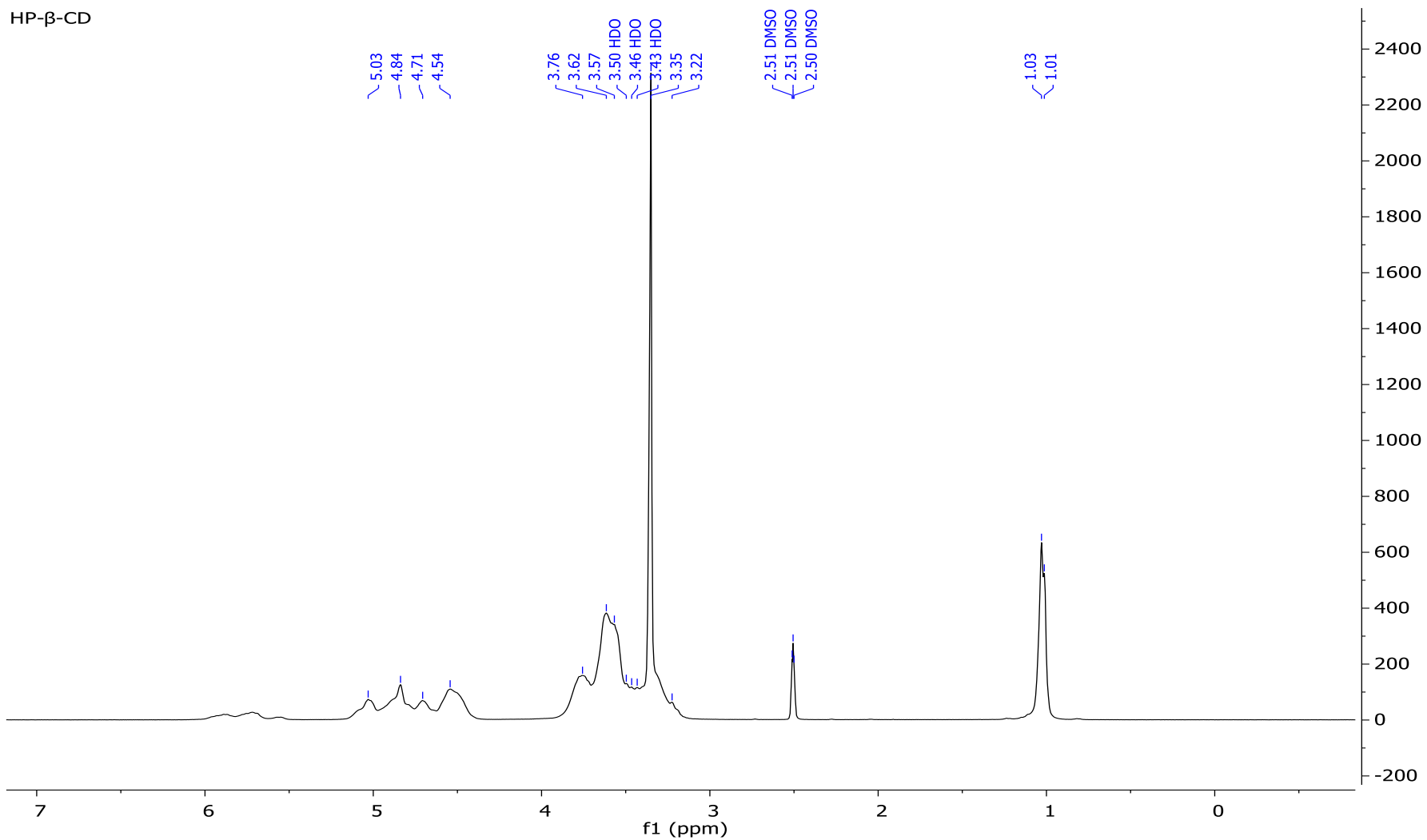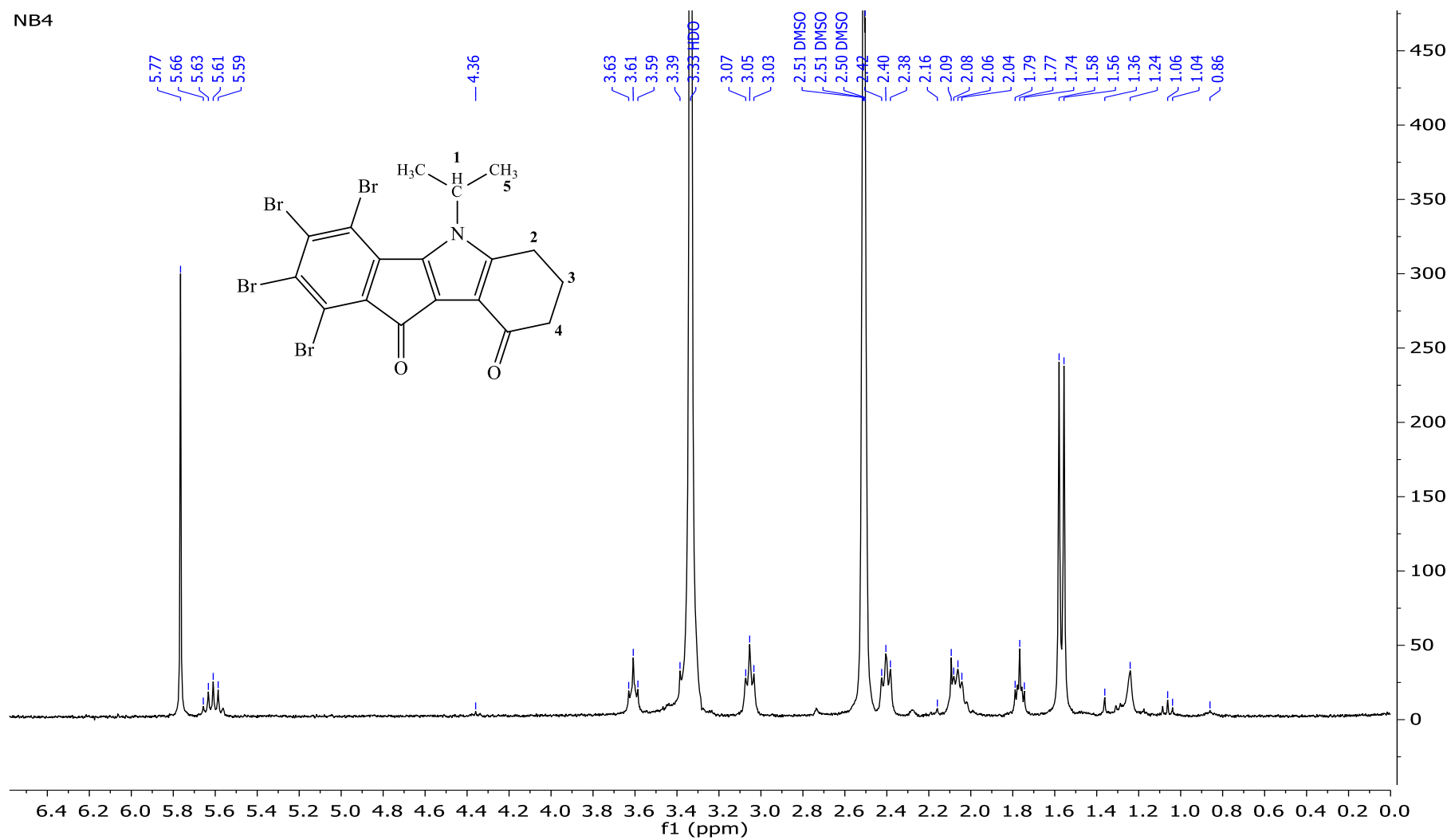
HP-β-CD

Figure S1. ^{1}H NMR Spectrum of HP-β-CD.
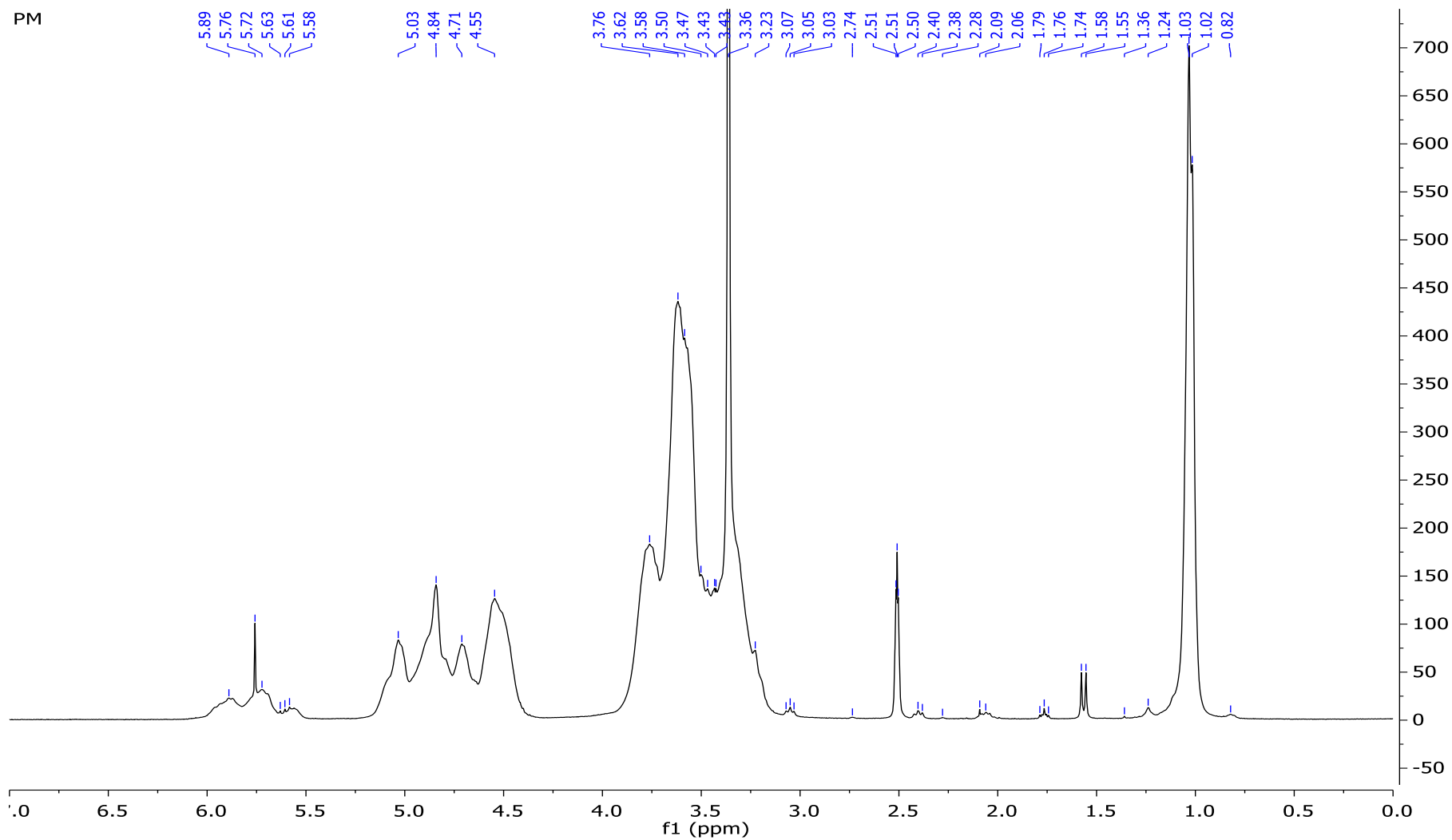
Figure S2. ^{1}H NMR Spectrum of NB4.

Figure S3. ^{1}H NMR Spectrum of PM inclusion complex.
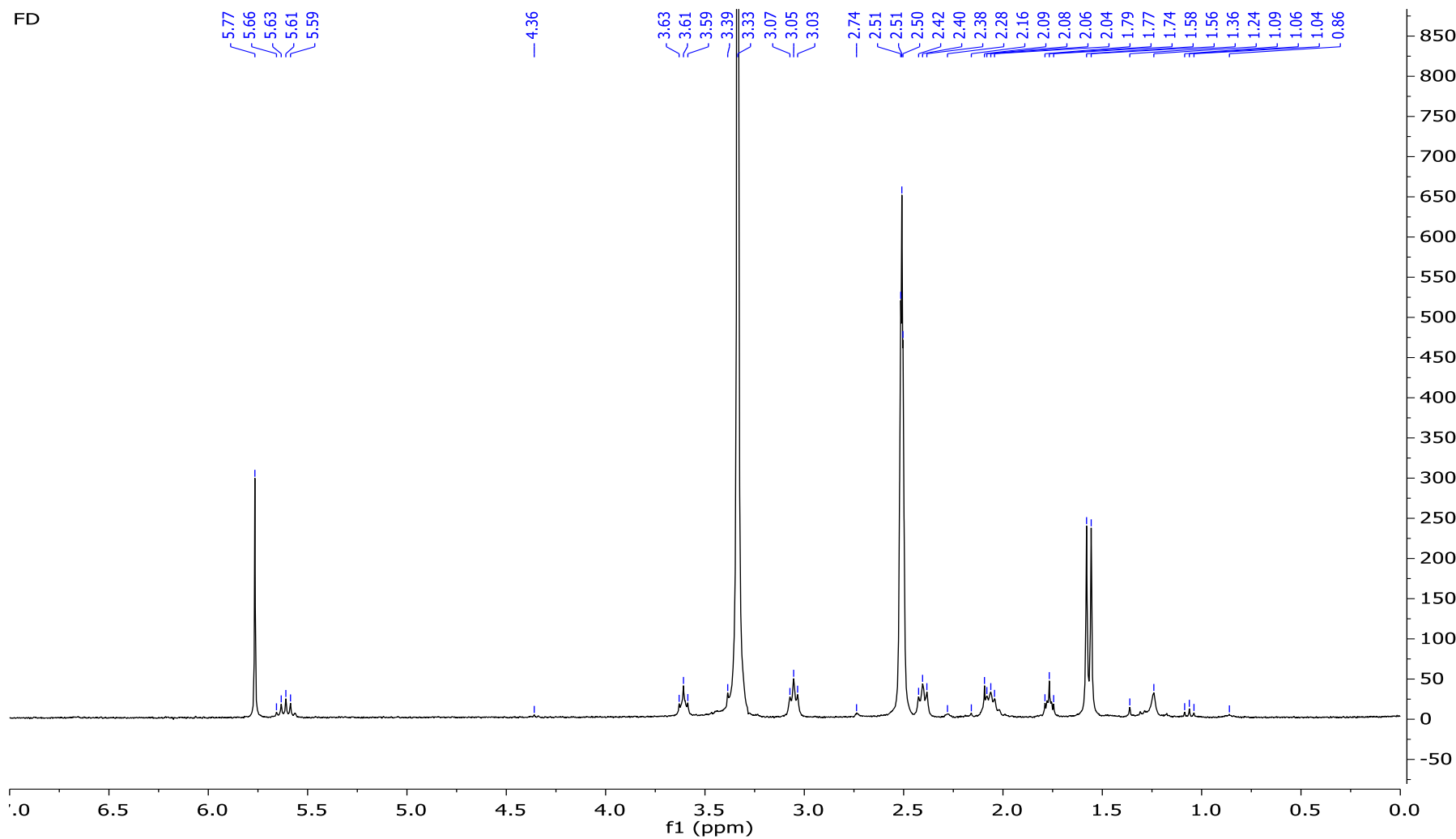
Figure S4. ^{1}H NMR Spectrum of FD inclusion complex.

Chapter III

Controlled release of active pharmaceutical ingredients

III.1 Introduction

From the earliest times, people have found ways to introduce drugs into the body. This process began with the chewing of leaves and roots of medicinal plants. Throughout the history of medicine delivery of drugs to humans has evolved from primitive extracts and inhalants to more reliable dosages forms, such as injections, tablets and capsules. These drug delivery systems are expected to be further optimized to increase drug activity and reduce toxicity. Drug delivery systems can influence the performance of a drug by manipulating its concentration, location and duration of exposure. Therefore, in controlled drug delivery systems, the active agent is released in a predesigned manner [1].

In the past 30 years, controlled drug delivery technology has represented one of the most rapidly advancing research areas [2]. The field is driven by the belief that controlled drug delivery will contribute significantly to human health. These drug delivery systems offer numerous advantages compared to conventional dosage forms [3]:

- ✓ Increasing the efficacy of currently used drugs
- ✓ Providing opportunities for the use of new agents currently precluded from clinical use due to challenges including low drug solubility and systemic toxicity
- ✓ Reducing harmful side effects
- ✓ Precise control of dose
- ✓ Decreasing number of dosages
- ✓ Improving patient compliance and convenience

III.2 Strategy of controlled release

In the conventional drug delivery, the drug concentration in the blood rises when drug is taken, then peaks and declines. Since each drug has a plasma level above which it is toxic and below which it is ineffective, the plasma drug concentration in a patient at a particular time depends on the compliance with the prescribed routine. In contrast, with controlled release systems, the drug concentration is within the therapeutic range for a longer time. This release pattern is highly beneficial for drugs that are rapidly metabolized and eliminated from the body after administration.

The second approach is to prepare feedback-controlled devices that release the appropriate amount of drug in response to a therapeutic marker. In recent years, several research

groups have been developing responsive systems [4]. These systems can be classified as external regulated and self regulated systems. The external controlled devices apply external triggers for pulsed delivery such as: magnetic, ultrasonic, thermal and electric triggers. In the self-regulated system, the release rate is controlled by feedback information. The self-regulated systems utilize several approaches such as pH-sensitive polymers, enzyme substrate reactions and competitive binding, as rate-control mechanisms.

The third strategy is to control drug distribution in the body. The idea is to deliver a drug to the precise location in the body where it will be most effective. There are two basic types of targeting systems: passive and active. Passive targeting systems rely on non-specific interactions such as hydrophobic or electrostatic interactions, and the body physical characteristics. The size of drug carriers has been extensively studied for passive targeting. It was found that particles larger than 5-7 μm in diameter usually become trapped in the lung [5] and particles smaller than 1 μm in diameter rapidly phagocytosed by the Kupffer cells of the liver [6]. When the particle size is reduced below 100 nm, the particles can appear in the bone marrow [7]. It was also demonstrated that drug carriers small than 200 nm can be accumulated efficiently in tumor through enhanced permeability and retention (EPR) effect due to the abnormality of tumor tissue, resulting in the enhanced vascular permeability compared to healthy tissues [8]. On the other hand, active targeting systems utilize specific interactions, such as antigen-antibody and ligand receptor binding, to achieve specific targeting goals. In this approach, the therapeutic index of drugs could be enhanced by keeping drugs away from healthy cells. The types of receptors that have been utilized for this purpose include transferrin receptors (tumor cells) [9], folate receptors (tumor cells) [10], albumin receptors (cardiac and lung) [11] and growth factors receptors [12].

While these fundamental ideas of controlled drug delivery are extremely attractive, achieving controlled drug delivery is not a simple or straightforward task. Currently, the vast majority of the work in this area is focusing on liposomes, micelles, drug conjugates, and nanoparticles.

In our work, halloysite nanotubes were chosen as a drug carrier for a sustained drug delivery system because of their characteristics already mentioned in chapter 1.

III.3. References

[1] M.S. Alqahtani, M. Kazi, M.A. Alsenaidy, M.Z. Ahmad, Advances in Oral Drug Delivery, Frontiers in Pharmacology. 12 (2021) 62. https://doi.org/10.3389/fphar.2021.618411.

[2] K. Park, The Controlled Drug Delivery Systems: Past Forward and Future Back, J Control Release. 190 (2014) 3–8. https://doi.org/10.1016/j.jconrel.2014.03.054.

[3] C. Li, J. Wang, Y. Wang, H. Gao, G. Wei, Y. Huang, H. Yu, Y. Gan, Y. Wang, L. Mei, H. Chen, H. Hu, Z. Zhang, Y. Jin, Recent progress in drug delivery, Acta Pharmaceutica Sinica B. 9 (2019) 1145–1162. https://doi.org/10.1016/j.apsb.2019.08.003.

[4] J.K. Patra, G. Das, L.F. Fraceto, E.V.R. Campos, M. del P. Rodriguez-Torres, L.S. Acosta-Torres, L.A. Diaz-Torres, R. Grillo, M.K. Swamy, S. Sharma, S. Habtemariam, H.-S. Shin, Nano based drug delivery systems: recent developments and future prospects, Journal of Nanobiotechnology. 16 (2018) 71. https://doi.org/10.1186/s12951-018-0392-8.

[5] M.F. Attia, N. Anton, J. Wallyn, Z. Omran, T.F. Vandamme, An overview of active and passive targeting strategies to improve the nanocarriers efficiency to tumour sites, Journal of Pharmacy and Pharmacology. 71 (2019) 1185–1198. https://doi.org/10.1111/jphp.13098.

[6] C.I. Colino, J.M. Lanao, C. Gutierrez-Millan, Targeting of Hepatic Macrophages by Therapeutic Nanoparticles, Front Immunol. 11 (2020) 218. https://doi.org/10.3389/fimmu.2020.00218.

[7] M. Longmire, P.L. Choyke, H. Kobayashi, Clearance Properties of Nano-sized Particles and Molecules as Imaging Agents: Considerations and Caveats, Nanomedicine (Lond). 3 (2008) 703–717. https://doi.org/10.2217/17435889.3.5.703.

[8] S.K. Golombek, J.-N. May, B. Theek, L. Appold, N. Drude, F. Kiessling, T. Lammers, Tumor Targeting via EPR: Strategies to Enhance Patient Responses, Adv Drug Deliv Rev. 130 (2018) 17–38. https://doi.org/10.1016/j.addr.2018.07.007.

[9] L. Woythe, N.B. Tito, L. Albertazzi, A quantitative view on multivalent nanomedicine targeting, Advanced Drug Delivery Reviews. 169 (2021) 1–21. https://doi.org/10.1016/j.addr.2020.11.010.

[10] B. Frigerio, C. Bizzoni, G. Jansen, C.P. Leamon, G.J. Peters, P.S. Low, L.H. Matherly, M. Figini, Folate receptors and transporters: biological role and diagnostic/therapeutic targets in cancer and other diseases, Journal of Experimental & Clinical Cancer Research. 38 (2019) 125. https://doi.org/10.1186/s13046-019-1123-1.

[11] M.T. Larsen, M. Kuhlmann, M.L. Hvam, K.A. Howard, Albumin-based drug delivery: harnessing nature to cure disease, Mol Cell Ther. 4 (2016) 3. https://doi.org/10.1186/s40591-016-0048-8.

[12] A. Bafico, S.A. Aaronson, Classification of Growth Factors and Their Receptors, Holland-Frei Cancer Medicine. 6th Edition. (2003). https://www.ncbi.nlm.nih.gov/books/NBK12423/ (accessed November 26, 2021).

III.3 Publication: Experimental and theoretical studies of the interaction of ketoprofen in halloysite nanotubes

Graphical Abstract
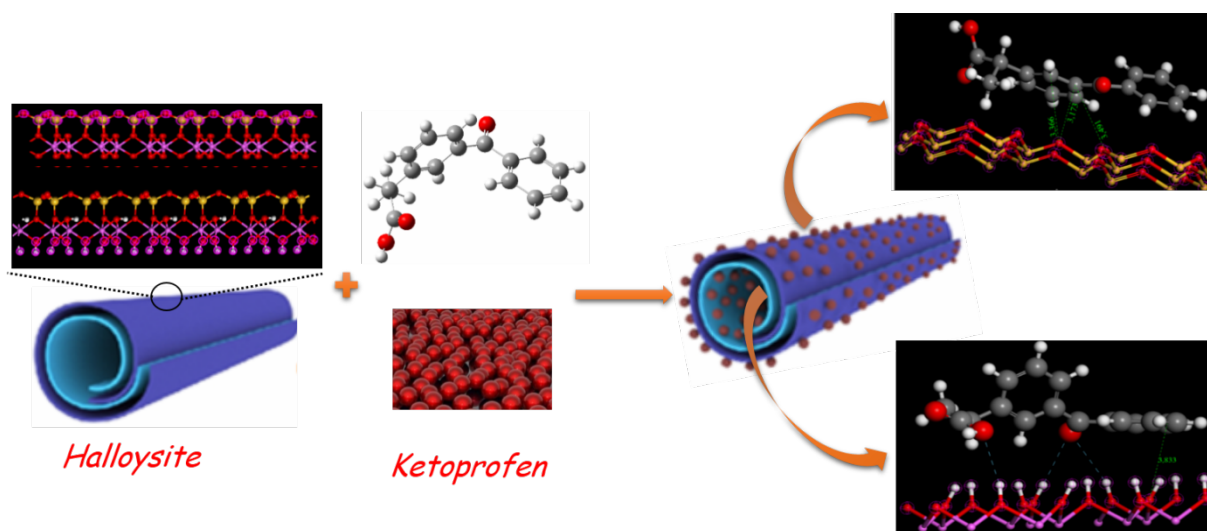
Highlights

- Halloysite was used as a drug carrier for the loading of ketoprofen
- Ketoprofen was successfully loaded to the halloysite with high entrapment efficiency
- The resulting materials were characterized by Zeta potential, N_2 adsorption, XRD, TEM, FTIR, TGA/DSC.
- The classical atomistic molecular simulation method was used for investigated the interaction mechanism between ketoprofen and the halloysite nanotubes.

Abstract

In recent years, the application of halloysite (HAL) in the conception of drug systems has become important due to its excellent physicochemical properties. Ketoprofen (KET) is widely used around the world as an anti-inflammatory drug. A formulation of HAL-KET was prepared. The interaction between the KET molecules and HAL has been investigated experimentally by Zeta potential, TEM, XRD, FTIR spectroscopy and TGA/DSC. In addition, this interaction was studied theoretically by using Monte-Carlo calculation method (MC). The results have shown that the interaction of KET is stabilized not only by electrostatic interactions and hydrogen

bonds with HAL but also via the delocalized π electrons density of phenyl groups of KET and the hydrogen atoms of HAL.

Keywords: Halloysite; Ketoprofen; interaction; Characterization; Molecular modeling; Pharmaceutical carrier

1. Introduction

Ketoprofen (KET) is well known by its analgesic, anti-inflammatory and antipyretic properties. It is indicated mainly for the symptomatic treatment of pain and inflammation of osteoarthritis and rheumatoid arthritis [1]. The main drawbacks for the KET are low bioavailability, large number of gastrointestinal side effects, short biological half-life and poor-water solubility [2]. Many researchers made attempts to solve these problems by designing new carriers to achieve controlled and prolonged release property [3–6].

Halloysite (HAL) is a clay mineral, physically and chemically analogous to kaolinite. HAL is characterized by a hollow nanotubular structure and composed by rolled kaolinite sheets [7]. The external diameter of the HAL tubes is from 50 to 200 nm with an internal diameter of 5 to 30 nm and a length of 0.5 to 25 μm. HAL nanotubes contain multiple rolled aluminosilicate layers [8]. HAL mainly occurs in two different form, the hydrated form (basal distance around 1.0 nm) with the formula $Al_2Si_2O_5 (OH)_4.nH_2O$ and the dehydrated form (basal distance about 0.7 nm) with the formula $Al_2Si_2O_5(OH)_4$, identical to kaolinite. The outer surface of HAL nanotubes is composed mainly of negatively charged SiO_2 and an inner surface composed of positively charged Al_2O_3. In addition, HAL nanotubes have a high specific surface area, good thermal stability, low cost and ability of loading drugs [9–12]. From these characteristics, HAL nanotubes have been widely used as supports for the loading and release of pharmaceutical agents as: 5-aminosalicylic acid [13], ibuprofen [14], diclofenac [15], dexamethasone[16], nifedipine [17], furosemide [18], resveratrol [19], diphenhydramine [20], 5-fluorouracil [21], paclitaxel [22], isoniazide [23], irinotecan [24], Pyrazole [3,4-*d*] pyrimidine derivatives [25], but not much molecular modelling work has been done on the mechanism of interaction of these pharmaceutical agents and HAL nanotubes.

Molecular modeling is a method that has been used to predict the mechanism of interaction between molecules with solid surfaces [26], such as the mechanisms of adsorption of metals, organic compounds or biomolecules on mineral surfaces. In the pharmaceutical field, molecular simulations have been used to study the mechanisms and interactions between

therapeutically active species and biologically inactive materials that can be used as carriers in drug delivery systems [27].

This work will focus on the physico-chemical characterization of KET, HAL and KET loaded HAL (HAL-KET) by TEM, XRD, FTIR and TGA/DSC techniques and will specify the interaction energies of KET on HAL adsorption sites in the presence and absence of water by applying the Monte-Carlo calculation method (MC) and we will correlate between the experimental results and those obtained by MC method. To our best knowledge, the study of the interaction between KET and HAL has not been previously reported.

2. Materials and Methods

2.1. Materials

The raw halloysite sample was directly collected from a mine of Djebbel Debbagh (Guelma, Algeria), ground, sieved and dried at 100°C for 24 h. The product was labeled as HAL-R. The drug ketoprofen (abbreviated as KET) (Formula: $C_{16}H_{14}O_3$, CAS number 22071-45-4, M_W: 254.3 g/mol, pKa=4.4, log K_{OW}=3.00, solubility in water at 25°C (S_W=21mg/L)) was supplied from SALEM Laboratories El-Eulma, Algeria. All reagents are used as received.

2.2. Halloysite Purification

In order to purify the HAL-R [28], 20 g of this sample is dispersed in 1L of distilled water and stirred for 24 h and then centrifuged at 5000 rpm for 5 min. The obtained precipitate was washed with 2 L of 0.1 M HCl under strong agitation and at room temperature for 4 h in order to remove the carbonates. Afterward, the obtained precipitate was repeatedly washed with distilled water and centrifuged successively for at least five centrifugations until the supernatant became neutral. For removing the organic matter, the solid residue is added to a solution of oxygenated water (10% v/v) and stirred overnight at room temperature. Then, the residual hydrogen peroxide is degraded by heating under the temperature of 70 °C for 30 min. The precipitate is washed with hot water and dried at 60°C for 24 h and stored in bottles. The resultant sample was denoted as HAL.

2.3. Ketoprofen loading

In order to obtain a saturated solution, 1g of KET was added in 250 mL of water. Then, 1 g of HAL was dispersed into this solution and mixed to obtain a homogeneous suspension. The suspension was placed in vacuum for 4 cycles, each for 30 min allowing air bubbles to be removed from HAL pores, which is generally indicated by a slight fizzing of the solution. Once

the vacuum is broken, the solution enters the lumen to ensure maximum loading **[29]**. The sample was removed and washed triply with 200 ml of water to remove excess drug not adsorbed. The sample denoted HAL-KET was dried at 60°C overnight and powdered.

2.4. Characterization techniques

The chemical composition of halloysite before and after purification was determined by X-ray fluorescence (XRF) using (Rigaku primus IV apparatus, Japan).

The zeta potential of the halloysite dispersion, versus pH, was measured using nano particle analyzer sz-100 (Horiba Scientific, Japan). In addition, the pH_{PZC} of halloysite was measured using the pH drift method **[30] (Fig. not shown).**

Nitrogen gas adsorption–desorption isotherms were measured using a Micromeritics Tristar 3000 instrument at 77 K. The measurements were made after degassing the samples under vacuum at 200°C for 3 h. The specific surface areas are determined according to the BET method at the relative pressure in the range of 0.05–0.35 **[31].** The total pore volume, V_{pore}, was directly determined from the Nitrogen adsorption at $P/P_o = 0.98$.

The analysis of the microstructures of HAL and HAL-KET were performed with Transmission Electronic Microscopy (TEM) using JEOL 1400 Flash apparatus, operating with an accelerating voltage of 120 kV. A droplet of 5 µl of HAL nanoparticles dispersed in distilled water was deposited onto a carbon coated copper grid (CF200-CU UL EMS). Excess solution was carefully blotted off using filter paper and air-dried at room temperature during one night for imaging. To obtain right distributions, more than 100 halloysite crystals dimensions were considered.

The structure of HAL-R, HAL, KET and HAL-KET samples was determined by XRD measurement (Bruker D8 advance diffractometer operating at 40 kV as acceleration tension and 30 mA as courant with Cu Kα1 radiation (λ=0.1542 nm)). Radial scans were recorded in the reflection scanning mode from 5 to 80° (2θ) with a scanning rate of 10 ° ·min^{-1}. Bragg's law, defined as nλ = 2d sinθ, was used to compute the interreticular distances (d) for the examined clay samples.

The infrared spectra of HAL, KET and HAL-KET were obtained using Fourier transformed infrared spectroscopy (FTIR-8400S Shimadzu (Japan) spectrophotometer from 400 to 4000 cm^{-1}, using KBr pellets technique.

Loading efficiency was determined using thermogravimetric analysis (TGA/DSC) on an EXTAR 6000 thermal analyzer (Seiko, Mahwa, NJ, USA) under nitrogen atmosphere at heating rate of 10 °C min^{-1}, from 30 to 900 °C.

2.5. Calculation methods

The chemical calculations were performed employing three softwares, Gaussian 9.5 W, the Forcite modulus and the Adsorption locator modulus included in Materials Studio software packages.

The geometrical optimizations of the KET and the water molecules were carried out with Gaussian 9.5W based on the Density Functional theory (DFT) with Beck's three parameter hybrid exchange Lee–Yang–Parr correlation (B3LYP) in conjunction with 6-31G (d, p) basis set [32,33]. Those parameters are well adapted for the small molecular structures [34–36]. To get more reliable data, the effect of the solvent was considered, which was defining as the water molecules.

The HAL has the same crystalline structure as kaolinite and morphologically, the planar form of HAL is comparable to that of kaolinite [7]. The lamellar kaolinite structure was developed using the crystallographic parameters defined in the AMCSD file 0012232. In order to develop the modeling of the adsorption, supercells of kaolinite (001) and (00-1) with the dimensions (1.5466 x 2.6834 x 1.1513 nm corresponding to 3 x 3 x 2 unit cells, these dimensions correspond to the ratio: 1 molecule of KET to 9 surface unit cell of kaolinite) **(Figure.1)** and 12 nm as vacuum slab are chosen which respecting the periodic boundary conditions at the interfaces. Those dimensions are largely sufficient to host the KET and the waters molecules. The geometrical optimization of the supercells was performed using Forcite modulus, based on classical theory; Universal Forcefield type and the ultrafine convergence criteria were used on basis set definitions.
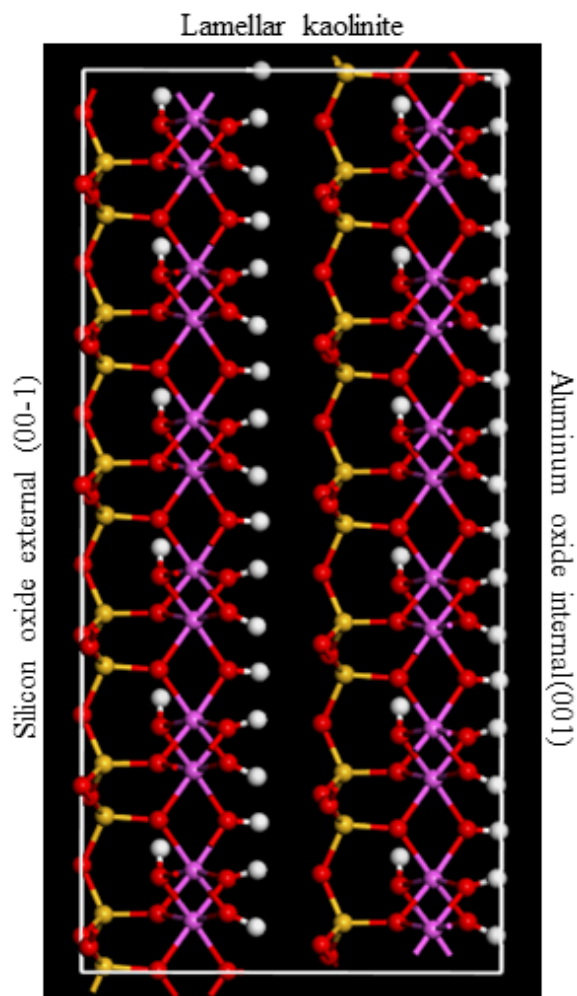
Figure 1: Supercell of kaolinite structure in the direction (001) (3 x 3 x 2).

Finally, the adsorption was modeled by the means of the canonical Molecular Dynamic Simulation (MDS), using adsorption locator modulus based on Monte Carlo (MC) theory, starting from the geometrical optimization of the pristine materials (KET and HAL substrate). A normal thermodynamic ensemble and a temperature of 25 ºC (this temperature is close to experimental one) were fixed. The equilibrium configurations were performed using the neutral charge of the both adsorbent and adsorbate, which considering the zero charge point of the system. The time step was 0.1 fs and the simulation time was 1 ns, moreover, the geometrical optimization of the adsorbed molecule was considered after 10 cycles and 100000 steps by cycle which taken at every step, $2*10^{-5}$ Kcal·mol^{-1} as cut off energy, 10^{-3} Kcal·mol^{-1}.Å^{-1} as max. force and 10^{-6} nm as max. displacement. The adsorption was simulated in the vacuum slab under 1.2 nm distance from the substrate.

3. Results and discussion

3.1. Experimental investigation

Chemical analyses of halloysite before (HAL-R) and after purification (HAL) are listed in **Table 1.** Purification shows an increase in the content of SiO_2 and decrease in the content of Al_2O_3. The ratio of SiO_2/Al_2O_3 increased slightly from 1.20 to 1.29. The decrease in the alumina content in the HAL can be ascribed to the leaching of Al ions from the octahedral layer due to hydrolysis under purification by acid. This dealumination is accompanied by the reduction of impurities CaO, Fe_2O_3, K_2O and MnO_2.

Table 1: Chemical composition of HAL-R and HAL

	SiO2	Al_2O_3	CaO	Fe_2O_3	K_2O	MgO	MnO	Na_2O	SiO_2/Al_2O_3	Others
HAL-R	49.8	41.4	0.713	0.593	0.586	0.0995	2.35	0.21	1.20	traces
HAL	52.4	40.7	0.174	0.521	0.482	0.105	2.09	0.27	1.29	traces

Zeta potential measurements of HAL (1g/L) are performed within the pH ranging from 2 to 11 **(Figure 2)**. This figure shows that the surface of the HAL was positively charged at very low pH and an increasingly negative value at the pH rises. The isoelectric point of HAL is around 3.6.
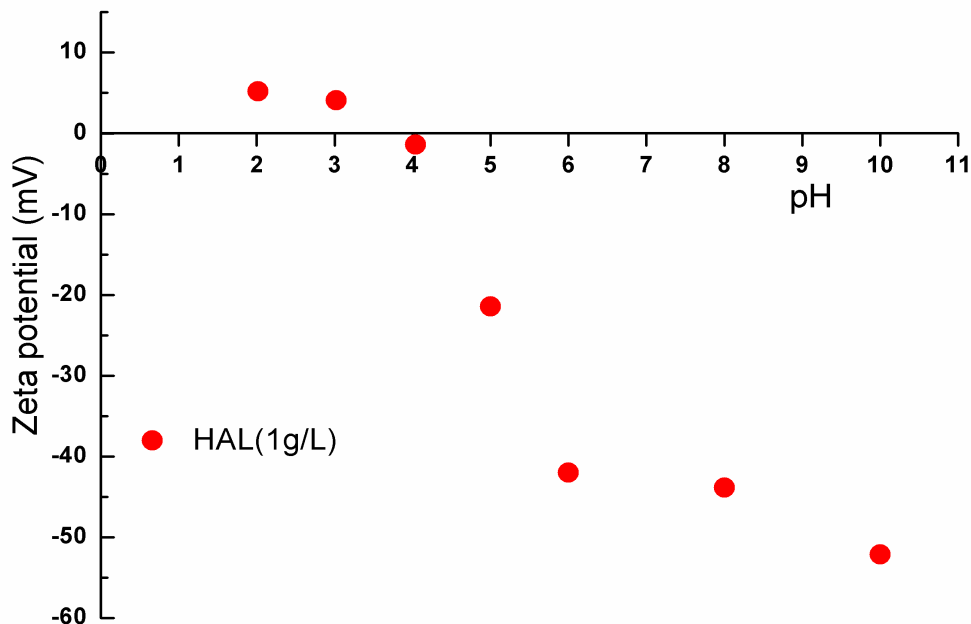

Figure.2: Zeta potential of HAL versus pH

The adsorption- desorption isotherms of HAL-R and HAL are presented in **Figure 3**. The isotherms of these samples are classified as type IV isotherms with H3 hysteresis loops **[37].**

This type of isotherm is a typical characteristic of mesopores structures. The S_{BET} and V_{pore} values of HAL-R and HAL are (150.3 m^2/g, 0.212 cm^3/g) and (191.2 m^2/g, 0.208 cm^3/g), respectively.
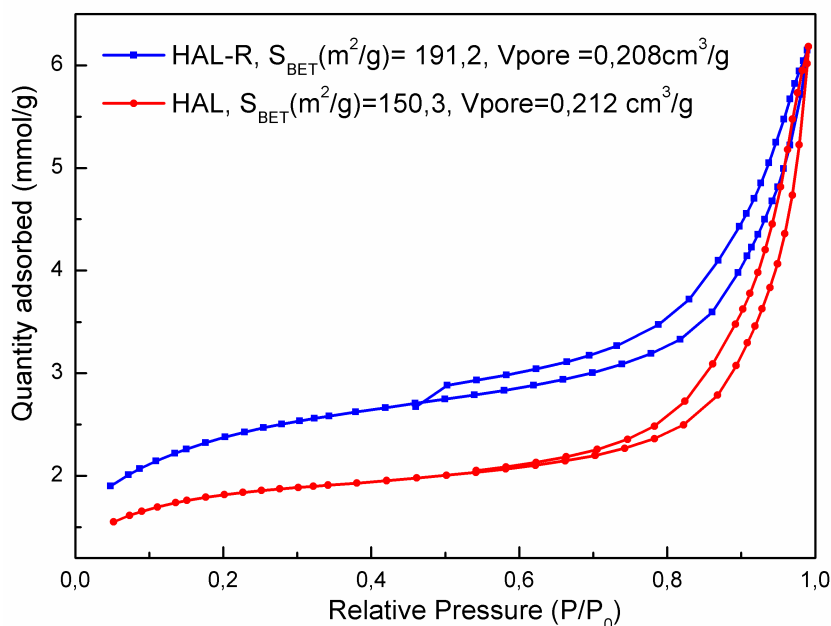
Figure 3: N$_2$ adsorption/desorption isotherms of HAL-R and HAL

The TEM images of HAL and HAL-KET are shown in **Figure 4**. The TEM images of HAL **(Figures 4a-c)** consist of various sizes of nanotubular shapes, the length of the HAL is comprise from 40 to 1300 nm, this result conforms to the conventional values of these clay minerals that are comprised between 20 and 2000 nm **[7]**. After addition of KET, the central part of the HAL lumen and outer surface of the nanotubes became darker which proves that the KET molecules were adsorbed on the internal and external surfaces, respectively **(Figures 4d-f)**.
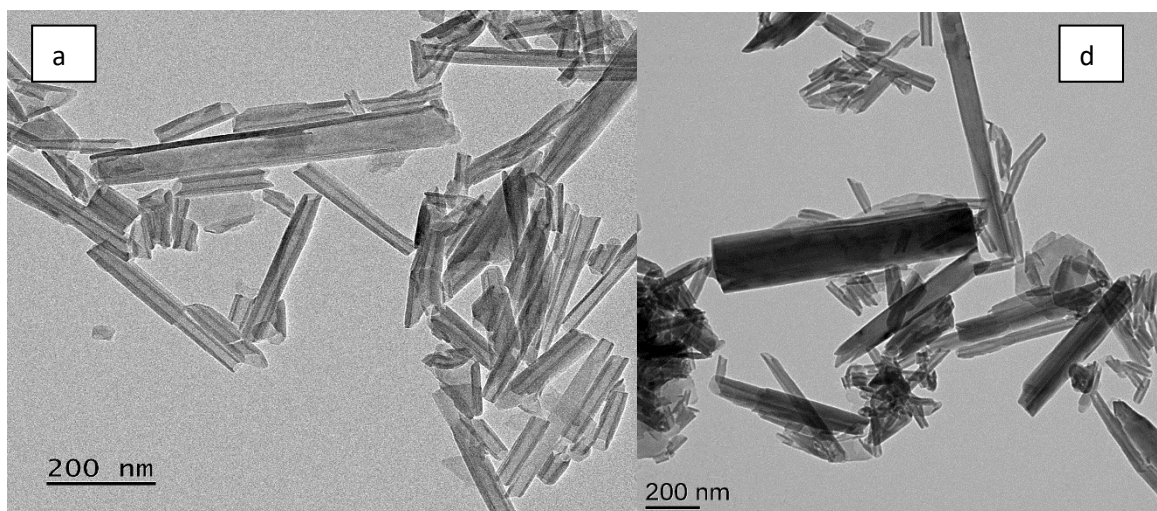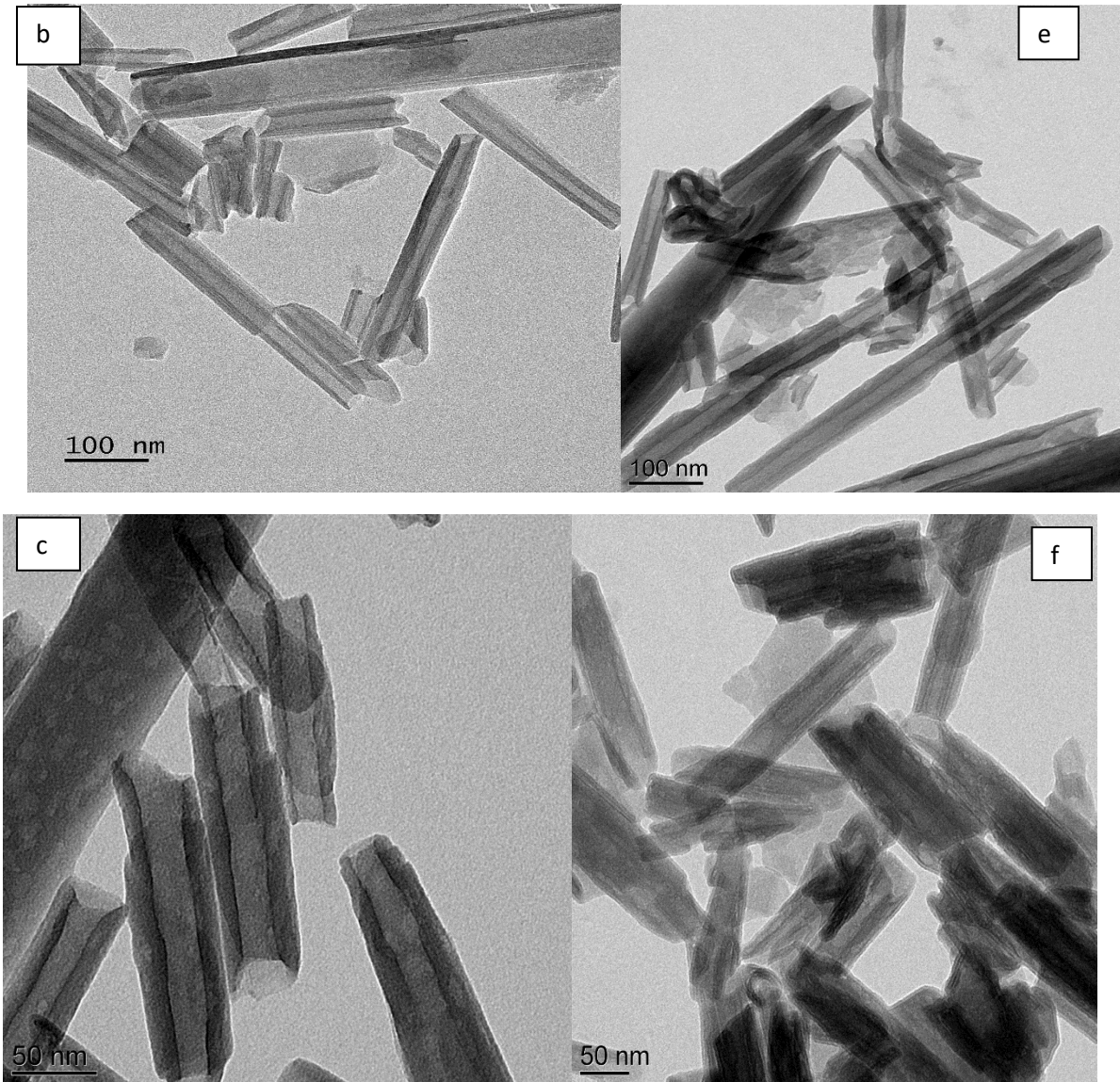
Figure 4: TEM images of (a, b, c) HAL and (d, e, f) HAL-KET

The **Figures 5a-b** presents the distribution of the external diameters of HAL-KET and HAL. They show that deposit is almost homogeneous, and the average external diameter estimated by the fit by Gaussian function is 35 ± 13 nm and 43 ± 13 nm with a width at mid-height of 25 and 25 nm respectively for HAL and HAL-KET. The estimated thickness of KET deposited on the outer surface in a homogeneous manner is about (43 - 35)/2= 4 nm. In addition, the **Figures 4d-f** shows that the lumen volume of HAL is filled by the KET molecules.
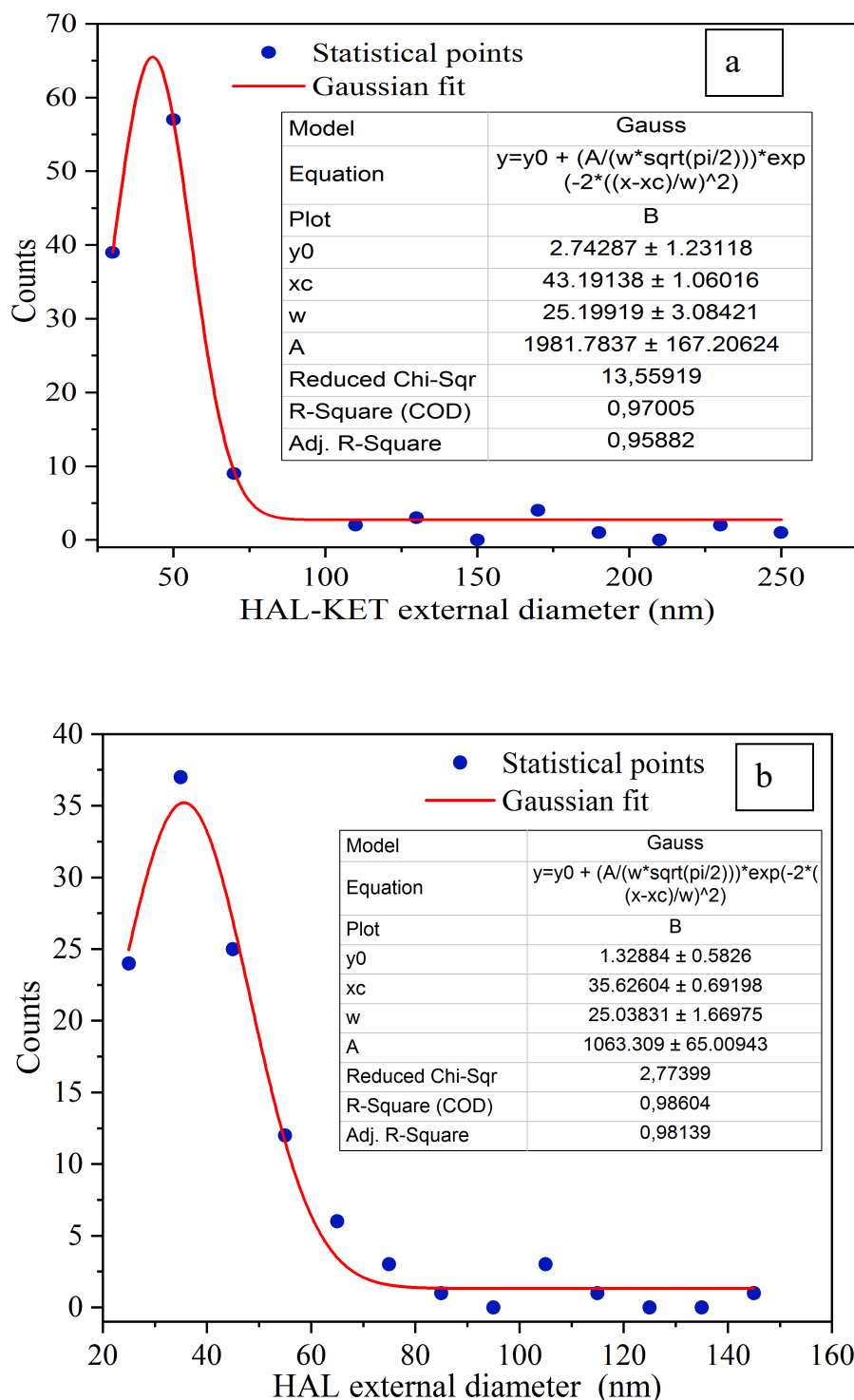
Figure 5: Distribution of the external diameters of (a) HAL-KET and (b) HAL

In order to modulate the adsorption of KET into HAL, the average internal diameter of the empty volume of the nanotubes of HAL-KET and HAL (considering the deposit homogenous) is estimated **(Figures.6c-d)**. The found values respectively are 16 ± 3 nm and 8 ± 3 nm which were obtained from the fit by Gaussian function of the diameter distribution, so the estimation of the average deposited homogeneous thickness is about $(16 - 8)/2 = 4$ nm.
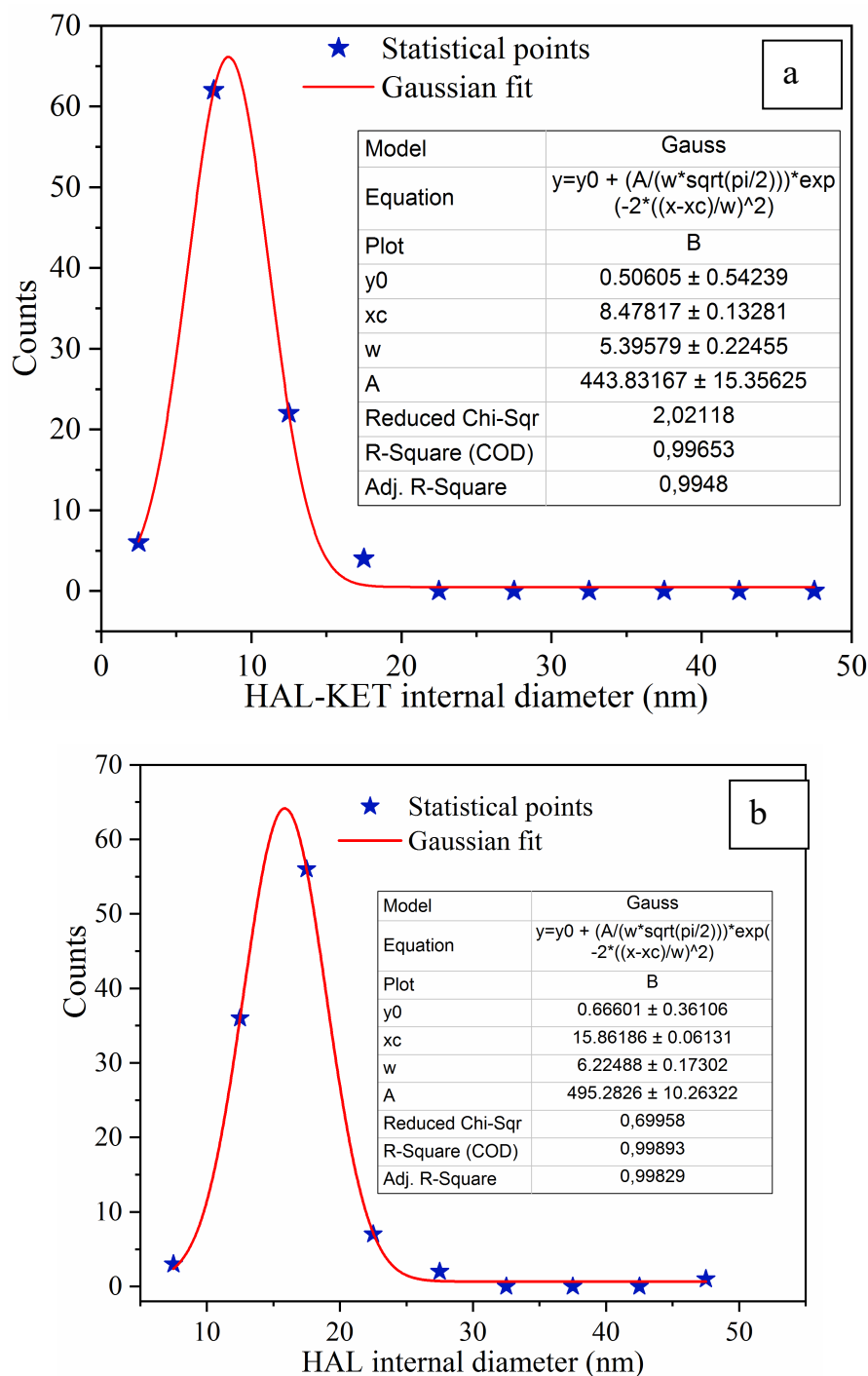
Figure 6: Distribution of the internal diameters of (a) HAL-KET and (b) HAL

The XRD patterns of HAL-R, HAL, KET and HAL-KET are shown in **Figure.7**. According to the XRD patterns, the pattern of HAL shows the characteristic diffraction peaks at the angular positions $2\theta=12.25, 20.24, 24.97, 35.27, 36.19, 55.31$ and 62.59 °, corresponding respectively to the Miller indices of the reticular planes: (001), (020), (002), (003), (200), (211) and (-3-31) **[38]**. The crystalline phases of quartz, carbonate, alumina and cristobalite are also

observed in the HAL-R and HAL samples but in small quantities in a trace **[39,40]**.The interreticular distances d $_{(001)}$=0.723 and d $_{(020)}$= 0.440 nm are characteristic of the dehydrated phase of HAL (Al$_2$Si$_2$O$_5$) that has a tubular morphology **[7]**. Otherwise, the KET exhibits diffraction peaks at the angular positions 13.48, 14.78, 17.68, 23.25, 28.13 and 32.94 ° because its crystallinity However, these characteristic peaks disappeared in KET loaded HAL (HAL-KET) which indicates that the KET changes its state from crystalline to amorphous nature. These results show as well that KET molecules were diluted in the HAL structure. This conclusion is consistent with the previous studied on drug-loaded HAL **[14,41,42]**. In addition, the KET is not intercalated between layers because the basal spacing of halloysite with KET anions is the same like in HAL sample, see **Figure 7.**
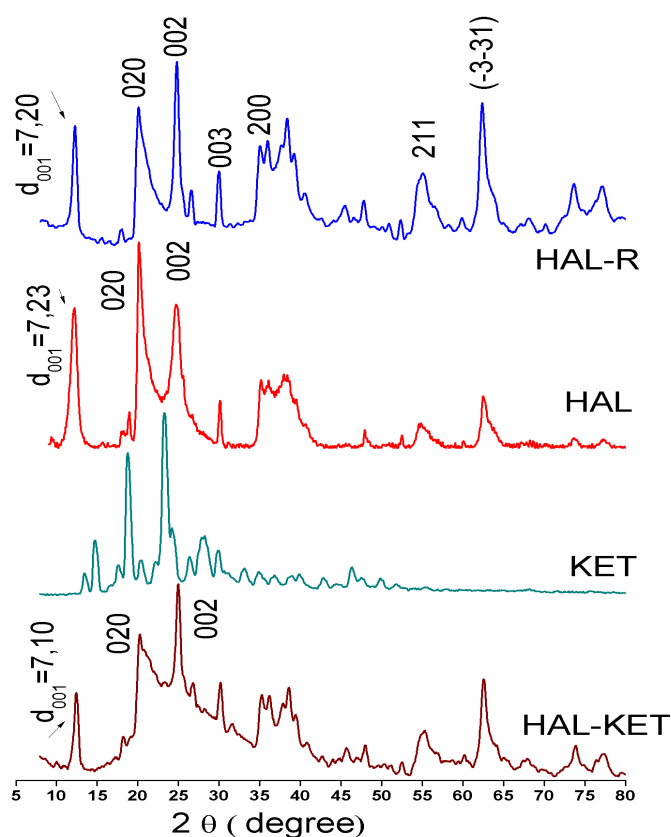
Figure 7: XRD patterns of HAL-R, HAL, KET and HAL-KET provided by the main characteristic plane Miller indices

The interaction between KET and HAL was studied by FTIR spectroscopy, as shown in the **Figure 8**. The spectrum of the HAL shows two bands centered at 3692 and 3626 cm^{-1}, belonging to the hydroxyl region (3000–4000 cm^{-1}), they were attributed to the stretching vibrations of inner-surface of Al$_2$-OH groups and the deformation vibration of interlayer water,

respectively. In addition, the wide bands centered at 3464 cm^{-1} and weak at 1639 cm^{-1} were attributed to the stretching and OH deformation vibration modes of the physically adsorbed water, respectively. The groups at 1090 and 1029 cm^{-1} correspond to the stretching vibrations of Si-O in the plane and Si-O-Si, respectively. The band at 916 cm^{-1} was attributed to the O-H deformation of the internal hydroxyl groups and that at 793 cm^{-1} was caused by a symmetrical stretching vibration of Si-O. The bands at 752 and 687 cm^{-1} were attributed to the perpendicular Si-O stretching vibrations. The three remaining bands at 540, 470 and 437 cm^{-1} can be attributed to the deformation vibrations of the groups Al-O-Si, Si-O-Si, and Si-O, respectively [43]. The FTIR spectrum of KET shows characteristic adsorption peaks at 3500 cm^{-1} due to O–H stretching and the bands at 2970 and 2930 cm^{-1} are due to C–H stretching asymmetric and symmetric of the methyl group respectively. Moreover, there was a stretching band at 1698 cm^{-1} (for C=C stretching of carboxylic acid), 1654 cm^{-1} (for ketone group attached to two aromatic rings), 1598 cm^{-1} and 1440 cm^{-1} (for C=C stretching from the aromatic ring), 1321 cm^{-1} (for CH deformation of CH$_3$ symmetrical), 1281 cm^{-1} (for C=C deformation of aromatic rings) [44]. Regarding the FTIR spectrum of HAL-KET sample, it was clear that the characteristic peaks of HAL were maintained, the presence of new peaks at the frequencies 1691 cm^{-1} (C=C stretching of carboxylic acid), 1660 cm^{-1} (C=O group), 1450 cm^{-1} (C=C stretching from the aromatic ring) and 1290 cm^{-1}(C=C deformation of aromatic rings), belonging to KET, prove the interaction of KET with HAL. Comparative results were found during the intercalation of KET on mesoporous silica nanoparticles [45].
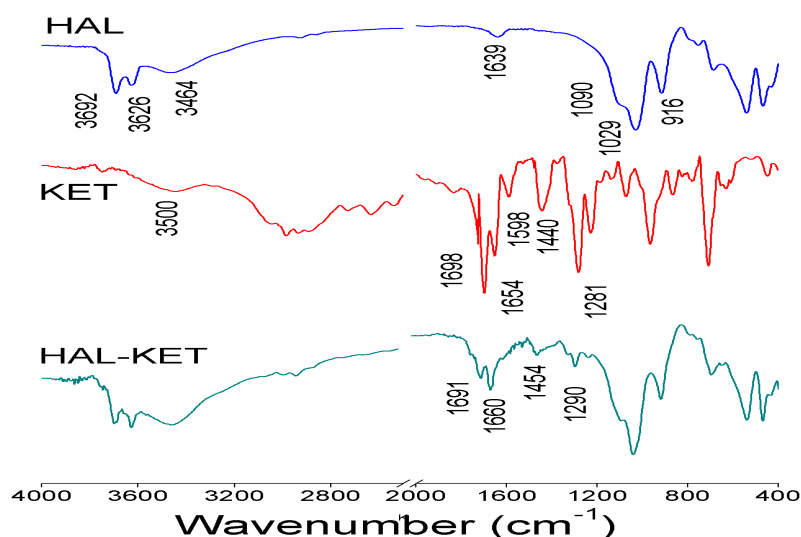

Figure 8: FTIR spectra of HAL, KET and HALKET samples

The thermal gravimetric analysis curves (TGA) of the HAL, KET and HAL-KET samples obtained under nitrogen atmosphere are shown in **Figure 9**. The TGA analysis for the HAL shows two significant mass losses clearly observed. The first mass loss takes place from 25 to 400 °C attributed to the dehydration of physically adsorbed water and interlamelar residual water. The second loss of mass between 400 and 600 °C can be attributed to the dehydratation of hydroxyl groups (Al-OH and Si-OH groups on HAL) **[46]**. This result is comparable to that observed in the literature concerning the dehydroxylation of HAL between 400 and 600 °C **[47]**.The TGA curve of KET shows thermal decompositions between 217-394 °C with a single mass loss, centered at 319°C. The TGA profiles indicate that KET are stable up to 167 and that there are no mass losses for KET before this temperature. The thermogram of HAL-KET can be seen as a superposition of thermograms of the pristine materials. The mass losses of HAL in HAL-KET show the same profiles as that of pure HAL, however the degradation profiles of KET change. Loading efficiency of KET (wt %) was calculated by the difference between the total weight loss of KET loaded HAL and unloaded HAL samples. According to following formula: loading efficiency (%)= W_1-W_0 (where W_1 and W_0 represent the % weight loss of KET loaded into HAL and the weight loss of unloaded HAL at 450 °C, respectively. The total mass losses obtained at T=450 °C for HAL and HAL-KET are 7.04 % and 24.96 %, respectively. The loading efficiency of KET in HAL is estimated to be 17.92%. This amount adsorbed on internal and external surfaces of HAL is close to the HAL loaded by drugs mentioned in the literature **[29]**. It should be noted that the degradation temperature of KET in the HAL-KET determined by DSC is different than that of pure KET **(Figure 9)**.
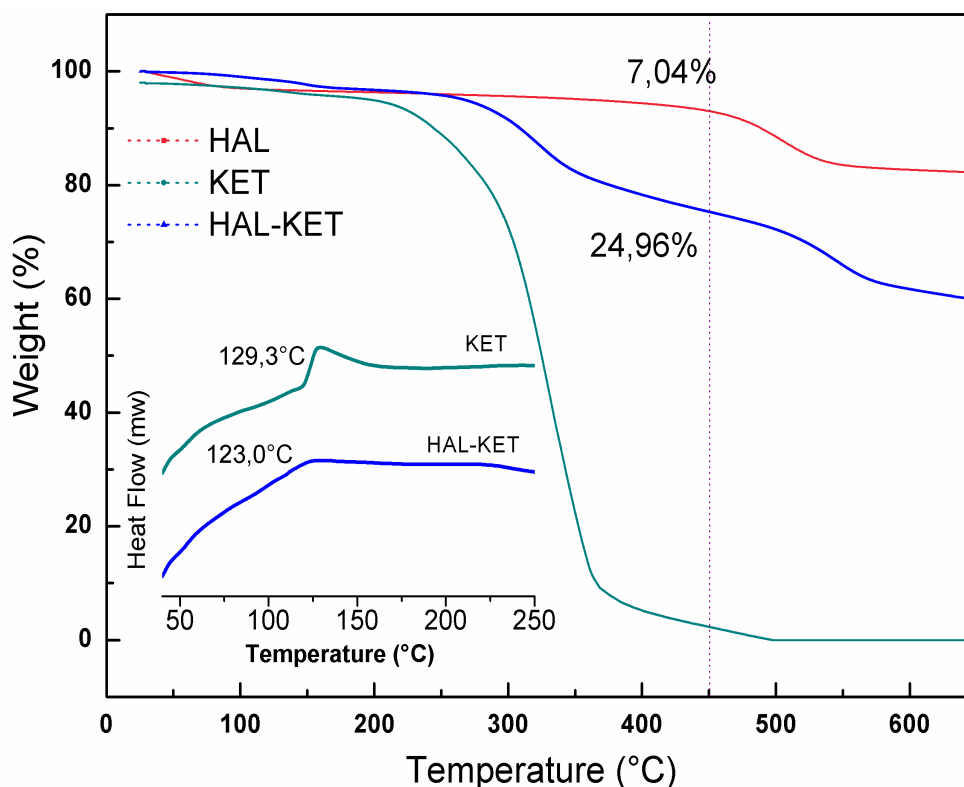
Figure 9: TG analysis of HAL, KET, and HAL-KET and DSC curve

The endothermic peak attributed to the KET melting in the HAL-KET sample shifts to lower values centered at 123 °C. The diminution of the value of the melting point may be attributed to the interaction of KET with HAL and the formation of amorphous phase of KET **[24,42]**, the low intensity of the signal is due probably to a dilution phenomenon. The XRD pattern of HAL-KET also confirms this claim where no peaks associated to KET were observed **(Figure 7)**.

3.2. Theoretical investigation

3.2.1. Equilibrium configurations
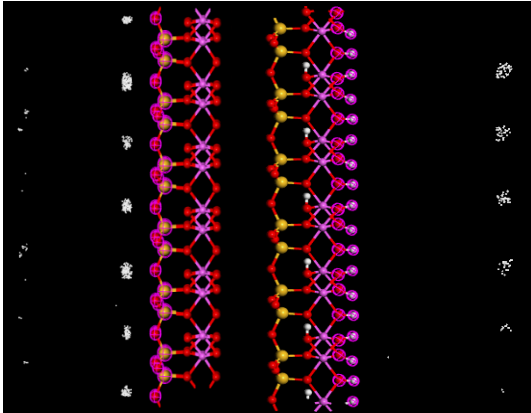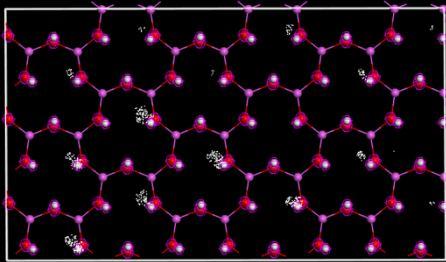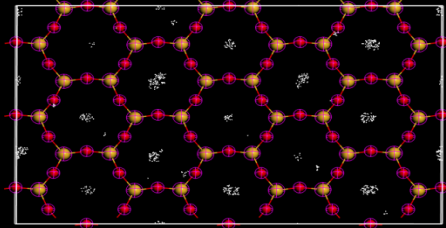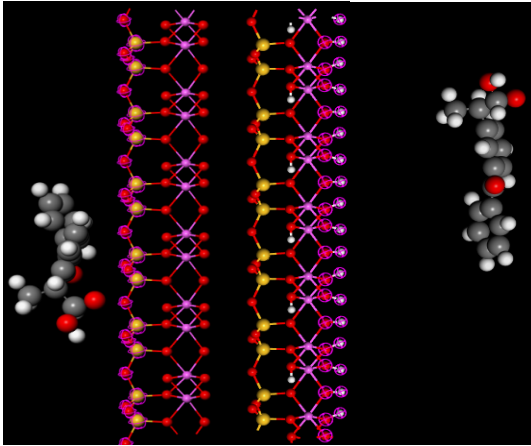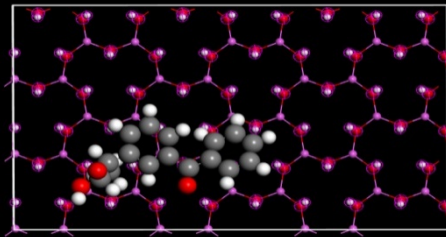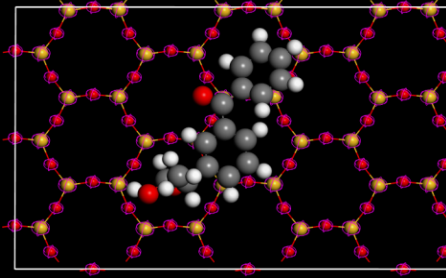
The MDS helps to find the most stable adsorption sites on external and internal kaolinite surfaces through minimization of the energy for each adsorption sites. The **Figure 10 shows** the equilibrium configurations of the ketoprofen and water molecules on kaolinite (001) and (00-1) surfaces, the external atomic layer illustrated by yellow color, is selected for the adsorption, and the **Table 2** summarizes their related output adsorption energies in kJ/mol, including, the total energy, the rigid adsorption energy, the deformation energy and dE$_{ads}$/dNi, the values of the energy were calculated taken the substrate energy as null.

Table 2: Adsorption energies (kJ/mol) of the ketoprofen and the water molecules

		Total Energy	Adsorption energy	Rigid adsorption energy	Deformation energy	Ketoprofen optimization mol : dEad/dNi	Water mol : dEad/dNi
(00-1) surface	Ketoprofen	3.741	-52.686	-35.423	-17.262	-52.686	/
	Water	-3.976	-4.935	-3.976	-0.959	/	-4.935
	Ketoprofen 30 water	-75.77	-151.386	-114.943	-36.442	-58.282	-4.409
(001) surface	Ketoprofen	3.286	-53.141	-36.297	-16.843	-53.141	/
	Water	-4.042	-5.510	-4.042	-1.468	/	-5.510
	Ketoprofen 30 water	-76.375	-162.169	-115.801	-46.368	-60.306	-4.110

The total energy is defined as the sum of the energies of the adsorbate molecules, it reports the energy released (or required) when the relaxed adsorbate molecules are adsorbed, it is defined as the sum of the rigid adsorption energy and the deformation energy. The rigid adsorption energy reports the energy released (or required) when the unrelaxed adsorbate molecules are adsorbed on the substrate. The deformation energy reports the energy released when the adsorbed adsorbate components are relaxed on the substrate surface. Finally, dE_{ads}/dNi is the energy of adsorbate-adsorbent configurations when one of the adsorbate molecules has been removed; the negative energy values indicate the spontaneity of the adsorption process.

The **Figure 10a** shows the most likely adsorption area of the water molecules projected on side and top views for both surfaces, on the surface (001) the water molecule prefers the top sites of the oxygen atoms, while, the hollows are the most likely adsorption sites for water molecules on the surface (00-1). According to the equilibrium configurations presented in the **Figure 10b**, it can be seen that of the ketoprofen molecule is adsorbed in longitudinal configuration, such that at least one aromatic ring finds a quasi-planar configuration with respect to the surface of the substrate for both orientations (001) and (00-1). At the last, the **Figure 10c** exhibits the closest configuration from the experiments, taken in account the adsorption if the KET with 30 water molecules. **Figure 10c** illustrates that the longitudinal configuration is almost conserved, in another words, the water molecules don't influence the affinity of the adsorption of the ketoprofen.

(a)

(b)

Figure 10: The equilibrium configurations of the KET and water molecules on HAL (100) substrate (a) the most likely adsorption area for the water molecules (b) KET (c) simulation of the experimental configuration.

3.2.2. Hydrogen bonding system

The equilibrium configurations illustrate a good affinity of the adsorption of the ketoprofen and water molecules on kaolinite (001) and (00-1) surfaces, the large distance between the adsorbate molecules and adsorbents surfaces substantiates the absence of covalent bonds, although weak bonds can be involved, where hydrogen bonds and van-der Waals-type dipolar electrostatic forces and π electrons interactions are mainly predominant.

The **Figure 11** shows the magnification of the adsorption contact provided by: the predicted extramolecular hydrogen bonding system, and by the distance between aromatic cycles of ketoprofen and the adsorbent surfaces.

For the surface (001), any hydrogen bonds below 3 Å of the distance H···Acceptor was predicted between the ketoprofen and this surface **(Fig.11d)**, and the distance between the longitudinal aromatic cycle and the surface is about 3.83 Å, at this distance, the short contact and the conjugated π electrons can be weakly involved in the adsorption mechanism, this result can be seen on the low the total adsorption energy of 3.286 kJ/ mol, otherwise, on this surface, the water molecules at the hollow sites can generate three hydrogen bonds between the oxygen of the water as donor and the oxygen of the adsorbent surface as acceptor **(Fig.11c)**, these three hydrogen bonds increase the total adsorption energy to the value -4.042 kJ/ mol.

For the adsorption on the surface (00-1), divers hydrogen bonds were predicted, this diversity may be related to the richness of this surface by the hydrogen. Two hydrogen bonds accurate between the oxygen of the surface as donor and the oxygen of the ketoprofen as acceptor, and another one between the oxygen of the hydroxyl group of the ketoprofen as donor and the oxygen of the surface as acceptor **(Fig.11b)**. In addition, the minimum distance between the longitudinal cycle and surface is about 3.17 Å, at this distance, the short contact and the π-electrons are involved in the adsorption mechanism, the total adsorption energy in this situation is 3.741 kJ/ mol. Finally, the adsorption of water molecule on this adsorbent surface occurs through one weak hydrogen bond between the oxygen of the surface as donor and the oxygen of water as acceptor **(Fig.11a)** with energy of -4,042 kJ/ mol. The **Table 3** summarizes the corresponding acceptor-donor bond lengths and angles measurements characteristic of the predicted hydrogen bonds.
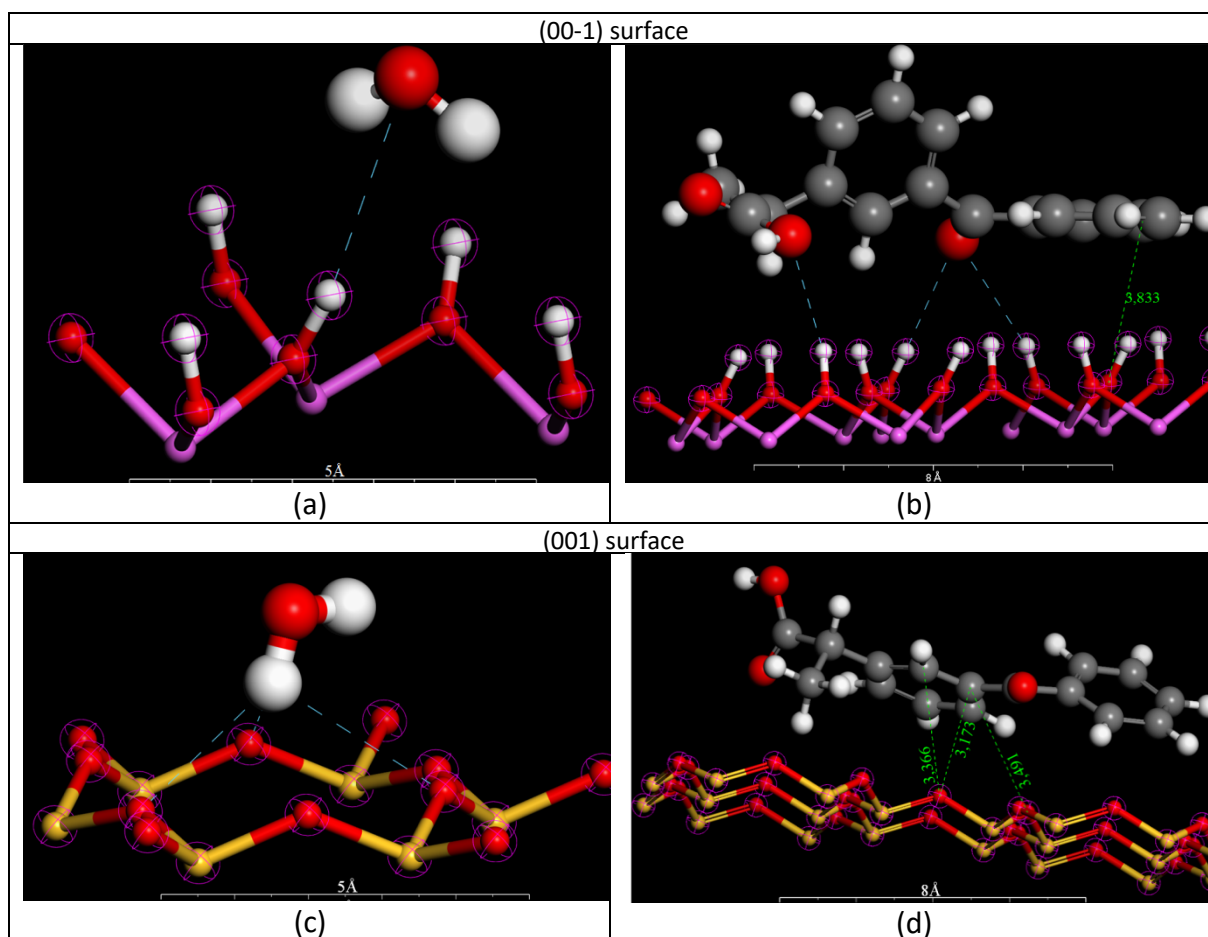

Figure 11: Local magnification of the adsorption configuration, (blue: possible hydrogen bonds, green: distance values)

Table 3: Geometric parameters of the predicted hydrogen bonds (Angle (°), Bond length (Å)) KET: Ketoprofen. W.: water

| | Angle (°) | Bond length (Å) | | |
	O-H···H	O-H	H···H	D···A
Ket.	155.959	0.979	2.861	3.776
	166.749	0.983	2.768	3.732
	160.428	0.976	2.820	3.754
W	147.393	0.979	2.845	3.707
	140.265	0.989	2.730	3.548
W	108.281	0.989	2.789	3.239
	109.070	0.989	2.782	3.243

3.3. Suggested adsorption mechanism

In this work, HAL was used as a drug carrier for the loading of KET by vacuum method. The use of vacuum to improve the loading efficacy into the halloysite nanotubes is well established experimentally but its interpretation has been reported recently. Of course, due to capillarity the nanotubes are quickly filled and there is no need for vacuum to remove air from inside **[48].** The mechanism of interaction of KET with HAL was evaluated by zeta potential, XRD, TEM, TGA / DSC and FTIR. After loading the HAL nanotubes with KET, the FTIR spectrum showed the appearance of new absorption peaks attributed to the KET molecules. According to TEM images, KET was mainly encapsulated in the lumen and loaded on the external surface of halloysite. The loading efficiency of KET introduced into HAL is 17.92%. But by DRX, no peaks relative to KET were observed, suggesting that the state of KET in HAL is in an amorphous state. As the zeta potential of HAL is between 3 and 4, this indicates that HAL is positive in the acidic medium and negative beyond pH greater than 3.6. On the other hand, KET presents a negative charge at pH = 7.4 and a positive charge at pH = 4 **[49].** Knowing that the oxygen of the carbonyl function and that of the carboxylic acid one are more electronegative than the carbon atoms, this will lead to the development positive charges on the KET molecule**.** To this the effect of conjugation due to the aromatic rings can be added. This might increase the probability of creating positive charges on the drug particles **[49].** The mechanism of interaction of KET in HAL nanotubes is determined by the functional groups existing on the surface which are Si-OH (electronegative), Al-OH (electropositive), and some Al-OH and Si-OH groups are located on surface defects of halloysite. These hydroxyl groups allow halloysite to carry a pH-dependent surface charge **[50].** The adsorption mechanism between the KET molecule and the surface can be proposed as follows:

1/ Electrostatic interactions

- Between the positive groups of the KET and the deprotonated silanols (Si-O⁻) and (Al-O⁻) located on surface defects of halloysite
- between the negative groups of the KET and the Al-OH of lumen surface
- Between the delocalized π electron density of benzene rings drug and the hydrogen atoms of the tetrahedral layer of Hal clay.

2/ Hydrogen bonds

- Between the hydrogen of the hydroxyl group of the KET and the oxygen atoms of the tetrahedral layer (Si-O⁻) of HAL surface.
- Between the oxygen atoms of the KET and the hydrogen atoms of the surface.

4. Conclusion

The present work reports the use of Algerian halloysite as a carrier for the loading of KET molecules. Physicochemical characterizations show that the KET was mainly loaded in internal and external surfaces of halloysite, respectively, and that ketoprofen is present in amorphous phase in HAL-KET composite. The TGA profiles show that the loading efficiency of KET introduced into HAL is 17.92%. This amount of KET is distributed homogeneously on the outer surface and in a non-homogeneous manner on the inner surface of the nanotubes. The study by Monte-Carlo theory illustrates a good affinity for adsorption of KET on the inner and outer surfaces, and these affinities of adsorption are not significantly influenced by the presence of water molecules. The mechanism of interaction of KET with HAL is physical, where several hydrogen bonds and electrostatic interaction are predominant.

References

[1] T.G. Kantor, Ketoprofen: A Review of Its Pharmacologic and Clinical Properties, Pharmacotherapy: The Journal of Human Pharmacology and Drug Therapy. 6 (1986) 93–102. https://doi.org/10.1002/j.1875-9114.1986.tb03459.x.

[2] S. Rençber, S.Y. Karavana, M. Özyazici, Bioavailability file: ketoprofen, FABAD Journal of Pharmaceutical Sciences. 34 (2009) 203.

[3] M. Kaleemullah, K. Jiyauddin, E. Thiban, S. Rasha, S. Al-Dhalli, S. Budiasih, O.E. Gamal, A. Fadli, Y. Eddy, Development and evaluation of Ketoprofen sustained release matrix tablet using Hibiscus rosa-sinensis leaves mucilage, Saudi Pharmaceutical Journal. 25 (2017) 770–779. https://doi.org/10.1016/j.jsps.2016.10.006.

[4] E.D. de Freitas, P.C.P. Rosa, M.G.C. da Silva, M.G.A. Vieira, Development of sericin/alginate beads of ketoprofen using experimental design: Formulation and in vitro dissolution evaluation, Powder Technology. 335 (2018) 315–326. https://doi.org/10.1016/j.powtec.2018.05.016.

[5] M.V. Harsha, S.R. Baratam, A.K. Kishore, Development and Evaluation of Ketoprofen Sustained delivery system using NeemGum, Research Journal of Pharmacy and Technology. 14 (2021) 817–822. https://doi.org/10.5958/0974-360X.2021.00144.X.

[6] M. Kamada, F. Hirayama, K. Udo, H. Yano, H. Arima, K. Uekama, Cyclodextrin conjugate-based controlled release system: repeated- and prolonged-releases of ketoprofen after oral administration in rats, Journal of Controlled Release. 82 (2002) 407–416. https://doi.org/10.1016/S0168-3659(02)00171-2.

[7] E. Joussein, S. Petit, J. Churchman, B. Theng, D. Righi, B. Delvaux, Halloysite clay minerals - a review, Clay Minerals. 40 (2005) 383–426. https://doi.org/10.1180/0009855054040180

[8] R. Yendluri, Y. Lvov, M.M. de Villiers, V. Vinokurov, E. Naumenko, E. Tarasova, R. Fakhrullin, Paclitaxel Encapsulated in Halloysite Clay Nanotubes for Intestinal and Intracellular Delivery, Journal of Pharmaceutical Sciences. 106 (2017) 3131–3139. https://doi.org/10.1016/j.xphs.2017.05.034.

[9] M. Liu, Z. Jia, D. Jia, C. Zhou, Recent advance in research on halloysite nanotubes polymer nanocomposite, Progress in Polymer Science. 39 (2014) 1498–1525. https://doi.org/10.1016/j.progpolymsci.2014.04.004.

[10] B. Wu, M. Jiang, X. Liu, C. Huang, Z. Gu, Y. Cao, Evaluation of toxicity of halloysite nanotubes and multi-walled carbon nanotubes to endothelial cells in vitro and blood

vessels in vivo,Nanotoxicology.14 (2020) 1017–1038.
https://doi.org/10.1080/17435390.2020.1780642.

[11] N. Alipoormazandarani, S. Ghazi hoseini, A. Mohammadi Nafchi, Preparation and characterization of novel bionano composite based on soluble soybean polysaccharide and halloysite nanoclay, Carbohydrate Polymers. 134 (2015) 745–751. https://doi.org/10.1016/j.carbpol.2015.08.059.

[12] S. Leporatti, Halloysite clay nanotubes as nano-bazookas for drug delivery, Polymer International. 66 (2017) 1111–1118. https://doi.org/10.1002/pi.5347.

[13] C. Aguzzi, C. Viseras, P. Cerezo, I. Salcedo, R. Sánchez-Espejo, C. Valenzuela, Release kinetics of 5-aminosalicylic acid from halloysite, Colloids and Surfaces B: Biointerfaces. 105 (2013) 75–80. https://doi.org/10.1016/j.colsurfb.2012.12.041.

[14] D. Tan, P. Yuan, F. Annabi-Bergaya, H. Yu, D. Liu, H. Liu, H. He, Natural halloysite nanotubes as mesoporous carriers for the loading of ibuprofen, Microporous and Mesoporous Materials. 179 (2013) 89–98. https://doi.org/10.1016/j.micromeso.2013.05.007.

[15] L. Lisuzzo, G. Cavallaro, S. Milioto, G. Lazzara, Layered composite based on halloysite and natural polymers: a carrier for the pH controlled release of drugs, New J. Chem. 43 (2019) 10887–10893. https://doi.org/10.1039/C9NJ02565K.

[16] N. G. Veerabadran, R. R. Price, Y. M. Lvov, Clay nanotubes for encapsulation and sustained release of drugs, NANO. 02 (2007) 115–120. https://doi.org/10.1142/S1793292007000441.

[17] R. Yendluri, D.P. Otto, M.M. De Villiers, V. Vinokurov, Y.M. Lvov, Application of halloysite clay nanotubes as a pharmaceutical excipient, International Journal of Pharmaceutics. 521 (2017) 267–273. https://doi.org/10.1016/j.ijpharm.2017.02.055.

[18] M. Hanif, F. Jabbar, S. Sharif, G. Abbas, A. Farooq, M. Aziz, Halloysite nanotubes as a new drug-delivery system: a review, Clay Minerals. 51 (2016) 469–477 https://doi.org/10.1180/claymin.2016.051.3.03.

[19] V. Vergaro, Y.M. Lvov, S. Leporatti, Halloysite Clay Nanotubes for Resveratrol Delivery to Cancer Cells, Macro-molecular Bioscience. 12 (2012) 1265–1271. https://doi.org/10.1002/mabi.201200121.

[20] H. Hemmatpour, V. Haddadi-Asl, H. Roghani-Mamaqani, Synthesis of pH-sensitive poly (N,N-dimethyl amino ethyl methacrylate)-grafted halloysite nanotubes for adsorption and controlled release of DPH and DS drugs, Polymer. 65 (2015) 143–153. https://doi.org/10.1016/j.polymer.2015.03.067.

[21]S. Harikrishnan, R. Sedev, C.C. Beh, C. Priest, N.R. Foster, Loading of 5-fluorouracil onto Halloysite nanotubes for targeted drug delivery using a subcritical gas antisolvent process (GAS), The Journal of Supercritical Fluids. 159 (2020) 104756. https://doi.org/10.1016/j.supflu.2020.104756.

[22]A. Borrego-Sánchez, M.E. Awad, C.I. Sainz-Díaz, Molecular Modeling of Adsorption of 5-Aminosalicylic Acid in the Halloysite Nanotube, Minerals. 8 (2018) 61. https://doi.org/10.3390/min8020061.

[23]E. Carazo1, A. Borrego-Sánchez1,2, F. García-Villén1, R. Sánchez-Espejo1, C. Aguzzi1, C.Viseras1,2, C.I. Sainz-Díaz2, P. Cerezo1, Assessment of halloysite nanotubes as vehicles of isoniazid, Colloids and Surfaces B: Biointerfaces Volume 160, 2017, Pages 337-344. https://doi.org/10.1016/j.colsurfb.2017.09.036

[24]Eleni Giannia,c, Konstantinos Avgoustakisb, Milan Pšeničkac, Miroslav Pospíšilc, Dimitrios Papoulisa, Halloysite nanotubes as carriers for irinotecan: Synthesis and characterization by experimental and molecular simulation methods, Journal of Drug Delivery Science and Technology, Journal of Drug Delivery Science and Technology 52 (2019) 568–576. https://doi.org/10.1016/j.jddst.2019.05.001

[25]Marina Massaro, Giampaolo Barone, Viviana Barra, Patrizia Cancemi, Aldo Di Leonardo, Giancarlo Grossi, Fabrizio Lo Celso, Silvia Schenone, Cesar Viseras Iborra Serena Riela, Pyrazole[3,4-*d*] pyrimidine derivatives loaded into halloysite as potential CDK inhibitors, International Journal of Pharmaceutics 599 (2021) 120281. https://doi.org/10.1016/j.ijpharm.2021.120281

[26]D. Sid, M. Baitiche, Z. Elbahri, F. Djerboua, M. Boutahala, Z. Bouaziz, M.L. Borgne, Solubility enhancement of mefenamic acid by inclusion complex with β-cyclodextrin: in silico modelling, formulation, characterisation, and in vitro studies, Journal of Enzyme Inhibition and Medicinal Chemistry. 36 (2021) 605–617. https://doi.org/10.1080/14756366.2020.1869225.

[27]S. Karimzadeh, B. Safaei, T.-C. Jen, Theorical investigation of adsorption mechanism of doxorubicin anticancer drug on the pristine and functionalized single-walled carbon nanotube surface as a drug delivery vehicle: A DFT study, Journal of Molecular Liquids. 322 (2021) 114890. https://doi.org/10.1016/j.molliq.2020.114890.

[28]Handbook of Clay Science, second edition, part B: Techniques and Applications Edited by F. Bergaya and G. Lagaly,2013.

[29]E. Abdullayev, Y. Lvov, Chapter 22 - Halloysite for Controllable Loading and Release, in: P. Yuan, A. Thill, F. Bergaya (Eds.), Developments in Clay Science, Elsevier, 2016: pp. 554–605. https://doi.org/10.1016/B978-0-08-100293-3.00022-4.

[30] S. Sahnoun, M. Boutahala, H. Zaghouane-Boudiaf, L. Zerroual, Trichlorophenol removal from aqueous solutions by modified halloysite: kinetic and equilibrium studies, Desalin. Water Treat. 57 (2016) 15941–15951, https://doi.org/10.1080/19443994.2015.1075159.

[31]S. Brunauer, P. H. Emmett, E. Teller, J. Am. Chem. Soc. 60 (1938) 309

[32]C. Lee, W. Yang, R.G. Parr, Development of the Colle-Salvetti correlation-energy formula into a functional of the electron density, Phys. Rev. B. 37 (1988) 785–789. https://doi.org/10.1103/PhysRevB.37.785.

[33]B. Miehlich, A. Savin, H. Stoll, H. Preuss, Results obtained with the correlation energy density functionals of becke and Lee, Yang and Parr, Chemical Physics Letters. 157 (1989) 200–206. https://doi.org/10.1016/0009-2614(89)87234-3.

[34]Y. Nishiyama, P. Langan, H. Chanzy, Crystal Structure and Hydrogen-Bonding System in Cellulose Iβ from Synchrotron X-ray and Neutron Fiber Diffraction, J. Am. Chem. Soc. 124 (2002) 9074–9082. https://doi.org/10.1021/ja0257319.

[35]L. Ouksel, S. Chafaa, R. Bourzami, N. Hamdouni, M. Sebais, N. Chafai, Crystal structure, vibrational, spectral investigation, quantum chemical DFT calculations and thermal behavior of Diethyl [hydroxy (phenyl) methyl] phosphonate, Journal of Molecular Structure. 1144 (2017) 389–395.https://doi.org/10.1016/j.molstruc.2017.05.029.

[36]R. Bourzami, L. Ouksel, N. Chafai, Synthesis, spectral analysis, theoretical studies, molecular dynamic simulation and comparison of anticorrosive activity of an ester and an acid α-Hydroxyphosphonates, Journal of Molecular Structure. 1195 (2019) 839–849. https://doi.org/10.1016/j.molstruc.2019.06.012.

[37]S. J. Gregg, K. S. W. Sing, Adsorption, surfaces area and porosity. Academic Press. London, (1982)

[38]G. Brown, Crystal Structures of Clay Minerals and their X-Ray Identification, The Mineralogical Society of Great Britain and Ireland, 1982.

[39]A. Aras, The change of phase composition in kaolinite- and illite-rich clay-based ceramic bodies, Applied Clay Science. 24 (2004) 257–269. https://doi.org/10.1016/j.clay.2003.08.012.

[40] S.R. Levis, P.B. Deasy, Characterization of halloysite for use as a microtubular drug delivery system, International Journal of Pharmaceutics. 243 (2002) 125–134. https://doi.org/10.1016/S0378-5173(02)00274-0.

[41] O. Sreekanth Reddy , M.C.S. Subha , T. Jithendra , C. Madhavi , K. Chowdoji Rao, Curcumin encapsulated dual cross linked sodium alginate/montmorillonite polymeric composite beads for controlled drug delivery, Journal of Pharmaceutical Analysis 11 (2021) 191-199. https://doi.org/10.1016/j.jpha.2020.07.002

[42] D. Tan, P. Yuan, F. Annabi-Bergaya, D. Liu, L. Wang, H. Liu, H. He, Loading and in vitro release of ibuprofen in tubular halloysite, Applied Clay Science. 96 (2014) 50–55. https://doi.org/10.1016/j.clay.2014.01.018.

[43] H. Sabahi, M. Khorami, A.H. Rezayan, Y. Jafari, M.H. Karami, Surface functionalization of halloysite nanotubes via curcumin inclusion, Colloids and Surfaces A: Physicochemical and Engineering Aspects. 538 (2018) 834–840. https://doi.org/10.1016/j.colsurfa.2017.11.038.

[44] R. Soto, M. Svärd, V. Verma, L. Padrela, K. Ryan, Å.C. Rasmuson, Solubility and thermodynamic analysis of ketoprofen in organic solvents, International Journal of Pharmaceutics. 588 (2020) 119686. https://doi.org/10.1016/j.ijpharm.2020.119686.

[45] A.A. Abd-Elrahman, M.A.E. Nabarawi, D.H. Hassan, A.A. Taha, Ketoprofen mesoporous silica nanoparticles SBA-15 hard gelatin capsules: preparation and in vitro/in vivo characterization, Drug Delivery. 23 (2016) 3387–3398. https://doi.org/10.1080/10717544.2016.1186251.

[46] S. Hendessi, E.B. Sevinis, S. Unal, F.C. Cebeci, Y.Z. Menceloglu, H. Unal, Antibacterial sustained-release coatings from halloysite nanotubes/water borne polyurethanes, Progress in Organic Coatings. 101 (2016) 253–261. https://doi.org/10.1016/j.porgcoat.2016.09.005.

[47] P. Yuan, D. Tan, F. Annabi-Bergaya, W. Yan, M. Fan, D. Liu, H. He, Changes in Structure, Morphology, Porosity, and Surface Activity Of Mesoporous Halloysite Nanotubes Under Heating, Clays and Clay Minerals. 60 (2012) 561–573. https://doi.org/10.1346/CCMN.2012.0600602.

[48] L. Lisuzzo, G. Cavallaro, P. Pasbakhsh, S. Milioto, G. Lazzara, Why does vacuum drive to the loading of halloysite nanotubes? The key role of water confinement, Journal of Colloid and Interface Science 547 (2019) 361–369, https://doi.org/10.1016/j.jcis.2019.04.012

[49] Adi I. Arida, Moawia M. Al-Tabakha, Encapsulation of ketoprofen for controlled drug release, European Journal of Pharmaceutics and Biopharmaceutics 66 (2007) 48-54. https://doi.org/10.1016/j.ejpb.2006.09.010

[50] N. G. Veerabadran, R. R. Price, Y. M. Lvov, Clay nanotubes for encapsulation and sustained release of drugs. Nano 2(2) 115-120 (2007).https://doi.org/10.1142/S1793292007000441

III.4 Publication: Improved biological performance of ketoprofen using novel modified halloysite clay nanotubes

Highlights

- Halloysite was modified by citric acid to obtain new clay nanotubes.
- Clay nanotubes were loaded with ketoprofen.
- Halloysite, modified halloysite and their corresponding formulations were fully characterized.
- New formulations exhibited promising anti-inflammatory and analgesic activities.
- Total protective effect against gastric damage was observed with ketoprofen-loaded modified halloysite clay nanotubes.

Abstract:

In the present work, elegant modification of halloysite (Hal) by citric acid (CA) was realized. The corresponding novel bio-composite (Hal-CA) was then used as drug carrier. To validate this concept, ketoprofen (KET), a known non-steroidal anti-inflammatory agent, was chosen as drug model. KET has low solubility and a short biological half-life, which can cause some limitations in its therapeutic use. In addition, its use is limited due to gastrointestinal side effects. All Hal, Hal-CA, Hal-KET and Hal-CA-KET samples were characterized using several techniques such as X-ray diffraction (XRD), Fourier transform infrared (FTIR) spectroscopy, transmission electron microscopy (TEM), N2 adsorption-desorption, thermogravimetric analysis (TGA) and differential scanning calorimetry (DSC). The release of KET from the prepared formulations was investigated at pH 1 and 6.8 by means of UV-Visible spectroscopy. In addition, kinetics of the release of KET from inclusion complexes were determined by fitting the release profiles to the first order, Korsmeyer–Peppas and Higuchi models. In order to assess these novel bio-composites, anti-inflammatory and anti-nociceptive activities were also evaluated *in vivo*. Finally, the ulcerogenic activity and the histopathological effects of all formulations were compared to that of pure KET. This work showed the increase of the anti-inflammatory and antinociceptive potentials of KET loaded in Hal-CA, as well as a maximum protection against ulcers. This suggests that Hal-CA can be considered as a new carrier for pharmaceutical formulations.

Keywords: Halloysite; Ketoprofen; Citric acid; Bio-composites; Release; *In vivo* performance

1. Introduction

Ketoprofen (KET) is a non-steroidal anti-inflammatory drug (NSAID) belonging to the class of 2-arylpropionic acids, well known for its analgesic, anti-inflammatory and antipyretic properties (Kantor, 1986). It is indicated mainly for the symptomatic treatment of pain and inflammation of osteoarthritis and rheumatoid arthritis (Freitas et al., 2018). In recent years, possible new therapeutic benefits of KET are gaining interest. The drug has proven its effectiveness in the prevention of the development of various cancers including colorectal and lung cancers as well as in the treatment of neurodegenerative disorders among which Alzheimer and Parkinson's diseases (Rençber et al., 2009). However, the use of KET is limited due to a large number of side effects; especially those related to gastrointestinal (GI) complications, abdominal pain, constipation and flatulence observed in more than 3% of patients (Kantor, 1986). In addition, its low solubility (0.05 mg·mL^{-1} at 25 °C in water), its short biological half-life (t$_{1/2}$= 2-4 h) lead to a low bioavailability of this active pharmaceutical ingredient (API). However, in order to overcome this drawback, high doses are recommended (maximum dose 300 mg per day) with a variable frequency of administration (2 to 4 times per day). High doses naturally increase the risk of developing side effects, limiting long-term use (Cerciello et al., 2015). For all these reasons, KET is a potential candidate for new development of controlled release formulations, capable of providing drug release systems with a predetermined rate and time (Joussein et al., 2005), having an improved solubility, and eventually reducing its well-known harmful effects. So far, many host materials were studied with KET such as synthetic polymers (Mangindaan et al., 2012), layered double hydroxides (San Román et al., 2012), biopolymers (Maestrelli et al., 2015; Matos Fonseca et al., 2019), cyclodextrins (Zhao et al., 2019), UiO-66 metal-organic frame (Li et al., 2019).These systems have been prepared by different methods, including intercalation, inclusion, mixing and kneading, and were then tested for their release properties of the guest ingredient.

Clay minerals have been used for different biomedical purposes since many years and new studies were recently published (Charaabi et al. 2019; Charaabi et al., 2021). Additionally, a particular attention is also given to halloysite (Hal) (Joussein et al., 2005). Hal is extracted from natural deposits with a natural aluminosilicate composition having a hollow nanotubular structure and formed by rolled kaolin sheets. The external diameter of the Hal tubes ranges typically from 50 to 200 nm with an internal diameter of 5 to 30 nm and a length of 0.5 to 25 μm. Hal nanotubes contain up to 10 to 15 rolled aluminosilicate layers with a repeat distance of 0.72 nm between layers (Yendluri et al., 2017a). The crystalline and chemical composition of Hal are similar to those of kaolinite but Hal can be intercalated by a monolayer of water

molecules increasing the basal spacing. Thus, Hal mainly occurs in two different polymorphs, the hydrated form (basal distance around 1.0 nm) with the formula $Al_2Si_2O_5(OH)_4.2H_2O$ and the dehydrated form (basal distance about 0.7 nm) with the formula $Al_2Si_2O_5(OH)_4$, identical to kaolinite. The outer surface of Hal nanotubes is composed mainly of negatively charged SiO_2 moieties and an inner surface composed of positively charged Al_2O_3 groups. In addition, Hal nanotubes have a high specific surface area and a good thermal stability. They are inert and chemically stable in a wide range of pH (3-10), non-toxic, biocompatible, abundant and low cost (Liu et al., 2014; Alipoormazandarani et al., 2015; Tharmavaram et al., 2018; Oliyaei et al., 2019). An important advantage of Hal clays, as compared with platy clays such as montmorillonite, kaolin and laponite, is that Hal do not need exfoliation and can be easily dispersed in water. For this, Hal nanotubes have been widely considered as supports for the encapsulation and release studies of medicines, inorganic salts, APIs, antiseptics, corrosion inhibitors, antibacterials, cosmetic additives, enzymes and proteins (Abdullayev and Lvov, 2016). On top of these applications, Hal was employed in numerous fields as a catalyst support (Massaro et al., 2017; Huang et al., 2021), as a filler for hydrogels and polymers (Bertolino et al., 2018), as composite bioplastics (Lisuzzo et al., 2020), as an adsorbent of pollutants (Xia et al., 2021). In addition, Hal nanotubes coated with octadecyltrimethoxysilane were investigated, their cellular uptake was confirmed and no apoptosis-inducing effect was observed on cells (Rozhina et al., 2020). It is now well established that Hal can fix active molecules through three different ways: (i) adsorption onto the external and internal walls of nanotubes, (ii) encapsulation in the internal space (lumen of the nanotubes) and (iii) intercalation between the layers (Abdullayev and Lvov, 2013). It has also been shown that the encapsulation in the internal space is the main mode for water-soluble active principles and this already allows a high capacity and a controlled release (Abdullayev and Lvov, 2013). A number of APIs has been encapsulated in Hal nanotubes, including 5-aminosalicylic acid (Aguzzi et al., 2013), ibuprofen (Tan et al., 2013), diclofenac (Lisuzzo et al., 2019), dexamethasone (Veerabadran et al., 2007), oflaxacin (Aguzzi et al., 2013), nifedipine (Yendluri et al., 2017b), furosemide (Hanif et al., 2016), diphenhydramine (Hemmatpour et al., 2015), 5-fluorouracil (Harikrishnan et al., 2020), resveratrol (Vergaro et al., 2012) and paclitaxel (Yendluri et al., 2017a). All of these drugs are sparingly soluble in water; therefore, intercalation in Hal nanotubes plays a major role in sustained release, but also ensures an effective dispersion in aqueous media. However, the practical applications of Hal are restricted by its rather low exchange capacity, due to the low degree of isomorphic substitution of silicium (Si) by aluminum (Al) in the tetrahedral layer, which leads to a low content and rapid release of molecules intercalated in Hal (Yang et al.,

2016). For example, when Hal is used as an unmodified support, only a weak affinity may be observed between Hal and APIs. In order to improve the performance of Hal, the properties of internal and/or external surfaces of this later should be adapted. In general, the modification of the surface relates to the introduction of functional groups on the surface of the Hal (e.g. surfactants, silanes, octadecyl phosphonic acid, polyethyleneimine) (Massaro et al., 2018). However, the toxicity and the cost of these modifying products limit their application in the modification of Hal. Therefore, it is essential to find a gentle, environmentally-friendly modifier to functionalize the Hal without compromising the drug's intercalation effectiveness.

Citric Acid (CA) is a natural organic acid commonly used as cross-linking agent. CA has three acid dissociation constants, namely pKa1 = 3.13 (H_2Cit^{1-}), pKa2 = 4.76 ($HCit^{2-}$) and pKa3 = 6.40 (Cit^{3-}). In a neutral aqueous solution, CA is completely ionized in its citrate form (Cit^{3-}) (Apelblat and Barthel, 1991). As a tricarboxylic acid, CA cross-linked materials have effective functional groups (-OH and -COOH). In recent years, certain biomaterials (e.g. bentonite) modified by CA have been proposed in the literature (Schilling et al., 2008; Ghorpade et al., 2016, 2017, 2018; Zhang et al., 2019).

In the present work, we consider the active role of Hal and Hal treated with CA (Hal-CA) as friendly drug carriers for KET. Such drug delivery systems (DDS) can assist in overcoming the side effects associated with KET by designing new oral DDS that can limit drug release in the stomach and enhance the release in the intestine. This may improve the drug efficiency together with the patient compliance. Further we detail the multi-step procedure used for the purification of the natural crude Hal. At this stage, it is possible to prepare organic/inorganic material (Hal-CA) using an esterification reaction between surface OH groups of Hal and COOH groups of CA (Sajab et al., 2011; Tcheumi et al., 2019; Zhang et al., 2019). Two formulations (Hal-KET and Hal-CA-KET) were produced and compared. KET loading and release kinetics were also investigated. All biomaterials and formulations were characterized by different techniques such as X-ray diffraction (XRD), Fourier transform infrared (FTIR) spectroscopy, transmission electron microscopy (TEM), N2 adsorption-desorption, thermogravimetric analysis (TGA) and differential scanning calorimetry (DSC). Release studies of formulations and their kinetics were also investigated. Finally, all formulations were evaluated for their pharmacological effects. *In vivo* studies on the anti-inflammatory and analgesic activities, after oral administration of Hal-KET and Hal-CA-KET, have been carried out on rodents. The ulcerogenic activity and histopathological effects of the formulations were also compared to that of pure KET.

2. Materials and methods

2.1. Materials

The raw halloysite material was obtained from the mine of Djebbel Debbagh (Guelma, Algeria). The mineral was first milled in a mortar, sieved at 45 µm and dried at 100 °C for 24 h. The drug ketoprofen (abbreviated as KET) (molecular formula: $C_{16}H_{14}O_3$, CAS number 22071-45-4, MW: 254.3 g·mol^{-1}, pKa= 4.4, log K_{OW}= 3.00, water solubility at 25 °C =21 mg·L^{-1}), was supplied by SALEM pharmaceutical Laboratories, El- Eulma, Algeria. Citric acid (CA) (2-hydroxypropane-1,2,3-tricarboxylic acid, CAS number 77-92-9, solubility in water 59.2% w/w at 20 °C) was purchased from Sigma Aldrich, USA. Lambda carrageenan was purchased from Sigma Aldrich. All other used chemicals are of analytical grades. All reagents are used as received.

2.2. Halloysite purification

The first step in the purification of the raw halloysite material consists in the removal of the water-soluble matter. To this end, 20 g of the material are dispersed in 1 L of distilled water and stirred for 24 h at room temperature. Then the suspension is centrifuged at 5000 rpm for 5 min. In order to remove the carbonates, the resulting powder was further suspended treated under vigorous stirring with 2 L 0.1 M HCl at room temperature for 4 h (Bergaya and Lagaly, 2013). After a second centrifugation the obtained precipitate was repeatedly washed with distilled water and centrifuged successively for five times to eliminate chloride ions (tested by $AgNO_3$ solution). Further purification consists in the elimination of the soil organic matter and this was achieved through a further treatment when submitting the solid residue to the action of an aqueous solution of (10% v/v) hydrogen peroxide (1 L) and stirred overnight at room temperature. Then, the residual hydrogen peroxide was degraded by heating the suspension at 70 °C for 30 min. The precipitate was washed with hot water (100 °C, 1 L) and dried for 24 h at 50 °C. The material was milled in a mortar, sieved at 45 µm, kept in a bottle and stored away from moisture. The resultant sample was denoted as Hal.

2.3. Preparation of halloysite modified by citric acid

A mixture of the Hal (1 g), CA (3 g, used as surface functionalization agent) and sodium dihydrogen phosphate (2 g, used as catalytic agent) was added to 25 mL of distilled water in a round bottom flask. Then, the suspension was heated at 100 °C under magnetic stirring for 1 h. The mixture was then cooled down to room temperature and sequentially washed three times

with (150 mL) portions of distilled water. The obtained residue was collected by centrifugation, dried at 50 °C for 24 h; the Hal-CA sample was obtained as a white solid, milled in a mortar, sieved at 45 µm and stored at 4 °C in an airtight container.

2.4. KET loading

In order to obtain a saturated solution, a total of 1 g of KET was added in 250 mL of water. Then, 1 g of either Hal or Hal-CA was added to the solution and mixed to obtain a homogeneous suspension. This later was placed in vacuum (600 mbar) for 4 cycles and for 30 min each. According to the most recent studies, the vacuum steps induced an optimization of the loading efficiency due to water removal from the inner cavity of Hal (Lisuzzo et al., 2021 and 2019). Then the solution entered the lumen to ensure maximum loading. The solid samples were recovered by centrifugation and washed three times with 200 mL portions of water to remove excess of non-retained drug. The samples were dried overnight, milled in a mortar, sieved at 45 µm and stored at 4 °C in an air-tight container. The samples were denoted Hal-KET and Hal-CA-KET.

2.5. Characterization techniques

X-ray diffraction (XRD) analysis for the Hal, Hal-CA, Hal-KET and Hal-CA-KET samples was performed using a Bruker D8 advance diffractometer operating at 40 kV and 30 mA with Cu Kα1 radiation (λ = 0.15418 nm). Radial scans were recorded in the reflection scanning mode from 2θ = 5 to 80° with a scanning rate of 10°/min. Bragg's law, defined as $n\lambda = 2\,d\,\sin\theta$, was used to compute the inter-reticular distance (d) for the examined clay samples. The mean diameter of crystallite found in Hal material is evaluated by Scherrer equation ($D = k\,\lambda/\beta\,\cos\theta$), where k is the shape factor close to 0.9, β is the width at half height of the reflection peaks, λ is the incident wavelength and 2θ is the Bragg angle.

FTIR study was carried out using Shimadzu Ftir-8400 spectrophotometer having a standard mid-IR DTGS detector. FTIR spectra were recorded in the range of 400–4000 cm^{-1} using the KBr pellets technique.

TEM investigations were performed with a JEOL JEM-1400 Flash electron microscope at "Centre Technologique des Microstructures de l'Université de Lyon 1", operating with an accelerating voltage of 120 kV. A droplet of 5 µL of Hal nanoparticles dispersed in distilled water was deposited onto a carbon coated copper grid (CF200-CU UL EMS). Excess solution was carefully blotted off using filter paper. The sample was air-dried at room temperature during one night before imaging.

Nitrogen gas adsorption–desorption isotherms were measured using a Micromeritics ASAP 2020 Plus Version 1.03 at 77 K. The measurements were taken after degassing the samples under vacuum at 120 °C for 3 h. The specific surface areas (S_{BET}) are determined according to the BET method at the relative pressure in the range of 0.05–0.35. The total pore volume (Vp) was directly determined from the nitrogen adsorption at P/P_o = 0.99. The pore diameter (Dp) was obtained by the formula: Dp = $4Vp/S_{BET}$ (Brunauer et al., 1938; Sahnoun et al., 2016).

Finally, thermogravimetric analysis/differential scanning calorimetry (TGA/DSC) were conducted on an EXTAR 6000 thermal analyzer (Seiko, Mahwa, NJ, USA) under the nitrogen flow of 15 $cm^3 \cdot min^{-1}$ for the sample and 10 $cm^3 \cdot min^{-1}$ for the balance. The samples were heated from 30 to 900 °C, with a rate of 10 $°C \cdot min^{-1}$.

2.6. In vitro drug release studies

In vitro release experiments of the KET from Hal, Hal-CA and pure KET were performed using the United States Pharmacopeia Paddle Method (Apparatus II) on Heidolph RZR 2041. The samples loaded with 50 mg of KET (i.e. 249.6 mg of Hal-KET and 193.8 mg of Hal-CA-KET) were placed into a hard gelatin capsules (size 00), and then soaked into 900 mL of simulated gastric medium (0.1 M HCl, i.e. pH 1) for 2 h. Then the acid medium was drained and replaced by 900 mL 0.01 M KH_2PO_4 buffer solution adjusted to pH 6.8 with 0.1 M NaOH, as simulated intestinal fluid. Temperature was maintained at 37 ± 0.5 °C during the entire release process and the release medium was stirred at 100 rpm. At suitable time intervals, 1 mL of the suspension medium was aliquoted, using a syringe, and filtered through 0.22 μm nylon disc filters. Then, an equivalent volume of fresh medium was added in order to maintain sinking conditions. The KET concentration was determined from the peak at 256 nm using an UV-Vis spectrophotometer (SHIMADZU UV-1800). Each drug release test was carried out in duplicate.

In addition, kinetics of the release of KET from inclusion complexes were determined by fitting the release profiles to the first order (equation 1) (Wagner, 1969), Korsmeyer–Peppas (equation 2) (Kim and Fassihi, 1997) and Higuchi (equation 3) (Higuchi et al., 1963) theoretical models, as follows:

F_t = 1-exp (-K_1.t),   (1)

Where F_t is the fraction of drug released at time t in the medium and K_1 is the first order release constant.

F_t = $K_{KP}t^n$,   (2)

Where K_{KP} is the Korsmeyer–Peppas constant, and n is the release exponent indicative of the drug release mechanism.

$$F_t = K_H t^{0.5} + a, \tag{3}$$

Where K_H is the Higuchi release constant and "a" is a constant characterizing the initial drug fraction.

Then, the selection of the best fit model is based on the regression coefficient value R^2.

2.7. Animals preparation

In this part of the study, male Swiss albino mice of 20-30 g weight and male Wistar rats of 150-200 g were used. These animals are brought from 'Institut Pasteur' of Algeria. Before the beginning of the experimentation, the animals were kept in polycarbonate cages for 7 days under ordinary laboratory conditions (12/12 h light/dark cycle, at 23 ± 2 °C with free food and water access).

2.8. Carrageenan-induced rat paw edema

To assess the *in vivo* anti-inflammatory effectiveness of the formulations (Hal-KET and Hal-CA-KET) in comparison with the pure drug, 24 male Wistar rats were distributed into four groups with six rats each. Therefore, the rats were kept under fasting overnight prior for conducting the experiments except water was fed, 2 mL solution of saline (0.9%, w/v) was administered orally to group I (control group), KET equivalent to body weight of 5 mg·kg^{-1} and dissolved in 2 mL solution of saline was introduced by gavage to group II (standard group), Hal-KET and Hal-CA-KET formulations equivalent to drug 5 mg·kg^{-1} body weight were administered orally to the groups III and VI (test groups), respectively, using 2 mL of NaCl (0.9%) solution.

An acute inflammation (edema) was instigated one hour after the administration of the pure drug and formulations. For this, we injected 0.1 mL of 1% (w/v) lambda carrageenan in saline into the sub-plantar zone of each Wistar rat's right-hand paw (Boppana et al., 2016). After the phlogistic agent has been injected, the volume of the paw was measured by a digital caliper at 0 h, every h for 6 h and finally at 24 h. The average increase in paw volume relatively to control animals can estimate edema. Therefore, the anti-inflammatory activity was determined by the percentage of edema reduction in treated rats in relation to controls as shown in the following equation:

$$\text{Inhibition \%} = \frac{(Vc-Vt)}{Vc} * 100, \tag{4}$$

Where Vc is changed in paw size of control and Vt is changed in treated paw size.

2.9. Acetic acid-induced writhings

Male Swiss mice (25-30 g, n = 6/group) were orally treated with NaCl 0.9% solution (control), KET, Hal-KET and Hal-CA-KET (5 mg·kg^{-1} of drug) before the intraperitoneal injection of 0.6% of acetic acid (100 µL/10 g). The analgesic activity was determined by the number of abdominal constrictions counted for 30 min (Cunha et al., 2016) and the % writhing inhibition was calculated using the following formula:

$$\%MPE = \frac{(\text{Mean no. of constrictions (control) - Mean no. of constriction (test))}}{\text{Mean number of constrictions (control)}} *100, \tag{5}$$

Where MPE is the percentage of maximum possible effect.

2.10. Ulcerogenicity study

For this part, the rats were under fasting and separately kept in wire mesh cages to avoid coprophagy except water was fed during 24 h prior to the start of experiments. Table 1 summarized the experimental design and animal groups. On the morning of the tests, magnetic agitation was used to achieve a well-dispersed suspension of pure drug and samples. Then 2 mL of gavage solutions equivalent to 500 mg per kg (body weight) of KET was then given orally for each fasted rat (Laudanno et al., 2000). After 6 h, each rat was sacrificed. The stomach was then removed and opened up along the greater curvature, gently washed by dipping in the saline solution.

Table 1: *In vivo* ulcerogenicity activity experiment design.

Groups (n=6)	Treatment	Dose (mg·kg^{-1}) of KET
I	Control (saline)	-
II	Pure KET	500
III	Hal-KET	500
VI	Hal-CA-KET	500

Then total area of the lesions and total area of the stomach were measured using AUTOCAD-2018 software. The percentage of ulceration is calculated according to the following formula:

$$\% \text{ ulceration} = \frac{\text{total lesion area}}{\text{total stomach area}} *100, \tag{6}$$

2.11. Histopathological examinations and assessments

Stomach sections were fixed in 10% formalin, then stomach tissues were processed by dehydration using xylene and ethanol then they were embedded in paraffin and then serially-sectioned (3-μm thick) using a Leica RM2135 microtome (Leica, Berlin, Germany), installed on glass slides and colored with hematoxylin and eosin (H&E) solution. The photographs were taken using binocular light microscope (CXRIII, Labomed, Mumbai, India).

2.12. Statistical analysis

Graph Pad Prism (version 8.3.0 for Windows) was used to carry out statistical test analysis. All *in vivo* results were indicated as mean ± standard error of mean (SEM). A one-way variance analysis (ANOVA) followed by Dunnet's test was used to analyze each assay. The *p*-values less than 0.05 were considered statistically significant.

3. Results and discussion

3.1. Characterization of the purified Hal

3.1.1. Powder x-ray diffraction

The XRD diagram of Hal is shown in Fig. 1(a). The results confirmed that Hal was not pure and traces of other minerals (e.g. alunite, quartz) coexisted with. The pattern showed the characteristic diffraction peaks at the angular positions 2θ = 12.3, 20.2, 25.0, 30.0, 35.3, 36.2, 55.3 and 62.6°. According to the powder diffraction file (JCPDS 29-1487) of 7 Å-Hal, these eight angular positions are related to the Miller indices of the reticular plane families (001), (020), (002), (113), (003), (200), (211) and (-3-31), respectively. In addition, the inter-reticular distances [d(001) =7.33 Å and d(020) = 4.41 Å] are characteristic of the dehydrated phase of 7 Å-Hal with the chemical formula $Al_2Si_2O_5$ having a tubular morphology (Yuan et al., 2012). The XRD pattern also illustrates the existence of trace of quartz, formed by the dissociative SiO_2 that segregated from the 7 Å-Hal. Its weak peaks are indexed by letter Q and are located at the six angular positions 10.2, 26.6, 39.2, 40.5, 45.5 and 47.8°. According to the diffraction file (JCPDS 78-2315), these peaks are related to the hexagonal phase planes of SiO_2(100), (1-1-1), (1-1-2), (2-20), (02-1) and (2-12), respectively (Segovia-Sandoval et al., 2018). Another phase is also observed which corresponds to alunite and indexed by letter A. Its four characteristic peaks are observed at the angular positions of 15.6, 18.0, 50.9 and 52.4°. These peaks are attributed to the (003), (100), (033) and (200) reflexions, respectively, according to

JCPDS 73-1652. Moreover, the crystallite seizes of Hal, quartz and alunite, are estimated using Scherrer method (Tan et al., 2013). Their values are close to 15.2, 13.1 and 11.7 nm, respectively, and when comparing the intensities, the main crystalline phase is that of the Hal.

3.1.2. FTIR spectroscopy

In the FTIR spectrum of Hal (Fig. 1(b)), two bands centered at 3692 and 3626 cm^{-1}, were attributed to the O-H stretching of the inner surface and the inner layers, respectively. In addition, the wide bands centered at 3464 cm^{-1} and the weak one at 1639 cm^{-1} were attributed to the O-H stretching and O-H deformation vibrations of the physically adsorbed water, respectively (Sabahi et al., 2018). The groups at 1090 cm^{-1} and 1029 cm^{-1} corresponded to the stretching vibrations of Si-O and Si-O-Si, respectively. The band at 916 cm^{-1} was attributed to the O-H deformation of the internal O-H groups, and the one at 793 cm^{-1} was caused by a symmetrical stretching vibration of Si-O. The bands at 752 and 687 cm^{-1} were attributed to the perpendicular Si-O stretching vibrations. The three remaining bands at 540, 470, and 437 cm^{-1} were attributed to the deformation vibrations of the groups Al-O-Si, Si-O-Si, and Si-O, respectively (Yuan et al., 2012). As a result, both X-ray diffraction and FTIR analyses confirmed the expected structure of Hal.

3.1.3. TEM analysis

The TEM image of Hal clearly showed that HAL particles have a typical cylindrical shape with a transparent central cylindrical area parallel to the tube axis (Fig. 1(c)), indicating that the particles are hollow and open-ended. Various sizes of the nanotubules were present in the sample, their lengths ranged from 40 to 1300 nm, and their widths from 25 to 85 nm. The size distribution of Hal reported in this study may be specific to the mine of Djebbel Debbagh (Guelma, Algeria) but it stays in the same order of magnitude than the other Hal obtained from other sources (Joussein et al., 2005b).
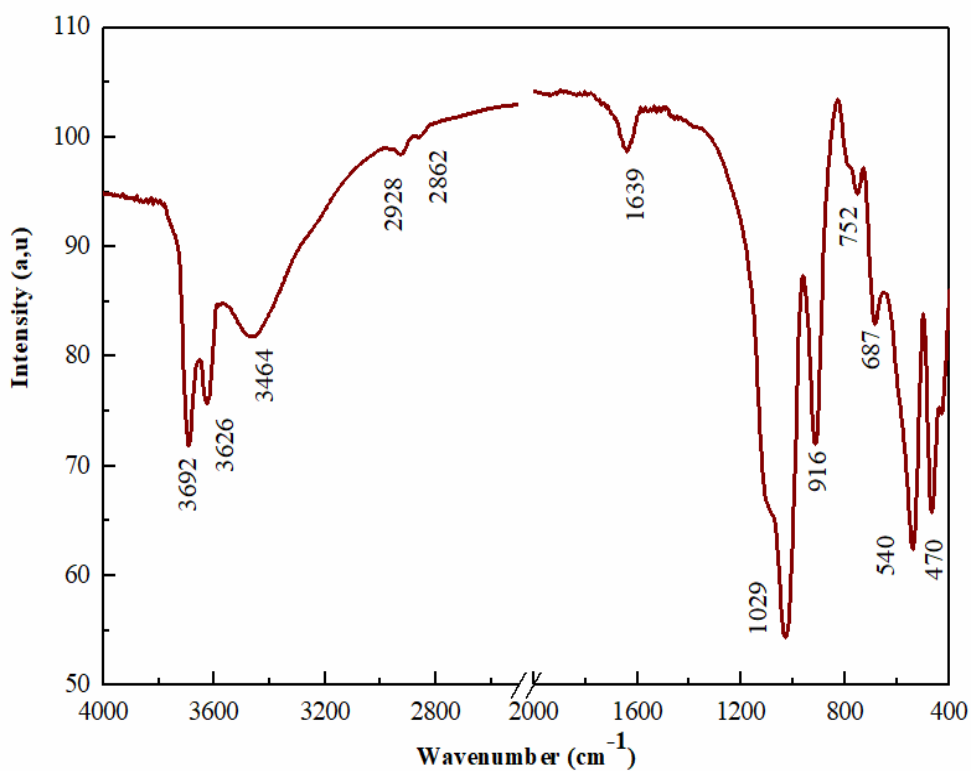
3.1.4. N$_2$ adsorption-desorption analysis

The N$_2$ adsorption-desorption isotherm of the Hal was presented in Fig. 1(d). The isotherm of this sample is classified as type II with H3 hysteresis loops, on the basis of IUPAC recommendations. The H3 hysteresis loop observed in this case where the adsorbent forms aggregates can be attributed to capillary condensation taking place in a non-rigid texture and is not characteristic of a defined mesoporosity (Greg et al., 1962; Torres et al., 1999). The S$_{BET}$, V$_{pore}$ and Dp values of Hal are 18.93 m$^2 \cdot$g^{-1}, 0.0576 cm$^3 \cdot$g^{-1} and 11.8 nm, respectively.

3.1.5. Thermogravimetric analysis

The TGA analysis for Hal showed two significant mass losses clearly observed (Fig. 1(e)). The first mass loss takes place from 50 to 200 °C, and is attributed to the dehydration of physically adsorbed water and interlamellar residual water (8% water content). The second loss of mass between 300 and 600 °C corresponds to a derivative thermogravimetry (DTG) peak centered at 480 °C. It can be attributed to the structural dehydration of the aluminol groups (Al-OH). This result is similar to that observed in the literature concerning the dehydroxylation of Hal between 400 and 600 °C (Yuan et al., 2012).
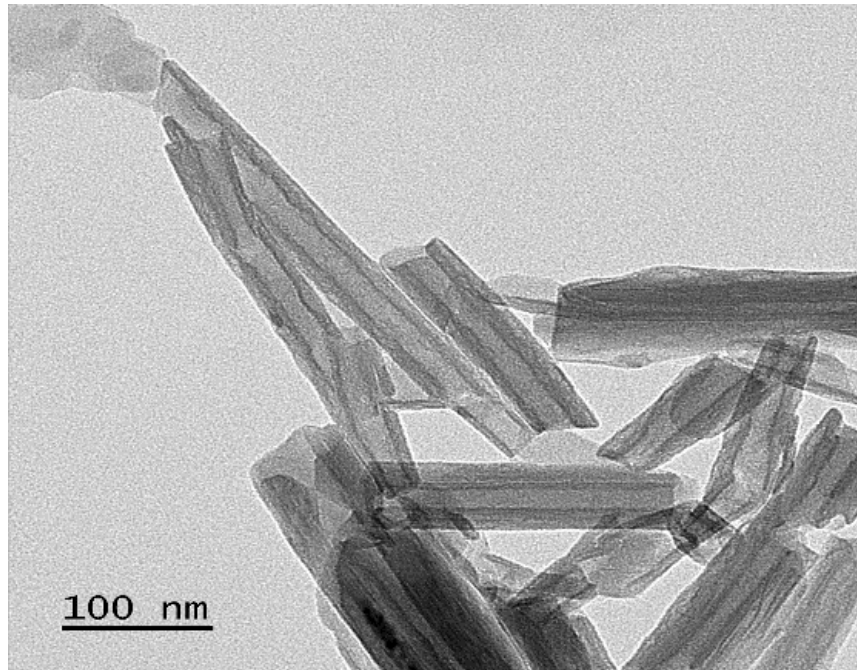
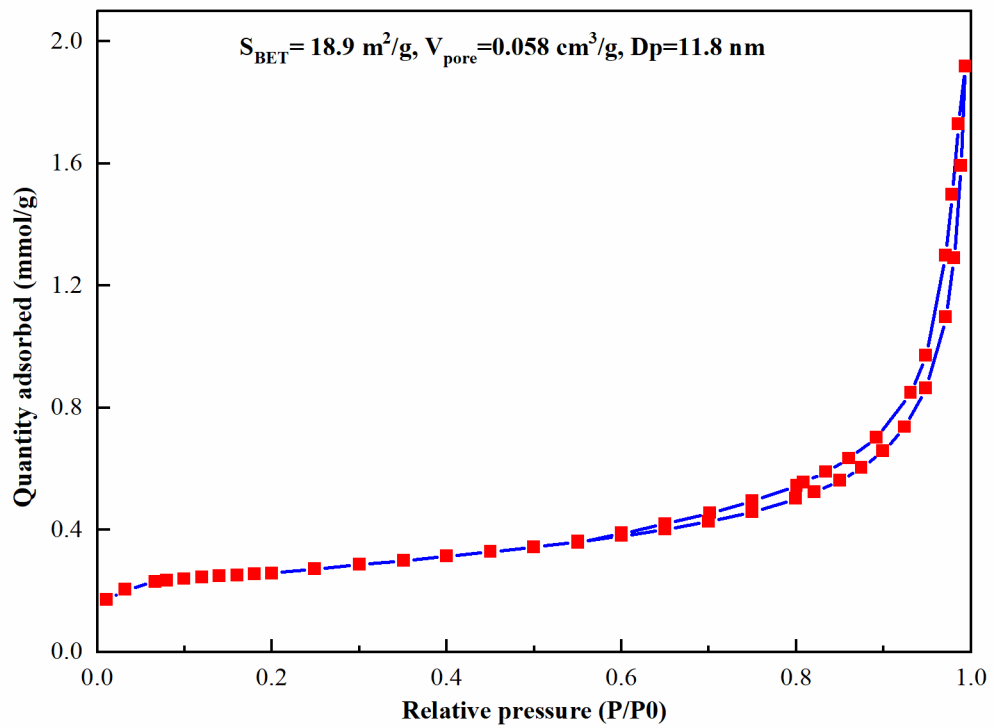**a)**

b)

c)

d)

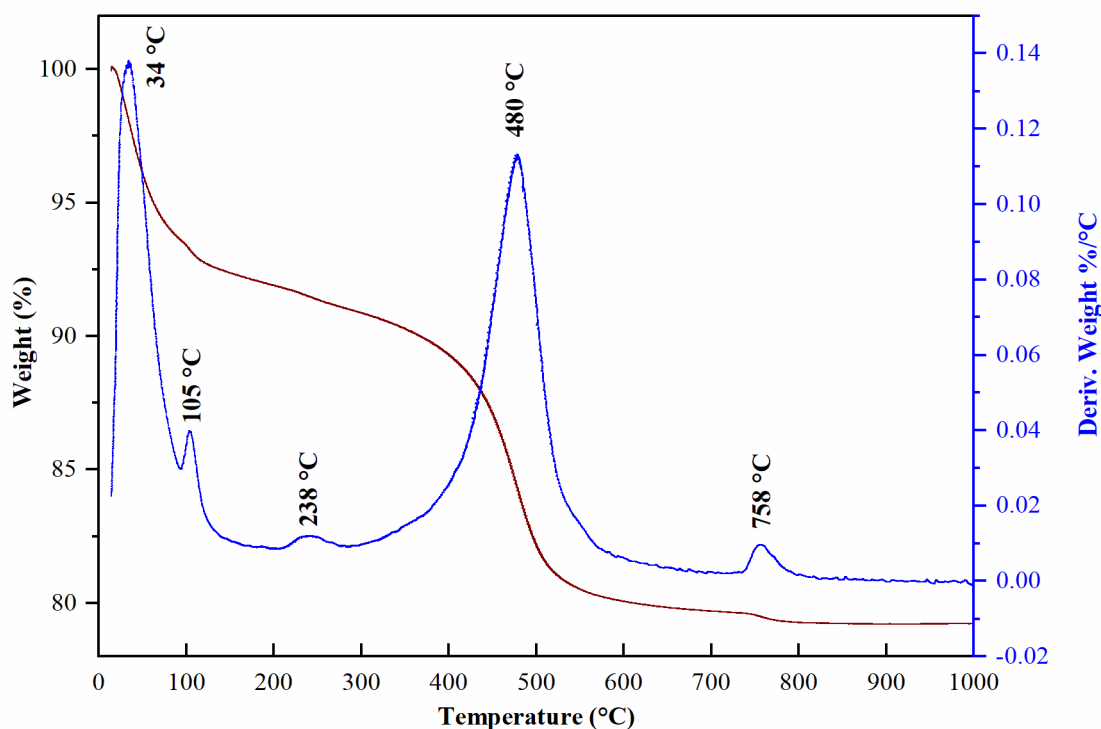$S_{BET}= 18.9\ m^2/g,\ V_{pore}=0.058\ cm^3/g,\ Dp=11.8\ nm$
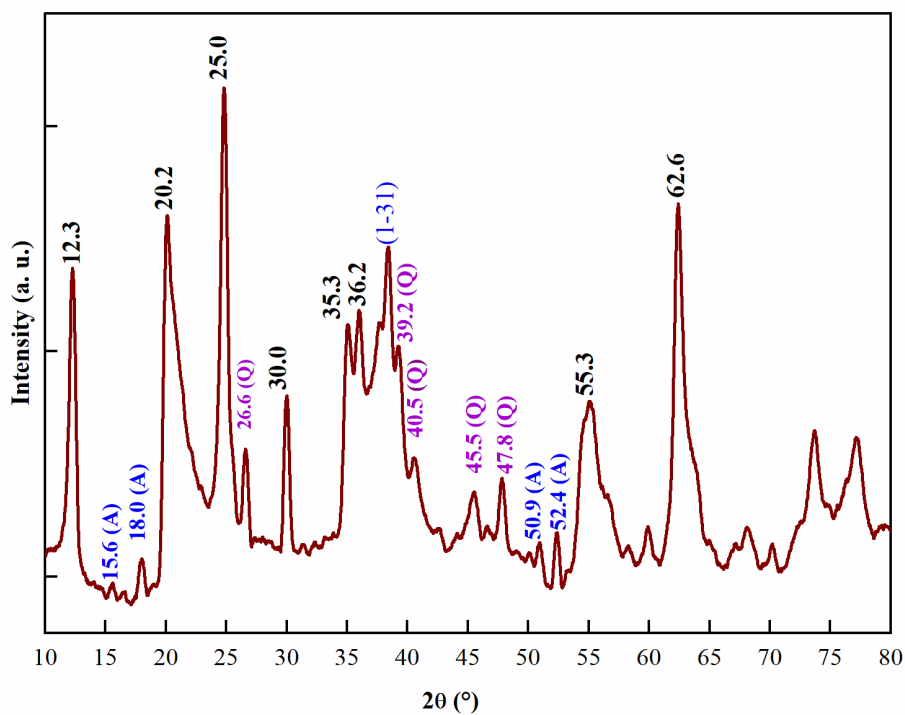
e)

Fig. 1. Characterization of purified Hal: X-ray diffractogram, Q: quartz, A: alunite (a); FTIR spectrum (b); TEM image (c); N$_2$ adsorption/desorption isotherms (d) and TGA-DTA (e).

3.2. Characterization of the CA–modified and KET-loaded halloysite samples

3.2.1. Powder x-ray diffraction

The XRD diagrams of the Hal-CA, KET and composites (Hal-KET and Hal-CA-KET) are displayed in Fig. 2. The 2θ-positions of the XRD reflection peaks of Hal-CA are almost unchanged compared to those of Hal. Nevertheless, the treatment with CA impacts the crystallinity of Hal, this result can be observed directly on the pattern by a marked decrease of the relative peak intensities. Moreover, the CA addition decreased the crystallite size of the Hal from 15.20 to 8.56 nm. In addition, the pattern of KET powder showed a crystalline structure. The most significant diffraction peaks are observed at angular positions of 2θ = 13.4, 14.8, 18.8, 23.3, 28.2 and 29.9°. These values are in fair agreement with previous results (Cervini-Silva et al., 2013).
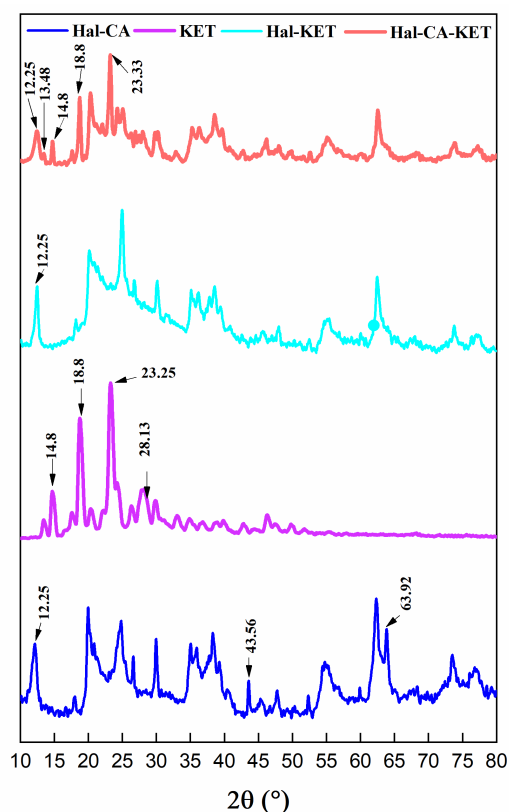
Fig. 2. X-ray diffractograms of samples.

Otherwise, the Hal-CA-KET pattern illustrates the appearance of KET diffraction peaks at the angular positions of 2θ = 13.4, 14.8, 18.8 and 23.3°. This confirms that the crystalline form of the molecular KET is not affected, while this crystalline structure is lost when KET is directly deposited on the unmodified Hal. This phenomenon probably shows that CA promotes the incorporation/adsorption of KET on Hal and further heterogeneous nucleation of KET crystals happens. In addition, the crystalline structure of Hal was poorly affected. This may be explained by the fact that KET is not interspersed in the interlamellar spacing, but rather deposited on the internal and external surfaces of Hal (Carretero and Pozo, 2010). Previously, the intercalation of organic molecules in Hal has been shown to depend on several factors, namely (i) the charge, the size of the organic molecule and the number of functional groups and (ii) the state of hydration of Hal (inter-lamellar water promoting further intercalation of organic molecules) (Tan et al., 2013). In our case, Hal is dehydrated and KET only exhibits one COOH group per molecule. These two characteristics do not favor the intercalation of KET in Hal. Comparable result was obtained concerning the intercalation of ibuprofen in Hal nanotubes (Tan et al., 2013).

3.2.2. FTIR spectroscopy

The interaction between KET and Hal or Hal-CA was further evaluated by FTIR spectroscopy (Fig. 3). The previously published spectrum of CA alone showed a broad band centered at 3291 cm^{-1} due to the stretching vibrations of the valence of OH (Segovia-Sandoval et al., 2018). Moreover, the peaks at 1725 cm^{-1}, 1400 cm^{-1} and 1222 cm^{-1} are due to the stretching vibrations of the carbonyl groups of CA. For the Hal-CA sample, in addition to the specific bands of Hal, the spectrum showed new bands characteristic of CA at 1765, 1735 and 1384 cm^{-1}. The peak at 1725 cm^{-1} (CA) moved to 1765 cm^{-1} (Hal-CA), thus demonstrating the functionalization of Hal through ester-type bonds (Sajab et al., 2011; Zhang et al., 2019).
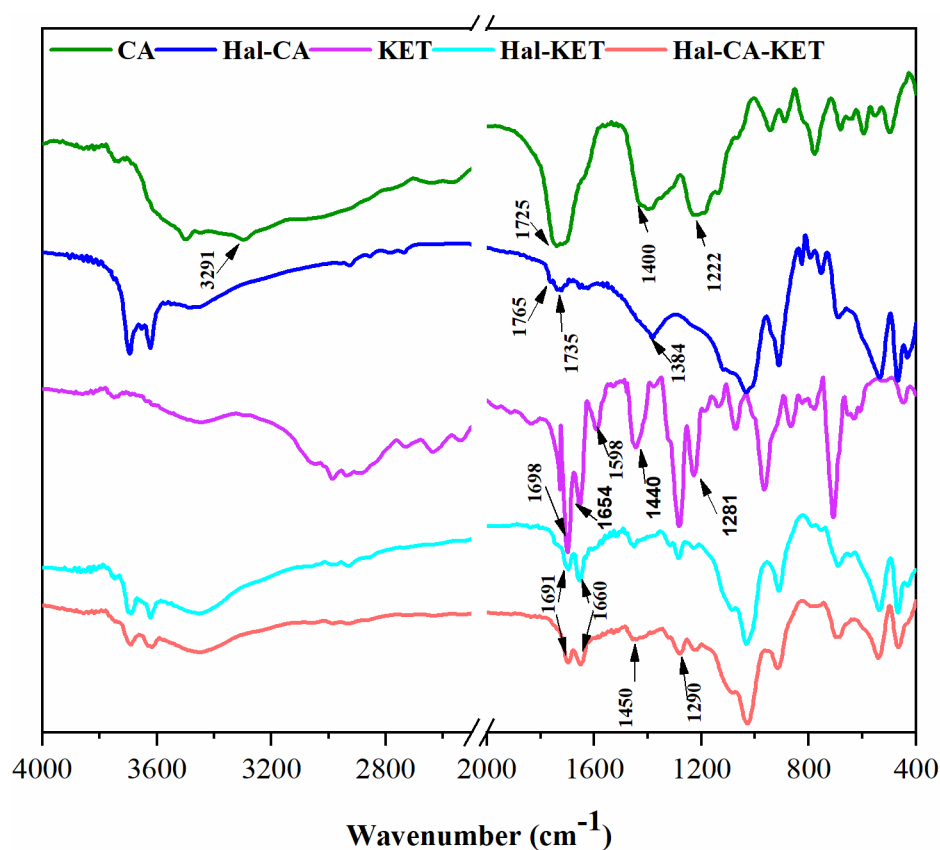

Fig. 3. FTIR spectra of samples (KET, Hal-KET, Hal-CA, Hal-CA-KET).

The spectrum of KET FTIR displayed characteristic adsorption peaks at 1698 cm^{-1} (C=C stretching of carboxylic acid), 1654 cm^{-1} (stretching of ketone group attached to two aromatic rings), 1598 cm^{-1} and 1440 cm^{-1} (C=C stretching from the aromatic ring), 1321 cm^{-1} (CH deformation of CH$_3$ symmetrical) and 1281 cm^{-1} (C=C deformation of aromatic rings). Concerning the Hal-KET and Hal-CA-KET samples, new peaks at 1691 cm^{-1}, 1660 cm^{-1}, 1450 cm^{-1} and 1290 cm^{-1}, belonging to KET, were observed. These shifted bands confirm that the KET molecules have been adsorbed from the surfaces of Hal and Hal-CA. The interaction

mechanisms between key groups of KET and Hal / Hal-CA (COOH, OH, Si-OH, Al-OH) should involve hydrogen bonds and/or Van der Waals interactions. These results are similar to that of 5-aminosalicylic acid and ibuprofen adsorbed on the external and internal surfaces of Hal (Aguzzi et al., 2013; Tan et al., 2013).

3.2.3. TEM analysis

Figure 4 shows the TEM images of Hal-KET, Hal-CA and Hal-CA-KET. Comparatively to the image of the Hal (Fig. 1(c)), the external diameter of Hal-KET and Hal-CA-KET was not significantly affected by the deposit of KET (Fig. S1). This result can conclude that the KET molecules were not inserted in the interlamellar spacing (Tan et al., 2013) although a change of the contrast in the lumen parts was observed on the TEM images of Hal-KET (Fig. 4(a)). Comparatively to Hal, this variation of the contrast confirms the presence of different electronic densities and may be related to the existence of KET molecules in the lumen.

Furthermore, the TEM images of Hal-CA and Hal-CA-KET present black spots (Fig. 4 (b) and (c)), illustrating that the surface of Hal was modified by CA-addition without a loss of the tubular morphology, and also, a slight degradation of the Hal was observed after the deposit treatment of CA and KET, these results are in good agreement with the XRD data.
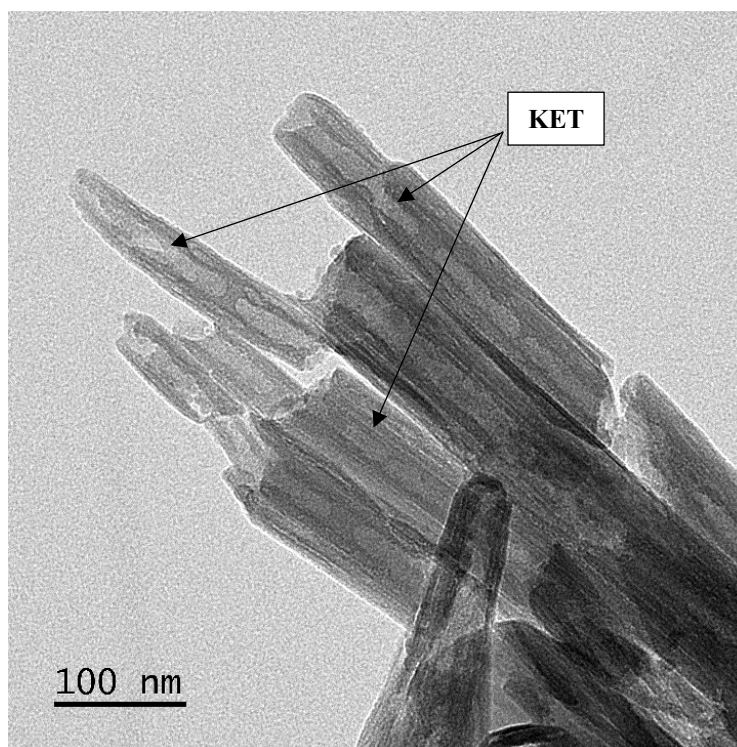
a)
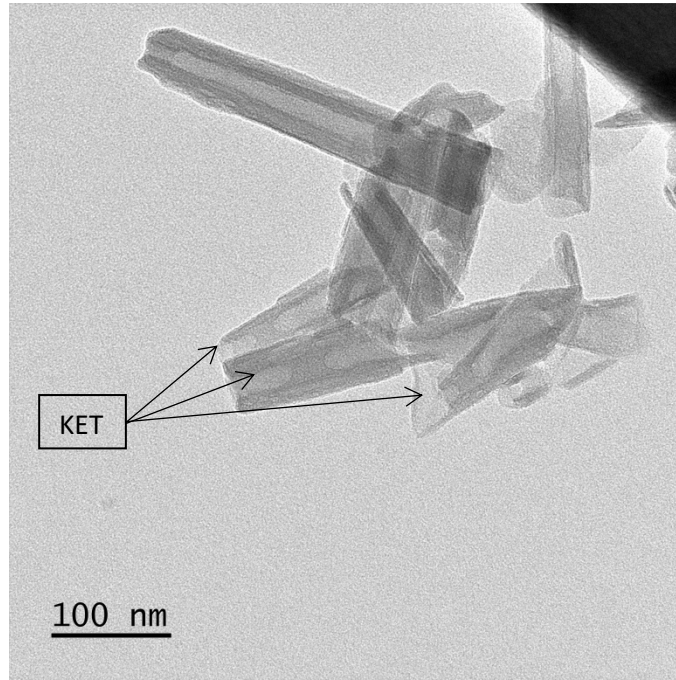
b)
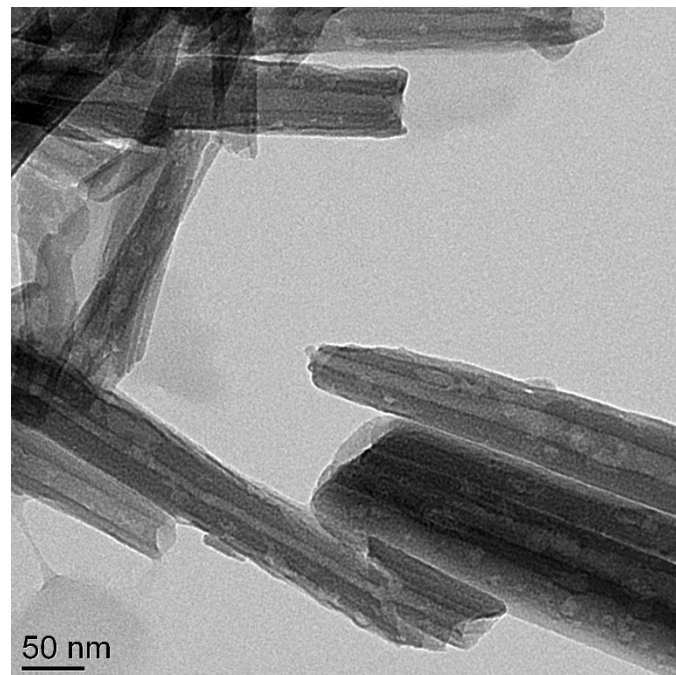
c)

Fig. 4. TEM images of Hal-*KET (a); Hal-CA (b) and Hal-CA-KET (c).*

3.2.4. N2 adsorption-desorption analysis

Figure 5 shows the adsorption–desorption isotherms of N_2, at 77 K, for the Hal-KET and Hal-CA-KET samples. The two isotherms are similar and belong to type II isotherms. This is characteristic of mesoporous/macroporous solids according to IUPAC classification, with H3 hysteresis loops. This indicates the presence of tubular pores (open at both ends) or of capillaries with an ink-well shape (San Roman et al., 2016). After activation of Hal with CA, the Hal surface area significantly decreases from 18.93 to 0.635 $m^2 \cdot g^{-1}$ (Figure not shown). This shows an interaction between CA and Hal indicating that the CA was inserted inside the pores interacting with the hydroxyl groups. After addition of KET, the S_{BET} and Vp values of the Hal-KET and Hal-CA-KET samples were increased. The corresponding values of S_{BET} and V_P are 40.7 $m^2 \cdot g^{-1}$ and 0.193 $cm^3 \cdot g^{-1}$ for Hal-KET and then 64.6 $m^2 \cdot g^{-1}$ and 0.296 $cm^3 \cdot g^{-1}$ for Hal-CA-KET. Furthermore, the pore diameter (Dp) increased from 11.8 nm (Hal) to 18.6 for Hal-KET and 18.0 nm for Hal-CA-KET. This change may have been due to the formation of micropores during surface breakage, resulting from structural rearrangement or transformation (Yuan et al.,

2012). Moreover, the values of 18.6 and 18.0 nm are of the same order of the internal diameter of the Hal (Tan et al., 2013).
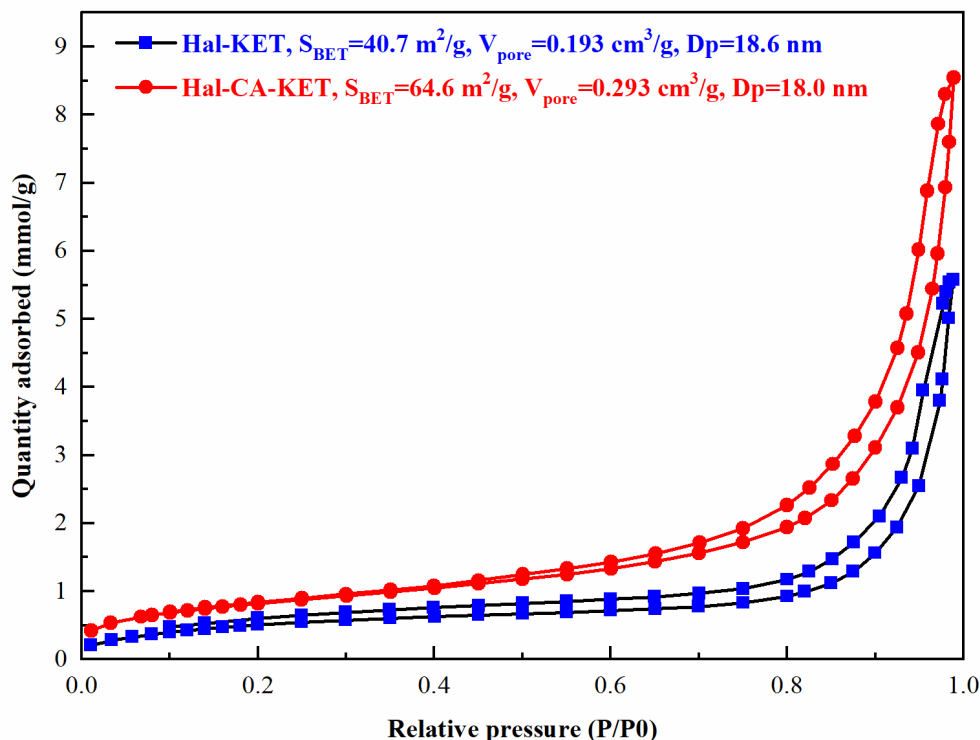

Fig. 5. N_2 adsorption/desorption isotherms of samples.

3.2.5. Thermogravimetric analysis

The thermogravimetry analysis (TGA) of Hal-CA, Hal-KET and Hal-CA-KET samples is shown in Fig. 6. The thermograms of CA and KET show thermal decompositions between 122-286 °C and 217-394 °C, respectively (Fig. S2). Under N_2 flow, they are fully decomposed into CO_2 and H_2O. These TGA profiles indicate that CA and KET should be considered as thermally stable up to 131 and 167 °C, respectively. The mass losses of Hal-KET and Hal-CA-KET show different profiles in comparison with pure Hal: the degradation profiles of KET, CA and Hal are largely impacted by the presence of the other constituents and resulting interactions. In particular, the degradation temperatures of KET in the two composites Hal-KET and Hal-CA-KET are shifted to higher temperatures in comparison with that of pure KET (Fig. 6). This strongly suggest that KET has been adsorbed in Hal and is more stable (Sabahi et al., 2018). KET degradation occurs above 500 °C, whereas the degradation peak is close to 480 °C for the pristine Hal. It is also observed that the remaining water content (determined from the mass loss between 20 and 200 °C) for the materials Hal-CA, Hal-KET and Hal-CA-KET are 5.80, 3.82 and 6.80%, respectively. These values are lower compared to pure Hal (10.71%). This

evidences the replacement of free and bound water from Hal by CA in Hal-CA and KET in Hal-KET and Hal-CA-KET. The total mass losses at 800 °C are 20.3, 20.2, 40.3 and 46% for the samples Hal, Hal-CA, Hal-KET and Hal-CA-KET, respectively. The increase in mass losses from pure Hal and Hal-CA to about 40-46% for Hal-KET and Hal-CA-KET is clearly due to the thermal degradation of KET retained by the aluminosilicate structure of the Hal. The intercalated quantities of KET in the Hal-KET and Hal-CA-KET samples are approximately 20 and 26%, respectively. These values were calculated using the following equations:

KET from HAL-KET % = (mass loss in HAL-KET) - (mass loss in HAL)，(7)

And

KET from HAL-CA-KET % = (mass loss in HAL-CA-KETO) - (mass loss in HAL-CA), (8)

These amounts adsorbed in Hal and Hal-CA are close to the amounts of other APIs adsorbed in Hal mentioned in the literature (Aguzzi et al., 2013; Abdullayev and Lvov, 2016). It is noted that the loading efficiency of active agents in clays can vary from 20 to 30%.
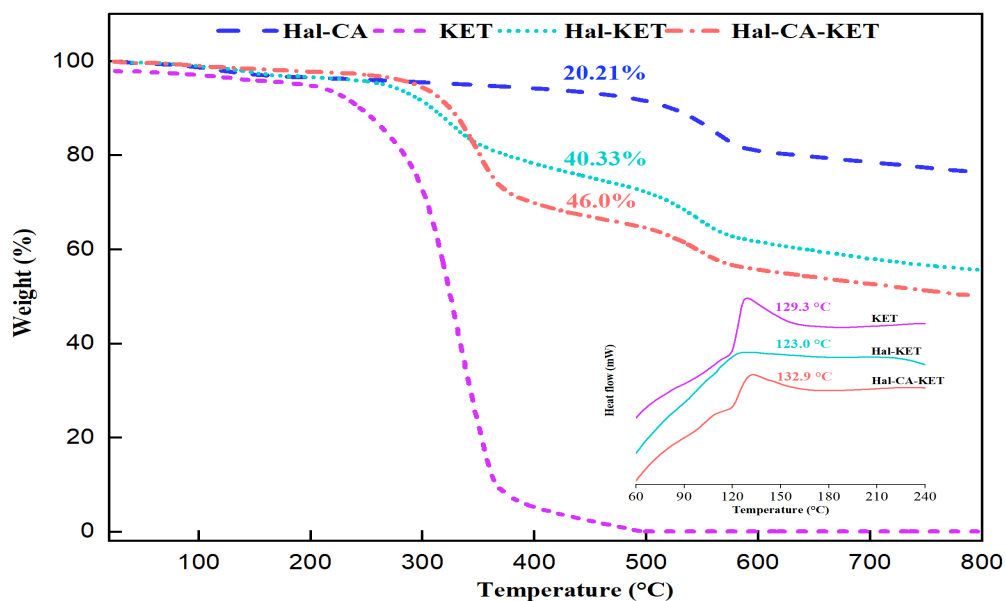

Fig. 6. ATG and DSC thermograms of samples.

3.3. In vitro drug release studies from unmodified and modified Hal

KET was successively released at pH 1 and then at pH 6.8 as displayed in Fig. 7. In fact, loading of KET in Hal and Hal-CA delayed the drug-release compared to the drug alone. Indeed, the cumulative release of KET from natural Hal was about 83% after 90 min. After treated with CA, an evident delay in the cumulative release to 34% after 90 min was clearly observed.
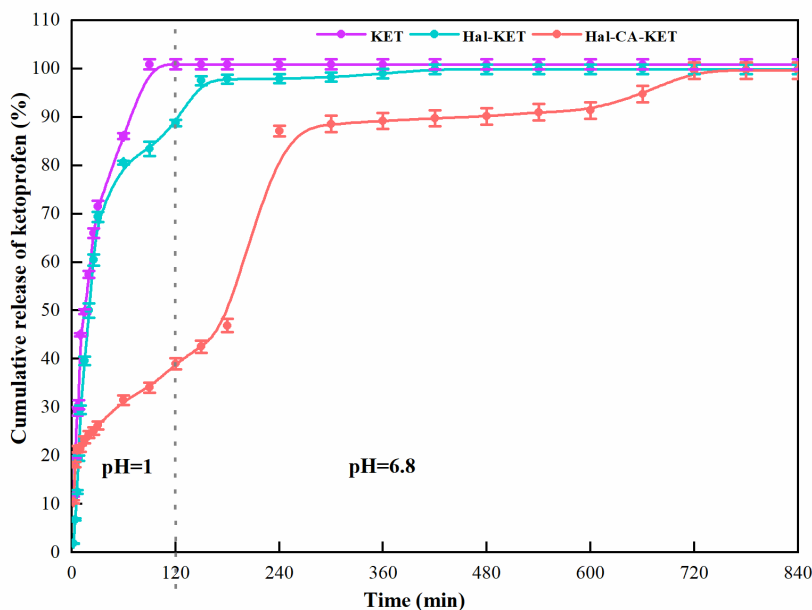

Fig. 7. Dissolution profiles of KET, KET from Hal and KET from Hal-CA.

At pH 1, the release of KET from the two formulations showed two stages, including a fast-bust release followed by a subsequent prolonged release. The fast release can be ascribed to the externally adsorbed KET, because the surface-loaded KET was weakly bonded through hydrogen bonding. The prolonged release of KET in Hal-KET can be ascribed to the release of the lumen-loaded KET, of which the diffusion was substantially delayed by the pseudo one-dimensional nanotube structure of Hal (Tan et al., 2013).

For the release of KET from CA-modified Hal, it is clearly observed that the burst release of KET was attenuated, and the prolongated release rate of KET was slower. The reason is the stronger interactions (hydrogen bonds) between KET and CA-modified Hal which delayed the dissolution and diffusion of KET from CA-modified Hal (Tan et al., 2013). Interestingly, pH impacted the release of KET with a faster release when the pH value of the medium reached 6.8. For Hal-KET and Hal-CA-KET, KET-release kinetics from Fig. 7 were fitted using three mathematical models as described in the literature (Costa and Sousa Lobo, 2001; Costa et al.,

2003; Dash et al., 2010). The best results were obtained with the Korsmeyer–Peppas model and are given in Table 2. Then KET demonstrates a quasi-Fickian release behavior (n<0.5) which indicates minimal interaction between KET and Hal-KET or Hal-CA-KET (Dantas de Freitas et al., 2018).

3.4. Carrageenan-induced rat paw edema

The carrageenan-induced paw edema is a popular test used in the screening of potential drugs and their corresponding formulations for anti-inflammatory activity. Results from the study indicate that pure KET caused 44% and 16% of paw edema inhibition at 3 h and 24 h, respectively (Fig. 8, Table S1).
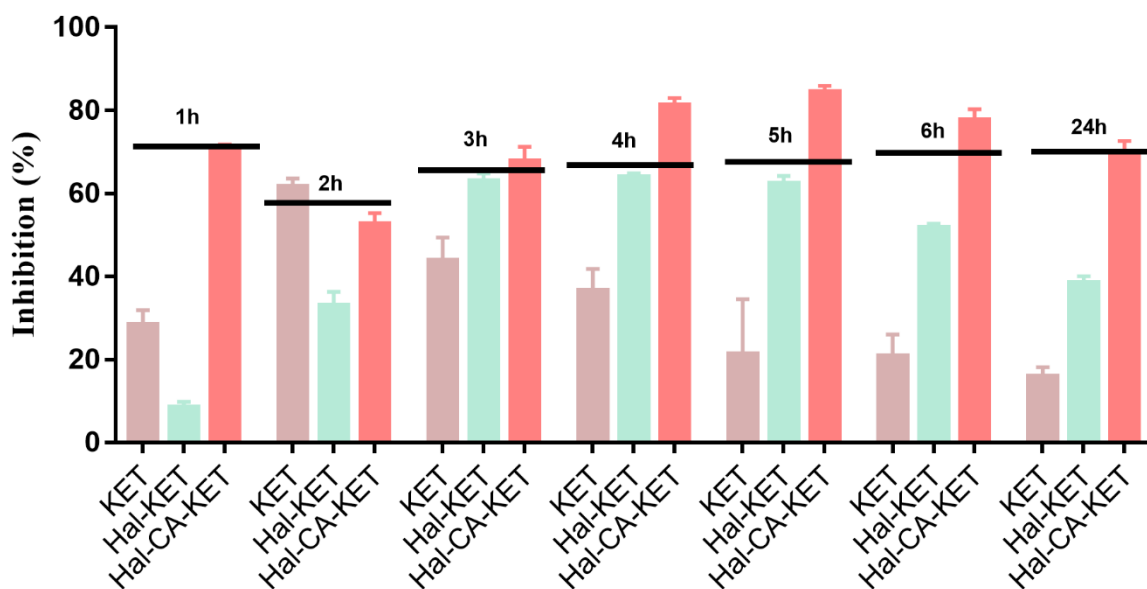
Fig. 8. Anti-inflammatory activity of KET, Hal-KET and Hal-CA-KET in rats.

KET-loaded Hal had greater anti-inflammatory effects than pure KET (Fig. 8, Table S1). Indeed, Hal-KET caused 63% and 39% of paw edema inhibition at 3 h and 24 h. This can be explained by a slower release of KET from Hal. With Hal-KET, the maximum inhibitory effect is obtained between 3 and 5 h, with a median value around 63%. This inhibitory effect is even more spectacular with the use of the Hal-CA-KET formulation, with inhibition values between 68% (3 h) and 70% (24 h) (Fig. 8, Table S1). The overall improvement of the anti-inflammatory effect is due to an initial fast release of KET from Hal-CA during the first h (inhibition effect

at 70%) and a subsequent slower release able to provide an effective concentration of KET for 24 h (with a maximum 85% at 5 h) (Table S1). Another issue is that simple Hal and Hal-CA formulations apparently also have their own anti-inflammatory effect (Cornejo-Garrido et al., 2012; Cervini-Silva et al., 2013). Between 2 and 24 h, the effect of Hal and Hal-CA is similar, around 20% inhibition (Fig. S3, Table S1). These observations strongly indicate that the Hal-CA-KET system is highly efficient for reducing inflammation, with a maximum inhibition of 83% between 4 and 5 h. This effect is maintained until 24 h, with 70% inhibition (only 16% for KET alone).

Table 2: Release parameters for formulations obtained after data fitting with Korsmeyer–Peppas model of drug release kinetics.

	Sample	K_{KP}	n	R^2
pH=1	Hal-KET	0.104±0.0271	0.473±0.0637	0.900
	Hal-CA-KET	0.115±0.0078	0.248±0.0177	0.981
pH=6.8	Hal-KET	0.899±0.0130	0.0161±0.0018	0.870
	Hal-CA-KET	0.116±0.0617	0.327±0.071	0.973

3.5. Acetic acid-induced writhings

The treatment with Hal and Hal-CA clay nanotubes by oral administration removed writhings and enhancing the anti-nociceptive effect, with values between 41% and 30% for Hal and Hal-CA, respectively **(Fig. S4)**. KET alone reduced writhings by 83%, on the other hand, a maximum effect of 100% both with Hal-KET and Hal-CA-KET **(Fig. 9)**.
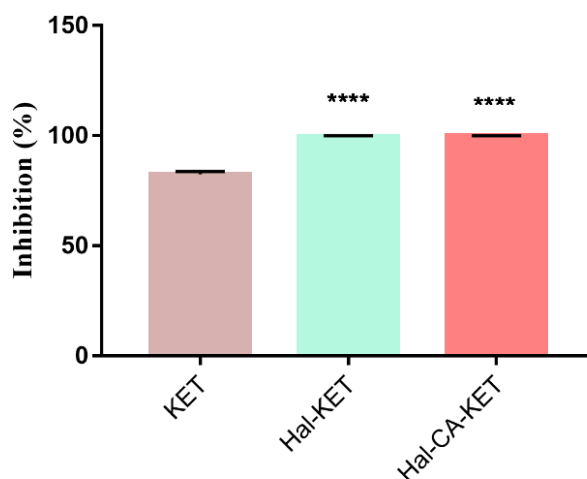

Fig. 9. Analgesic effect of KET, Hal-KET and Hal-CA-KET on acetic acid-induced writhings in mice. **** p <0.0001 very highly significantly.

3.6. Ulcerogenicity study

A systematic macroscopic examination of all rat stomach (n = 24) was performed. For each group, a typical representative image of the stomach (fundus-corpus) is shown (Fig. 10). Negative control group displayed a healthy corpus (Fig. 10(a)), whereas the KET administration generated well-defined hemorrhagic streak ulcers (Fig. 10(b)) with a maximum percentage of ulceration area close to 11% (Fig. 11).

Hal-KET demonstrated a significant protective effect of stomach (Fig. 10(c)) in comparison with KET-treated rats, with also only 0.3% of ulceration (Fig. 11). Nevertheless, Hal-CA-KET provided the total mucosa protection (Fig. 10(d)). In addition, it is important to note that Hal and Hal-CA may adhere to the GI mucous membrane and then protect the stomach wall (e.g. by increasing the viscosity and stability of the gastric mucus) (Carretero and Pozo, 2010; Awad et al., 2017).
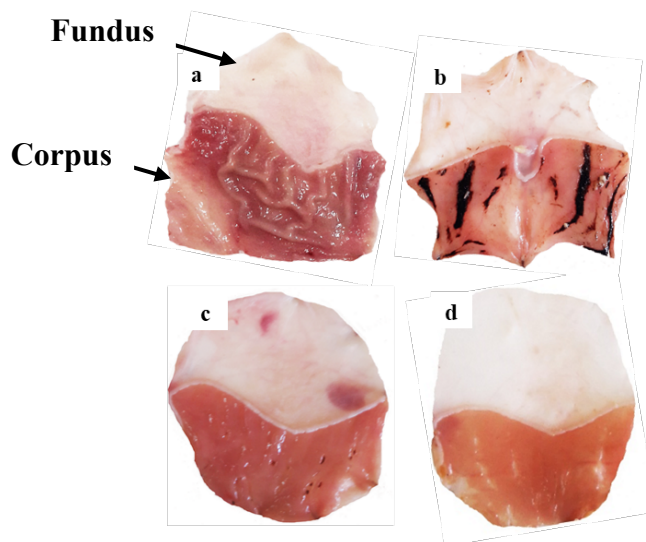

Fig. 10. Macroscopic findings of KET-induced gastric mucosal lesions.
Control (a); KET (b); Hal-KET (c) and Hal-CA-KET (d).
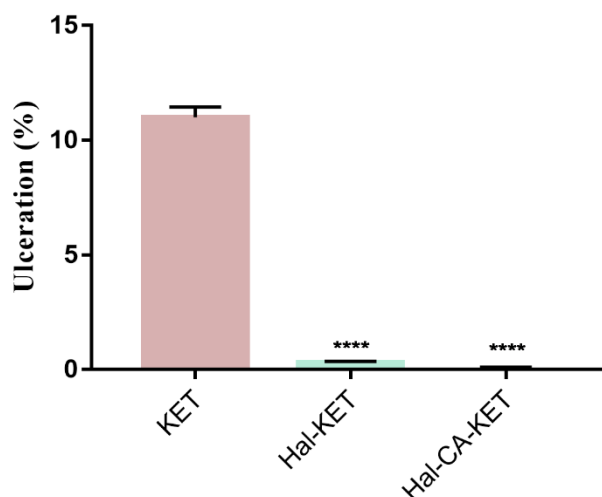
Fig. 11. Percentage of KET-induced ulceration (total area of lesions).
**** p <0.0001 very highly significantly.

3.7. Histopathological studies

Histopathological studies were conducted in rats. It was observed no gastric damage in the negative control group (saline) as shown in Fig. 12($a_{1,2}$). In the positive control group (KET), necrotic gastric mucosa was found with external hemorrhages and deeply penetrated injuries into the gastric epithelium (Fig. 12($b_{1,2}$)). Severe congestion, dilated blood vessels (Fig. 12(b_3)) and infiltration of neutrophil inflammatory cells (Fig. 12(b_4)) were also present. On the other hand, KET-loaded Hal decreased the pathological structure of the gastric mucosa when compared with those of the KET group (Fig. 12($c_{1,2}$)). Nevertheless, histopathological examination revealed that stomach tissue showed sub-mucosal congestion and mild inflammation (Fig. 12($c_{1,2}$)). In the case of KET-loaded Hal-CA, histopathological examination revealed that stomach tissue showed normal gastric mucosa (Fig. 12($d_{1,2}$)). The results of macroscopic and microscopic observations were then strongly correlated.

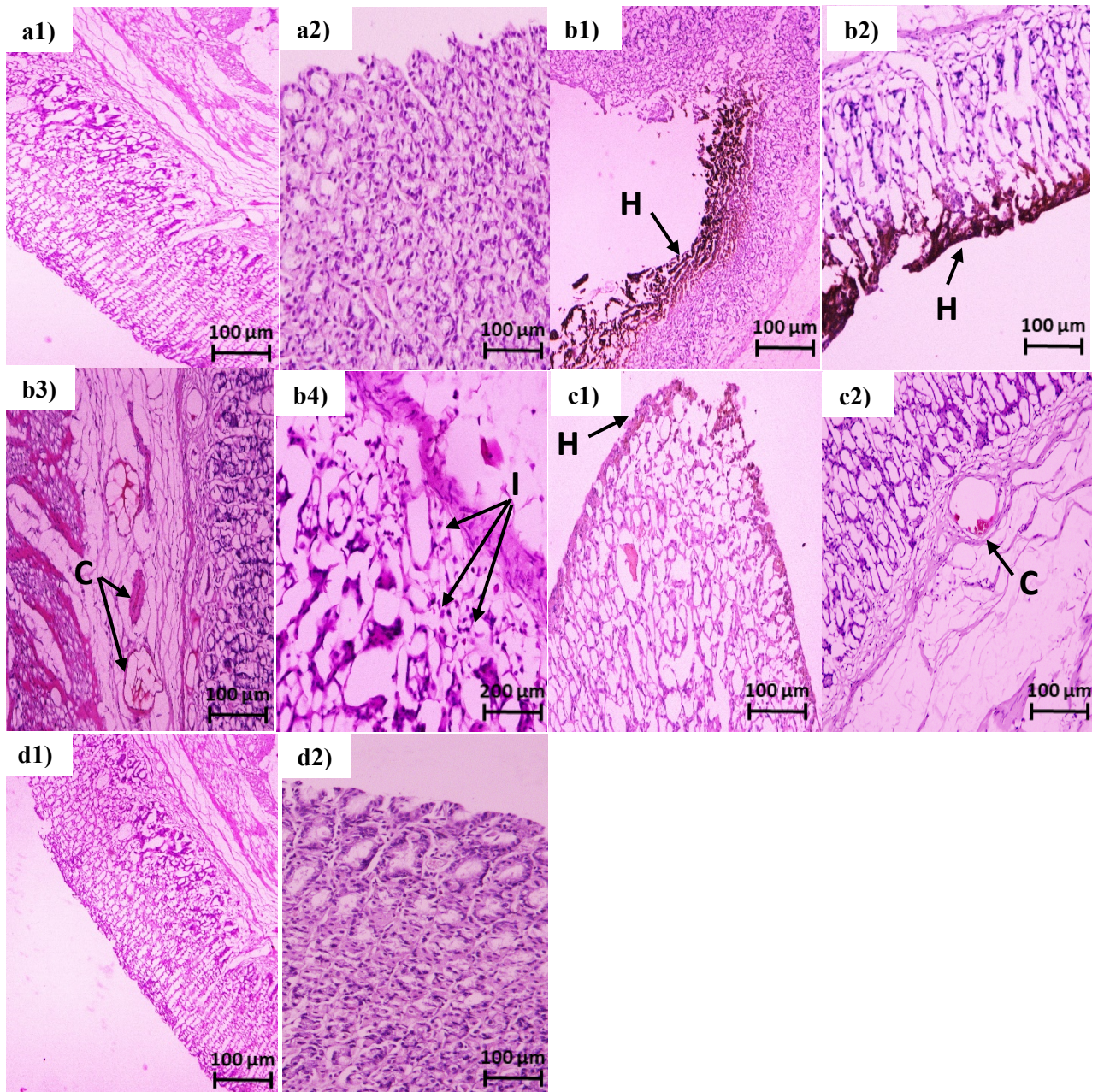**Fig. 12.** Stomach histopathology: control rats (a$_1$,a$_2$); rats treated with KET (b$_1$-b$_4$); rats treated with Hal-KET (c$_1$,c$_2$) and rats treated with Hal-CA-KET (d$_1$,d$_2$). Congestion (**C**), infiltration (**I**), hemorrhagic bands in the gastric mucosa (**H**).

4. Conclusions

The present study successfully endorsed the development and evaluation of a novel formulation which ensures both the increase in the therapeutic effectiveness of KET and a decrease in the gastric damage related to its main side effects. Hal and Hal-CA were found to be a convenient and reliable nanoscale carrier platform for loading of KET. In addition, results of the physicochemical characterization confirmed the interaction between HAL-CA and KET, both in the luminal space and external surfaces. *In vitro* release kinetics of the Hal-CA clay nanotubes revealed an effective release for 24 h. *In vivo* studies indicated clearly that the treatment of animals with formulations reduced carrageenan-induced paw edema and the number of writhings induced by acetic acid. Moreover, Hal-CA-KET provides a total gastric mucosa protection. Hal-CA can be considered as a promising and credible tool for future pharmaceutical formulations.

Ethics statement

The animal studies were carried out after getting the clearance of the Ethics Committee of the Université Ferhat Abbas Sétif 1 (ref. CED/01/03-2019), and the experiments were conducted in strict compliance following the ethical principles provided by the Committee for the Purpose of Control and Supervision of Experiments on Animal (CPCSEA).

References

Abdullayev, E., Lvov, Y., 2016. Chapter 22 - Halloysite for Controllable Loading and Release, in: Yuan, P., Thill, A., Bergaya, F. (Eds.), Developments in Clay Science, Nanosized Tubular Clay Minerals. Elsevier, pp. 554–605. https://doi.org/10.1016/B978-0-08-100293-3.00022-4.

Abdullayev, E., Lvov, Y., 2013. Halloysite clay nanotubes as a ceramic "skeleton" for functional biopolymer composites with sustained drug release. J. Mater. Chem. B 1, 2894–2903. https://doi.org/10.1039/C3TB20059K.

Aguzzi, C., Viseras, C., Cerezo, P., Salcedo, I., Sánchez-Espejo, R., Valenzuela, C., 2013. Release kinetics of 5-aminosalicylic acid from halloysite. Colloids Surf. B Biointerfaces 105, 75–80. https://doi.org/10.1016/j.colsurfb.2012.12.041.

Alipoormazandarani, N., Ghazihoseini, S., Mohammadi Nafchi, A., 2015. Preparation and characterization of novel bionanocomposite based on soluble soybean polysaccharide and halloysite nanoclay. Carbohydr. Polym. 134, 745–751. https://doi.org/10.1016/j.carbpol.2015.08.059.

Apelblat, A., Barthel, J., 1991. Conductance studies on aqueous citric acid. Z. Naturforsch. A 46, 131–140. https://doi.org/10.1515/zna-1991-1-222.

Awad, M.E., López-Galindo, A., Setti, M., El-Rahmany, M.M., Iborra, C.V., 2017. Kaolinite in pharmaceutics and biomedicine. Int. J. Pharm. 533, 34–48. https://doi.org/10.1016/j.ijpharm.2017.09.056.

Bergaya, F., Lagaly, G., 2013. Chapter 7.1 - Purification of Natural Clays, in: Bergaya, Faïza, Lagaly, Gerhard (Eds.), Developments in Clay Science, Handbook of Clay Science. Elsevier, pp. 213–221. https://doi.org/10.1016/B978-0-08-098258-8.00008-0.

Bertolino, V., Cavallaro, G., Lazzara, G., Milioto, S., Parisi, F., 2018. Halloysite nanotubes sandwiched between chitosan layers: a novel bionanocomposite with multilayer structure. New J. Chem. 42, 8384–8390. https://doi.org/10.1039/C8NJ01161C.

Boppana, R., Kulkarni, R.V., Mohan, G.K., Mutalik, S., Aminabhavi, T.M., 2016. In vitro and in vivo assessment of novel pH-sensitive interpenetrating polymer networks of a graft copolymer for gastro-protective delivery of ketoprofen. RSC Adv. 6, 64344–64356. https://doi.org/10.1039/C6RA04218J.

Brunauer, S., Emmett, P. H, Teller, E., 1938. Adsorption of gases in multimolecular layers. J. Am. Chem. Soc. 60, 309–319. https://doi.org/10.1021/ja01269a023.

Carretero, M.I., Pozo, M., 2010. Clay and non-clay minerals in the pharmaceutical and cosmetic industries Part II. Active ingredients. Appl. Clay Sci. 47, 171–181. https://doi.org/10.1016/j.clay.2009.10.016.

Cerciello, A., Auriemma, G., Morello, S., Pinto, A., Del Gaudio, P., Russo, P., Aquino, R.P., 2015. Design and in vivo anti-inflammatory effect of ketoprofen delayed delivery systems. J. Pharm. Sci. 104, 3451–3458. https://doi.org/10.1002/jps.24554.

Cervini-Silva, J., Nieto-Camacho, A., Palacios, E., Montoya, J.A., Gómez-Vidales, V., Ramírez-Apán, M.T., 2013. Anti-inflammatory and anti-bacterial activity and cytotoxicity of halloysite surfaces. Colloids Surf. B Biointerfaces 111, 651–655. https://doi.org/10.1016/j.colsurfb.2013.06.056.

Charaabi, S., Tchara, L., Marminon, C., Bouaziz, Z., Holtzinger, G., Pensé-Lhéritier, A., Le Borgne, M., Issa, S., 2019.A comparative adsorption study of benzophenone-3 onto synthesized lipophilic organosilicate, Laponite and montmorillonite. Appl. Clay Sci. 170, 114–124. https://doi.org/10.1016/j.clay.2019.01.005.

Charaabi, S., Absi, R., Pensé-Lhéritier, A., Le Borgne, M., Issa, S., 2021. Adsorption studies of benzophenone-3 onto clay minerals and organosilicates: Kinetics and modelling. Appl. Clay Sci. 202, 105937. https://doi.org/10.1016/j.clay.2020.105937.

Cornejo-Garrido, H., Nieto-Camacho, A., Gómez-Vidales, V., Ramírez-Apan, M.T., del Angel, P., Montoya, J.A., Domínguez-López, M., Kibanova, D., Cervini-Silva, J., 2012. The anti-inflammatory properties of halloysite. Appl. Clay Sci. 57, 10–16. https://doi.org/10.1016/j.clay.2011.12.001.

Costa, F.O., Sousa, J.J.S., Pais, A.A.C.C., Formosinho, S.J., 2003. Comparison of dissolution profiles of ibuprofen pellets. J. Control. Release, 89, 199–212. https://doi.org/10.1016/S0168-3659(03)00033-6.

Costa, P., Sousa Lobo, J.M., 2001. Modeling and comparaison dissolution profiles of ibuprofen pellets. Eur. J. Pharm. Sci., 13, 123–133. https://doi.org/10.1016/s0928-0987(01)00095-1.

Cunha, V.R.R., Guilherme, V.A., de Paula, E., de Araujo, D.R., Silva, R.O., Medeiros, J.V.R., Leite, J.R.S.A., Petersen, P.A.D., Foldvari, M., Petrilli, H.M., Constantino, V.R.L., 2016. Delivery system for mefenamic acid based on the nanocarrier layered double hydroxide: Physicochemical characterization and evaluation of anti-inflammatory and antinociceptive potential. Mater. Sci. Eng. C 58, 629–638. https://doi.org/10.1016/j.msec.2015.08.037.

Dantas de Freitas, E., Pires Rosa, P.R., Carlos da Silva, M.G., Adeodato Vieira, M.G., 2018. Development of sericin/alginate beads of ketoprofen using experimental design: Formulation and *in vitro* dissolution evaluation. Powder Technol. 335, 315–326. https://doi.org/10.1016/j.powtec.2018.05.016.

Dash, S., Murphy, P.N., Nath, I., Chowdhury, P., 2010. Kinetic modeling on drug release from controlled drug delivery systems. Acta Pol. Pharm., 67, 217–223.

Freitas, E.D. de, Rosa, P.C.P., Silva, M.G.C. da, Vieira, M.G.A., 2018. Development of sericin/alginate beads of ketoprofen using experimental design: Formulation and in vitro dissolution evaluation. Powder Technol. 335, 315–326. https://doi.org/10.1016/j.powtec.2018.05.016.

Ghorpade, V.S., Yadav, A.V., Dias, R.J., 2017. Citric acid crosslinked β-cyclodextrin/carboxymethylcellulose hydrogel films for controlled delivery of poorly soluble drugs. Carbohydr. Polym. 164, 339–348. https://doi.org/10.1016/j.carbpol.2017.02.005.

Ghorpade, V.S., Yadav, A.V., Dias, R.J., 2016. Citric acid crosslinked cyclodextrin/hydroxypropylmethylcellulose hydrogel films for hydrophobic drug delivery. Int. J. Biol. Macromol. 93, 75–86. https://doi.org/10.1016/j.ijbiomac.2016.08.072.

Ghorpade, V.S., Yadav, A.V., Dias, R.J., Mali, K.K., Pargaonkar, S.S., Shinde, P.V., Dhane, N.S., 2018. Citric acid crosslinked carboxymethylcellulose-poly(ethylene glycol) hydrogel films for delivery of poorly soluble drugs. Int. J. Biol. Macromol. 118, 783–791. https://doi.org/10.1016/j.ijbiomac.2018.06.142.

Gregg, S.J., Sing, K.S.W., 1982. Adsorption, surface area and porosity. 2nd ed. Academic Press, London. https://doi.org/10.1002/bbpc.19820861019.

Hanif, M., Jabbar, F., Sharif, S., Abbas, G., Farooq, A., Aziz, M., 2016. Halloysite nanotubes as a new drug-delivery system: a review. Clay Miner. 51, 469–477. https://doi.org/10.1180/claymin.2016.051.3.03.

Harikrishnan, S., Sedev, R., Beh, C.C., Priest, C., Foster, N.R., 2020. Loading of 5-fluorouracil onto Halloysite nanotubes for targeted drug delivery using a subcritical gas antisolvent process (GAS). J. Supercrit. Fluids 159, 104756. https://doi.org/10.1016/j.supflu.2020.104756.

Hemmatpour, H., Haddadi-Asl, V., Roghani-Mamaqani, H., 2015. Synthesis of pH-sensitive poly (N,N-dimethylaminoethyl methacrylate)-grafted halloysite nanotubes for adsorption and controlled release of DPH and DS drugs. Polymer 65, 143–153. https://doi.org/10.1016/j.polymer.2015.03.067.

Huang, J., Zhang, Y., Zhang, Y., 2021. Preparation and characterization of manganese oxides supported on functionalized halloysite nanotubes with enhanced catalytic oxidation for toluene. Appl. Clay Sci. 209, 106147. https://doi.org/10.1016/j.clay.2021.106147.

Joussein, E., Petit, S., Churchman, J., Theng, B., Righi, D., Delvaux, B., 2005. Halloysite clay minerals - a review. Clay Miner. 40, 383–426. https://doi.org/10.1180/0009855054040180.

Kantor, T.G., 1986. Ketoprofen: A review of itspharmacologic and clinicalproperties. Pharmacotherapy 6, 93–102. https://doi.org/10.1002/j.1875-9114.1986.tb03459.x.

Kim, H., Fassihi, R., 1997. Application of binary polymer system in drug release rate modulation. 2. Influence of formulation variables and hydrodynamic conditions on release kinetics. J. Pharm. Sci. 86, 323–328. https://doi.org/10.1021/js960307p.

Laudanno, O.M., Cesolari, J.A., Esnarriaga, J., San Miguel, P., Bedini, O.A., 2000. In vivo selectivity of nonsteroidalantiinflammatorydrugs and gastrointestinal ulcers in rats. Dig. Dis. Sci. 45, 1359–1365. https://doi.org/10.1023/A:1005508120776.

Li, Z., Zhao, S., Wang, H., Peng, Y., Tan, Z., Tang, B., 2019. Functional groups influence and mechanism research of UiO-66-type metal-organic frameworks for ketoprofen delivery. Colloids Surf. B Biointerfaces 178, 1–7. https://doi.org/10.1016/j.colsurfb.2019.02.027.

Lisuzzo, L., Cavallaro, G., Milioto, S., Lazzara, G., 2019. Layered composite based on halloysite and natural polymers: a carrier for the pH controlled release of drugs. New J. Chem. 43, 10887–10893. https://doi.org/10.1039/C9NJ02565K.

Lisuzzo, L., Cavallaro, G., Milioto. S., Lazzara, G., 2020. Effects of halloysite content on the thermo-mechanical performances of composite bioplastics, Appl. Clay Sci. 185, 105416. https://doi.org/10.1016/j.clay.2019.105416.

Lisuzzo, L., Cavallaro, G., Milioto. S., Lazzara, G., 2021. Halloysite nanotubes filled with salicylic acid and sodium diclofenac: effects of vacuum pumping on loading and release properties. J. Nanostruct. Chem. https://doi.org/10.1007/s40097-021-00391-z.

Lisuzzo, L., Cavallaro, G., Pasbakhsh, P., Milioto, S., Lazzara, G., 2019. Why does vacuum drive to the loading of halloysite nanotubes? The key role of water confinement. J. Colloid Interface Sci. 547, 361–369. https://doi.org/10.1016/j.jcis.2019.04.012.

Liu, M., Jia, Z., Jia, D., Zhou, C., 2014. Recent advance in research on halloysite nanotubes-polymer nanocomposite. Prog. Polym. Sci. 39, 1498–1525. https://doi.org/10.1016/j.progpolymsci.2014.04.004.

Maestrelli, F., Zerrouk, N., Cirri, M., Mura, P., 2015. Comparative evaluation of polymeric and waxy microspheres for combined colon delivery of ascorbic acid and ketoprofen. Int. J. Pharm. 485, 365–373. https://doi.org/10.1016/j.ijpharm.2015.02.073.

Mangindaan, D., Chen, C.-T., Wang, M.-J., 2012. Integrating sol–gel with cold plasmas modified porous polycaprolactone membranes for the drug-release of silver-sulfadiazine and ketoprofen. Appl. Surf. Sci. 262, 114–119. https://doi.org/10.1016/j.apsusc.2012.03.003.

Massaro, M., Colletti, C.G., Lazzara, G., Milioto, S., Noto, R., Riela, S., 2017. Halloysite nanotubes as support for metal-based catalysts. J. Mater. Chem. A 5, 13276–13293. https://doi.org/10.1039/C7TA02996A.

Massaro, M., Cavallaro, G., Colletti, C.G., Lazzara, G., Milioto, S., Noto, R., Riela, S., 2018. Chemical modification of halloysite nanotubes for controlled loading and release. J. Mater. Chem. B 6, 3415–3433. https://doi.org/10.1039/C8TB00543E.

de Matos Fonseca, J., de Fátima Medeiros, S., Alves, G.M., Santos, D.M.D., Campana-Filho, S.P., Santos, A., 2019. Chitosan microparticles embedded with multi-responsive poly(N-vinylcaprolactam-co-itaconic acid-co-ethylene-glycol dimethacrylate)-based hydrogel nanoparticles as a new carrier for delivery of hydrophobic drugs. Colloids Surf. B Biointerfaces 175, 73–83. https://doi.org/10.1016/j.colsurfb.2018.11.042.

Oliyaei, N., Moosavi-Nasab, M., Tamaddon, A.M., Fazaeli, M., 2019. Preparation and characterization of porous starch reinforced with halloysite nanotube by solvent exchange method. Int. J. Biol. Macromol. 123, 682–690. https://doi.org/10.1016/j.ijbiomac.2018.11.095.

Rençber, S., Karavana, S.Y., Özyazici, M., 2009. Bioavailability file: Ketoprofen. FABAD J. Pharm. Sci. 34, 203–216.

Rozhina, E., Panchal, A., Akhatova, F., Lvov, Y., Fakhrullin, R., 2020. Cytocompatibility and cellular uptake of alkylsilane-modified hydrophobic halloysite nanotubes. Appl. Clay Sci. 185, 105371. https://doi.org/10.1016/j.clay.2019.105371.

Sabahi, H., Khorami, M., Rezayan, A.H., Jafari, Y., Karami, M.H., 2018. Surface functionalization of halloysite nanotubes via curcumin inclusion. Colloids Surf. A Physicochem. Eng. Asp. 538, 834–840. https://doi.org/10.1016/j.colsurfa.2017.11.038.

Sahnoun, S., Boutahala, M., Zaghouane-Boudiaf, H., Zerroual, L., 2016. Trichlorophenol removal from aqueous solutions by modified halloysite: kinetic and equilibrium studies. Desalination Water Treat. 57, 15941–15951. https://doi.org/10.1080/19443994.2015.1075159.

Sajab, M.S., Chia, C.H., Zakaria, S., Jani, S.M., Ayob, M.K., Chee, K.L., Khiew, P.S., Chiu, W.S., 2011. Citric acid modified kenaf core fibres for removal of methylene blue from aqueous solution. Bioresour. Technol. 102, 7237–7243. https://doi.org/10.1016/j.biortech.2011.05.011.

San Román, M.S., Holgado, M.J., Salinas, B., Rives, V., 2012. Characterisation of diclofenac, ketoprofen or chloramphenicol succinate encapsulated in layered double hydroxides with the hydrotalcite-type structure. Appl. Clay Sci. 55, 158–163. https://doi.org/10.1016/j.clay.2011.11.010.

San Roman, S., Gullón, J., Del Arco, M., Martin, C., 2016. Influence of the surface acidity of the alumina on the sustained release of ketoprofen. J. Pharma. Sci, 105, 2146-2154. https://doi.org/10.1016/j.xphs.2016.04.029.

Schilling, S.U., Bruce, C.D., Shah, N.H., Malick, A.W., McGinity, J.W., 2008. Citric acid monohydrate as a release-modifying agent in melt extruded matrix tablets. Int. J. Pharm. 361, 158–168. https://doi.org/10.1016/j.ijpharm.2008.05.035.

Segovia-Sandoval, S.J., Ocampo-Pérez, R., Berber-Mendoza, M.S., Leyva-Ramos, R., Jacobo-Azuara, A., Medellín-Castillo, N.A., 2018. Walnut shell treated with citric acid and its application as biosorbent in the removal of Zn(II). J. Water Process Eng. 25, 45–53. https://doi.org/10.1016/j.jwpe.2018.06.007.

Tan, D., Yuan, P., Annabi-Bergaya, F., Yu, H., Liu, D., Liu, H., He, H., 2013. Natural halloysite nanotubes as mesoporous carriers for the loading of ibuprofen. Micropor. Mesopor. Mat. 179, 89–98. https://doi.org/10.1016/j.micromeso.2013.05.007.

Tcheumi, H.L., Tassontio, V.N., Tonle, I.K., Ngameni, E., 2019. Surface functionalization of smectite-type clay by facile polymerization of β-cyclodextrin using citric acid cross linker: Application as sensing material for the electrochemical determination of paraquat. Appl. Clay Sci. 173, 97–106. https://doi.org/10.1016/j.clay.2019.03.013.

Tharmavaram, M., Pandey, G., Rawtani, D., 2018. Surface modified halloysite nanotubes: A flexible interface for biological, environmental and catalytic applications. Adv.Colloid Interface Sci. 261, 82–101. https://doi.org/10.1016/j.cis.2018.09.001.

Torres Sànchez, R.M., Basaldella, E.I., Marco, J.F., 1999. The effect of thermal and mechanical treatment on Kaolinite: Characterization by XPS and IEP measurements. J. Colloid Interf. Sci. 215, 339–344. https://doi.org/10.1006/jcis.1999.6241.

Veerabadran, N.G., Price, R.R., Lvov, Y.M., 2007. Clay nanotubes for encapsulation and sustained release of drugs. Nano 02, 115–120. https://doi.org/10.1142/S1793292007000441.

Vergaro, V., Lvov, Y.M., Leporatti, S., 2012. Halloysite claynanotubes for resveratrol delivery to cancer cells. Macromol. Biosci. 12, 1265–1271. https://doi.org/10.1002/mabi.201200121.

Wagner, J.G., 1969. Interpretation of percent dissolved-time plots derived from in vitro testing of conventional tablets and capsules. J. Pharm. Sci. 58, 1253–1257. https://doi.org/10.1002/jps.2600581021.

Xia, M., Liu, H., Wang, H., Sun, F., Zou, X., Chen, T., Chu, Z., Chen, D., Zhou, Y., Xie, Q., 2021. Impact of the interaction between hematite and halloysite on environmental fate of organic pollutants. Appl. Clay Sci. 209, 106123. https://doi.org/10.1016/j.clay.2021.106123.

Yang, H., Zhang, Y., Ouyang, J., 2016. Chapter 4 - Physicochemical Properties of Halloysite, in: Yuan, P., Thill, A., Bergaya, F. (Eds.), Developments in Clay Science, Nanosized Tubular Clay Minerals. Elsevier, pp. 67–91. https://doi.org/10.1016/B978-0-08-100293-3.00004-2.

Yendluri, R., Lvov, Y., de Villiers, M.M., Vinokurov, V., Naumenko, E., Tarasova, E., Fakhrullin, R., 2017a. Paclitaxel encapsulated in halloysite clay nanotubes for intestinal and intracellular delivery. J. Pharm. Sci. 106, 3131–3139. https://doi.org/10.1016/j.xphs.2017.05.034.

Yendluri, R., Otto, D.P., De Villiers, M.M., Vinokurov, V., Lvov, Y.M., 2017b. Application of halloysite clay nanotubes as a pharmaceutical excipient. Int. J. Pharm. 521, 267–273. https://doi.org/10.1016/j.ijpharm.2017.02.055.

Yuan, P., Tan, D., Annabi-Bergaya, F., Yan, W., Fan, M., Liu, D., He, H., 2012. Changes in structure, morphology, porosity, and surface activity of mesoporous halloysite nanotubes underheating. Clays Clay Miner. 60, 561–573. https://doi.org/10.1346/CCMN.2012.0600602.

Zhang, H., Zhou, J., Muhammad, Y., Tang, R., Liu, K., Zhu, Y., Tong, Z., 2019. Citric acid modified bentonite for Congo Red adsorption. Front. Mater. 6, 1–5. https://doi.org/10.3389/fmats.2019.00005.

Zhao, Q., Gao, H., Su, Y., Huang, T., Lu, J., Yu, H., Ouyang, D., 2019. Experimental characterization and molecular dynamic simulation of ketoprofen-cyclodextrin complexes. Chem. Phys. Lett. 736, 136802. https://doi.org/10.1016/j.cplett.2019.136802.

Supplementary information for the publication: Improved biological performance of ketoprofen using novel modified halloysite clay nanotubes
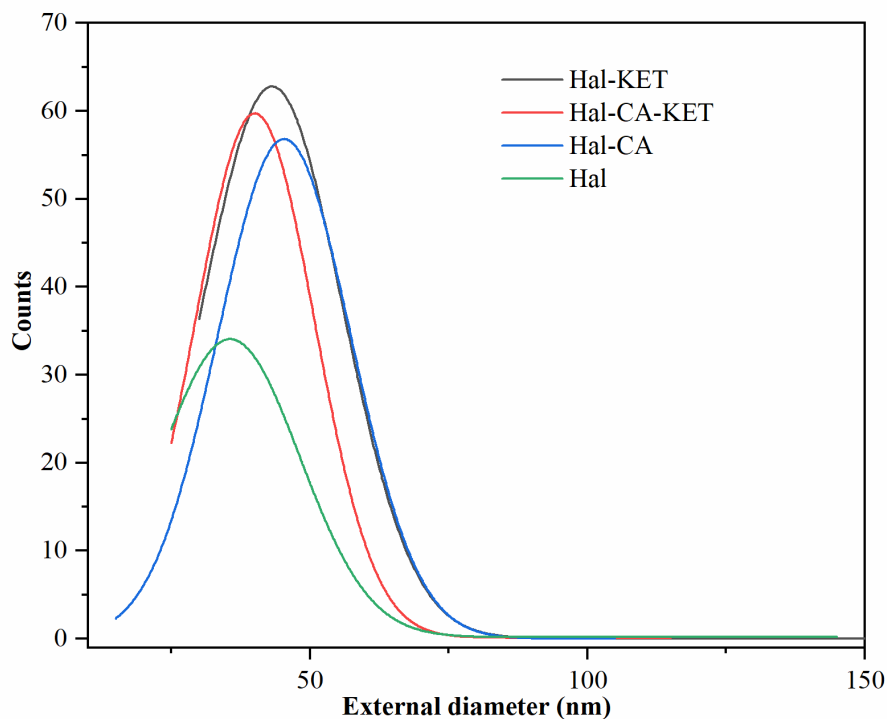

Fig. S1. Distribution of the external diameter of Hal, Hal-CA, Hal-KET and Hal-CA-KET.
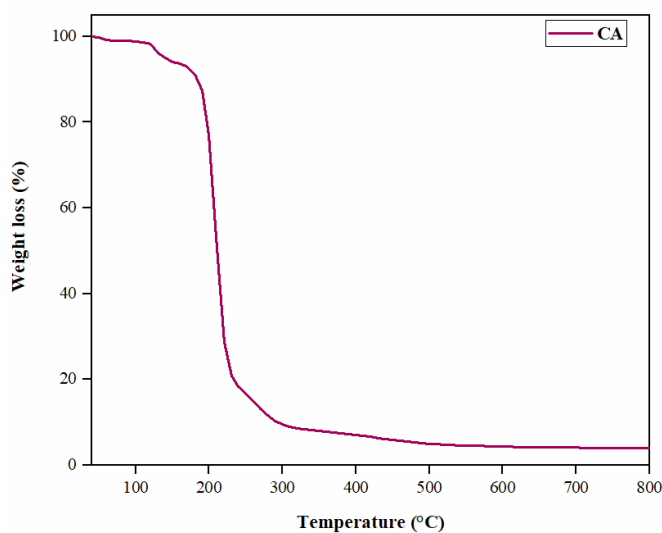

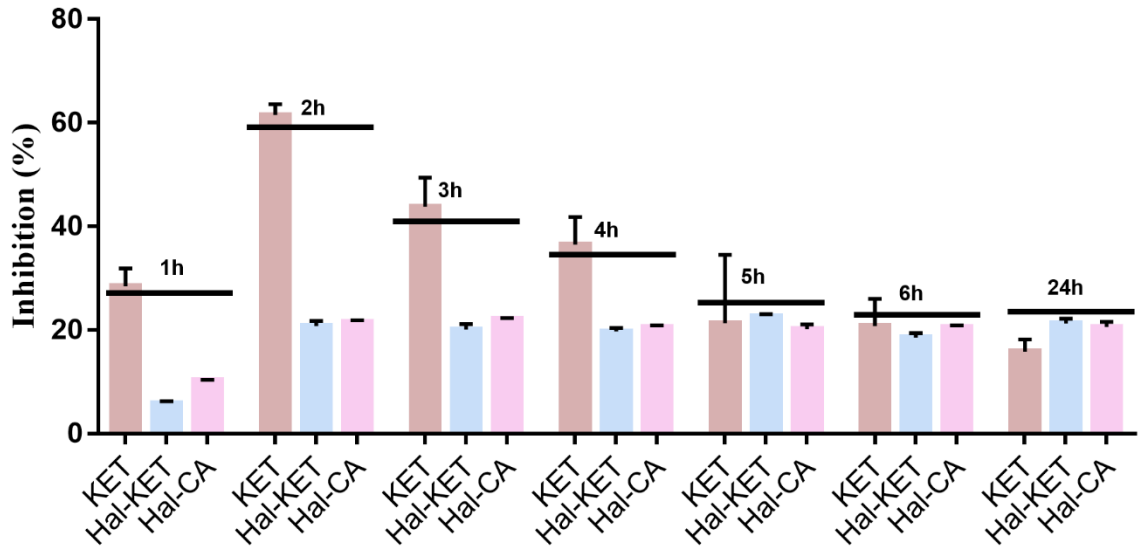**Fig. S2.** ATG thermogram of citric acid.

Fig. S3. Anti-inflammatory activity of KET, Hal-KET and HAL-CA in rats, between 1 and 24 h.
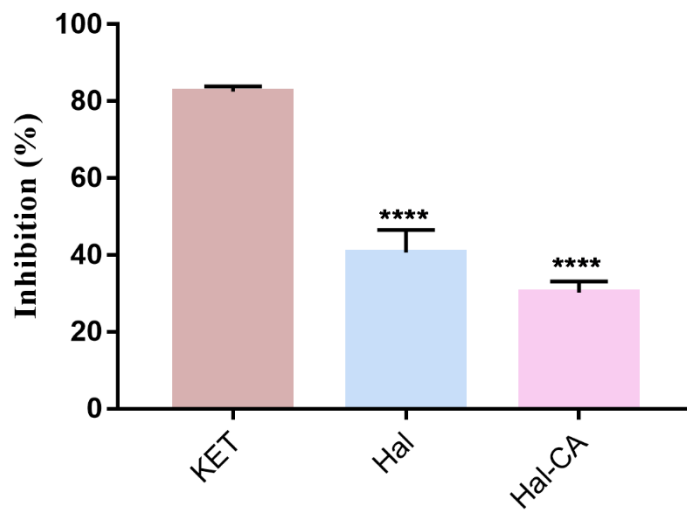
Fig. S4. Analgesic effects of KET, Hal-KET and Hal-CA on acetic acid-induced writhings in mice, at 30 min.

Table S1. Observation of anti-inflammatory activity between 1 and 24 h using Hal, Hal-CA and the corresponding formulations.

time (h)	KET		Hal-KET		Hal-CA-KET		Hal		Hal-CA	
	MEAN	SEM	MEAN	SEM	MEAN	SEM	MEAN	SEM	MEAN	SEM
1	28.42	3.49	8.42	1.4	69.9	1.91	5.87	0.4	10.35	0.02
2	61.5	2.12	32.96	3.31	53.66	2.65	20.79	0.95	21.45	0.32
3	43.8	5.61	63.04	1.8	67.8	3.43	20.09	1.01	22.14	0.17
4	36.5	5.33	63.89	0.97	81.24	1.74	19.7	0.69	20.54	0.33
5	21.8	13.22	62.33	1.89	84.43	1.46	22.71	0.34	20.16	0.93
6	20.8	5.21	51.67	1.05	77.69	2.61	18.57	0.82	20.52	0.34
24	15.84	2.33	38.49	1.57	69.98	2.69	21.27	0.89	20.57	1.02

Conclusion

The purpose of drug delivery is to get an administered drug distributed to tissues or organs that are infected or diseased. The action of the drug that is not targeted mostly generates unwanted side effects.

In controlled and sustained drug delivery, drugs are mostly contained   in carriers which form a vehicle that encapsulates the drug and keeps it sheltered from outside influences.

Two major problems may be encountered in the release of drugs: Their low solubility and their poor site specific release or unwanted degradation in the stomach or bloodstream.

Thus, when a drug is administered, an initial high concentration of drug is made available to the tissues through a phenomenon called "burst release". In this mode, the drug could degrade before reaching the target site and bioavailability of the drug cannot be prolonged and predicted over a period of time.

The objective of this research was on one hand to increase the solubility of two active ingredients (mefenamic acid and an indeno-indole derivative) by using β-cyclodextrin and hydroxypropyl-β-cyclodextrin as encapsulating matrix by forming microparticulate inclusion complexes and on the other hand to obtain a sustained release of ketoprofen using a biocompatible nanoparticulate clay such as halloysite with high surface area nanotubes with ability to interact with drug molecules by adsorption, encapsulation or ion exchange.

The work of this thesis is three-fold:

- First, a bibliographic synthesis on matrices for active ingredients used in this work has been established. Namely, cyclodextrins (native and modified as well as their inclusion complexes) and clays, in particular native and functionalized halloysite have been presented.
- For the second part of the thesis, we pursue the research objective in the contexts of improvement of the solubility of an anti-inflammatory and an anticancer agent while maintaining the extended release with the aim of minimizing the side effects caused by the therapeutic molecules used. So, this experimental section can be divided into two parts:

1) In this part, the phase solubility diagram and job's plot experiment were used to determine the stoichiometry of the MA: β-CD complex. Then molecular modeling approach helped:

✓ to select the most stable inclusion complex (2:1),

✓ to determine intermolecular energy contributions,

✓ to predict hydrophilic surfaces and drug solubility (e.g. solvation energy).

Inclusion complexes of MA:β-CD in the 2:1 molar ratio were prepared using three methods, namely PM, KN, and CE.

FTIR and NMR studies showed no evidence of chemical reactions between the drug and β-CD. DSC, XRPD, and SEM experiments confirmed partial amorphism of the MA after inclusion complexation indicating that MA was well dispersed in the β-CD cavities.

These results suggest an enhanced dissolution profile compared to the crystalline form. All three formulations showed a significant improvement of the MA dissolution; however, the CE complex exhibited the highest KH value. The CE method is thus the most appropriate method to get improved MA dissolution properties.

Actually, the (2:1) MA:β-CD binary complex obtained by CE method constitutes an interesting alternative to formulate MA.

Protein denaturation and membrane stabilisation assays also confirmed the therapeutic benefits of MA when used as (2:1) MA:β -CD complex.

Finally, this approach of preparing inclusion complexes in an optimised ratio could allow other poor-water soluble NSAIDs to be studied again.

2) The work of this part has been devoted to the synthesis of a potent serine / threonine kinase CK2 inhibitor (IC50 = 16 nM) within EA 4446 B2MC laboratory (Claude Bernard University).

This inhibitor named 1,2,3,4-tetrabromo-5-isopropyl-7,8-dihydroindeno [1,2-b] indole-9,10 (5H, 6H) -dione) and coded NB4 has also anti-leukemic activity on multiresistant lines (IPC, Bcl-2). The current limit of its use is the low water solubility (<< 0.002 mg / mL, LogP = 6.31). In order to get around this problem, the use of two cyclodextrins (β-CD or hydroxypropyl-β-CD) in different molar ratios has been studied *in silico*.

The results indicate that the NB4-hydroxypropyl-β-CD complex with a 1: 1 ratio is the most stable and thermodynamically favored. First, the Job's plot was used to confirm the stoichiometry of the NB4: HP-β-CD complex and then its stability was confirmed by the Benesi – Hildebrand plot.

On this basis, the NB4-HP-β-CD system was prepared by the method of freeze drying. The complex was analyzed by different techniques namely: ^{1}H NMR, FTIR and DSC.

The dissolution study showed significantly improved profiles of NB4-HP-β-CD compared to pure NB4. The theoretical model has been successfully validated, with a good correlation between the experimental data and *in silico*.

- The third and last portion of the work reports the use of Algerian halloysite as a carrier for the loading of KET molecules.

Physicochemical characterizations show that the KET was mainly loaded in internal and external surfaces of halloysite, respectively, and that ketoprofen is present in amorphous phase in HAL-KET composite.

The TGA profiles show that the loading efficiency of KET introduced into HAL is around 18%. This amount of KET is distributed homogeneously on the outer surface and in a non-homogeneous manner on the inner surface of the nanotubes.

The study by Monte-Carlo theory illustrates a good affinity for adsorption of KET on the inner and outer surfaces, and these affinities of adsorption are not significantly influenced by the presence of water molecules.

The mechanism of interaction of KET with HAL is physical, where several hydrogen bonds and electrostatic interactions are predominant.

This theoretical study was completed by a development and evaluation of a novel formulation which ensures both the increase in the therapeutic effectiveness of KET and a decrease in the gastric damage related to its main side effects.

Hal and Hal-CA were found to be a convenient and reliable nanoscale carrier platform for loading of KET. In addition, results of the physicochemical characterization confirmed the interaction between Hal-CA and KET, both in the luminal space and external surfaces. *In vitro* release kinetics of the Hal-CA clay nanotubes revealed an effective extended release for 24 h.

In vivo studies indicated clearly that the treatment of animals with formulations reduced carrageenan induced paw edema and the number of writhings induced by acetic acid. Moreover, Hal-CA-KET provides a total gastric mucosa protection. Hal-CA can be considered as a promising and credible tool for future pharmaceutical formulations.

Résumé :

La faible solubilité aqueuse de certaines molécules thérapeutiques est un facteur limitant pour leur utilisation clinique. Le premier axe de cette thèse a été orienté vers une étude de chemoinformatique pour surmonter le problème de solubilité d'un inhibiteur de la protéine kinase CK2 et actif sur différentes lignées de cellules leucémiques (un dérivé d'indéno-indole) par son inclusion dans l'hydroxypropyl-β-cyclodextrine ainsi que celle d'un anti-inflammatoire tel que l'acide méfénamique en utilisant une β-cyclodextrine native. L'effet des CDs sur la solubilité des principes actifs a été déterminé par des études de phase de solubilité. Les constantes d'association K ont également été calculées à partir des diagrammes de phase des solubilités obtenus. Les résultats ont été exploités en termes de gain de solubilité des molécules encapsulées comparativement à leur solubilité aqueuse intrinsèque. Le Job's plot a été utilisé pour déterminer la stœchiométrie des complexes et leur stabilité a été confirmée in silico aussi bien que par le Benesi–Hildebrand plot. Les systèmes ainsi préparés ont été caractérisés par ^{1}H and ^{13}C RMN, FTIR, ATG, MEB et DSC. L'étude de la dissolution a montré des profils significativement améliorés des complexes d'inclusion microparticulaires par rapport aux principes actifs purs et a permis de générer des systèmes de libération prolongée. L'étude théorique in silico conforte les résultats expérimentaux. Le deuxième axe qui a été abordé dans cette thèse est celui des nanotubes d'argile naturelle et biocompatibles qui sont parmi les meilleurs matériaux inorganiques pour les nanoformulations de médicaments. Des nanotubes d'halloysite ont servi de matrice encapsulante d'un anti-inflammatoire tel que le Kétoprofène. Pour faciliter la dispersion de ce support médicamenteux dans des milieux physiologiques, sa surface a été modifiée par une molécule qui lui augmente sa polarité telle que l'acide citrique. Dans cette optique de recherche, deux formulations (Hal-KET et Hal-CA-KET) ont été préparées et caractérisés par DRX, FTIR, TEM, ATG, DTA et DSC. Les tests de dissolution ont donné des profils de libération prolongée. Aussi une évaluation de leurs effets pharmacologiques in vivo par l'étude des activités anti-inflammatoire et analgésique, après administration orale de Hal-KET et Hal-CA-KET, a été réalisée sur des rongeurs. L'activité ulcérogènique et les effets histopathologiques des formulations ont également été comparés à celui du KET pur.

Mots clés : Encapsulation, libération prolongée, cyclodextrines, halloysite, stabilité, chemoinformatique.

Summary

The poor aqueous solubility of some pharmaceutical ingredients is a limiting factor in its clinical use. This study was undertaken to overcome the solubility limitation of an inhibitor of protein kinase CK2 (an indeno-indole derivative) by its inclusion in Hydroxypropyl-β-cyclodextrin as well as an anti-inflammatory such as mefenamic acid by using a native β-cyclodextrin. The effect of CDs on the solubility of active ingredients was determined by phase solubility studies. Association constants K were also calculated from the solubility phase diagrams obtained. The results were exploited in terms of gain in solubility of the encapsulated molecules compared to their intrinsic aqueous solubility. The Job's plot was used to determine the stoichiometry of the complexes and their stability was confirmed in silico as well as by the Benesi-Hildebrand plot. The systems thus prepared were characterized by ^{1}H and ^{13}C NMR, FTIR, ATG, MEB and DSC. The study of dissolution has shown significantly improved profiles of microparticulate inclusion complexes compared to pure active ingredients and allows the generation of sustained release systems. The theoretical study in silico confirms the experimental results. The second axis which was approached in this thesis is that of natural and biocompatible clay nanotubes which are among the best inorganic materials for drug nanoformulations. Halloysite nanotubes served as an encapsulating matrix for an anti-inflammatory such as Ketoprofen. To facilitate the dispersion of this medicinal support in physiological media, its surface has been modified by a molecule which increases its polarity, such as citric acid. In this research perspective, two formulations (Hal-KET and Hal-CA-KET) were prepared and characterized by DRX, FTIR, TEM, ATG, DTA and DSC. Dissolution tests gave sustained release profiles. Also, an evaluation of their pharmacological effects in vivo by studying anti-inflammatory and analgesic activities, after oral administration of Hal-KET and Hal-CA-KET, was carried out in rodents. The ulcerogenic activity and histopathological effects of the formulations were also compared with that of pure KET.

Key words: Encapsulation, sustained release, cyclodextrins, halloysite, stability, chemoinformatics

ملخص

بعد ضعف الذوبان المائي لبعض المكونات الصيدلانية عاملاً مقيّداً للاستخدام السريري. أجريت هذه الدراسة للتغلب على محدودية قابلية الذوبان لمثبط بروتين كيناز 2CK (مشتق إندينو إندول) من خلال إدراجه في هيدروكسي بروبيل بيتا سيكلوديكسترين بالإضافة إلى مضاد للالتهابات مثل حمض الميفيناميك باستخدام مركب بيتا سيكلوديكسترين الأصلي. . تم تحديد تأثير الأقراص المدمجة على قابلية ذوبان المكونات النشطة من خلال دراسات الذوبان في المرحلة. كما تم حساب ثوابت الرابطة K من مخططات مرحلة الذوبان التي تم الحصول عليها. تم استغلال النتائج من حيث الزيادة في قابلية ذوبان الجزيئات المغلفة مقارنة بقابليتها للذوبان في الماء. تم استخدام. Job Plot لتحديد قياس العناصر المتكافئة للمجمعات وتم تأكيد استقرارها في السيليكو وكذلك من خلال Benesi-Hildebrand تميزت الأنظمة المعدة على هذا النحو بـNMR و FTIR و ATG و MEB و DSC. أظهرت دراسة الذوبان ملامح محسنة بشكل ملحوظ لمجمعات تضمين الجسيمات الدقيقة مقارنة بالمكونات النشطة النقية وتسمح بتوليد أنظمة إطلاق مستدامة.

تؤكد الدراسة النظريةفي السيليكو نتائج التجربة. المحور الثاني الذي تم تناوله في هذه الأطروحة هو محور الأنابيب النانوية الطينية الطبيعية والمتوافقة حيوياً والتي تعد من بين أفضل المواد غير العضوية للتشكيلات النانوية للأدوية. تعمل الأنابيب النانوية هالويسايت كمصفوفة مغلفة لمضاد للالتهابات مثل كيتوبروفين. لتسهيل تشتت هذا الدعم الطبي في الوسط الفسيولوجي، تم تعديل سطحه بواسطة جزيء يزيد قطبيته ، مثل حامض الستريك. في هذا المنظور البحثي ، تم تحضير صيغتين (Hal-KET و Hal-CA-KET) وتميزتا بـ DRX و FTIR و TEM و ATG و DTA و DSC. أعطت اختبارات الذوبان ملامح إطلاق مستدامة. أيضًا ، تم إجراء تقييم لتأثيراتها الدوائية في الجسم الحي من خلال دراسة الأنشطة المضادة للالتهابات والمسكنات ، بعد تناول Hal-KET و Hal-CA-KET عن طريق الفم ، في القوارض.القرحة

الكلمات الدالة: المعلوماتية الكيميائ,التضمين,سيكلودكسسترين,الاستقرار